SEISMIC RESPONSE OF MULTI-SPAN HIGHWAY BRIDGES WITH TWO-COLUMN REINFORCED CONCRETE BENTS INCLUDING FOUNDATION AND COLUMN FLEXIBILITY

A THESIS SUBMITTED TO
THE GRADUATE SCHOOL OF NATURAL AND APPLIED SCIENCES
OF
MIDDLE EAST TECHNICAL UNIVERSITY

BY

TANER YILMAZ

IN PARTIAL FULFILLMENT OF THE REQUIREMENTS
FOR
THE DEGREE OF MASTER OF SCIENCE
IN
CIVIL ENGINEERING

DECEMBER 2008

Approval of the thesis:

SEISMIC RESPONSE OF MULTI-SPAN HIGHWAY BRIDGES WITH TWO-COLUMN REINFORCED CONCRETE BENTS INCLUDING FOUNDATION AND COLUMN FLEXIBILITY

submitted by **TANER YILMAZ** in partial fulfillment of the requirements for the degree of **Master of Science in Civil Engineering Department, Middle East Technical University** by,

Prof. Dr. Canan Özgen _____
Dean, Graduate School of **Natural and Applied Sciences**

Prof. Dr. Güney Özcebe _____
Head of Department, **Civil Engineering**

Asst. Prof. Dr. Alp Caner _____
Supervisor, **Civil Engineering Dept., METU**

Examining Committee Members:

Prof. Dr. Polat Gülkan _____
Civil Engineering Dept., METU

Asst. Prof. Dr. Alp Caner _____
Civil Engineering Dept., METU

Assoc. Prof. Dr. Ahmet Yakut _____
Civil Engineering Dept., METU

Asst. Prof. Dr. M. Altuğ Erberik _____
Civil Engineering Dept., METU

Assoc. Prof. Dr. Murat Dicleli _____
Dept. of Engineering Sciences, METU

Date: 02.12.2008

I hereby declare that all information in this document has been obtained and presented in accordance with the academic rules and ethical conduct. I also declare that, as required by these rules and conduct, I have fully cited and referenced all material and results that are not original to this work.

Name, Last Name : **TANER YILMAZ**

Signature :

ABSTRACT

SEISMIC RESPONSE OF MULTI-SPAN HIGHWAY BRIDGES WITH TWO-COLUMN REINFORCED CONCRETE BENTS INCLUDING FOUNDATION AND COLUMN FLEXIBILITY

Yılmaz, Taner

M.S., Department of Civil Engineering

Supervisor: Asst. Prof. Dr. Alp Caner

December 2008, 204 pages

Seismic design of highway bridges has improved as a result of the experience gained from large earthquakes of the last thirty years. Ductility demand and reserved capacity are extremely important response measures used in new bridge designs to assess target damage levels. However, the application of practical design approaches specified in bridge design codes is not well-defined for bridges over flexible foundations. Within the scope of this research, thirty two bridge models having varying column aspect ratio, amount of column longitudinal reinforcement and foundation flexibility parameters are investigated through a series of analyses such as response spectrum analysis and inelastic time-history analysis under "safety evaluation earthquake" hazard level with a return period of 1000 years, and push-over analysis. Using the results of analyses, seismic response of the investigated bridges are identified with several measures such as displacement capacity over demand ratio, global displacement ductility demand, and response modification factor, along with maximum concrete and steel strains of columns. A correlation between concrete and steel strains and seismic response

measure values is constructed to estimate damage levels with commonly used response measures. The findings of this research revealed that global displacement ductility demand is not a favorable response measure for assessing damage levels. On the other hand, displacement capacity over demand ratios can be suggested for estimation of damage levels especially where foundation flexibility effects are extensive as system yielding is not taken into consideration.

Keywords: Seismic design, displacement ductility demand, foundation flexibility, damage level, highway bridge

ÖZ

İKİ KOLONLU BETONARME ORTA AYAKLARA SAHİP ÇOK AÇIKLIKLI KARAYOLU KÖPRÜLERİNİN ZEMİN VE KOLON ESNEKLİĞİNİ KAPSAYAN DEPREM DAVRANIŞI

Yılmaz, Taner
Yüksek Lisans, İnşaat Mühendisliği Bölümü
Tez Yöneticisi: Yrd. Doç. Dr. Alp Caner

Aralık 2008, 204 sayfa

Karayolu köprülerinin sismik tasarımı, son otuz yıldaki büyük depremlerden kazanılan tecrübelerin sonucunda gelişmiştir. Süneklilik istemi ve rezerv kapasite, hedef hasar seviyelerinin değerlendirilmesi için yeni köprü tasarımlarında kullanılan son derece önemli tepki ölçüleridir. Ancak köprü tasarım yönetmeliklerinde belirtilen pratik tasarım yaklaşımlarının uygulaması, esnek temeller üzerindeki köprüler için iyi tanımlanmamıştır. Bu araştırma kapsamında, değişken kolon boy/çap oranı, kolon boyuna donatı oranı ve zemin esnekliği parametrelerine sahip otuz iki köprü modeli, 1000 senelik tekrarlama periyoduna sahip "güvenlik değerlendirmesi depremi" altındaki tepki spektrumu analizi ve elastik ötesi zaman tanım analizi, ve artımsal itme analizi gibi bir dizi analiz aracılığıyla incelenmiştir. Analiz sonuçları kullanılarak incelenen köprülerin deprem davranışları, kolonların maksimum beton ve donatı birim şekil değiştirmeleri ile birlikte deplasman kapasite istem oranı, global deplasman süneklilik istemi, tepki modifikasyon faktörü gibi çeşitli tepki ölçülerine gore belirlenmiştir. Çokça kullanılan tepki ölçüleri ile hasar seviyelerini tahmin etmek

için beton ve donatı birim şekil değiştirmeleri ve sismik tepki ölçüleri arasında bir ilişki kurulmuştur. Bu araştırmadaki bulgular, global deplasman süneklilik isteminin hasar seviyelerinin tayini için uygun bir tepki ölçüsü olmadığını göstermiştir. Diğer taraftan; hasar seviyelerinin tahmini için, özellikle zemin esnekliği etkisinin çok olduğu yerlerde sistemin akması dikkate alınmadığından dolayı deplasman kapasite istem oranları önerilebilir.

Anahtar kelimeler: Deprem tasarımı, deplasman süneklilik istemi, zemin esnekliği, hasar seviyesi, karayolu köprüsü

ACKNOWLEDGEMENTS

This study was conducted under the supervision of Asst. Prof. Dr. Alp Caner. I would like to express my sincere appreciation and gratitude for the guidance, encouragement, and support that he has provided me throughout the research.

I would also like to thank to my friends Durukan Bedük, Murat Şahin, Onur Yücel, Salih Yılmaztekin, Ali Ali Türkkan and Atilla Bayraktar for their friendship and encouragement throughout this study.

Finally, my mother Betül Neşe Yılmaz, my father Talat Yılmaz, my sister Ufuk Yılmaz Aygün, my brothers Dursun Murat Yılmaz and Cengiz Yılmaz deserve special thanks for their invaluable support and unlimited understanding.

TABLE OF CONTENTS

ABSTRACT....iv
ÖZ....vi
ACKNOWLEDGEMENTS....viii
TABLE OF CONTENTS....ix
CHAPTER
1. INTRODUCTION....1
1.1 Background....1
1.2 Statement of Problem....3
1.3 Aim and Scope of the Study....4
2. LITERATURE REVIEW....6
2.1 Seismic Design Approaches of Highway Bridges....6
2.2 Published Researches....15
3. METHOD OF ANALYSIS....19
3.1 Flowchart....19
3.2 Investigated Responses....19
3.2.1 Response Measures....21
3.2.2 Concrete and Steel Strains....27
3.3 Correlation of Investigated Responses....29
4. ANALYSIS PROCEDURE....31
4.1 Description of Bridges....31
4.2 Material Properties....36
4.2.1 Design Properties....36
4.2.2 Expected Material Properties....37
4.2.3 Material Models....39
4.3 Local Soil Condition....40
4.4 Investigated Cases....41

4.5 Computer Modeling 42
4.5.1 Superstructure 42
4.5.2 Substructure 44
4.5.3 Superstructure Supports 56
4.5.4 Lateral Soil Response 66
4.5.5 Element Types 70
4.6 Seismic Hazard 70
4.6.1 Seismic Hazard Level 1: Design Earthquake 71
4.6.2 Seismic Hazard Level 2: Safety Evaluation Earthquake 71
4.7 Response Spectrum Analysis 74
4.7.1 Modal Analysis 78
4.7.2 Shear Design of Columns 81
4.8 Push-Over Analysis 84
4.9 Inelastic Time-History Analysis 87
4.9.1 Response Spectrum Compatible Time-History Records 88
4.9.2 Rayleigh Damping 101
5. ANALYSES RESULTS 103
5.1 Introduction 103
5.2 Structural Displacement Ductility Capacities 103
5.3 Maximum Displacement Ratios 105
5.4 Displacement Capacity over Demand Ratios 108
5.5 Global Displacement Ductility Demands 113
5.6 Response Modification Factors for Columns 116
5.7 Concrete and Steel Strains 118
5.8 Correlation of Damage Levels with Response Measures 121
6. DISCUSSION OF RESULTS AND CONCLUSIONS 132
6.1 Discussion of Results 132
6.2 Summary and Conclusions 145
6.3 Recommendations for Further Studies 146
REFERENCES 147

APPENDICES

A. MATERIAL MODELS 154
B. ATTENUATION RELATIONSHIPS 158
C. LOAD-DEFLECTION (P-Y) CURVES FOR SAND 160
D. CONSTRUCTION OF RESPONSE SPECTRUM CURVES 162
E. SHEAR STRENGTH FORMULAS 165
F. MODAL ANALYSES RESULTS 167
G. RESPONSE SPECTRA OF TIME-HISTORY RECORDS 168
H. ANALYSES OUTPUTS 172
I. RESPONSE MEASURE VALUES 191
J. DEMONSTRATION OF CAPACITIES AND DEMANDS 197

CHAPTER 1

INTRODUCTION

1.1 Background

Seismic design of highway bridges has improved as a result of the experience gained from major earthquakes such as Loma Prieta (1989), Northridge (1994), Kobe (1995) and Chi-Chi (1999). Significant damage and even total failure at bridge columns observed in these earthquakes has shown that estimation of ductility demands and reserved capacities is extremely important for future bridge designs. In new designs, damage levels are directly or indirectly set at different seismic hazard levels to develop an economical design.

Force based design, utilizing elastic analysis, were used in design of many bridges till the last decade. Damage levels could not be assessed properly by forced based design and reliability in designs had typically large deviations from one bridge to another. The current trend is to use forced based methods in conjunction with displacement based methods, which provides a good estimation of damage levels.

Priestley et al. [44] stated that displacement based design was established on determination of the optimum strength to achieve a given performance limit state, related to a defined level of damage, under a specific level of seismic intensity. Damage levels are mainly measured in terms of concrete and steel strains. Instead of utilizing strains in assessing damage levels, design codes recommend using equivalent displacement ductility demands or response modification factors which allows a more practical engineering design approach.

Bridge design codes have been adapting this philosophy but there are some cases where generally accepted rules or recommendations for design can be insufficient in assessment. Response modification factors or displacement ductility demands are not defined as a function of foundation flexibility including potential soil yielding.

In seismic design of multi-span highway bridges, damage is allowed to develop at plastic hinge zones of columns avoiding brittle shear failure as shown in Figure 1.1. In such a design, foundation and cap beams remain essentially elastic and capacity protected. Damage levels are typically measured at plastic hinge zones of columns due to flexural behavior. Typical capacity curves of two similar bridges, one over competent soil and other one over poor soil, are presented with assessed damage levels as shown in Figure 1.2.

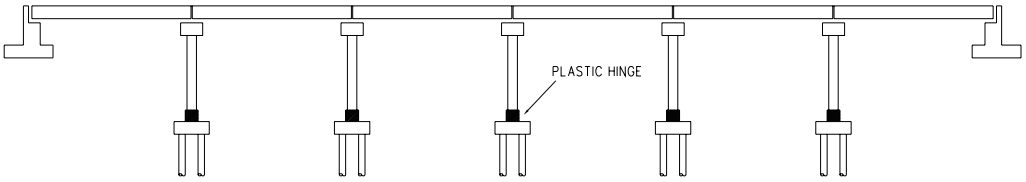

(a) In Longitudinal Direction

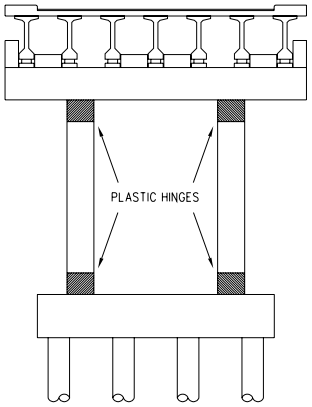

(b) In Transverse Direction

Figure 1.1: Potential Plastic Hinge Regions

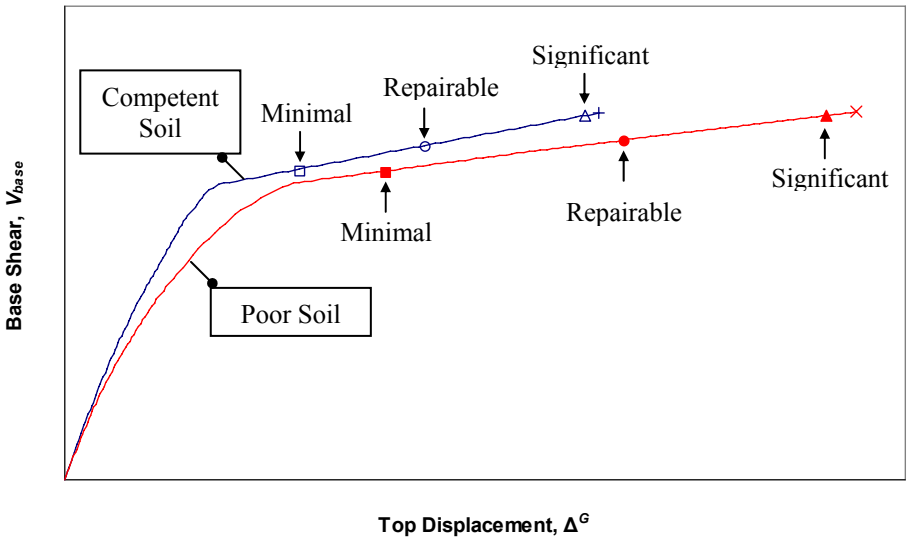

Figure 1.2: Typical Capacity Curves of Similar Bridges at Competent and Poor Soil Conditions, and Assessed Damage Levels

Over the past years, bridges were typically designed for a single hazard level representing an earthquake with a return period of 475 years. In new bridge designs, performance objectives are defined as a function of expected damage levels and serviceability conditions at different hazard levels according to the importance category of the bridge considered.

1.2 Statement of Problem

Engineering judgment is typically used to overcome difficulties arisen from uncertainties found in bridge design codes. Uncertainties involved in analysis and in design can be compiled as assessing material properties, modeling assumptions, element behaviors, soil conditions and hazard level at the site considered, limiting response modification factors, ductility demands, and capacity over demand ratios.

It has been evaluated that limited knowledge is available on the following issues:

- Effect of foundation flexibility on seismic response
- Identification of damage states with commonly used response measures
- Selecting hazard level and corresponding target damage levels
- Variation in concrete and steel strains with respect to the same damage level defined in different codes or researches
- Correlation of importance categories to target damage levels

1.3 Aim and Scope of the Study

The aim of this study can be summarized as:

- To study seismic response of standard multi-span highway bridges with different column slenderness and longitudinal reinforcement ratios at competent and poor soil conditions.
- To identify differences in seismic response measures.
- To identify seismic response measure values corresponding to different damage levels.

Within the scope of this study, thirty two bridge models with varying column aspect ratio, amount of longitudinal reinforcement and foundation flexibility parameters are investigated through a series of analyses as briefly explained below:

- Response spectrum analysis per AASHTO-LRFD [2] is performed. Elastic internal forces corresponding to “design earthquake” hazard are obtained.
- Response spectrum analysis per AASHTO-Seismic [28] is performed. Elastic displacement demands corresponding to “safety evaluation earthquake” hazard are obtained.
- Push-over analyses is performed from which capacity curves are obtained.

- For each model, a total of eight inelastic time-history analyses are performed with generated accelerograms compatible with the spectra used for “safety evaluation earthquake” hazard. Inelastic displacement demands and plastic rotations are obtained.

Utilizing the outputs of the steps mentioned above, the following results are achieved:

- Amount of necessary column confining reinforcement is determined.
- Several response measures, namely structural displacement ductility capacities, maximum displacement ratios, displacement capacity over demand ratios, global displacement ductility demands, and response modification factors are obtained. Maximum concrete and steel strains of columns are computed.
- Correlation between concrete and steel strains with seismic response measures is constructed. Approximate damage levels are estimated with the commonly used response measures.

CHAPTER 2

LITERATURE REVIEW

2.1 Seismic Design Approaches of Highway Bridges

Researches and practice performed mainly in United States lead improvements on seismic design of highway bridges. Several government agencies such as Federal Highway Administration (FHWA), American Association of State Highway and Transportation Officials (AASHTO), California Department of Transportation (Caltrans) and Applied Technology Council (ATC) have been contributing to these improvements intensively. A brief summary of the history of improvements on seismic design criteria of highway bridges is given in reference [22] as follows:

- Prior to 1971 San Fernando Earthquake, lateral force requirements for buildings which consider 2 % to 6 % of dead loads were applied for bridges.
- In 1973, Caltrans developed new seismic design criteria related to site, seismic response of the soils at the site, and the dynamic characteristics of bridges. AASTHO modified the 1973 Provisions slightly, and adopted Interim Specifications.
- In 1981, ATC developed guidelines ATC-6 [7] for seismic design of bridges.
- In 1983, AASHTO adopted ATC-6 as the Guide Specifications.
- In 1991, AASHTO incorporated the Guide Specifications into Standard Specifications for Highway Bridges.

- In 1996 and in 1997, ATC published improved seismic design criteria recommendations for California Bridges [8] and for U.S. bridges and highway structures [9], respectively.
- In 1999, Caltrans published the new Seismic Design Methodology [14] and the first version of Seismic Design Criteria.
- In 2006, Caltrans published the latest version of Seismic Design Criteria (version 1.4) [15].

In 2001, the joint venture of ATC and Multidisciplinary Center for Earthquake Engineering Research (MCEER) carried out a research [11] for National Cooperative Highway Research Program (NCHRP) project no. 12-49 [12] to develop recommended specifications for seismic design of highway bridges. As an outcome, ATC and MCEER published the document "Recommended LRFD Guidelines for the Seismic Design of Highway Bridges" [10] and submitted to the AASHTO Bridge Subcommittee. Due to the unresolved issues evaluated through trial designs, these guidelines were not adopted by AASHTO Bridge Subcommittee. In order to reformat the document [10] and to integrate the material of Caltrans-SDC [15], ATC-32 [8], and South Carolina Seismic Design Specifications [46], in 2006, Imbsen Consulting, completed a research project called "Development of LRFD Guidelines for the Seismic Design of Highway Bridges, Version 2" for the NCHRP project no. 20-07/Task 193. In 2007, the resulting document "Proposed AASHTO Guide Specifications for LRFD Seismic Bridge Design" [28] is published.

Three major sources, AASHTO-LRFD, Caltrans-SDC and Proposed AASHTO Guide Specifications for LRFD Seismic Bridge Design (AASHTO-Seismic hereafter), related to seismic design of highway bridges are discussed further:

AASHTO LRFD Bridge Design Specifications [2]

In AASHTO-LRFD [2], bridge structures are classified into three importance categories as critical bridges, essential bridges and other bridges. The importance classification of a bridge is made according to the social/survival and security/defense requirements. Design is checked with respect to a single level hazard. The design earthquake, for which acceleration contour maps are given for U.S. is an event having a return period of 475 years. The target damage levels are not explicitly stated but the service conditions for essential and critical bridges after a design earthquake is specified. Essential bridges are required to be open to emergency vehicles and for security/defense purposes immediately after the design earthquake. Critical bridges are required to remain open to all traffic after the design earthquake and be usable by emergency vehicles immediately after a large earthquake with a higher return period e.g. 2500 years.

AASHTO-LRFD utilizes a forced-based method for design of structural elements. Site effects are taken into consideration for determination of elastic design forces according to the soil profile at the site. Four types of soil profiles are defined. The construction of response spectra is explained in APPENDIX D. Inelastic design forces can be obtained from dividing elastic forces to proper response modification factors providing ductile behavior. Recommended response modification factors for substructure elements are shown in Table 2.1.

Inelastic hinges are permitted at locations in columns where they can be readily inspected and/or repaired. Capacity protection design principles are applied to avoid brittle failure. Essential elastic response of capacity protected members such as foundation elements, superstructure and connections is required.

Table 2.1: Response Modification Factors for Substructure Elements [2]

Substructure	Importance Category		
	Critical	Essential	Other
Wall-type piers-larger dimension	1.5	1.5	2
Reinforced concrete pile bents			
- Vertical piles only	1.5	2	3
- With batter piles	1.5	1.5	2
Single columns	1.5	2	3
Steel or composite steel and concrete pile bents			
- Vertical piles only	1.5	3.5	5
- With batter piles	1.5	2	3
Multiple column bent	1.5	3.5	5

ATC-32 Improved Seismic Guidelines for California Bridges [8]

ATC-32 [8] proposes a two level performance objective as a function of ground motion at the site and criticality or importance of the bridge structure. (Table 2.2)

Table 2.2: Two Level Performance Objectives Defined in ATC-32

Ground Motion at Site		Ordinary Bridges	Important Bridges
Functional Evaluation	Service Level	*Immediate*	*Immediate*
	Damage Level	*Repairable*	*Minimal*
Safety Evaluation	Service Level	*Limited*	*Immediate*
	Damage Level	*Significant*	*Repairable*

The terms defined in Table 2.2 are explained as follows:

Importance definitions

Important bridge: Any bridge satisfying one or more of the following:

- Required to provide secondary life safety.
- The time for restoration of functionality after closure would create a major economic impact.
- Formally designated as critical by a local emergency plan.

Ground Motion Levels

Safety Evaluation Earthquake (SEE): Deterministically assessed ground motion from maximum credible earthquake or probabilistically assessed ground motion with a long return period (approximately 1000 to 2000 years).

Functional Evaluation Earthquake (FEE): Probabilistically assessed ground motion that has 60 % probability of not being exceeded during the useful life of the bridge.

Service level definitions

Immediate : Full access to normal traffic available almost immediately.

Limited : Limited access possible within days; full service restorable within months

Damage level definitions

Minimal : Essentially elastic performance.

Repairable : No collapse. Damage that can be repaired with a minimum risk of losing functionality

Significant : A minimum risk of collapse, but damage that would require closure for repair.

Caltrans Seismic Design Criteria (Caltrans-SDC) [15]

Seismic performance goals of Caltrans are outlined in Seismic Design Methodology document [14]. Required performance objectives are almost identical with the recommendations of ATC-32 [8]. It is stated that an explicit functional evaluation is not required for ordinary bridges provided that the safety-evaluation performance criteria and the seismic design requirements are satisfied.

Seismic design philosophy of Caltrans can be summarized as expressed in [14] and as follows:

- The assessment of FEE is required to be reviewed by a Caltrans-approved consensus group rather than giving a probabilistic definition. SEE for ordinary bridges shall be based on deterministic assessment corresponding to the maximum credible earthquake. Spectral acceleration values for SEE for ordinary bridges can be estimated from the response spectra curves in Caltrans-SDC [15]. The safety evaluation and functional evaluation earthquakes for important bridges may be determined either deterministically or probabilistically. The approximate return period of SEE is between 1000 to 2000 years.
- All structural components shall be designed to provide sufficient strength and ductility, with a reasonable amount of reserve capacity, to ensure collapse will not take place during maximum credible earthquake.
- Caltrans takes advantage of ductility and post elastic strength to meet performance criteria with a minimal capital investment. One of the most desirable types of ductile response in bridge systems is sustained hysteric force-deformation cycles that dissipate energy. This type of response can be generated internally by flexural plastic hinges.
- Inelastic behavior shall be limited to pre-determined locations within the bridge that can be easily inspected and repaired following an earthquake.
- An adequate margin of strength shall be provided between the designated ductile failure mode and non-ductile failure mode. Components not explicitly designated for ductile performance or as sacrificial components shall be designed to remain essentially elastic under seismic loads.
- The estimated displacement demands generated by the design earthquake shall not exceed the structure's global displacement capacity or the local displacement capacity of any of its individual components.

Caltrans Seismic Design Criteria [15] specifies minimum design requirements that are necessary to meet the performance goals established for ordinary bridges in Seismic Design Methodology Document.

- The entire structural system as well as its individual subsystems shall meet the displacement ductility demand requirement as shown in Table 2.3. Displacement ductility demand is defined as:

$$\mu_D = \Delta_D / \Delta_Y \tag{2.1}$$

where;

Δ_D : Estimated global displacement demand

Δ_Y : Global yield displacement

Table 2.3: Maximum Displacement Ductility Demand Requirements for Bridges on Fixed Foundations [15]

Single column bents supported on fixed foundation		$\mu_D \leq 4$
Multi-column bents supported on fixed or pinned footings		$\mu_D \leq 5$
Pier walls supported on fixed or pinned footings	Weak direction	$\mu_D \leq 5$
	Strong direction	$\mu_D \leq 1$

Displacement ductility demand limits displayed in Table 2.3 are for fixed-base cantilever columns. However, limiting values are not clearly stated when the flexibility of foundation elements or cap beams are included in demand. For such situations, a greater percentage of flexibility of components other than the ductile members within the frame contributes to global displacements. Therefore, the global displacement ductility demand requirements in Table 2.3 may not be satisfied. It is also stated that "columns or piers with flexible foundations will naturally have low displacement ductility demands because of the foundation's contribution to Δ_Y" [15]. Lower limit for global displacement ductility demand is not dictated to encourage designs having flexible systems.

- Each bridge or frame shall satisfy global displacement criteria:

$$\Delta_C / \Delta_D > 1.0 \qquad (2.2)$$

where;

Δ_C : Global displacement capacity

Δ_D : Global displacement demand

- Each ductile member shall have a minimum local displacement ductility capacity of μ_c = 3 to ensure dependable rotational capacity in the plastic hinge region. The local displacement ductility capacity is defined as:

$$\mu_c = \Delta_c / \Delta_Y^{col} \qquad (2.3)$$

where;

Δ_C : Displacement capacity measured from the point of maximum moment to the contra-flexure point

Δ_Y^{col} : Yield displacement measured from the point of maximum moment to the contra-flexure point

Proposed AASHTO Guide Specifications for LRFD Seismic Bridge Design (AASHTO-Seismic) [28]

A single level performance objective, called "life safety", is specified for the design earthquake having a probability of exceedance 7 % in 75 years (return period of 1000 years). The expected performance for life safety is that the bridge has a low probability of collapse but, may suffer significant damage and significant disruption to service is possible.

Significant damage includes permanent offsets and damage consisting of cracking, reinforcement yielding, and major spalling of concrete for reinforced concrete elements. Significant disruption to service includes closure of the bridge to repair the damages, partial or complete replacement of columns and limited access (reduced lanes, light emergency traffic) on the bridge.

The performance definition states the minimum conditions, which correspond to the performance objectives specified for ordinary bridges in ATC-32 [8] under safety evaluation earthquake. It is expressed that bridge owners can specify higher level of performance objectives such as assigning repairable damage under the same hazard level to improve service conditions after the design earthquake. This is equivalent to increasing the importance level of the bridge from ordinary to important.

AASHTO-Seismic presents three types of earthquake resisting systems. Design strategy for conventional earthquake resisting systems, ductile substructure with essentially elastic superstructure, is identical with AASHTO-LRFD. However, some earthquake resisting elements such as in-ground hinging or passive abutment resistance are allowed with the approval of the owner.

In the general procedure, acceleration response parameters are constructed using the hazard maps produced for a ground motion having a probability of exceedance 7 % in 75 years. The construction of response spectra curves is shown in APPENDIX D. Besides, site-specific procedures are required as mandatory for bridges having high level of poor soil conditions or importance, or for sites located close to a known fault.

The design requirement of global displacement capacity shall be greater than global displacement demand defined in Caltrans-SDC [15] is also required in AASHTO-Seismic. AASHTO-Seismic also requires a local displacement ductility demand check for the elements having plastic displacements as shown in Table

2.4. The definition of displacement ductility demand is different than the displacement ductility demand definition of Caltrans.

$$\mu_D = 1 + \Delta_{pd} / \Delta_{yi} \tag{2.4}$$

where;

Δ_{pd} : Plastic displacement demand

Δ_{yi} : Idealized yield displacement corresponding to idealized yield curvature

These displacements are measured from the point of maximum moment to the contra-flexure point.

Table 2.4: Member Ductility Demand Requirements [28]

Single columns bents		$\mu_D \leq 5$
Multiple column bents		$\mu_D \leq 6$
Pier walls	Weak direction	$\mu_D \leq 5$
	Strong direction	$\mu_D \leq 1$

2.2 Published Researches

Damage levels of reinforced concrete elements are generally evaluated using concrete and steel strains at sections where deformations are maximized. The seismic performance requirements recommended by ATC-32 [8] are increasingly adopted by design manuals and project based design criteria. Quantitative damage limits corresponding to different performance levels has not been specified in Caltrans-SDC [15], AASHTO-LRFD [2] and ATC-32 [8] because of lack of consensus [22]. Strain and ductility limit values corresponding to three damage levels are proposed in reference [22] as shown in Table 2.5.

The concrete strain limits specified in Table 2.5 accounts for confinement effect of concrete. Increasing confinement upgrades the limiting damage levels. The

concrete strain limits divide the entire stress-strain diagram of a typical well-confined section to three equal regions. A corrected version of steel strain values for repairable and significant damage levels are shown in Table 2.5 as it is questionable that there may be a typing error given in the original document which is quite illogical.

Table 2.5: Strain and Ductility Limits for Different Damage Levels Proposed in Reference [22]

	Strain		Ductility	
Damage level	Concrete	Steel	Curvature μ_ϕ	Displacement μ_Δ
Significant	ε_{cu}	0.08	8~10	4~6
Repairable	Larger $\begin{cases} 0.005 \\ (2/3)\varepsilon_{cu} \end{cases}$	Larger $\begin{cases} \varepsilon_{sh} \\ 0.053 \end{cases}$	4~6	2~4
Minimum	Larger $\begin{cases} 0.004 \\ (1/3)\varepsilon_{cu} \end{cases}$	Larger $\begin{cases} 0.003 \\ 1.5\varepsilon_y \end{cases}$	2~4	1~2

The parameters shown in Table 2.5 are explained as follows:

ε_{cu} = Ultimate concrete compression strain depending on confinement
ε_y = Yield strain of steel
ε_{sh} = Hardening strain of steel
μ_ϕ = Curvature ductility (ϕ_u / ϕ_y)
μ_Δ = Displacement ductility (Δ_u / Δ_y)

A parametric study is included in ATC-32 [8] for the evaluation of the effectiveness of the proposed ATC-32 Recommendations in meeting the mandated performance criteria for several of the ATC-32 designed columns. In this study, concrete strain of 0.004 and steel strain of 0.01 are assumed for minimal damage level. For repairable damage level, a maximum concrete strain of 0.007 and a steel strain of 0.025 are assumed. Table 2.6 shows the

recommendations of reference [35] which are almost identical with the strains assumed in ATC-32 document except the steel strain for repairable damage level. Different references are directed for significant damage level.

Table 2.6: Quantitative Column Performance Requirements Recommended in Reference [35]

Damage level	Concrete Strain	Steel Strain
Minimal	0.004	0.01
Repairable	0.007	0.015
Significant (assumed as concrete cover has spalled)	For confined concrete, the energy model of Chang and Mander (1994) for confined concrete should be used.	Low cycle fatigue capacity recommendations of Dutta and Mander (1998) for plastic strain should be followed.

Kowalsky [29] employed the concrete compression and steel tension strain limits shown in Table 2.7 for different limit states.

Table 2.7: Strain Limits Employed in Reference [29] for Different Limit States

Limit state	Concrete strain limit	Steel strain limit
Serviceability	0.004 (compression)	0.015 (tension)
Damage control	0.018 (compression)	0.060 (tension)

Lehman et al. [32] made an experimental research to assess seismic performance of several well-confined, circular-cross-section, reinforced concrete bridge columns at a range of damage states and found out that damage states of residual cracking, cover spalling, and core crushing can best be related to engineering parameters, such as longitudinal reinforcement tensile strain and concrete compressive strain, using cumulative probability curves. Lu et al. [33] investigated evaluation of probabilistic drift limits of reinforced concrete columns at three distinctive performance levels, namely functional, damage control and ultimate level, by means of statistical simulation. Kowalsky [29] developed

dimensionless curvature limit states for circular reinforced concrete columns and used these to establish, curvature ductility, displacement ductility, drift ratio, and equivalent viscous damping capacities for the design limit states considered. It is stated that uniform damage cannot in general be achieved with uniform force-reduction or ductility factors that are typical in current design methods [29].

Various researches exist in literature related to the effect of foundation flexibility on seismic response which are compiled as:

- Budek et al. [13] made a research on inelastic seismic response of extended pile-shafts.
- Chai [18] derived an analytical model relating local curvature ductility demand to global displacement ductility demand of the soil-pile system of extended pile-shafts.
- Ciampoli and Pinto [20] made a research to assess the relevance of soil-structure interaction effects on the dynamic response of bridge piers responding in the inelastic range. It is indicated that an increase of the maximum displacements are produced as a result of soil-structure effects and inelastic demands in terms of curvature essentially remain unaffected by soil-structure interaction, showing a tendency to decrease.
- Ucak and Tsopelas [51] investigated the effect of soil-structure interaction on seismic isolated bridges.

CHAPTER 3

METHOD OF ANALYSIS

3.1 Flowchart

An analysis procedure is developed as shown in Figure 3.1 to clarify uncertain issues identified at the beginning of this study. The reason of performing two response spectrum analyses is to capture seismic responses of the investigated bridges which are designed in accordance with AASHTO-LRFD [2] for a major earthquake. Therefore, two seismic hazard levels are defined: *Design earthquake*, which is specified in AASHTO-LRFD and *Safety Evaluation Earthquake (SEE)*, which accounts for a major earthquake. These events have return periods of 475 and 1000 years, respectively.

The items shown in Figure 3.1 are explained in detail in Section 4.

3.2 Investigated Responses

A representative analytical model of the investigated type of bridges and positive sign convention of global orthogonal axes are shown in Figure 3.2. X, Y and Z denote longitudinal, transverse and vertical axes, respectively.

Seismic responses of the bridges under consideration are investigated along two orthogonal directions, transverse and longitudinal. The piers making maximum deformation can be observed from the modal shapes for the fundamental modes along transverse and longitudinal directions as shown in Section 4.7.1. The middle pier (pier #3) is considered to be the most critical under a seismic loading in transverse direction. Although all of the piers undergo similar deformations, pier #

1 is chosen to be the critical location under a seismic loading in longitudinal direction.

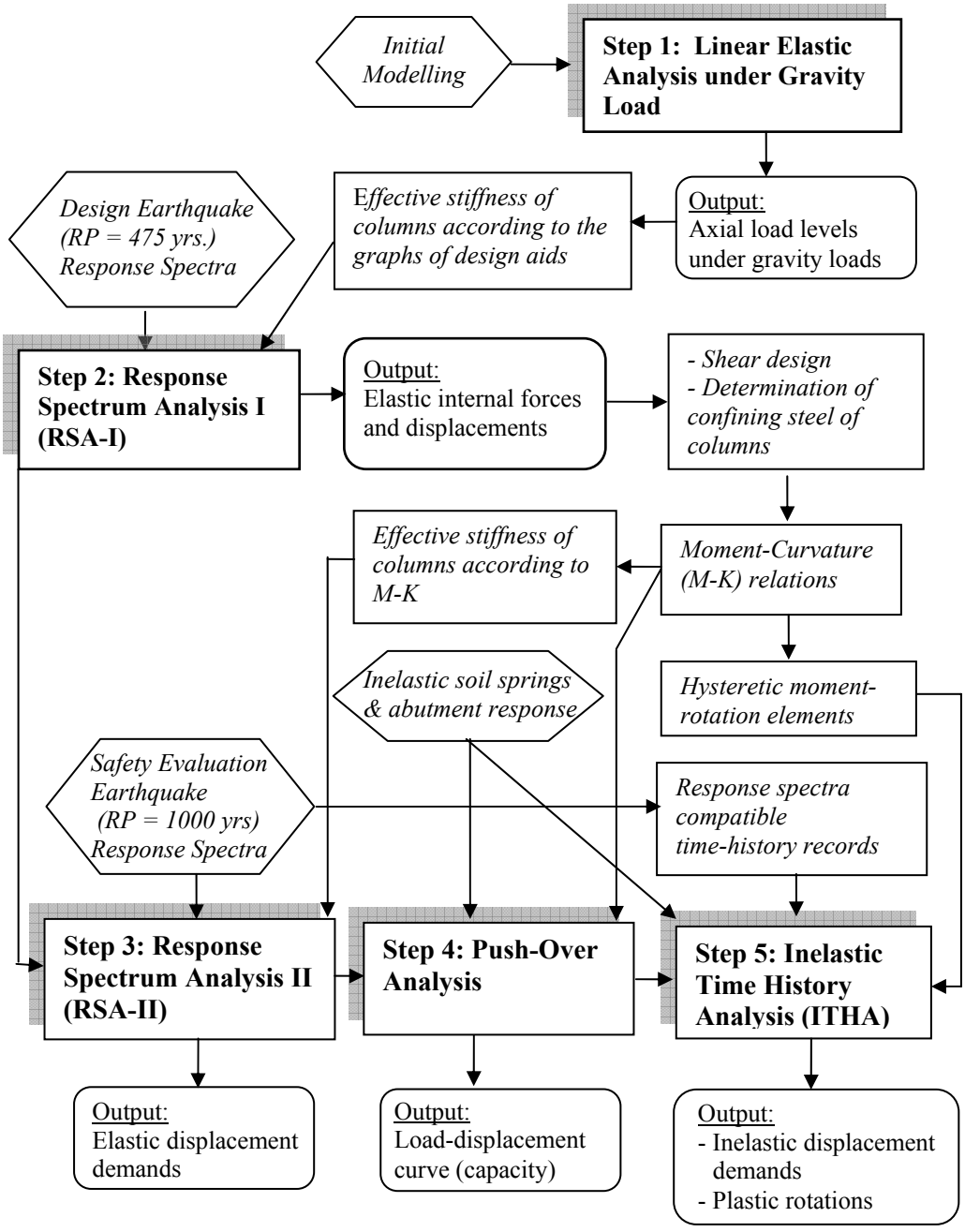

Figure 3.1: Analyses Flowchart

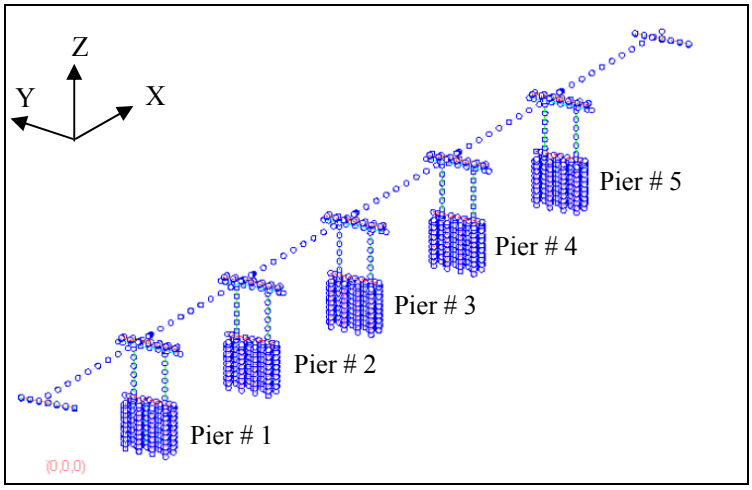

Figure 3.2: Global Axes and Numeration of Piers

3.2.1 Response Measures

The following outputs, as shown in Figure 3.3, are attained from RSA-II, push-over and inelastic time-history analyses:

Δ_t : Translational displacement of foundation measured at the centerline of pile cap

θ_f : Rotation of foundation

Δ^G : Global top displacement measured at the centerline of cap beam

V_{base} : Base shear, taken as summation of column shear forces

The reason of not using the displacement measured at the elevation of superstructure as the reference top displacement is the existence of relatively low longitudinal stiffness of elastomeric bearings between superstructure and substructure.

Global top displacement, Δ^G includes foundation deformation and structural deformation which mainly originates from columns. For a bent making plastic structural deformation, global top displacement could be expressed as:

$$\Delta^G = \Delta_f + \Delta_y + \Delta_p \tag{3.1}$$

where;

Δ_f : Displacement due to foundation flexibility

Δ_y : Idealized yield displacement of structure

Δ_p : Plastic displacement of structure

Displacement due to foundation flexibility consists of displacements attributed to translational displacement and rotation of foundation as shown in equation 3.2.

$$\Delta_f = \Delta_t + \theta_f H_n \tag{3.2}$$

where H_n is the net height of column measured from the top of pile cap to the bottom of cap beam. Center-to-center height of columns is not used for the computation of displacement attributed to rotation of foundation in order to eliminate the parameters of pile cap and cap beam dimensions. The additional displacement resulting from the rotation of foundation considering center-to-center height of columns is ignored. The top and bottom displacements of a pile cap or a cap beam element are assumed to be the same with the displacement measured at the centerline.

Global yield displacement is defined as:

$$(\Delta_Y)^G = \Delta_f + \Delta_y \tag{3.3}$$

Top displacement from which the contribution of foundation flexibility is excluded can be expressed with relative displacement, Δ^R.

$$\Delta^R = \Delta^G - \Delta_f \tag{3.4}$$

The superscript with the capital 'G' denotes *global* and 'R' denotes *relative*, hereafter.

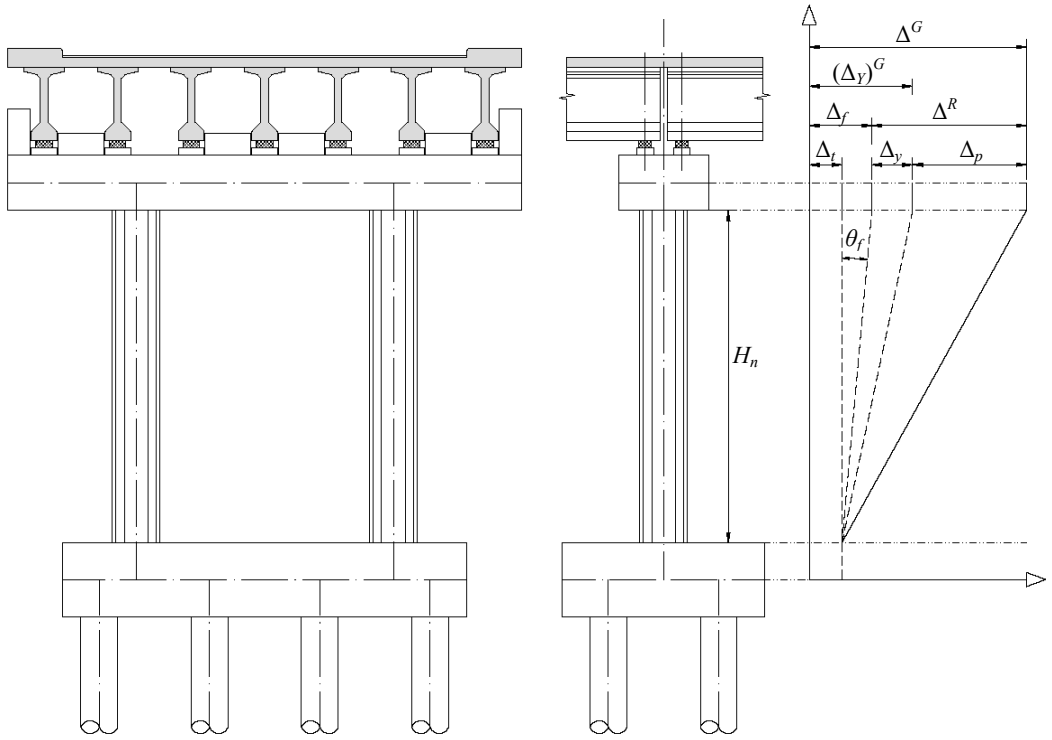

Figure 3.3: Output Parameters Attained from RSA-II, Push-over Analysis and Inelastic Time History Analyses

For the construction of global load-displacement relationships, base shear is taken as the total shear force of the most critical pier, not the total shear force of the whole bridge. A typical presentation of idealized capacity curve, elastic and inelastic top displacement demands with corresponding base shear forces are shown in Figure 3.4. The parameters drawn on Figure 3.4 are defined as:

$(\Delta_Y)^G$: Global yield displacement

$(\Delta_C)^G$: Global displacement capacity

F_Y : Base shear corresponding to the global yield displacement

F_C : Base shear corresponding to the global displacement capacity

$(\Delta_D)^G_{elastic}$: Global elastic displacement demand resulting from RSA-II

$(\Delta_D)^G_{inelastic}$: Global inelastic displacement demand resulting from ITHA

$(F_D)_{elastic}$: Base shear corresponding to the elastic displacement demand

$(F_D)_{inelastic}$: Base shear corresponding to the inelastic displacement demand

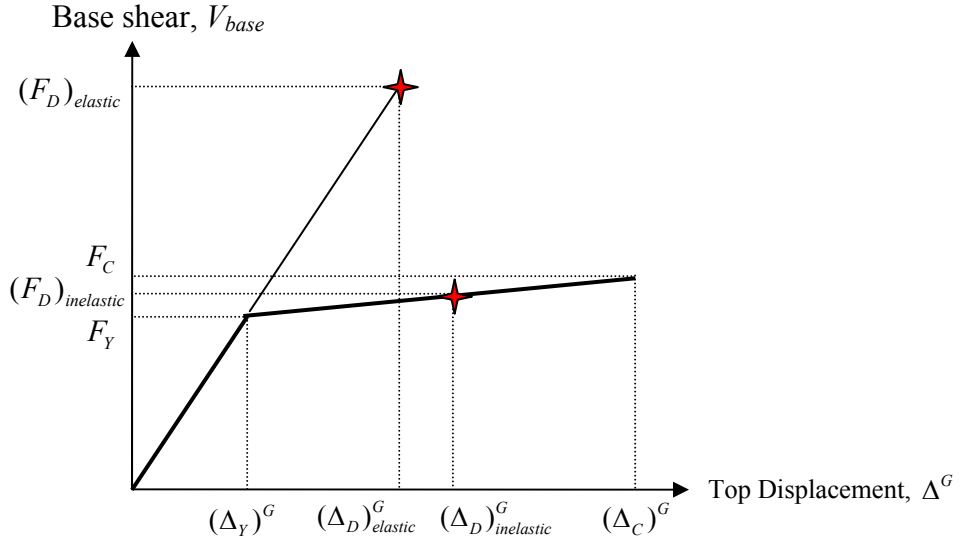

Figure 3.4: Typical Presentation of Capacity Curve, Global Elastic and Inelastic Demands

Three displacement parameters shown in Figure 3.4 can also be defined by using the *relative* definition:

$(\Delta_C)^R$: Relative displacement capacity at the point when failure occurs

$(\Delta_D)^R_{elastic}$: Relative elastic displacement demand resulting from RSA-II

$(\Delta_D)^R_{inelastic}$: Relative inelastic displacement demand resulting from ITHA

The average of maximum demands obtained from all inelastic time-history analyses is considered to be the inelastic displacement demand.

Five response measures are utilized in this study. The ones compiled below from *i* to i*v* are system-based response measures which are calculated using the parameters defined above. The last one is an element-based response measure which is computed based on the outputs obtained from RSA-I. The first response measure is utilized for evaluation of capacity while the others are used for evaluation of seismic demands.

i. Structural Displacement Ductility Capacity

Deformability capacity of a bridge considering only structural deformation can be expressed with structural displacement ductility capacity, μ_C which is defined as:

$$\mu_C = \frac{(\Delta_C)^R}{\Delta_y} \tag{3.5}$$

In the definition above displacement attributed to foundation flexibility is excluded and an equivalent fixed base condition is considered.

ii. Maximum Displacement Ratio

Maximum displacement ratio, C_1 is defined as the ratio of maximum global top displacement demand obtained from inelastic response to the one obtained from linear elastic response.

$$C_1 = \frac{(\Delta_D)^G_{inelastic}}{(\Delta_D)^G_{elastic}} \tag{3.6}$$

The definition of maximum displacement ratio used in this study is almost identical with the coefficient C_1 of displacement coefficient method defined in FEMA 356 [25].

iii. Displacement Capacity over Demand Ratio

Displacement capacity over demand ratio, *C/D* indicates how close a structure is to failure. Two types of displacement capacity over demand ratio are defined: using global displacements and using relative displacements. Relative displacement capacity over demand ratio is fairly a new response measure. The number of *C*/*D* ratio definitions can be increased up to four by either using displacement demands as elastic or inelastic. Global and relative displacement capacity over demand ratios are respectively defined as:

$$(C/D)^G = \frac{(\Delta_C)^G}{(\Delta_D)^G} \tag{3.7}$$

$$(C/D)^R = \frac{(\Delta_C)^R}{(\Delta_D)^R} \tag{3.8}$$

where;

$$(\Delta_D)^G = \begin{cases} (\Delta_D)^G_{elastic} \\ (\Delta_D)^G_{inelastic} \end{cases} \quad \& \quad (\Delta_D)^R = \begin{cases} (\Delta_D)^R_{elastic} \\ (\Delta_D)^R_{inelastic} \end{cases}$$

iv. Global Displacement Ductility Demand

Displacement ductility demand is generally used in practice to limit the flexibility of systems by specifying certain limits. In this study, global displacement ductility demand, which shows the extent of inelastic action of the global system, is defined as:

$$\mu_D = \frac{(\Delta_D)^G}{(\Delta_Y)^G} \tag{3.9}$$

v. Response Modification Factors for Columns

In forced based design, elastic design moments are divided to recommended response modification factors (*R*-factors) to supply necessary moment capacities to sections. In this study, a backward procedure is applied to find out necessary response modification factors for columns of the investigated cases, whose nominal moment capacities are known, to resist elastic moment demands. Response modification factor for columns is defined as:

$$R = \frac{M_D}{M_C} \tag{3.10}$$

where;

M_D : Elastic moment demand obtained from RSA-I

M_C : Factored moment capacity for the corresponding axial force

Response modification factors computed in this study are in accordance with the AASHTO-LRFD [2] seismic design procedure. Elastic moment demands are obtained from the RSA-I analysis, which include load factors. Slenderness effects are taken into account following the approximate method recommended in AASHTO-LRFD [2]. Resistance factors for seismic conditions are utilized for the calculation of reduced moment capacities. The maximum of the *R*-factors computed for both columns is considered to be the most critical.

3.2.2 Concrete and Steel Strains

In general, a relationship between concrete and steel strains and damage states of a reinforced concrete section can be established. Maximum concrete and steel strains are computed following the steps described below:

- From each inelastic time history analysis, plastic rotations -if there exists any- and corresponding axial forces are obtained when maximum inelastic displacement (target displacement) occurs along the direction considered.
- Total curvature of plastic hinges is computed by converting plastic rotation to plastic curvature and adding to yield curvature.

$$\phi_{total} = \phi_p + \phi_y \tag{3.11}$$

$$\phi_p = \theta_p / L_p \tag{3.12}$$

where;

ϕ_{total} : Total curvature

ϕ_p : Plastic curvature

θ_p : Plastic rotation

L_p : Plastic hinge length

- Concrete and steel strains are determined at the total curvatures under the corresponding axial forces.
- The maximum of the strains computed for left and right columns is taken as the critical. The average of all critical strains obtained from each ITHA is considered to be the final concrete and steel strains.
- Some columns make no plastic rotation that indicates they are in elastic range. These columns are excluded from averaging.

It is accepted that concrete and steel strain values found for the most critical column will govern the damage state of the complete structural system. The reason is that any damage occurring in any of the columns of the most critical bent directly affects the vulnerability of the whole investigated bridge system. This assumption would not be true for a redundant structural system such as a building with many load-carrying columns.

3.3 Correlation of Investigated Responses

ATC-32 [8] specifies three damage levels, namely minimal, repairable and significant in the definition of performance objectives for new bridge designs. As stated above in this document, the decision of assigning strains to damage levels is a controversial issue. In any case, in this study the strain values shown in Table 3.1 are accepted to represent damage levels of columns. Concrete strain limits for all damage levels and steel strain limits for significant and repairable damage levels are adopted from the proposed values given in reference [22]. The strain limit for minimal damage level is adopted from the utilized value in a research included in ATC-32 [8].

Table 3.1: Accepted Concrete and Steel Strains for Different Damage Levels

Damage level	Concrete strain	Steel strain
Significant	ε_{cu}	0.08
Repairable	Larger $\begin{cases} 0.005 \\ (2/3)\,\varepsilon_{cu} \end{cases}$	Larger $\begin{cases} \varepsilon_{sh} \\ 0.053 \end{cases}$
Minimum	Larger $\begin{cases} 0.004 \\ (1/3)\,\varepsilon_{cu} \end{cases}$	0.01

The concept of correlation of investigated responses is shown in Figure 3.5. For all cases, seismic response measures and corresponding strain values are drawn on same graphs. Seismic response measure values corresponding to the strains specifying damage levels are estimated using trend lines. The most critical value obtained from either concrete strain relation or steel strain relation is taken as the final limiting seismic response measure value for the damage level considered.

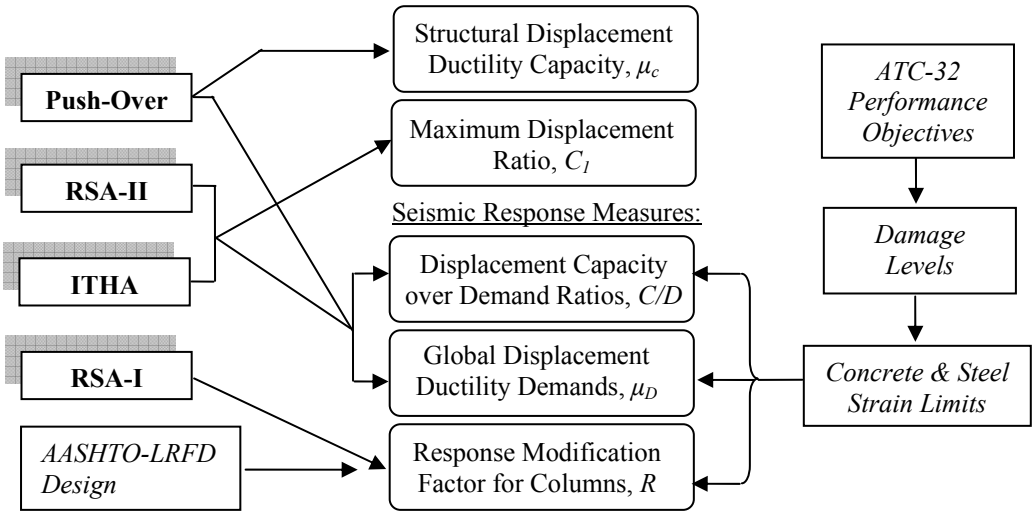

Figure 3.5: Correlation of Investigated Responses

CHAPTER 4

ANALYSIS PROCEDURE

4.1 Description of Bridges

The investigated bridge system in this study originates from the general practice in Turkey. Nevertheless, this study is not intended to be limited to Turkish practice in terms of the results attained at the end. Investigation of bridge practice at North American, Europe and Asian countries indicated that the bridge type selected for this research was very common in these countries as well. Therefore, it is aimed to generate a common practice that has many examples of application in many different parts of the world. A similar approach is used by ATC-32 [8] to generate design aid graphs for California bridges. The general principles of several design standards and reports currently under consideration in United States such as AASHTO-LRFD [2], Caltrans-SDC [15] and ATC-32 [8] are taken as a guide for design of bridges around the world. Thus, the results of this study could be beneficial for similar practices around the world.

Simply supported pre-stressed I girders with composite slab is the most common type of superstructure in Turkey for the last decade. Therefore, other types of superstructures such as post-tensioned box girder or steel plate girder are not usually considered at preliminary design stage.

Majority of bridges have seat type abutments. For standard highway bridges in Turkey, span lengths range from 10 to 40 meters, number of spans range from 1 to 9 and $L_{cap\ beam}/H_{column}$ ratio of bents range between 1 and 2 [48]. More than 50 % of these bridges have cap beam to column inertia ratios of 0.1 in Turkey [48], while this ratio is typically 1.5 in California [8]. Columns being stronger than cap

beams applied in Turkish practice may cause an undesirable result of cap beam failure which also violates modern seismic design criteria.

The investigated bridge has six equally spaced spans of 40 m length measured between pier axes. Total length of the bridge is 239 meters measured between the centers of bearings at two abutments. The platform width is 14 meters which can accommodate three lanes. The bridge is assumed to have no skew in plan besides it is assumed not to be a curved bridge. The plan and elevation view of the bridge is shown in Figure 4.1.

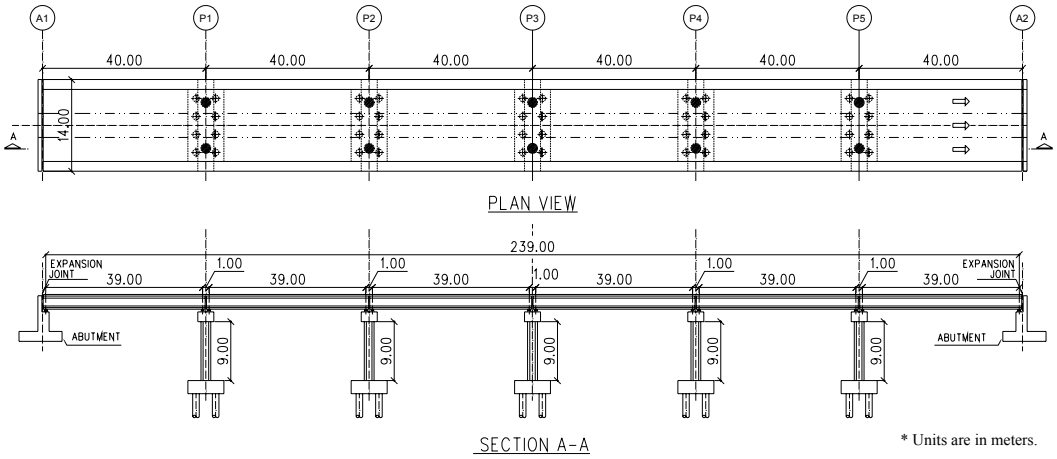

Figure 4.1: Elevation and Plan View of the Investigated Bridge

Seven pre-stressed I girders with a height of 200 cm and a length of 39.8 m supporting a 25 cm thick reinforced concrete slab constitutes the superstructure. Spacing between adjacent girders is designed to be 2 meters. Recently in Turkey, I girders are accommodated side by side leaving no space to avoid formwork resulting uneconomical designs. However, in this study an optimum design for superstructure is intended conforming to AASHTO-LRFD [2] design standards. There are totally 4 diaphragm beams -2 at supports and 2 at span- for proper live load distribution. Sectional view of superstructure is shown in Figure 4.2.

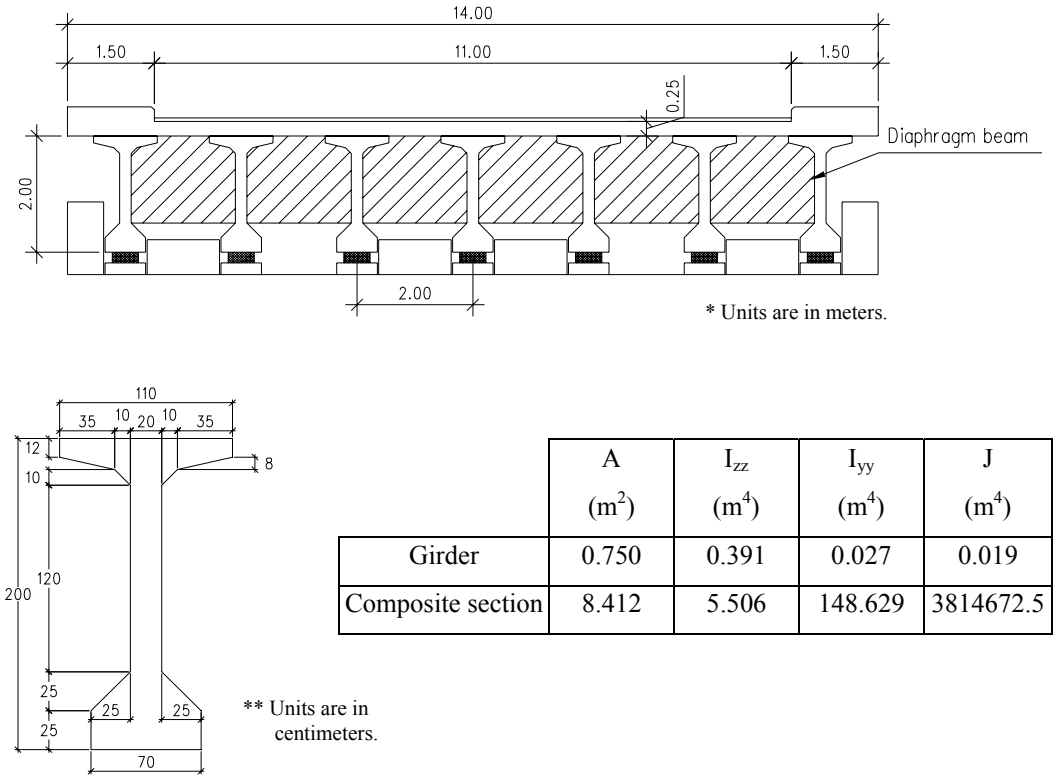

	A (m^2)	I_{zz} (m^4)	I_{yy} (m^4)	J (m^4)
Girder	0.750	0.391	0.027	0.019
Composite section	8.412	5.506	148.629	3814672.5

Figure 4.2: Sectional View and Properties of Superstructure

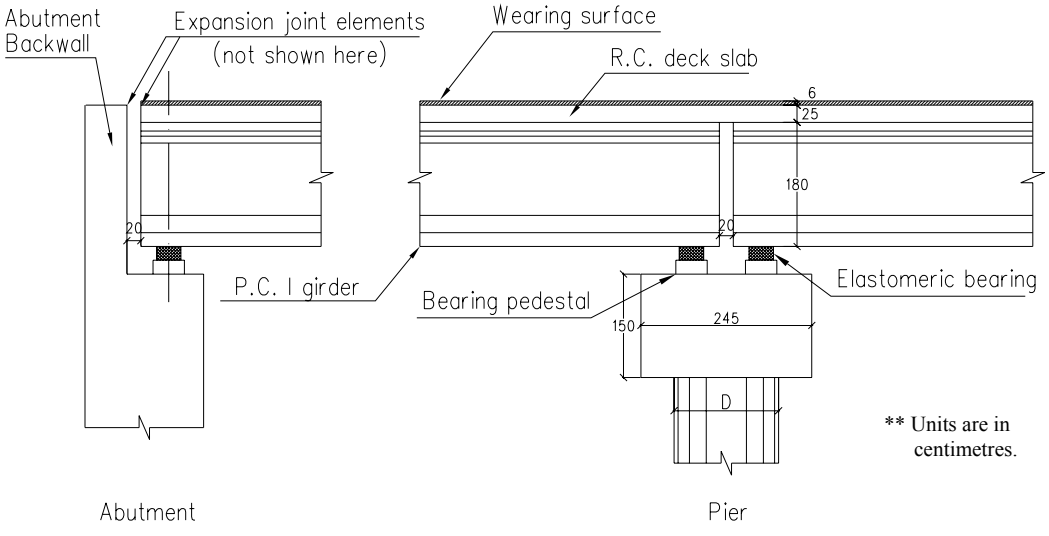

Figure 4.3: Superstructure Details at Abutments and at Piers

Continuity at slab level is common in engineering practice [16]. Expansion joints are only present at two abutments leaving a gap of 20 cm for longitudinal movements caused by thermal, shrinkage or earthquake effects. Figure 4.3 shows the details of superstructure at interior piers and at abutments.

Elevation view of a typical pier is shown in Figure 4.4. The net column height (H_n) of each two-column bent is 9.0 meters. As it is shown in Figure 4.4, L is the center-to-center distance between two columns, and H is the center-to-center distance between pile cap and cap beam. L/H ratio is 0.651.

It is shown in Figure 4.4 that two rows of concrete piles of each row composed of 4 piles with a rigid pile cap constitute the foundation. Each pile has a diameter of 1.0 meter and spaced 3 meters with the adjacent pile. Foundation layout does not change from one model to another.

Cap beam of each bent has a width of 2.45 meters and a height of 1.5 meters. The large width of cap beam is a result of minimum support length requirement described in Caltrans-SDC [15]. Being out of scope of the subject, it is assumed that this width is satisfactory and unseating is assumed not to occur in any of the cases investigated. Cap beam dimensions are kept constant for all models for the assignment of mass and weight of the bridge itself. However the ratio of cap beam moment of inertia to column moment of inertia is kept constant with varying column dimensions for each case in the plane perpendicular to the bridge longitudinal axis. This ratio is 2.77 which is calculated with gross moment of inertia values. The reason of having a high value for this ratio is to eliminate the effect of cap beam flexibility.

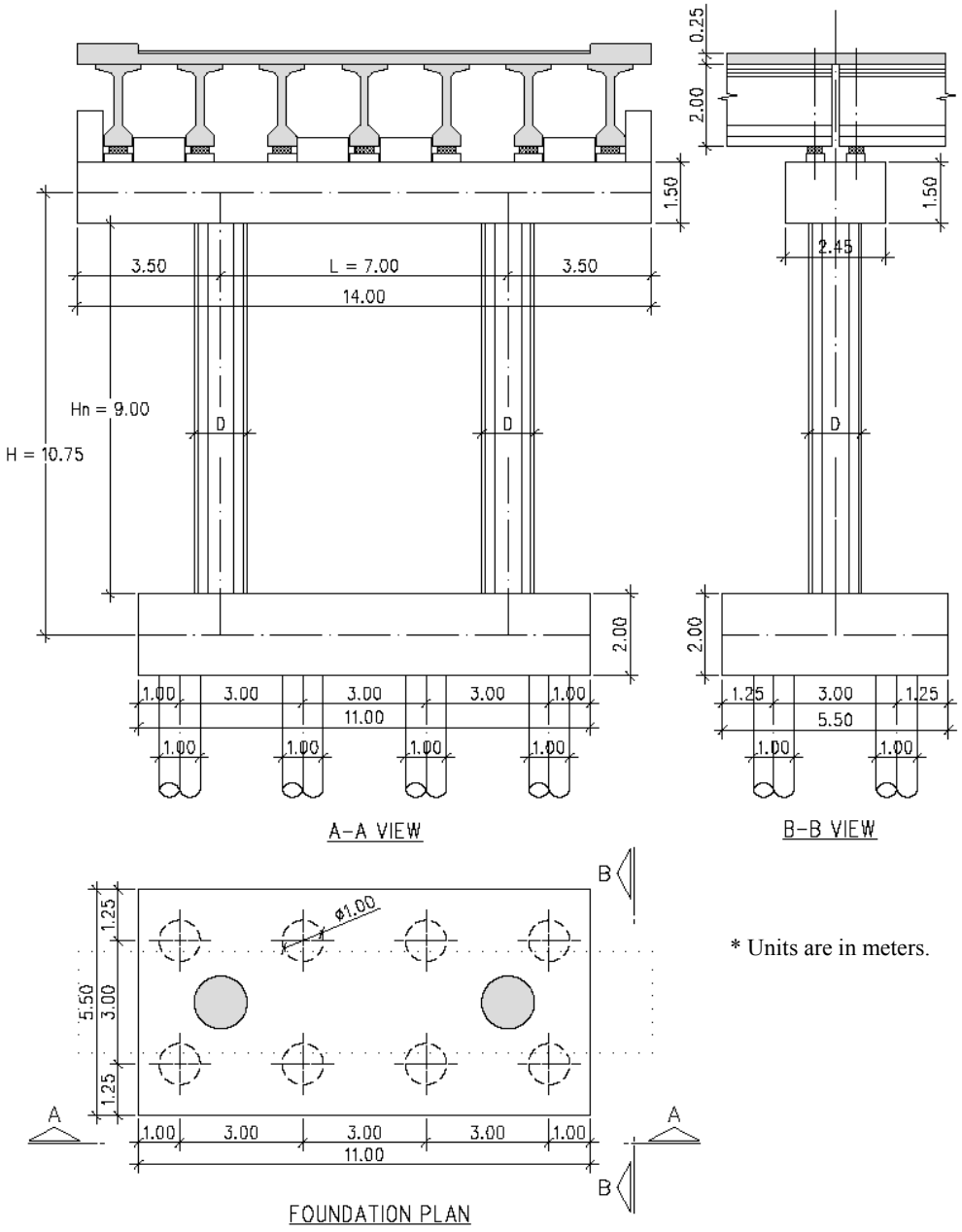

Figure 4.4: Foundation Plan and Elevation View of a Typical Bent

4.2 Material Properties

4.2.1 Design Properties

Design material properties are used in the first response spectrum analysis, RSA-I. Minimum design values of compressive strength of concrete and corresponding modulus of elasticity values of structural elements are listed in Table 4.1.

Table 4.1: Concrete Design Compressive Strength and Corresponding Modulus of Elasticity Values

Structural element	f'_c (MPa)	E_c (MPa)
Columns	30	29440
Piles	30	29440
Pile cap	30	29440
Cap beam	40	33994
Pre-stressed I girders	45	36057
Superstructure composite slab	25	26875

Modulus of elasticity is calculated from the formula stated in AASHTO-LRFD [2]:

$$E_c = 0.043\, w_c^{1.5} \sqrt{f'_c} \quad \text{(in MPa)} \tag{4.1}$$

where;

w_c : Unit weight of concrete (in kg/m^3)

f'_c : Compressive strength of concrete (in MPa)

Unit weight and Poisson's ratio of concrete are taken as 2500 kg/m^3 and 0.2, respectively. Minimum design yield strength and modulus of elasticity of both longitudinal and transverse reinforcing steel are taken as f_y = 420 Mpa and E_s = 200 000 MPa, respectively.

4.2.2 Expected Material Properties

Expected material properties are used in the second response spectrum analysis (RSA-II), push-over analysis, and inelastic time history analysis. ATC-32 [8] and Caltrans-SDC [15] recommend using expected material properties rather than design values to get a better estimate for the capacity of structural components except shear. Per ATC-32 [8] and Priestley et al. [43], expected material properties originate from several factors such as:

- Permissible range of yield strength of A706 steel is between 414 Mpa $\leq f_y \leq$ 534 that the upper limit is 30 % higher than the specified design value.
- The conservatism in mix designs makes 28-day concrete strengths about 20-25 % higher than the specified strength. Strength gain in 1 year is expressed to be 20 % above the 28-day strength. The specified strength value often goes up to 100 % or more after 30 years.
- It is expected that compression strength enhancement with confinement is about 50 % above actual unconfined strength.

Similar strength gains over 28-day compressive concrete strength of bridges in Turkey were observed during field inspections. [17]

Recommended values for the expected material properties in ATC-32 [8] are:

Expected compressive strength of concrete $f'_{ce} = 1.3\, f'_c$ (4.2)

Expected yield strength of reinforcing steel $f_{ye} = 1.1\, f_y$ (4.3)

where;

f'_c : Minimum design compressive strength of concrete

f_y : Minimum design yield strength of reinforcing steel

Factors composing the single overstrength factor of 1.3 used for capacity protection computations in AASHTO-LRFD [2] are based on recommended increased values of material properties:

Increased f_y (minimum) = 1.25 f_y
Increased f'_c = 1.5 f'_c
Increased ε_c = 0.01

Strain hardening is included in increased reinforcement yield strength. Conservatism in mix design, age effects, confinement effects and rapid loading effects are all included in increased compressive strength. Increase of ultimate compressive strain in confined concrete is taken into consideration with the increased crushing strain value.

Caltrans-SDC [15] requirements are used for the calculation of expected material properties in this study. Expected values for concrete compressive strength and corresponding modulus of elasticity values of structural elements are listed in Table 4.2. Recommended values that are used in this study for expected yield and ultimate strengths of reinforcing steel are:

f_y = 420 MPa $\quad$ f_{ye} = 475 MPa
f_u = 550 MPa $\quad$ f_{ue} = 655 MPa

where;
f_u : Minimum tensile strength of reinforcing steel
f_{ue} : Expected tensile strength of reinforcing steel

Table 4.2: Concrete Expected Compressive Strength and Corresponding Modulus of Elasticity Values

Structural element	f'_c (MPa)	E_c (MPa)
Columns	39	33567
Piles	39	33567
Pile cap	39	33567
Cap beam	52	38760
Pre-stressed I girders	58.5	41111
Superstructure composite slab	32.5	30642

4.2.3 Material Models

Mander's [34] material model is used for stress-strain relation of both confined and unconfined concrete under compression. Unconfined concrete compressive strain at maximum compressive stress and ultimate unconfined compression strain are taken as $\varepsilon_{co} = 0.002$ and $\varepsilon_{sp} = 0.005$, respectively.

Vebe's [52] model is used for stress-strain relation of concrete under tension. Modulus of rupture of concrete is calculated as:

$$f_r = 0.64\sqrt{f'_{co}} \tag{4.4}$$

where;

f'_{co} : Compressive strength of unconfined concrete

The material model used for reinforcing steel is composed of three parts: linear elastic part with a slope equal to the modulus of elasticity of steel until yielding, a yielding portion with zero slope until the onset of strain hardening and a nonlinear strain hardening portion until rupture. Strain softening after maximum steel stress is ignored. The stress-strain relation of hardening portion is taken as described in Turkish Earthquake Code [37]. Caltrans-SDC [15] recommends different values

for ultimate strain (ε_{su}) and strain at the onset of strain hardening (ε_{sh}) for different bar diameters. As specified amount of reinforcement could be attained with unlike bar diameters, common values are used for the ultimate strain as ε_{su} = 0.1 and strain value at the onset of strain hardening as ε_{sh} = 0.008.

Material models used are explained in Appendix A.

4.3 Local Soil Condition

In this study, two scenarios for local soil condition are investigated. The simplistic soil classification stated in Caltrans-SDC [15] is the basis for these two scenarios which are called *competent soil* and *poor soil* conditions.

Competent soils provide stiff foundations that experience small deformations while resisting maximum credible earthquakes. In this scenario, the dynamic characteristics of the bridge system is hardly affected by soil conditions that simple models are generally used in demand and capacity assessment ignoring foundation elements. Poor soils make bridge systems become non-standard and require project-specific design criteria to be applied. Soil-structure interaction has to be included in analysis to get the effect of foundation flexibility on the response of the entire bridge. [15]

The two scenarios explained above may be associated with uncorrected standard penetration test (SPT) blow numbers (N values). N is taken as 20 and 10 for the upper 10 meters of the soil profiles at competent and poor soil sites, respectively. Investigated soil conditions are also classified according to AASHTO-LRFD [2] and AASHTO-Seismic [28] for the construction of response spectra to be used in RSA-I and RSA-II analyses, respectively. Classification of the soil conditions investigated in this study according to different sources is summarized in Table 4.3.

Table 4.3: Site Class Definitions According to Different Sources

	Soil Type	
	Competent	Poor
Caltrans-SDC	$N > 20$	$N < 10$
AASHTO-LRFD	type II	type III
AASHTO-Seismic	site class D	site class E

4.4 Investigated Cases

32 different cases with varying soil conditions, column aspect ratios and column longitudinal reinforcement ratios are investigated. Each investigated case is given a different code as shown in Table 4.4. In a code, the first character denotes soil type, the second one denotes column aspect ratio and the last character denotes column longitudinal reinforcement ratio. The parameters demonstrated in Table 4.4 are defined as:

H_n : Net height of column measured from the top of pile cap to the bottom of cap beam

D : Column diameter

H_n / D : Column aspect ratio

ρ_l : Column longitudinal reinforcement ratio

The range of column aspect ratio parameters investigated in this study is believed to reflect bridge design practice sufficiently. The lower limit of column aspect ratio parameter is taken as 5. Considering a lower aspect ratio would be meaningless as elastic response mainly governs the design of bridge columns with low aspect ratios. AASHTO-LRFD [2] states that for columns with an aspect ratio less than 2.5, the forces resulting from plastic hinging generally exceed the elastic design forces.

Table 4.4: Investigated Cases

H_n (m)	D (m)	H_n / D	ρ_l	Code: Competent Soil	Code: Poor Soil
9.00	1.80	5	1%	***C51***	***P51***
			2%	***C52***	***P52***
			3%	***C53***	***P53***
			4%	***C54***	***P54***
9.00	1.50	6	1%	***C61***	***P61***
			2%	***C62***	***P62***
			3%	***C63***	***P63***
			4%	***C64***	***P64***
9.00	1.286	7	1%	***C71***	***P71***
			2%	***C72***	***P72***
			3%	***C73***	***P73***
			4%	***C74***	***P74***
9.00	1.125	8	1%	***C81***	***P81***
			2%	***C82***	***P82***
			3%	***C83***	***P83***
			4%	***C84***	***P84***

4.5 Computer Modeling

Computer models are generated in structural analysis software, LARSA 4D [31].

4.5.1 Superstructure

Superstructure is modeled in its simplest form since concentration is given to substructure. Modeling of composite slab with shell elements would increase the number of joints and exponentially increase computer run times. The whole superstructure could be represented using a beam element with transformed stiffness and identical mass properties as shown in Figure 4.5. Transformation of superstructure stiffness to elastic properties of girders is achieved by applying proper modular ratio, $n_{deck/girder}$ to the elastic properties of deck. Domaniç [21] found out that the effect of modeling whole superstructure with a single beam

element with equivalent sectional properties does not bring too much error in the overall dynamic response.

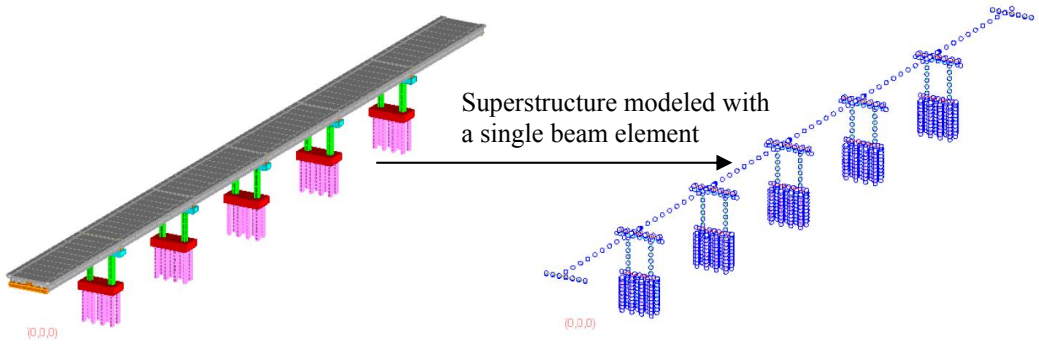

Figure 4.5: Representation of Superstructure

The link slab between adjacent spans is represented with a beam element using cracked sectional properties. (Figure 4.6)

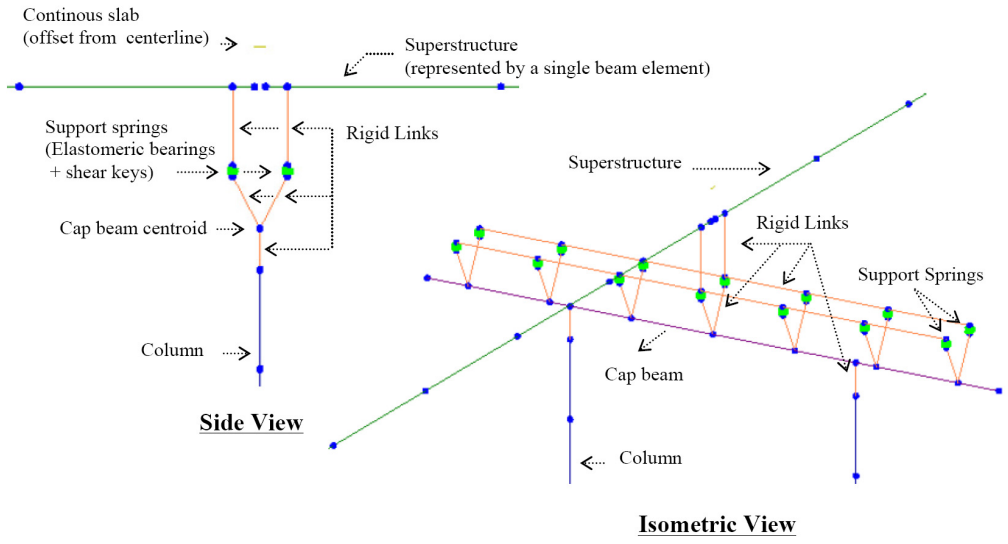

Figure 4.6: Modeling of Superstructure and Supports at Piers

For spans supported over elastomeric bearings with no horizontal restraints, superstructure may pound to adjacent spans, stem walls of inverted-T caps, or abutment backwalls during a seismic event. Substructure forces determined from elastic dynamic analysis are usually underestimated for bridges with inverted-T

cap beams which are close to a fault line, since pounding can not be modeled properly [40]. For the investigated bridge system rectangular section is preferred for cap beams. In any case, pounding effect is eliminated by replacing expansion joints with link slabs at deck level. Thus out of phase movement spans is eliminated, too. Superstructure element is divided into 10 equal parts along its length to have a better mass distribution. ATC-32 [8] and Priestley et al. [43] also suggested to form similar superstructure models to investigate seismic response of bridge piers.

4.5.2 Substructure

Columns

Moment-curvature diagrams and moment-axial load interaction diagrams of circular columns are obtained from a computer program developed in Microsoft Excel. (Figure 4.7) The program can modify an actual moment-curvature curve to an idealized bilinear curve using the method proposed by Priestley et al. [44] Concrete cover is accepted as unconfined and inner core is accepted as confined concrete. At each curvature point, concrete and steel strains are recorded.

Moment-Curvature Analysis

- The material models mentioned in Section 4.2.3 are used for determining moment curvature diagrams.
- Clear cover is 5 cm for all sections.
- Strain hardening is taken into consideration.
- Tension in concrete is not ignored.
- The analysis stops either when the extreme compression fiber of confined concrete reaches the ultimate strain of confined concrete (ε_{cu}) or steel ruptures.
- Effective confinement ratio for all sections is assumed to be 0.95

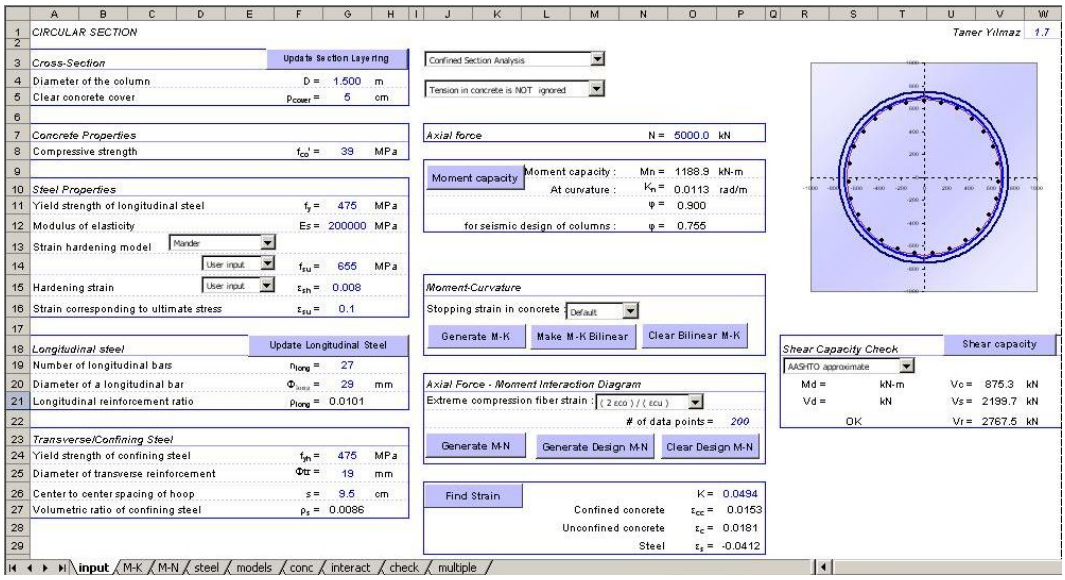

Figure 4.7: Moment-Curvature Program

Comparison of moment-curvature diagrams of a circular section having diameter of D = 1.5 meters with a longitudinal reinforcement ratio of ρ_l = 1 % at different axial load levels is shown in Figure 4.8. The parameter, α shown on the figure is the axial load ratio which is defined as:

$$\alpha = \frac{P}{f_c' A_c} \tag{4.5}$$

where;

P : Axial load acting on the section (compression is taken as positive)

A_c : Area of the section

f_c' : Compressive strength of concrete

Comparison of moment-curvature diagrams of the same section with different longitudinal reinforcement ratios and with the same volumetric ratio of confining reinforcement (ρ_s = 0.0086) is shown in Figure 4.9.

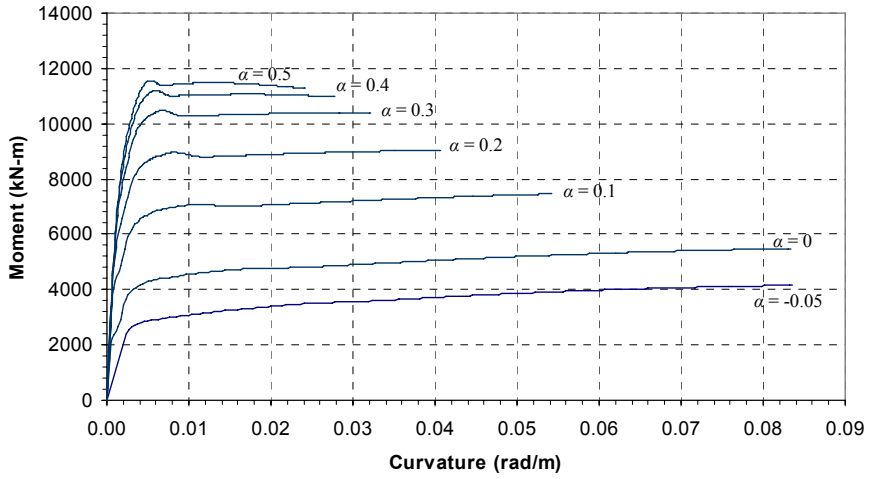

Figure 4.8: Effect of Axial Load Level on Moment-Curvature Diagrams

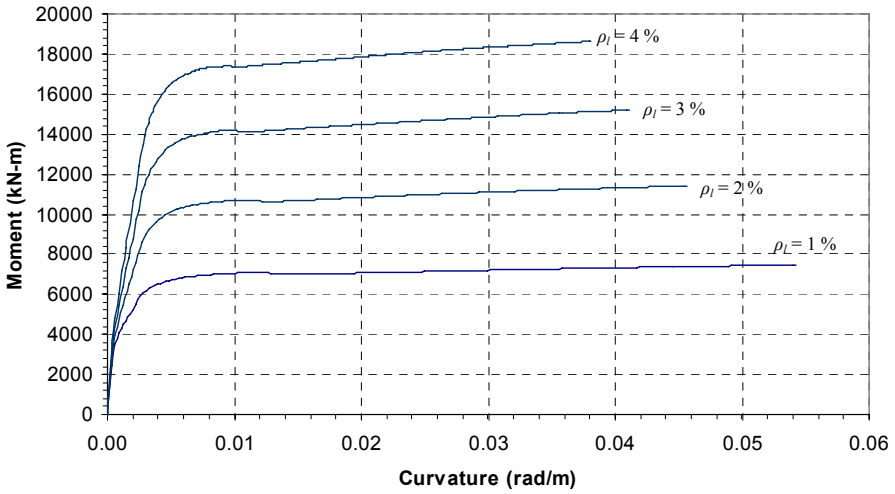

Figure 4.9: Effect of Longitudinal Reinforcement Ratio on Moment Curvature Diagrams

Steps of bilinear idealization process [44] are given as follows:

- The first yield (ϕ'_y, M_y) point is defined as the point when the extreme tension reinforcement reaches yield strain, or when the extreme concrete compression fiber reaches a strain of 0.002, whichever occurs first.

- The line connecting the origin and the first yield point is extrapolated up to the nominal moment capacity (M_n) to find yield curvature (ϕ_y). Nominal moment capacity is defined as the point when the extreme compression fiber reaches a strain of 0.004 or extreme tension reinforcement reaches a strain of 0.015, whichever occurs first.
- Post elastic branch is constructed by connecting the nominal yield point with the ultimate point (ϕ_u , M_u) which is the stopping point of the original moment-curvature diagram.

Figure 4.10 shows an example of bilinear idealization for the moment-curvature diagram of the circular column shown in Figure 4.8.

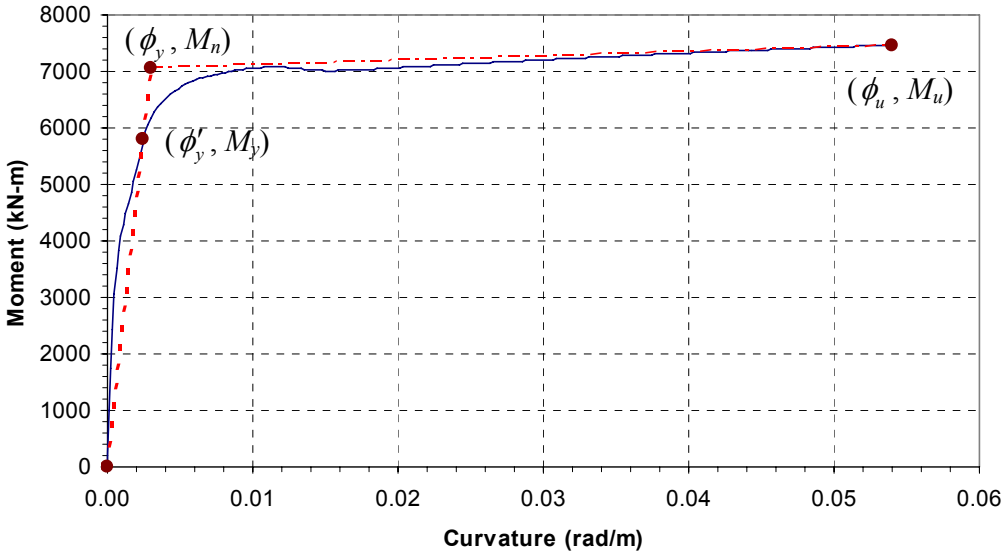

Figure 4.10: Bilinear Idealization of a Moment-Curvature Diagram

Modeling of Column Elements

Different types of elements are evaluated for modeling of columns. In response spectrum analysis, columns are modeled with linear elastic frame elements. The elastic behavior of reinforced concrete sections is not based on initial uncracked

section stiffness; instead secant stiffness is used for effective elastic stiffness. Uncracked section properties can only be used at low levels of seismic response [44]. The effective stiffness can be computed from the formula:

$$EI_{eff} = \frac{M_y}{\phi'_y} = \frac{M_n}{\phi_y} \tag{4.6}$$

One other way of estimating effective elastic stiffness is utilizing design aids. Caltrans-SDC [15] presents graphs showing the variation of elastic stiffness ratio with respect to axial load level and longitudinal reinforcement ratio for rectangular and circular sections. The graph for circular sections is shown in Figure 4.11

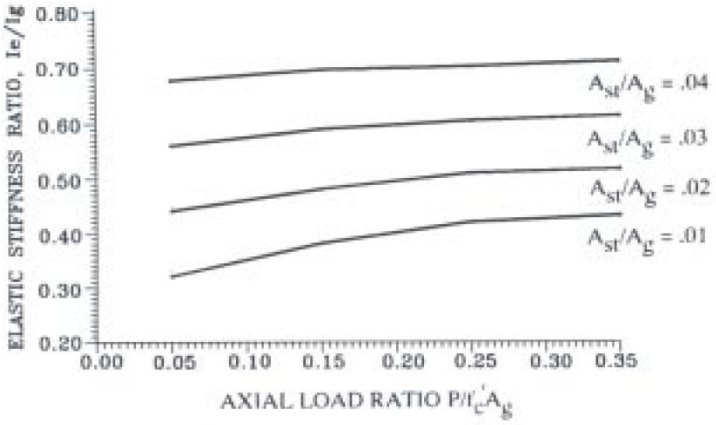

Figure 4.11: Elastic Stiffness Ratios for Circular Columns at Different Axial Load Levels and Longitudinal Reinforcement Ratios [15]

Effective stiffness values of columns are estimated from Figure 4.11 in RSA-I and from moment-curvature diagrams in RSA-II under the axial load levels obtained from gravity analyses. As shown in Figure 4.12, elastic stiffness ratios using moment-curvature relationships are smaller than the ones obtained from Figure 4.11. It is also observed that higher effective elastic stiffness ratios are achieved with greater amount of longitudinal reinforcement ratio.

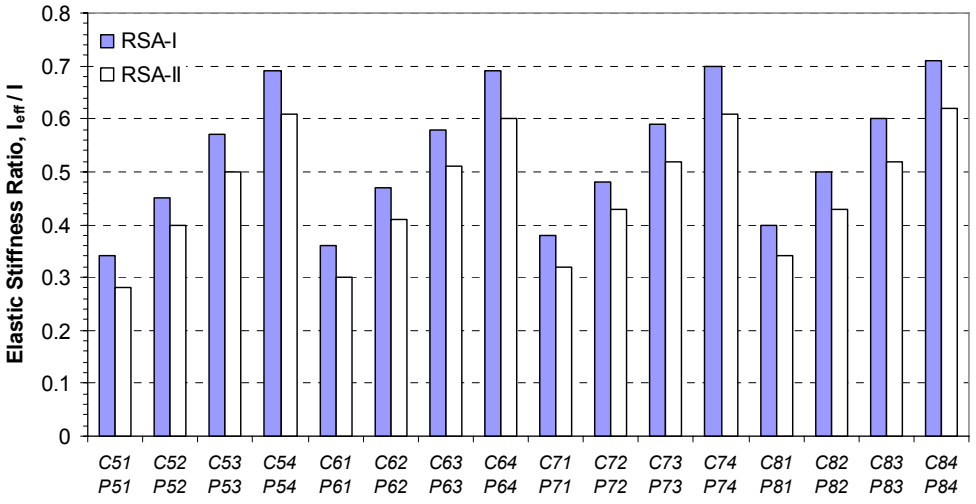

Figure 4.12: Comparison of Elastic Stiffness Ratios Used in RSA-I and RSA-II

In push-over and inelastic time history analyses, inelastic properties are introduced to column frame elements. In AASHTO-LRFD [2] it is stated that the inelastic model shall be based upon the results of physical tests or upon a representation of load-deformation behavior that is validated by tests. Hence, responses of three types of inelastic elements are compared with the test results found in literature which take confinement effects and cyclic loading into account. These elements are defined as:

i. Moment-Curvature Element

Larsa 4D [31] describes the moment-curvature element as follows:

- The formulation of the element is based on spread plasticity to capture the variation of sectional flexibility and combine them to determine the element stiffness matrix.
- Instead of using the material stress-strain relationships directly, this element uses the section axial force-centroidal strain and moment-curvature relationships to reduce computation.

- Force-interpolation functions are used that necessitates an element level state determination procedure to determine the element end forces and strains at Gaussian points.

In computer models, several moment-curvatures at different axial load levels can be introduced to the sectional properties of columns along two orthogonal directions.

ii. Hysteretic Moment-Rotation Elements (Connection Beams)

Lumped plasticity at column ends is used in the formulation of hysteretic moment-rotation element. Larsa 4D [31] describes hysteretic moment-rotation element as follows:

- It consists of an elastic beam with built-in yielding springs at the end.
- There can be up to four such end-springs, two springs at each end, one for each direction of bending.
- Moment-rotation curves are assigned to the end springs to model inelastic behavior of the end connections with the selection of appropriate parameters that determine hysteretic behavior.

Column ends are regarded as potential plastic hinge regions. A typical plastic hinge undergoes flexural yielding and plastic rotations while still retaining sufficient flexural strength [28]. As a result of bilinear idealization of curvature distribution, plastic hinge length is to be estimated to generate moment-rotation curves. Analytical plastic hinge length is defined in Caltrans-SDC [15] with the following formula:

$$L_p = 0.08\,L + 0.022\,f_{ye}\,d_{bl} \geq 0.044\,f_{ye}\,d_{bl} \tag{4.7}$$

where;

L : Length of column from the point of maximum moment to the point of contra-flexure

f_{ye} : Expected yield strength of column longitudinal reinforcing steel bars

d_{bl} : Nominal diameter of column longitudinal reinforcing steel bars

Generation of idealized moment-rotation curves from idealized moment-curvature relations is as follows assuming column ends yield simultaneously.

Yield Rotation: $$\theta_y = \frac{\phi_y L}{3} \quad (4.8)$$

Ultimate Rotation: $$\theta_u = \theta_y + (\phi_u - \phi_y) L_p \quad (4.9)$$

The inelastic hysteretic springs defined in Larsa 4D [31] is based on the reference [49]. The parameters describing hysteretic behavior are listed as follows:

- *Backbone*: Either bilinear or trilinear curves are defined.
- *Polygonal hysteretic model*: The type of cyclic behavior can be bilinear, vertex-oriented, or yield oriented
- *Alpha*: Stiffness degradation parameter
- *Beta1*: Ductility-based strength degradation parameter
- *Beta2*: Energy-based strength degradation parameter
- *Gamma*: Slip parameter

Detailed information on these parameters is presented in reference [49].

iii. Lumped fiber element

This element combines the idea of fiber element and lumped plasticity. As it is shown in Figure 4.13, only estimated plastic hinge length is modeled with fibers and the remaining portion of the column is modeled with an elastic beam element. Detailed information on fiber elements can be attained from reference [44].

Along the plastic hinge length, several inelastic spring elements exist for representation of concrete and steel areas. The inelastic properties of these spring elements are constituted from material models of confined and unconfined concrete, and reinforcing steel. Besides, large shear stiffness values are assigned

for these spring elements and they are connected to the elastic beam with rigid links.

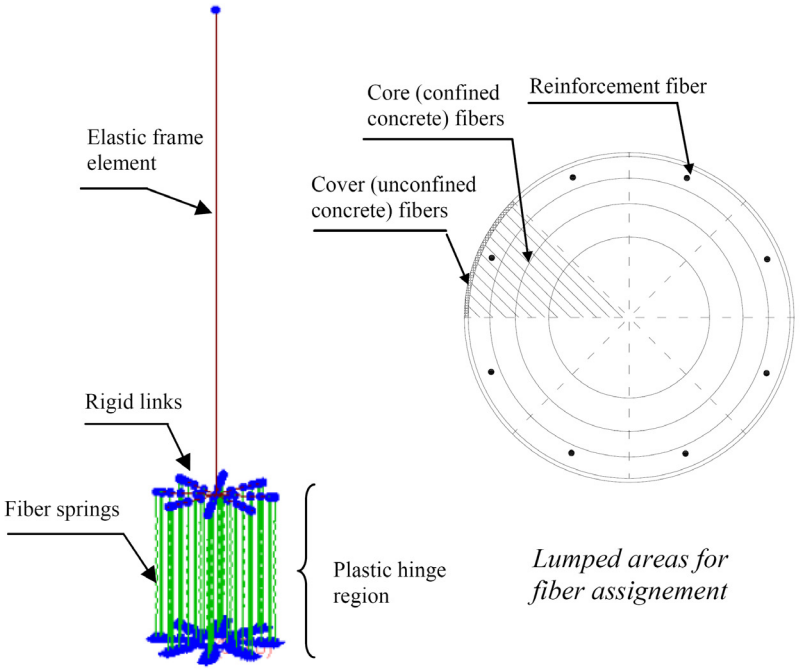

Figure 4.13: Modeling of a Cantilever Column with Lumped Fiber Element

Figure 4.14 shows two graphs comparing the analytical load-displacement response of the elements defined above with the output of test results provided from Peer Structural Performance Database [42]. The tests used for comparison are Moyer and Kowalsky [38] and Saatcioglu and Baingo [45].

It is observed that the curve obtained from using moment-rotation element matches with the test data better than the one obtained from using moment-curvature element. The use of moment-curvature element yields slightly stiffer initial slope for both test data. This may be due to the formulation of moment-curvature element as spread plasticity is utilized. However, the difference between the initial slopes gets smaller for the output of the second test data in which high strength concrete is utilized. Relatively high initial stiffness and overestimation of yielding force is observed for the curve obtained from using lumped fiber

element. The reason for this behavior may be due to utilizing insufficient number of nonlinear spring elements in the plastic hinge region.

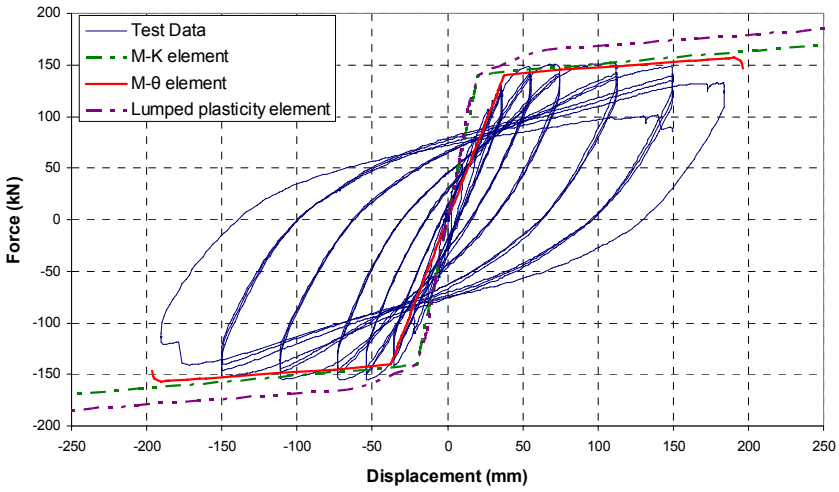

(a) Test Data of Reference [38]

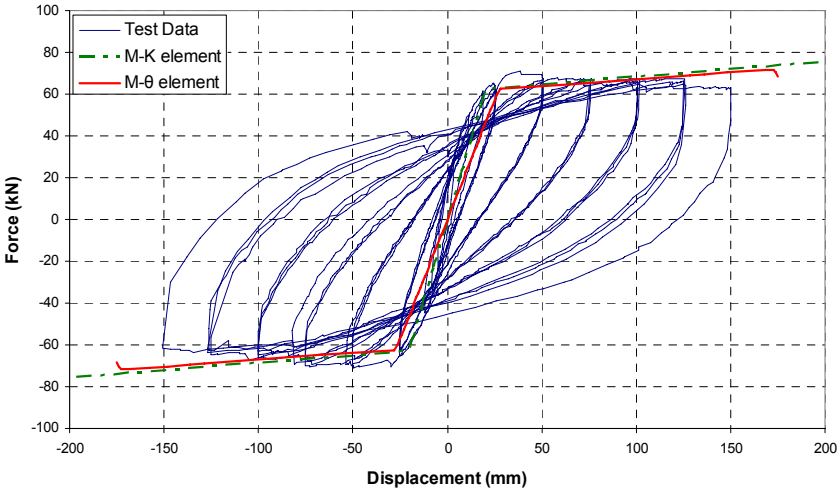

(b) Test Data of Reference [45]

Figure 4.14: Comparison of Inelastic Column Element Responses with the Real Test Outputs

Lumped fiber element is not preferred because modeling is not practical. It is evaluated that using either moment-curvature element or hysteretic moment-rotation element will not bring too much error in terms of modeling inelastic

behavior. The deficiency of moment-curvature elements in the structural analysis program, Larsa 4D is that the stopping (failure) point is estimated manually. In this study, moment-curvature elements are used in push-over analyses while hysteretic moment-rotation elements are used in inelastic time history analyses.

For hysteretic moment-rotation elements, bilinear hysteresis rule is adopted with the following parameters which represent the hysteretic behavior as defined above.

Alpha	*Beta1*	*Beta2*	*Gamma*
20000	0.01	0.01	1

Modeling of columns could be enhanced by the application of modified Takeda hysteresis rules which are characterized by unloading and reloading stiffnesses that are significantly lower than the initial elastic stiffness [44]. However, bilinear hysteresis rule is believed to be sufficient for investigated bridges due to the following reasons:

- Difference of responses obtained from using bilinear hysteresis rule and modified Takeda hysteresis rule is not significant in the range of periods of the bridges investigated in this study. The hysteretic component of equivalent viscous damping computed for both hysteresis rules are observed to be very close according to a research presented in reference [44]. Besides, it is evaluated from an inelastic time history analysis that the results obtained from using Takeda hysteresis rule and the results obtained from using bilinear hysteresis rule are consistent.
- Extra input parameters related to inelastic behavior of structural elements are needed for Modified Takeda hysteresis rule. This may bring uncertainty for new designs.

Foundation Elements

Modeling of foundation elements is shown in Figure 4.15 and described below as follows:

- Vertical displacement of the system is restrained at the bottom of each pile. Piles are locked into hard soil or rock.
- It is accepted that no shear failure occurs at piles and cap beams as these elements are capacity protected.
- Concrete piles are accepted to be capable of structurally resisting internal forces in essentially elastic range to eliminate any costly repair of pile damages induced by seismic event.
- Lateral movement at piles develops between pile cap and depth of fixity. A standard design effective stiffness is assigned to pile sections based on current engineering practice. Yüksekol [53] compared an iterative procedure of determining effective moment of inertia (I_e) of a pile section and the general assumption of taking I_e as half of the gross moment of inertia (I_g) in terms of the relationship between depth of fixity and pile length. It is found out that the general assumption of taking $I_e = 0.5\ I_g$ does not bring too much error. Therefore, in all type of analysis, effective moment of inertia of pile sections are taken as half of the gross moment of inertia.
- Depth of fixity can range from 5 to 8 diameters [53]. In this study, 9.0 meters portion of piles are modeled that is considered to be sufficient for bridges having a pile diameter of 1.0 meter.
- The group effect for laterally loaded piles has been investigated by many researchers as summarized in reference [53]. Pile group stiffness including soil contribution can be less than single pile response multiplied by number of piles in a group. In such a case, subgrade modulus can be reduced in a pile group. However in this study no reduction of capacity is applied to pile group as recommended by ATC-32 [8] and Caltrans-SDC [15]. In these documents it is stated that the group effect can be neglected for earthquake loading at three center to center spacing or higher since static load tests are said to overestimate group effect.
- The lateral resistance provided by pile cap is ignored as usually done in practice.

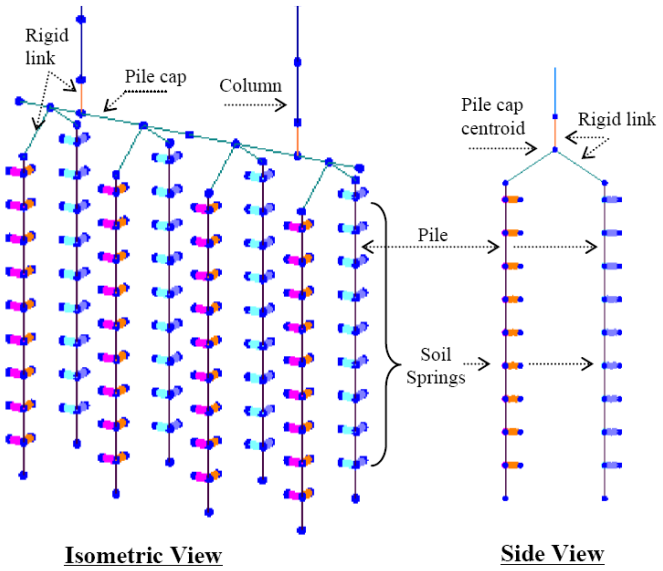

Figure 4.15: Modeling of Foundation Elements

4.5.3 Superstructure Supports

Superstructure elements join to substructure elements at support locations. Elastomeric bearings, shear keys and abutment longitudinal response are modeled using spring elements.

Elastomeric Bearings

A horizontal spring along longitudinal direction, a vertical spring and a rotational spring around the axis perpendicular to the longitudinal axis represents the stiffness of elastomeric bearings at support location. The stiffness of these linear elastic springs is computed as follows:

Horizontal Stiffness of an Elastomeric Bearing along Longitudinal Direction

Maximum horizontal load of an elastomeric bearing:

$$H_m = \frac{G\,A\,\Delta_s}{h_{rt}} \qquad \text{(in kN)} \tag{4.10}$$

where;

G : Shear modulus of elastomer (kN/m)

A : Plan area of elastomeric element or bearing (m^2)

Δ_s : Maximum shear deformation of elastomer (m)

h_{rt} : Total elastomer thickness (m)

Horizontal stiffness of an elastomeric bearing in longitudinal direction:

$$K_{h,long} = \frac{H_m}{\Delta_s} = \frac{G\,A}{h_{rt}} \qquad \text{(in kN/m)} \tag{4.11}$$

Vertical Stiffness of an Elastomeric Bearing

As the thicknesses of interior and exterior layers are different, the individual deflection resulting from each layer is calculated as:

Deflection due to interior layers: $$\delta_1 = \frac{P}{A\,E_1} n_{inner}\, h_{inner} \tag{4.12}$$

Deflection due to exterior layers: $$\delta_2 = \frac{P}{A\,E_2} \cdot 2 \cdot h_{exterior} \tag{4.13}$$

Total deflection: $$\delta = \delta_1 + \delta_2 \tag{4.14}$$

where;

h_{inner} : Inner elastomer layer thickness (m)

$h_{exterior}$: Exterior (cover) elastomer layer thickness (m)

E_1 : Effective modulus of elastomer in compression for interior layers (kN/m^2)

E_2 : Effective modulus of elastomer in compression for exterior layers (kN/m^2)

n_{inner} : Number of interior layers

P : Vertical load on elastomeric bearing (kN)

Effective modulus of elastomer in compression for interior and exterior layers can be approximately calculated as:

$$E_1 = 6\,G\,S_1 \tag{4.15}$$

$$E_2 = 6\,G\,S_2 \tag{4.16}$$

where;

S_1 : Shape factor for interior layers

S_2 : Shape factor for exterior layers

Shape factor is defined as: $S = \dfrac{LW}{2h(L+W)}$ (4.17)

where;

L : Length of elastomeric bearing

W : Width of elastomeric bearing

h : Thickness of elastomer (interior or exterior)

Equivalent effective modulus of elastomer bearing:

$$E_{c,eqv} = \frac{h_{rt}}{(n_{inner}\, h_{inner}) / E_1 + (2\, h_{exterior}) / E_2} \quad (4.18)$$

Vertical stiffness of elastomer: $K_v = \dfrac{E_{c,eqv}\, A}{h_{rt}}$ (in kN/m) (4.19)

Rotational Stiffness of an Elastomeric Bearing about the axis Perpendicular to Longitudinal Axis

Maximum bending moment for an elastomeric bearing:

$$M_m = \frac{0.5\, E_{c,eqv}\, I_{bearing}\, \theta_m}{h_{rt}} \quad \text{(in kN-m)} \quad (4.20)$$

where;

$I_{bearing}$: Moment of inertia of bearing in the direction of bending (m^4)

θ_m : Maximum design rotation (rad)

E_c : Effective modulus of elastomeric bearing in compression (kN/m)

h_{rt} : Total elastomer thickness (m)

Rotational stiffness: $K_\theta = \frac{M_m}{\theta_m} = \frac{0.5\,E_{c,eqv}\,I_{bearing}}{h_{rt}}$ (kN-m/rad) (4.21)

Input parameters of elastomeric bearings and the resulting stiffness values for one spring element are presented in Table 4.5.

Table 4.5: Input Parameters of Elastomeric Bearings and the Resulting Stiffness Values

L	(cm)	35	A	(cm^2)	1575	$K_{h,long}$	(kN/m)	1141.3
W	(cm)	45	$I_{bearing}$	(cm^4)	160781	K_v	(kN/m)	577157
h_{inner}	(mm)	11	S_1		8.95	K_θ	(kN/rad)	2945.9
$h_{exterior}$	(mm)	8.5	S_2		11.58			
n_{inner}		11	E_1	(kPa)	480615			
h_{rt}	(mm)	138	E_2	(kPa)	804578			
G	(kPa)	1000	$E_{c,eqv.}$	(kPa)	505699			

Shear Key Response

Shear keys are essential sacrificial structural members providing transverse restraint under seismic loading for bridges having superstructures not monolithically cast with substructure. Caltrans-SDC [15] expects abutment shear keys transmit the lateral shear forces generated by small earthquakes and service loads and recommends shear key capacity for seat-type abutments limited to the smaller of 75 % of the sum of the lateral pile capacity or 30 % of the axial dead load reaction at the abutment. AASHTO-Seismic [28] states that sacrificial shear keys can serve as structural fuses to limit the demand and control the damage in the abutments and supporting piles.

In this study, abutments are accepted to be rigid in transverse direction. Thus only shear keys contribute to stiffness in transverse direction at abutment location. Stiffness values of shear keys at abutments are assumed as half of the ones at piers. There are two reasons for this assumption. The first one is that the capacity

of shear keys at abutments can be intentionally specified lower by using a lower reinforcement ratio to decrease damage at abutments by dictating these elements as sacrificial. The second reason is to account for a relative lower lateral stiffness at abutments along transverse direction in case of a shear key failure. Dimensions of a typical internal and an external shear key at pier location are shown in Figure 4.16.

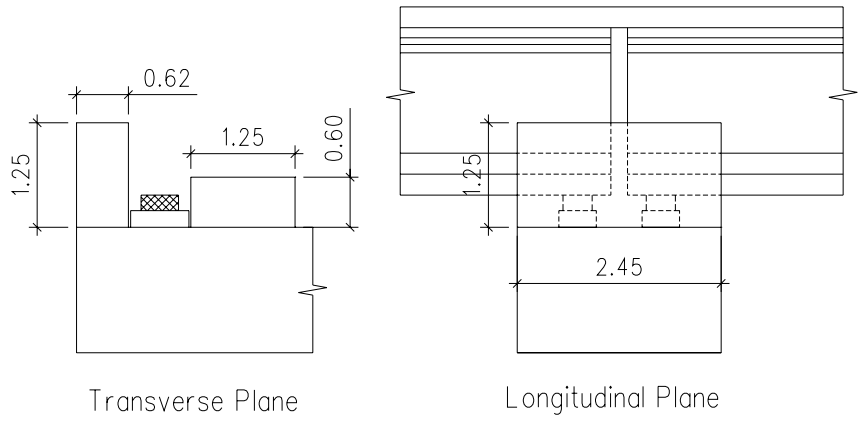

Figure 4.16: Dimensions of a Typical Internal and an External Shear Key at Pier Location

To find proper transverse stiffness of the shear keys at piers, shear key mechanism should be understood first. It is proposed in reference [36] that an internal shear key capacity can be calculated based on its category:

$\alpha < 0.5$	Shear friction
$0.5 < \alpha < 1.0$	Bracket and corbel
$\alpha > 1.0$	Flexural (cantilever beam)

α is height to depth ratio of shear key. These categories are determined according to the type of failure. As can be observed from Figure 4.16, $\alpha = 0.48$ for the internal shear keys of the investigated bridge. It is observed that bridges in Turkey generally have "shear friction" type internal shear keys. Hence, shear friction

capacity (V_n) is computed as traditionally done with the formula given in ACI Building Code [4]:

$$V_n = A_{vf}\, f_y\, \mu \tag{4.22}$$

where;

A_{vf} : Area of vertical reinforcing bars crossing the shear plane

f_y : Yield strength of steel

μ : Coefficient of friction

Coefficient of friction, μ is taken as 1.0 as recommended for concrete placed against hardened concrete with surface intentionally roughened.

The external shear keys are selected as "flexural" type on purpose. Use of flexural shear key is found to be successful in terms of ductility and damage control [36]. For the supplied amount of reinforcement, idealized shear force versus displacement curve of the external shear key is computed from a simple push-over analysis as shown in Figure 4.17.

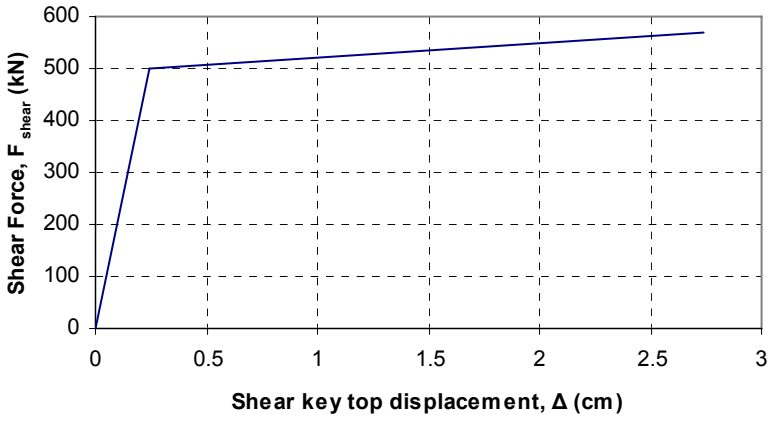

Figure 4.17: Idealized Shear Force versus Displacement Curve of an External Shear Key

Input parameters and resulting capacities of a single internal and external shear key are demonstrated in Table 4.6. Lateral stiffness supplied by shear keys at each support location are computed as follows:

$$\Sigma V_n = \Sigma V_{n,internal} + \Sigma V_{n,external} \quad (4.23)$$

$$\Sigma K_{s.k.} = \Sigma V_n / \Delta_{transverse} \quad (4.24)$$

$$K_{h,trans} = \Sigma K_{s.k.} / n_{support} \quad (4.25)$$

where;

$\Sigma V_{n,internal}$: Total shear force supplied from internal shear keys

$\Sigma V_{n,external}$: Total shear force supplied from external shear keys

$\Delta_{transverse}$: Assumed lateral yield displacement of shear keys

$n_{support}$: Number of support locations

$\Delta_{transverse}$ is accepted as 0.25 cm which is also the yield displacement of an external shear key. $n_{support}$ is equal to 14 as spring elements representing supports are modeled at each girder location and each shear key is resisting forces coming from adjacent superstructure portions.

Table 4.6: Input Parameters and Resulting Capacities of a Single Internal and External Shear Key

Internal Shear Key		
$A_{s,shear}$	(mm^2)	9883
ρ_{shear}	(%)	0.32
f_y	(MPa)	420
$V_{n,\ internal}$	(kN)	4151.0

External Shear Key		
$A_{s,flexural}$	(mm^2)	2614
$\rho_{flexural}$	(%)	0.17
f'_c	(MPa)	25
$V_{n,\ external}$	(kN)	498.3

Resulting transverse stiffness at each support location is $K_{h,trans}$ = 488637 kN/m. This value is rounded up to $K_{h,trans}$ = 500 000 kN/m to be used at piers. $K_{h,trans}$ = 250 000 kN/m at abutments. Detailed information on behavior of internal and external shear keys can be found from reference [36].

Abutment Longitudinal Response

Abutment longitudinal response is modeled as described in Caltrans-SDC [15]. Nonlinear behavior of abutment embankment stiffness is defined as follows referring to the nomenclature of Figure 4.18:

$$K_{abut} = K_i \cdot w \cdot (h_{bw} / 1.7) \tag{4.26}$$

$$P_{bw} = A_e \cdot 239 \cdot (h_{bw} / 1.7) \tag{4.27}$$

where;

K_i : Initial abutment stiffness based on test results (11.5 kN/mm/m)

K_{abut} : Initial abutment stiffness adjusted to backwall height

P_{bw} : Maximum passive pressure force

Δ_{gap} : Gap distance between superstructure and backwall

w_{bw} : Width of the backwall

h_{bw} : Height of the backwall

A_e : Effective abutment area (area of the backwall herein)

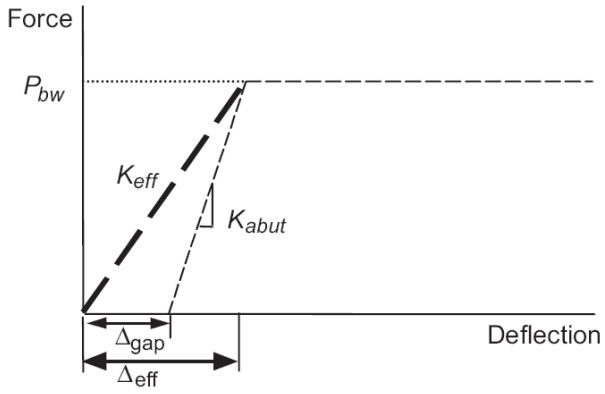

Figure 4.18: Abutment Embankment Stiffness [15]

Horizontal force developed on elastomers (P_{el}), which is obtained from multiplying the gap distance with total longitudinal stiffness of elastomers (K_{el}), contributes to abutment longitudinal response in the closing direction of expansion gap. Load-displacement curve of total abutment longitudinal response is shown in Figure 4.19 and related parameters are presented in Table 4.7.

Table 4.7: Parameters for the Construction of Total Abutment Longitudinal Response Curve

Δ_{gap}	(cm)	20	K_{abut}	(kN/m)	232029.4
h_{bw}	(m)	2.45	P_{el}	(kN)	1597.8
w_{bw}	(m)	14	P_{bw}	(kN)	11814.3
A_e	(m^2)	34.3	Δ_{eff}	(m)	0.25
K_{el}	(kN/m)	$7 \times K_{h,long}$ = 7989.1			

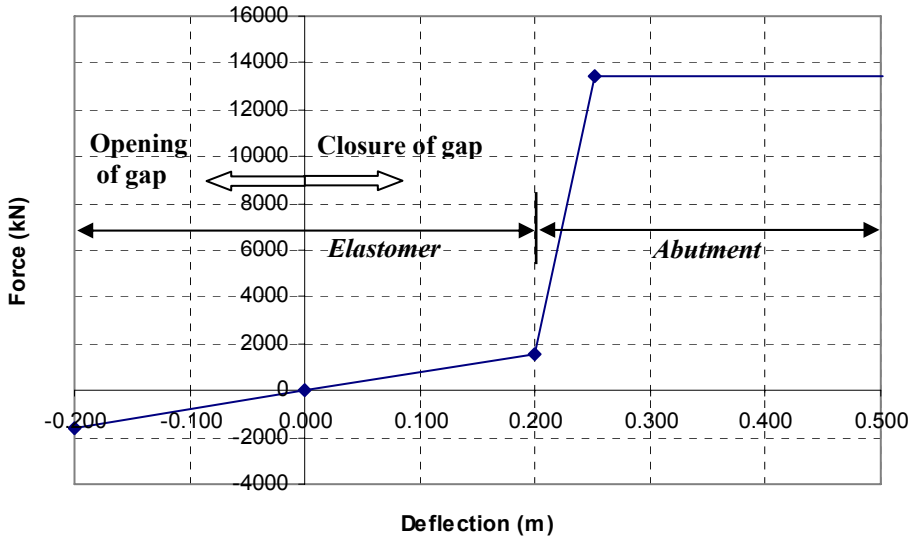

Figure 4.19: Load-Displacement Curve of Total Abutment Longitudinal Response

Abutment longitudinal response is modeled at each girder location using the same stiffness properties. For inelastic type of analyses, the opening and closing of expansion gap at abutments are directly taken into consideration with the true

inelastic curve which combines the load-displacement curve of elastomer and abutment longitudinal response as shown in Figure 4.19. On the other hand; in elastic analysis such as response spectrum analysis, the closing of gap at one abutment is modeled with effective abutment stiffness while opening of gap at the other abutment is modeled with elastomer longitudinal stiffness. Effective abutment stiffness mentioned in Caltrans-SDC [15] is determined through an iterative procedure. An example of this procedure is shown in Figure 4.20. Several values are assigned for $K_{h,long}$ and resulting displacements at the centerline of the superstructure with the corresponding spring forces are drawn on the same graph with the capacity curve. The intersection point of the two curves designates a good approximation of longitudinal displacement of superstructure along the closing direction.

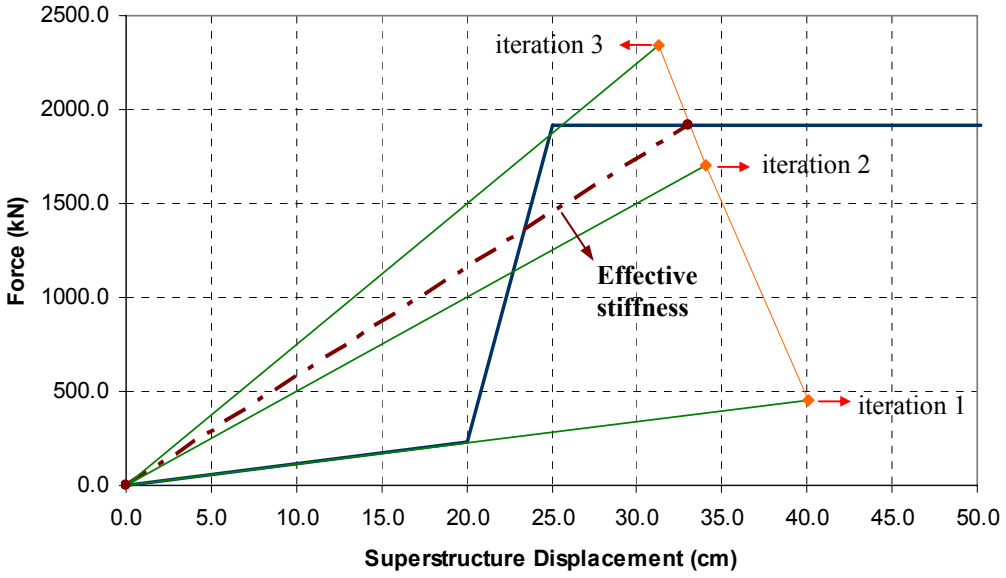

Figure 4.20: Iteration Procedure for Finding Abutment Effective Longitudinal Stiffness

Pounding between superstructure and abutment backwall is indirectly modeled with the procedure described above. (Figure 4.19) A more rigorous model accounting for pounding in detail is not needed in the scope of this study. Besides,

hysteretic characteristic of abutment is ignored. As a summary, Figure 4.21 shows the components of springs at support locations.

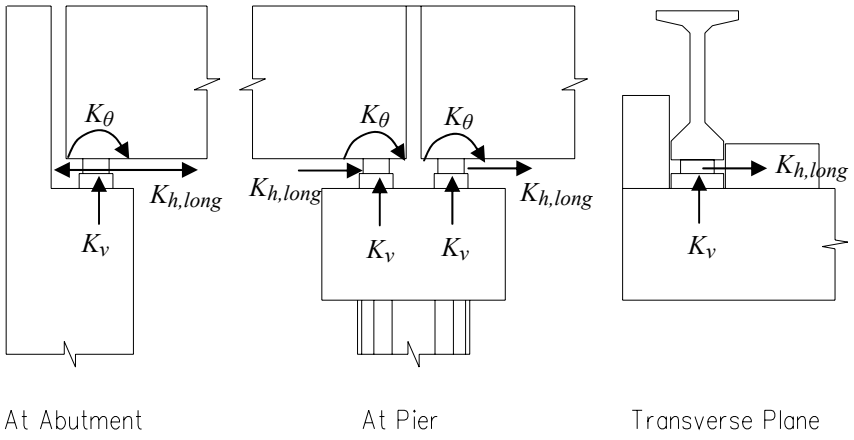

Figure 4.21: Components of Springs at Support Locations

4.5.4 Lateral Soil Response

Lateral soil response can be represented with nonlinear spring elements. The nonlinear properties for different soil conditions of these springs can be taken from the p-y curves recommended by several researchers. In this study, the p-y curves recommended by American Petroleum Institute [6] for sands are chosen to represent the two soil conditions compared throughout this study as recommended by AASHTO-LRFD [2]. The construction of these curves is explained in Appendix C. The required parameters for construction of p-y curves are derived from SPT N values, which are the basis parameters of the two scenarios investigated for local soil conditions.

Dunhum [23] proposes a correlation between internal friction angle and SPT N values for round grains of uniform size:

$$\phi' = \sqrt{12N} + 15 \tag{4.28}$$

To estimate relative density with SPT blow counts, the relation proposed by Meyerhof (1956) is used. (Table 4.8)

Table 4.8: Relative Density versus SPT N Values According to Meyerhof (1956)

N	Relative density, D_r (%)
< 4	< 20
4 ~ 10	20 ~ 40
10 ~ 30	40 ~ 60
30 ~ 50	60 ~ 80
> 50	> 80

Effective unit weight of soil is taken as 18 kN/m^3. The response is computed for cyclic loading case and the soil profile is assumed to be under water table. The parameters used for competent and poor soil conditions are summarized in Table 4.9.

Table 4.9: Parameters Used for Construction of P-y Curves

			Competent Soil	Poor Soil
SPT blow count	N		20	10
Internal friction angle (predicted)	$Ø'$	(degrees)	30.5	26
Relative density (predicted)	D_r	(%)	50	40

Soil springs are located at every 1.0 meter. P-y curves for competent and poor soil conditions for upper 9 meters are shown in Figure 4.22 with z being equal to the depth of a spring from the bottom of pile cap.

In push-over and inelastic time history analyses, soil springs are defined as inelastic where complete load-deflection curves are assigned. However for a linear elastic analysis, such as response spectrum analysis, it is impossible to model soil springs as inelastic. Therefore, an iterative procedure is applied to obtain the effective stiffness value. The algorithm of this procedure is summarized below for a single soil spring:

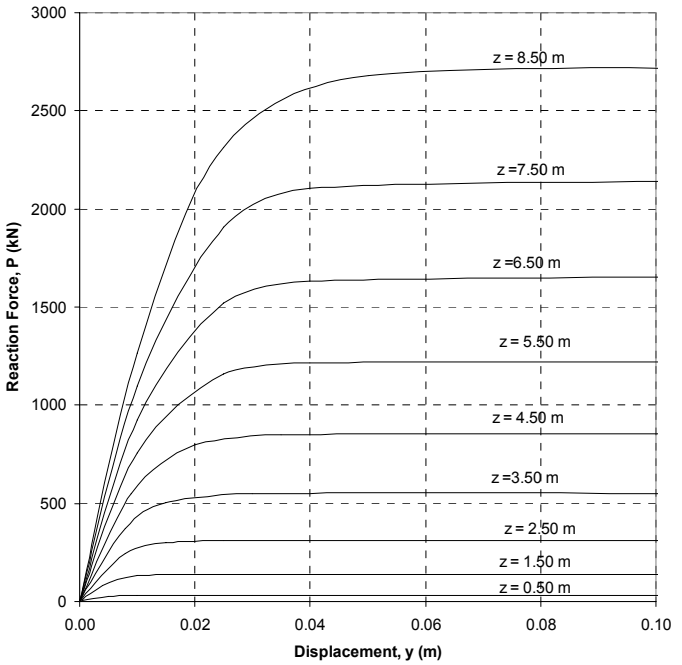

(a) For Competent Soil

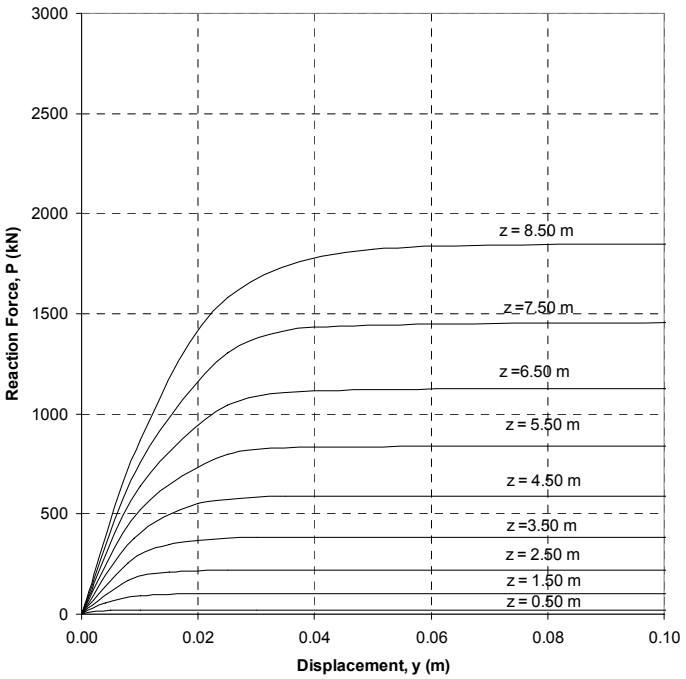

(b) For Poor Soil

Figure 4.22: P-y Curves

Step 1 Assign a stiffness value to the linear elastic spring. In the first iteration, generally the initial stiffness of p-y curve is assigned.

Step 2 Run analysis and obtain displacements.

Step 3 Using the joint displacement at the considered spring, compute the related lateral response force and stiffness value from p-y curves.

Step 4 If the difference between the stiffness values in step 1 and step 3 is within tolerable limits, stop iteration. Else, return to step 2 with the latest stiffness value computed in step 4.

This iterative procedure is applied for all soil springs simultaneously for both lateral directions. The iteration applied for one of the upmost springs at the middle pier of model *C81* along transverse direction is shown as an example in Figure 4.23. In this figure, 'i' denotes the iteration number.

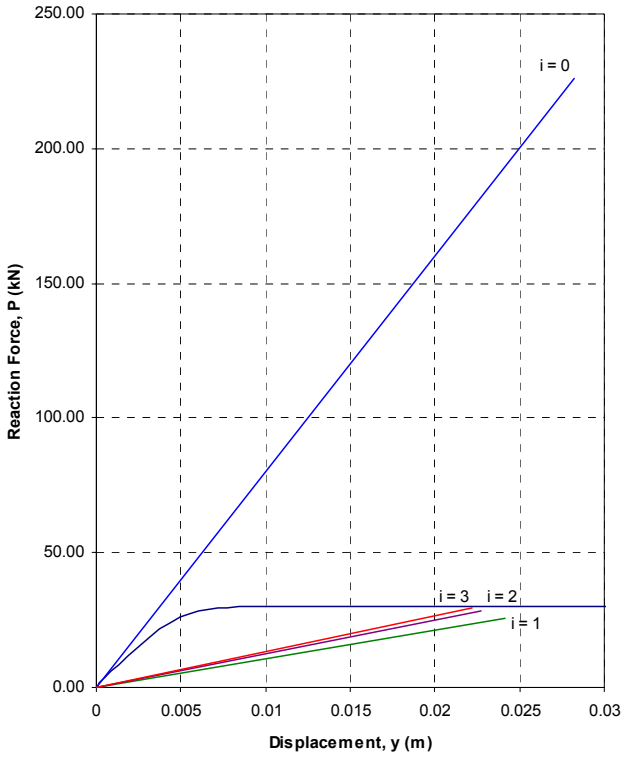

Figure 4.23: An example of the Iteration Procedure for Determining Effective Stiffness for Soil Springs

4.5.5 Element Types

The type of elements modeled in all analyses are summarized in Table 4.10.

Table 4.10: Element Types Used in all Analyses

	Response Spectrum Analysis		Push-Over Analysis	NLTH Analysis
Element	**RSA-I**	**RSA-II**		
Superstructure	*Linear elastic*	*Linear elastic*	*Linear elastic*	*Linear elastic*
Columns	*Linear elastic (effective stiffness)*	*Linear elastic (effective stiffness)*	*Moment-Curvature Elements*	*Hysteretic Moment-Rotation Elements*
Cap Beams	*Linear elastic*	*Linear elastic*	*Linear elastic*	*Linear elastic*
Foundation Elements (Piles, pile cap)	*Linear elastic*	*Linear elastic*	*Linear elastic*	*Linear elastic*
Bearings, Shear Keys	*Linear elastic*	*Linear elastic*	*Linear elastic*	*Linear elastic*
Abutment Longitudinal Response	*Linear elastic (effective stiffness)*	*Linear elastic (effective stiffness)*	*True Inelastic Curve*	*True Inelastic Curve*
Soil Springs	*Linear elastic (effective stiffness)*	*Linear elastic (effective stiffness)*	*True Inelastic Curve*	*True Inelastic Curve*

4.6 Seismic Hazard

Two seismic hazard level definitions are used in this study: design earthquake as defined in AASHTO-LRFD [2], and safety evaluation earthquake (SEE) as defined in Section 2.1. In this study, the seismic hazard definition is independent of any specific location while reflecting an earthquake prone region. This region is accepted as seismic zone I defined in the seismic zoning map of Turkey [26] (Figure 4.24).

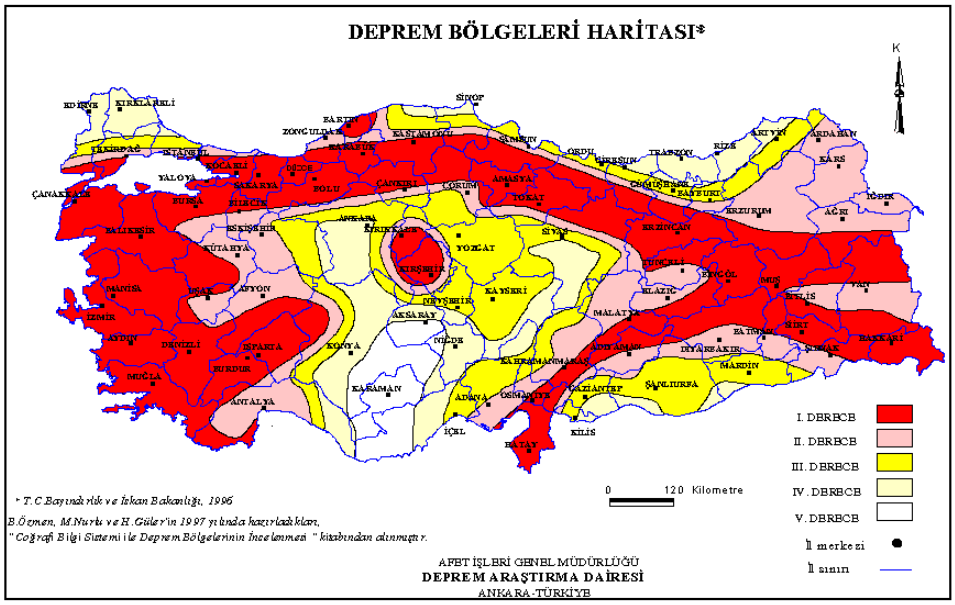

Figure 4.24: Seismic Zones of Turkey [26]

4.6.1 Seismic Hazard Level 1: Design Earthquake

AASHTO-LRFD [2] defines the *design earthquake* as an event having a probability of exceedance of 10 % in 50 years interval (corresponding to a return period of 475 years). Acceleration coefficients at this hazard level are determined from the contour maps prepared for United States. In this study, the acceleration coefficient is determined from the seismic zoning map of Turkey. For Zone I, peak ground acceleration is expected to be higher than 0.4 g for an event having a probability of exceedance of 10 % in 50 years. But, peak ground acceleration is taken as 0.4 g as applied in Turkish Earthquake Code [37].

4.6.2 Seismic Hazard Level 2: Safety Evaluation Earthquake

The hazard level specified in AASHTO-Seismic [28] is considered as the s*afety evaluation earthquake* used in this research. Safety evaluation earthquake is originally specified in ATC-32 [8] as an event having a return period of

approximately 1000-2000 years. AASHTO-Seismic has adopted this hazard level as defining an earthquake having a probability of exceedance of 7 % in 75 years (corresponding to a return period of 1000 years) for life safety assessment. New acceleration contour maps of United States prepared according to this new hazard level provides PGA and spectral acceleration values at short (0.2 seconds) and long periods (1.0 second) for the construction of response spectra.

An empirical method is followed to obtain PGA and spectral acceleration values at 0.2 and 1.0 seconds. The peak ground acceleration value for an event with a return period of 1000 years is estimated from using the acceleration value for an event with a return period of 475 years as shown in Figure 4.25. The acceleration value for an event with a return period of 1000 years (probability of not exceedance is 95 % in 50 years interval) is determined as 0.5 g.

For determining spectral acceleration values at 0.2 and 1.0 seconds, the attenuation relationships of Abrahamson&Silva [3] and Idriss [27] are used. A scenario earthquake of moment magnitude M_w = 7.5 is presumed to create peak ground acceleration of 0.5 g at rock. The distances necessary to create this target peak ground acceleration with one standard deviation of error are found from the mentioned attenuation relationships. The reason for using 84th percentile value is that if the median value is taken as target value, distances would be so close to the source. Near fault effect is ignored in the scope of this study. The results when both median and 84th percentile values are taken as target peak ground accelerations are both shown in Table 4.11.

Using the distances computed as explained above, corresponding spectral acceleration values at 0.2 and 1.0 second periods are also calculated using the same attenuation relationships. The average of values coming out from both attenuation relationships is taken as the final acceleration values at 0.2 and 1.0 second periods which are determined as 1.25 g and 0.57 g, respectively. As it is shown in Figure 4.26, design spectrum shape at rock is approximated well with

the ones obtained from attenuation relationships using the 0.2 and 1.0 second spectral accelerations found above. Attenuation relationships are explained in Appendix B in detail.

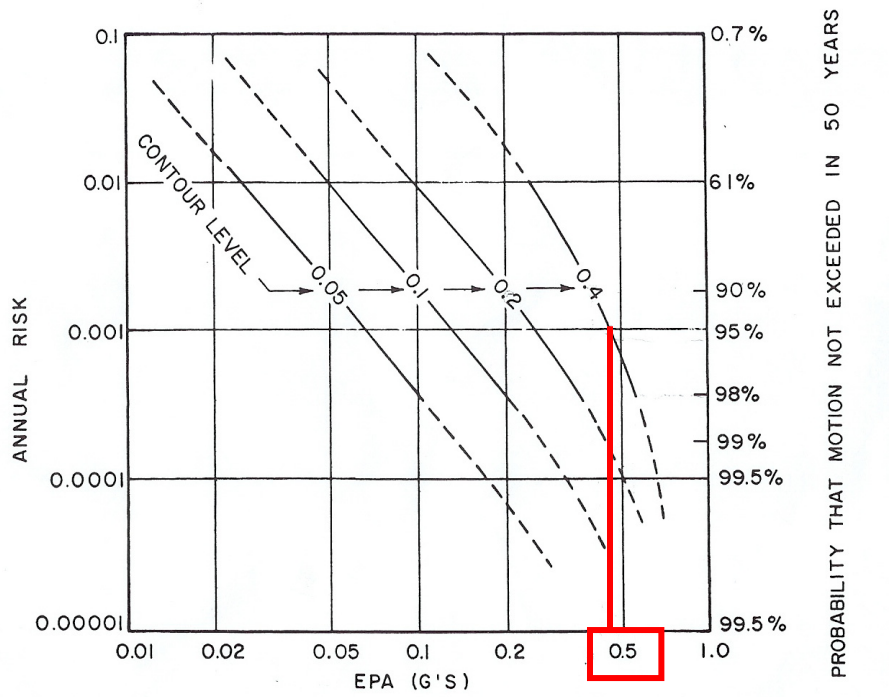

Figure 4.25: Determination of Effective Peak Acceleration Values at Different Hazard Levels with Known Values [24]

Table 4.11: Determination of 0.2 and 1.0 Second Spectral Acceleration Values

		Abrahamson & Silva		Idriss		Average		Used
		Target PGA (g)		Target PGA (g)		Target PGA (g)		
		when s = 0	when s = 1	when s = 0	when s = 1	when s = 0	when s = 1	
PGA (g)	(s = 0)	0.5	0.326	0.5	0.319	0.5	0.3225	
	(s = 1)	0.768	**0.5**	0.783	**0.5**	0.776	0.5	
R (km)		13.1	19.6	6.6	14.1	9.85	16.85	
S_s (g)		1.162	1.255	1.114	1.235	1.138	1.245	**1.25**
S_1 (g)		0.426	0.565	0.439	0.579	0.433	0.572	**0.57**

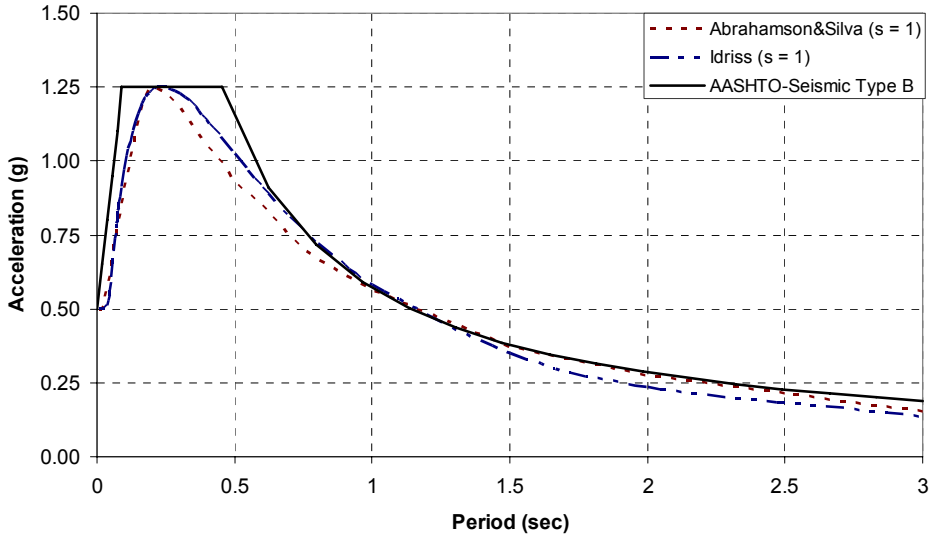

Figure 4.26: Response Spectra Obtained from Two Attenuation Relationships and Design Spectrum at Rock

4.7 Response Spectrum Analysis

Two response spectrum analyses with different hazard levels and response spectrum curves are performed. In the first analysis, (RSA-I) the standard procedure defined in AASHTO-LRFD [2] is followed. Hazard level for this analysis is as explained in Section 4.6.1. The aim in this step is to design columns for shear and determine response modification factor demands for each investigated cases. The response spectra with damping ratios of ξ = 5% for competent and poor soil conditions are constructed by using the curves associated with “type II” and “type III” soil profiles as shown in Figure 4.27.

In the second analysis (RSA-II), the response spectrum curve defined in AASHTO-Seismic [28] is utilized. Hazard level for this analysis is as explained in Section 4.6.2 The response spectra with damping ratios of ξ = 5% for competent and poor soil conditions are constructed by using the curves associated with ”site class D” and “site class E” as shown in Figure 4.28.

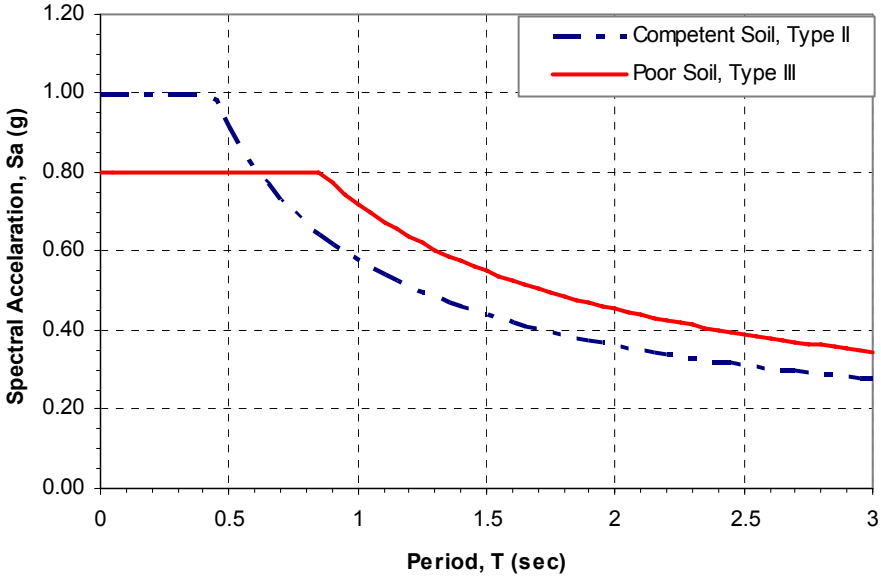

Figure 4.27: Response Spectra Used in RSA-I

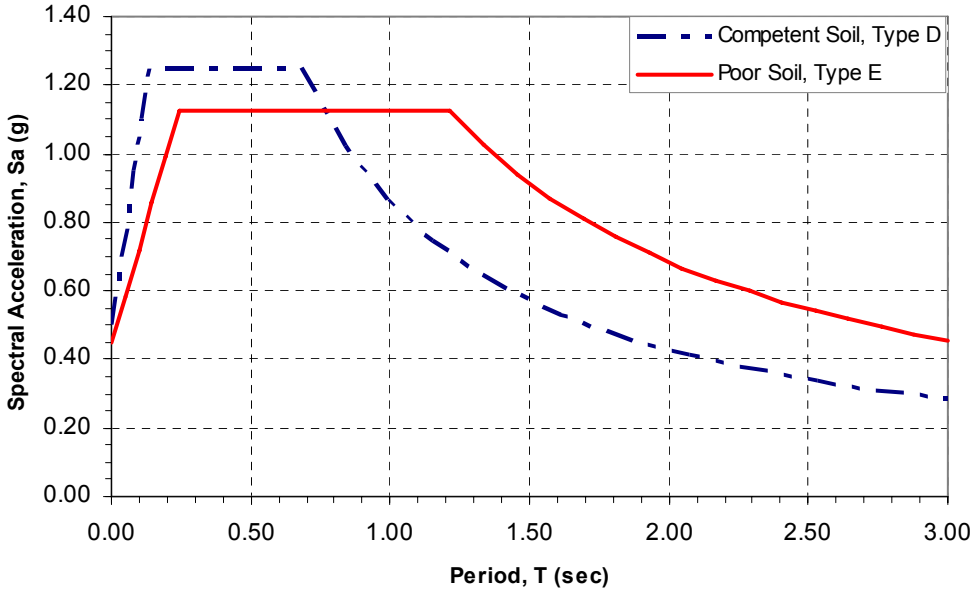

Figure 4.28: Response Spectra Used in RSA-II

Detailed explanation of construction of response spectrum curves is given in Appendix D.

Loading Combinations

Response spectrum analysis is typically performed in global orthogonal directions. Nevertheless, the direction of an earthquake motion is uncertain in real so to account for this uncertainty; resulting responses from analyses in two perpendicular directions are combined as recommended by AASHTO-LRFD [2]:

Load Combination 1: 1.0 EQ_X + 0.30 EQ_Y
Load Combination 2: 1.0 EQ_Y + 0.30 EQ_X

where;
EQ_X : Response value in longitudinal direction (X)
EQ_Y : Response value in transverse direction (Y)

Some references such as ATC-32 [8], NYCDOT [39] recommend to account for response from analysis in vertical direction. However, the effect of vertical response is out of scope of this study so it is not included to the load combinations stated above.

The first response spectrum analysis (RSA-I) is performed for design so the load factors proposed in AASHTO-LRFD is used as follows:

Comb 1 (longitudinal) : 1.25 DC + 1.50 DW + 0.5 LL + 1.0 EQ_X + 0.3 EQ_Y
Comb 2 (transverse) : 1.25 DC + 1.50 DW + 0.5 LL + 1.0 EQ_Y + 0.3 EQ_X

where;
DC : Dead load of structural attachments and nonstructural attachments
DW : Dead load of wearing surfaces and utilities such as barriers
LL : Live loads

Load factors recommended by AASHTO-LRFD for DC and DW are ranging between 0.9-1.25 and 0.65-1.50 respectively. In the beginning of RSA-I, the number of combinations was determined as 4 instead of 2 by also accounting for the lower load factors and ignoring live load cases. In this manner, a heavy and light case would be investigated. However, it is evaluated that there is not a significant difference between the analyzed combinations and the ones which are not shown here.

The issue of consideration of live load for response spectrum analysis is controversial. In this study, half of the live load is taken as recommended by AASHTO-LRFD which is thought to be reasonable for a wide range of values of average daily truck traffic. AASHTO-Seismic states that for bridges located in metropolitan areas where traffic congestion might occur, the probability of a large live load being on the bridge during an earthquake should be considered. Lane loading on 3 lanes with multiple presence factor and pedestrian live load defined in AASHTO-LRFD is taken as live loads. In Table 4.12, gravity loads are summarized with their values for unit length of superstructure.

Table 4.12: Gravity Load Cases

	Load Case	**w (kN/m)**
DC	Girders + deck	Directly computed by program
	Diaphragm beams	9.41
DW	Wearing surface and barriers	16.52
LL	Pedestrian live load	7.80
	Design lane load	23.72

For the second response spectrum analysis (RSA-II), two load combinations are analyzed to determine response of the investigated cases under seismic loadings in longitudinal and transverse direction.

Comb 1 (longitudinal) : $1.0\,DC + 1.0\,DW + 0.5\,LL + 1.0\,EQ_X + 0.3\,EQ_Y$

Comb 2 (transverse) : $1.0\,DC + 1.0\,DW + 0.5\,LL + 1.0\,EQ_Y + 0.3\,EQ_X$

Assignment of masses is as important as stiffness properties of structural members that can change modal characteristics of bridges. Structure's self weight and external load cases are considered as mass sources with proper units. Again, half of the live load contributes to mass characteristics. No factor is assigned to masses.

4.7.1 Modal Analysis

For the investigated bridge system, there are three fundamental vibration modes in orthogonal directions. The first two modes are clearly identified due to the large mass participation ratios in longitudinal and transverse directions. The third fundamental mode is identified in vertical direction with a smaller cumulative mass participation ratio. There are several modes between the fundamental modes along transverse and vertical direction as a result of a mixed behavior.

Modal shapes for the first and second modes are shown in Figure 4.29. There are slight differences in modal characteristics computed in RSA-I and RSA-II. The values of first two periods computed in both analyses are presented in Appendix F. This difference is due to different assignment of effective stiffness of columns, lateral soil response, and abutment longitudinal response. Periods of first two modes computed in RSA-II are shown in Figure 4.30. For the investigated cases, the period in longitudinal direction (first mode) is ranging between 1.47-1.70 seconds at competent soil while it is ranging between 1.62-1.90 seconds at poor soil. The period in transverse direction (second mode) is ranging between 0.63-1.20 seconds at competent soil while it is ranging between 0.68-1.22 seconds at poor soil. Poor soil elongates periods especially in longitudinal direction. This is mostly due to the difference between abutment longitudinal stiffness values. Besides, for cases with identical column aspect ratios, periods shorten slightly as longitudinal reinforcement ratio increases. This is due to the different effective stiffness assignment according to different longitudinal reinforcement ratios.

The vertical period of vibration is about 0.30 seconds at both soil conditions.

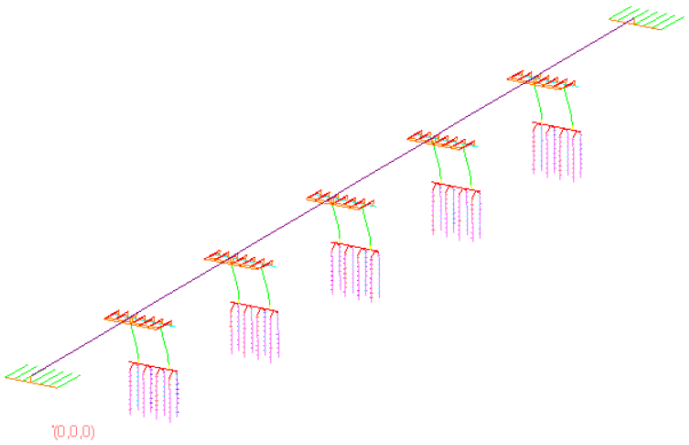

(a) 1ST Mode in Longitudinal Direction

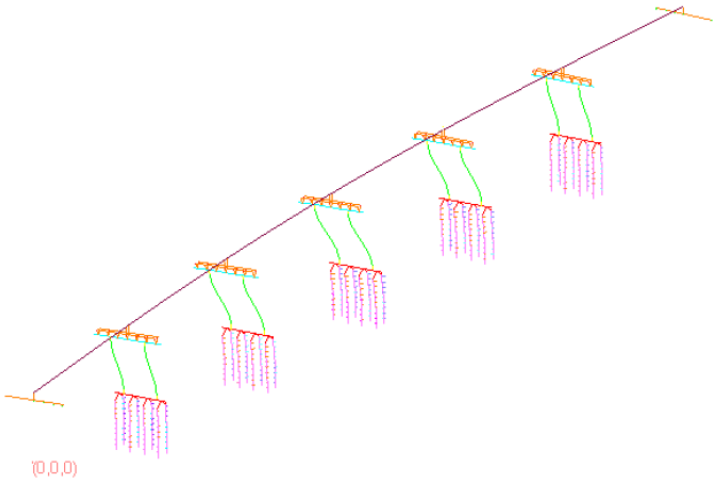

(b) 2nd Mode in Transverse Direction

Figure 4.29: Modal Shapes for the First and Second Mode

In response spectrum analyses, maximum responses of each mode are combined with CQC rule. 60 modes are computed in order to have total mass participated larger than 90 %.

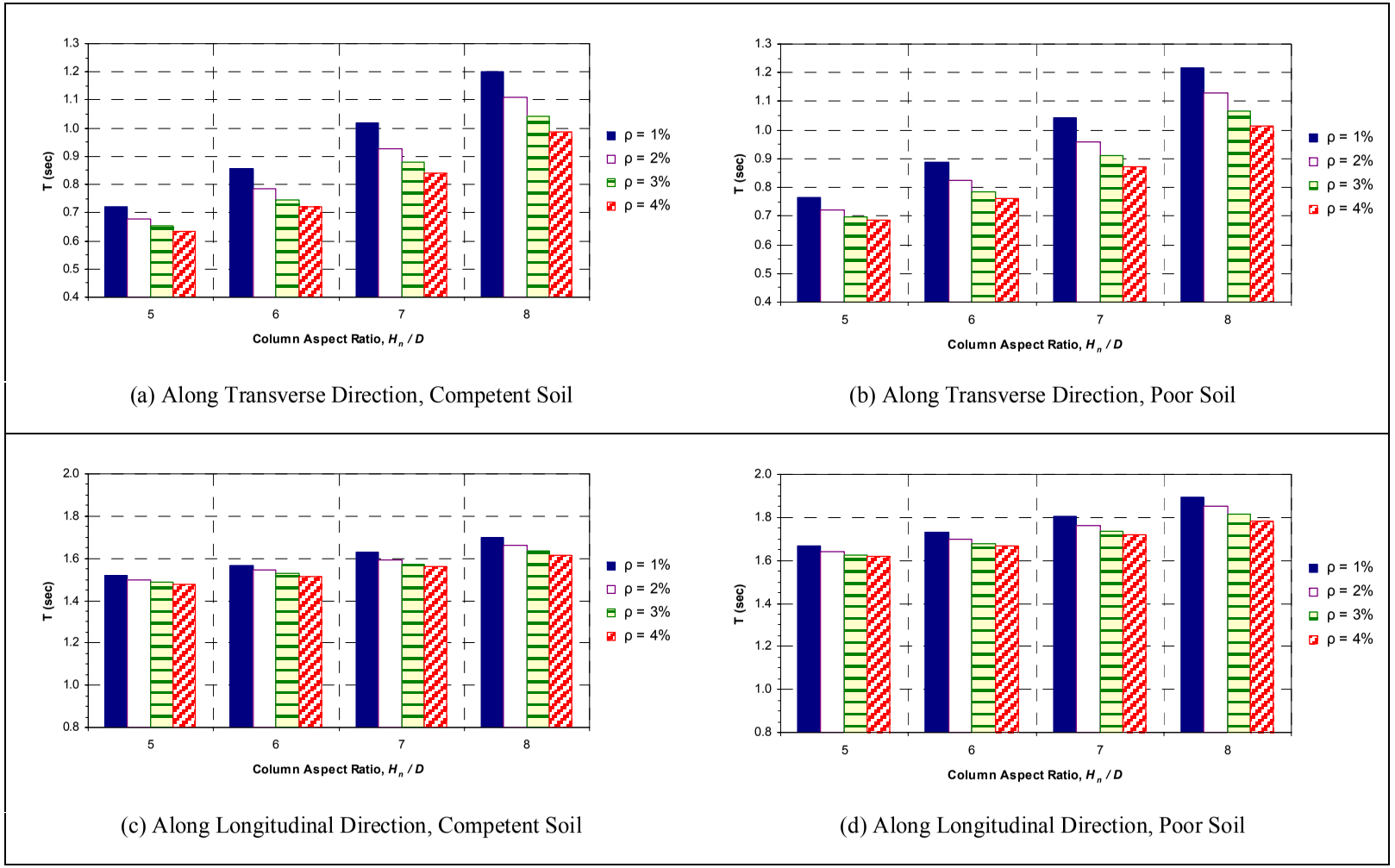

(a) Along Transverse Direction, Competent Soil

(b) Along Transverse Direction, Poor Soil

(c) Along Longitudinal Direction, Competent Soil

(d) Along Longitudinal Direction, Poor Soil

Figure 4.30: Fundamental Periods of Vibration Obtained from RSA-II

4.7.2 Shear Design of Columns

The smaller of elastic shear and inelastic hinging forces is used as design shear force. For oversized columns the forces resulting from an inelastic hinging analysis may exceed elastic forces. The procedure explained in AASHTO-LRFD [2] is followed for finding inelastic hinging forces. The iterative procedure for multiple columns is not explained here. As longitudinal reinforcement of each investigated case is known, nominal moment capacity (M_n) can be determined for a given axial load. The nominal moment capacity of reinforced concrete sections is calculated as recommended by Priestley et al. [44] that is also explained in section 4.5.2. The overstrength moment resistance is obtained from multiplying nominal moment capacity with $\varphi = 1.3$.

It is stated in AASHTO-Seismic [28] that for sections that are expected to accommodate a significant amount of plastic deformation, it is inapplicable to use the shear design provisions in AASHTO-LRFD. The reason is within the plastic hinge region as ductility demands increase, concrete shear strength degrades. Therefore, the shear strength formulas presented in AASHTO-Seismic [28] are used for estimating shear strength of columns. These formulas, which are given in Appendix E, are very similar to the ones stated in Caltrans-SDC [15]. It is shown in Figure 4.31 that shear strength values estimated from AASHTO-Seismic is slightly more conservative than the ones estimated from Caltrans-SDC.

In transverse reinforcement design, minimum shear capacity is tried to be supplied to sections making shear capacity over demand ratios, V_r / V_d near 1.0. The minimum requirement of confining reinforcement recommended in AASHTO-LRFD [2] is considered as the minimum transverse reinforcement.

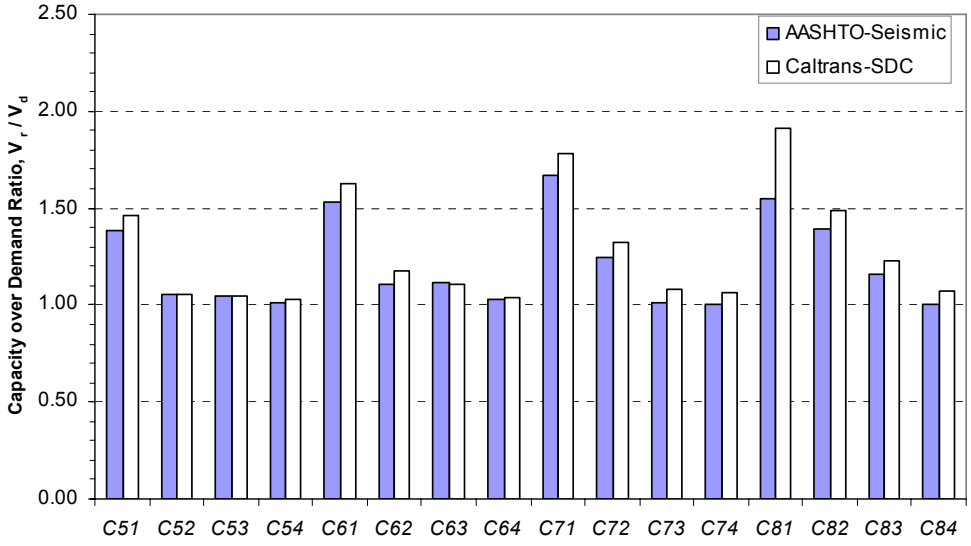

(a) Competent Soil Cases

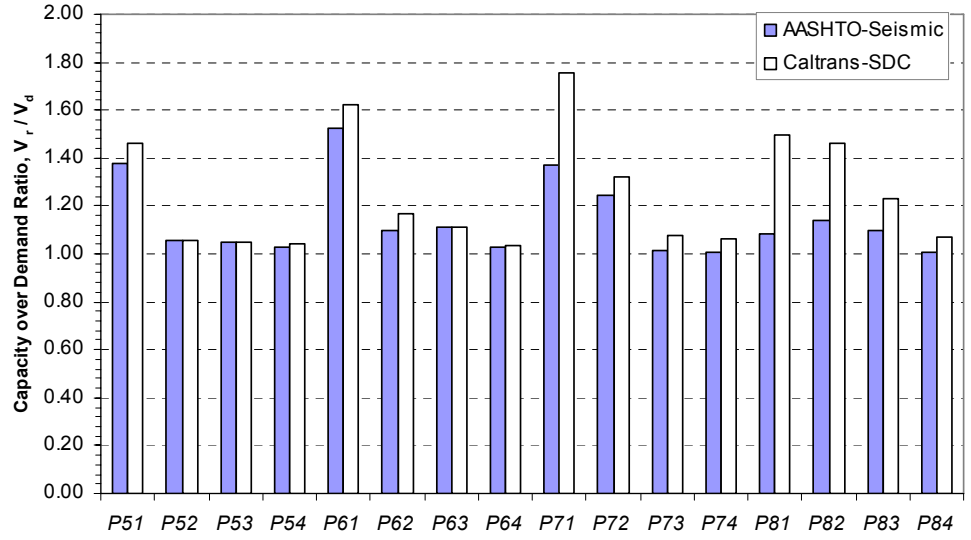

(b) Poor Soil Cases

Figure 4.31: Shear Capacity over Demand Ratios

Volumetric ratio of transverse reinforcement shall satisfy the larger of:

$$\rho_s \geq 0.12 \frac{f_c'}{f_y} \tag{4.29}$$

$$\rho_s \geq 0.45\left(\frac{A_g}{A_c}-1\right)\frac{f_c'}{f_y} \tag{4.30}$$

where;

f_c' : Compressive strength of concrete

f_y : Yield strength of reinforcing bars

A_g : Gross area of concrete section

A_c : Core area of concrete section measured to the outside diameter of the spiral

According to the results coming out from the equations above, the first requirement yields higher minimum volumetric reinforcement ratio giving $\rho_{s,min}$ = 0.0086. The volumetric ratios of transverse reinforcement supplied to the columns of all cases are shown in Figure 4.32.

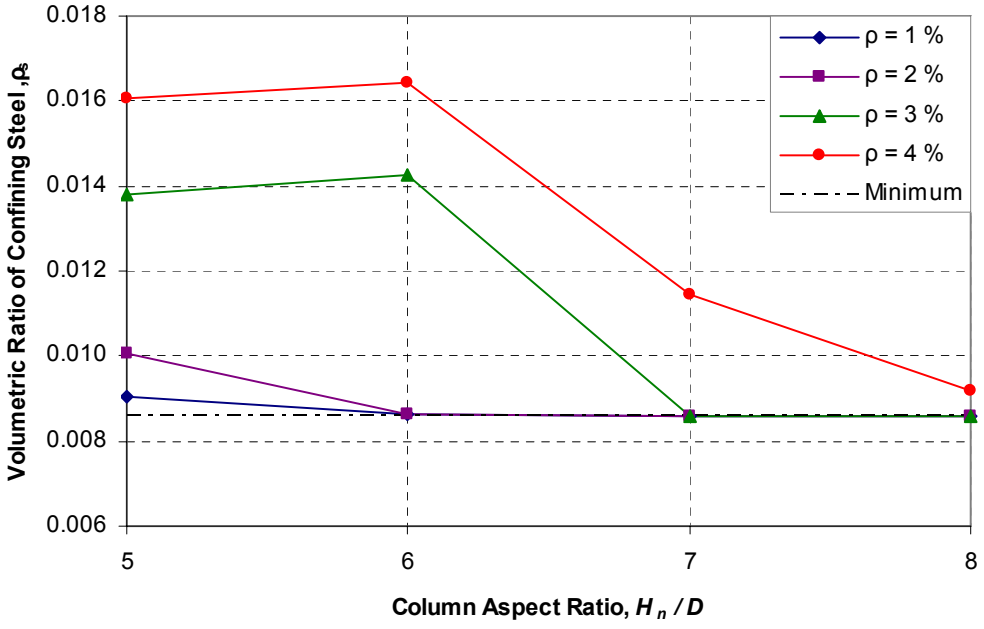

Figure 4.32: Volumetric Ratios of Confining Steel Supplied to the Sections

The transverse reinforcement supplied to the competent soil cases and poor soil cases are the same. The reason is design shear forces generally originate from inelastic hinging forces. The following interpretations can be made according to Figure 4.32:

- As columns get slender, the minimum confining reinforcement requirement governs the design.
- For the cases with identical aspect ratios, higher transverse reinforcement ratios have to be supplied to the ones having higher longitudinal reinforcement amounts.

4.8 Push-Over Analysis

The deformation capacity of a system along a desired direction can be determined from push-over analysis. Each bridge model is incrementally pushed until the failure of stability.

The bridge system is pushed according to a displacement profile related to the fundamental mode along the direction pushed. The modal displacement of each joint is scaled with an arbitrary constant creating the incremental joint forces:

$$(F_Y)_i = K_Y \cdot (\delta_Y)_i \tag{4.31}$$

$$(F_X)_i = K_X \cdot (\delta_X)_i \tag{4.32}$$

where;

$(F_Y)_i$: Incremental pushing force of joint *i* along Y (transverse direction)

$(F_X)_i$: Incremental pushing force of joint *i* along X (longitudinal direction)

$(\delta_Y)_i$: Modal displacement of joint *i* along Y

$(\delta_X)_i$: Modal displacement of joint *i* along X

K_X, K_Y : Arbitrary scaling coefficients along X and Y respectively.

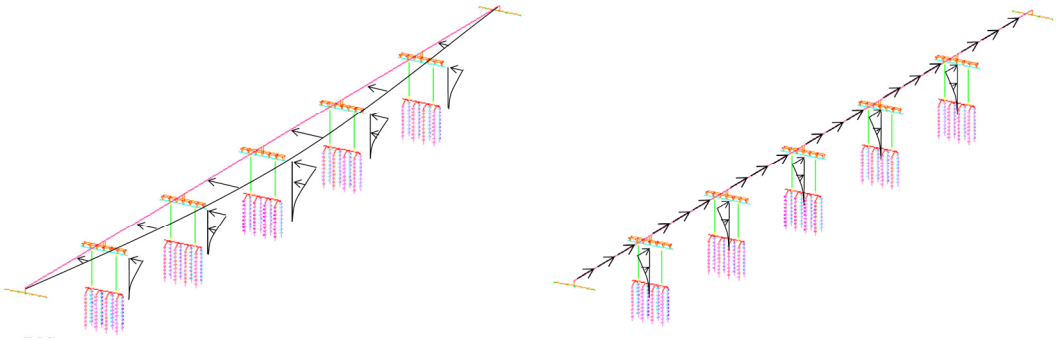

Figure 4.33: Isometric View of Pushing Force Profile

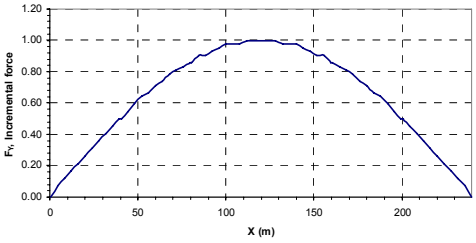

(a) F_Y vs. X for Push-over Analysis in Transverse Direction

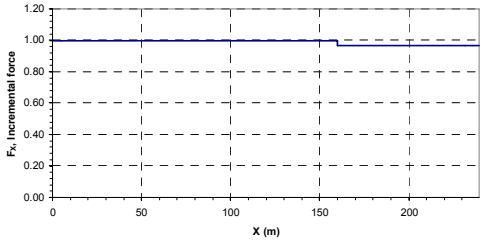

(b) F_X vs. X for Push-over Analysis in Transverse Direction

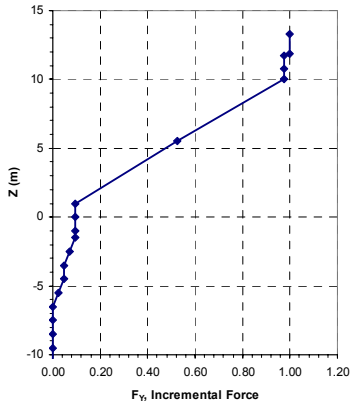

(c) F_Y vs. Z for Push-over Analysis in Longitudinal Direction

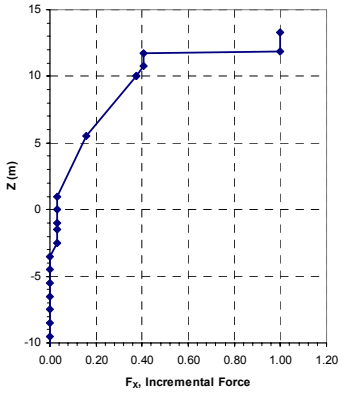

(d) F_X vs. Z for Push-over Analysis in Longitudinal Direction

Figure 4.34: Distribution of Incremental Joint Forces along the Length and Elevation of the Bridge

The distribution of joint forces is more important than the magnitudes of these forces since the program can automatically adjust incremental joint forces at each step. It may be seen from Figure 4.33 that vertical distribution of forces resemble the deflection shapes of first two modes. In Figure 4.34, incremental pushing force distribution along X (longitudinal direction) and Z (elevation) is shown with normalized values with respect to the highest value.

Idealized yield displacement of structure, Δ_y is obtained from converting the nonlinear push-over curve constructed using relative displacements to the idealized bilinear form according to the recommendation of FEMA 356 [25] as shown in Figure 4.35.

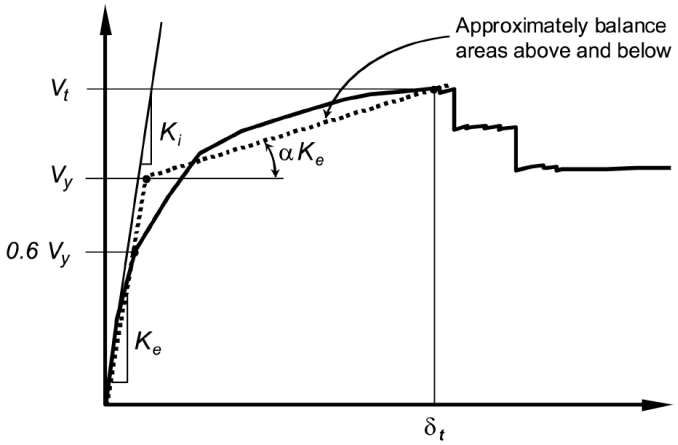

Figure 4.35: Idealized Force-Displacement Curve as Recommended in [25]

The parameters shown in Figure 4.35 are as follows:

K_i : Elastic lateral stiffness of the structure in the direction under consideration

K_e : Effective lateral strength of the structure

V_y : Effective yield strength of the structure

α : Post yield slope

δ_t : Target displacement (considered as ultimate displacement capacity)

The force displacement curve of model *P81* in transverse direction is shown in Figure 4.36 as an example of bilinear idealization.

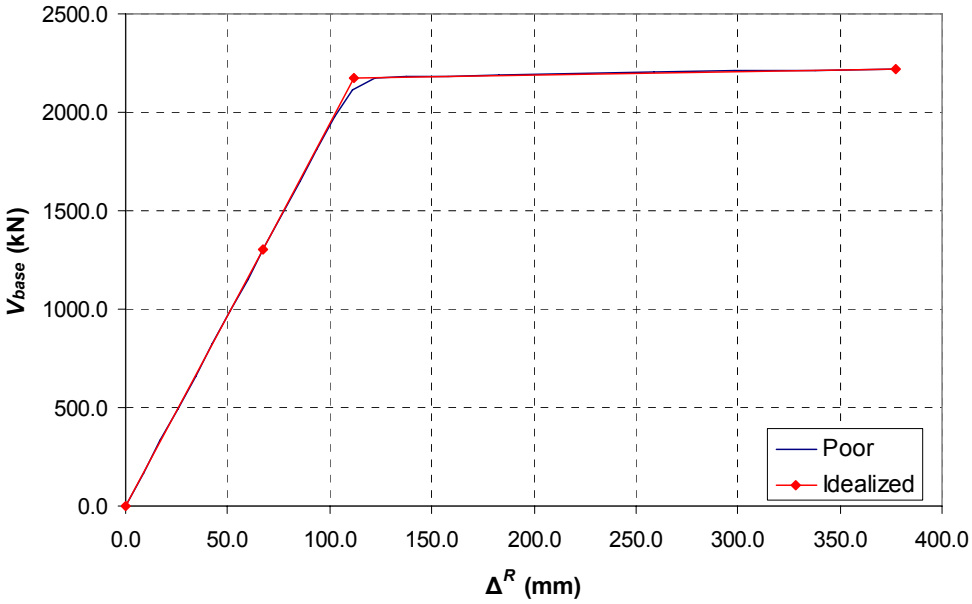

Figure 4.36: An Example of Idealized Force-Displacement Curve

4.9 Inelastic Time-History Analysis

Inelastic time-history analysis is the ultimate analysis for determination of the most accurate response of a structure under seismic loading. The number and type of inelastic elements assigned and number of data of ground motion affect run times significantly making this analysis type as very exhaustive.

The results of an inelastic time-history analysis are very dependent to selected ground motions. It is recommended to take the average value of the response parameter of interest if seven or more time-history analyses are performed or the maximum response of the parameter of interest if three time-history analyses are performed [1]. In this study, 8 analyses with 4 different sets of accelerograms are performed. A total of 24 spectrum compatible accelerograms are generated.

4.9.1 Response Spectrum Compatible Time-History Records

For seismic design of structures, generally response spectrum curves recommended by design codes are utilized. These curves mainly originate from ground motion data. Therefore, a generated time-history record has to reflect the seismic input which is defined in the form of response spectra by matching the ordinates of the response spectrum curve.

The parameters effective in the formation of ground motion data such as type of fault, earthquake magnitude, distance of the recording station, local soil conditions, etc. have to be considered in generation of time-history records. The assigned time-history record should be compatible with the soil conditions of the investigated case. The outcomes of this study are all about safety evaluation earthquake. Therefore, the generated time-histories for competent and poor soil conditions shall match with the response spectra constructed for site classes D and E respectively for an earthquake event with a return period of 1000 years.

In inelastic time-history analysis, all of the orthogonal components of generated accelerograms are applied on to the structure simultaneously. Horizontal components of generated time history records are spectrally compatible with horizontal elastic response while vertical component is spectrally compatible with vertical response spectra. The horizontal response spectra used in this study is presented in Section 4.7. The vertical response spectrum is constructed by multiplying the ordinates of the spectrum for horizontal motion with a factor of 2/3 as recommended by AASHTO [2].

The modified version of the freeware program called “RSCA”, released under GNU public license by Thiele, M. is used for generation of response spectrum compatible time-history records. Domaniç [21] made some modifications on the original program such as improving calculation routines and user interface. More

information on the original program and the modification process is available in references [50] and [21], respectively.

The general properties of the generated time-history records are shown in Table 4.13. The motions produced can be divided into two groups as synthetic records and modified records.

Spectrum compatible synthetic accelerograms are obtained from the program "RSCA" by the method of filtering of white noise. In this method, an intensity function that will simulate the characteristics of real accelerograms is chosen and the scaling scheme is applied to generated white-noise [21]. Exponential intensity functions are used for both synthetic record sets. For the generation of the first set, arbitrary exponential intensity functions are used for all orthogonal components; while for the generation of the second set, each component of the generated record has an exponential intensity function which is the approximation of the intensity of the corresponding component of the NGA 1158 record as shown in Figure 4.37.

The third and fourth sets of motions are obtained by modifying existing accelerograms. The intensities of input accelerograms are preserved for all orthogonal components. The existing accelerograms are taken from the PEER NGA database [41] where earthquake and local soil information is nicely presented with processed ground motion data. Selected existing ground motions are:

NGA 1158 : At Kocaeli Earthquake (M_w = 7.51), Düzce station on 17.08.1999

NGA 0764 : At Loma Prieta Earthquake (M_w = 6.59), CDMG 57476 Gilroy - Historic Bld. station on 18.10.1989

NGA 0732 : At Loma Prieta Earthquake (M_w = 6.59), USGS 1002 APEEL 2 - Redwood City station on 18.10.1989

Table 4.13: General Properties of the Generated Time-History Records

			Competent Soil		Poor Soil	
	Type	**Intensity**	**Input Accelerogram**	**Generated Record**	**Input Accelerogram**	**Generated Record**
Motion 1	Synthetic Record	Random exponential	-	*D_synth_1*	-	*E_synth_1*
Motion 2	Synthetic Record	Approximated exponential	-	*D_synth_2*	-	*E_synth_2*
Motion 3	Modified from real record	of input accelerogram	NGA 1158 Kocaeli	*D_real_1*	NGA 1158 Kocaeli	*E_real_1*
Motion 4	Modified from real record	of input accelerogram	NGA 0764 Loma Prieta	*D_real_2*	NGA 0732 Loma Prieta	*E_real_2*

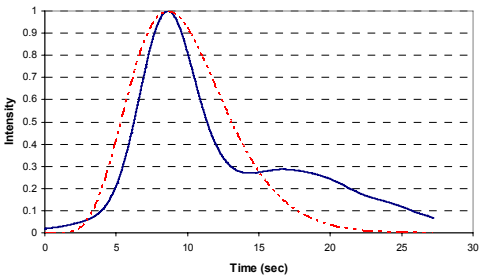

(a) N-S component from NGA1158 (270)

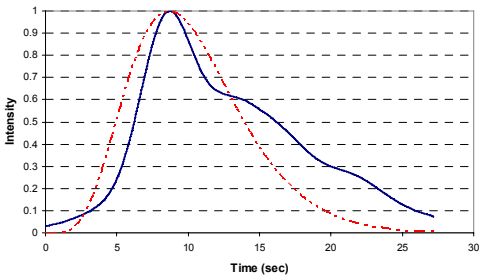

(b) E-W component from NGA1158 (180)

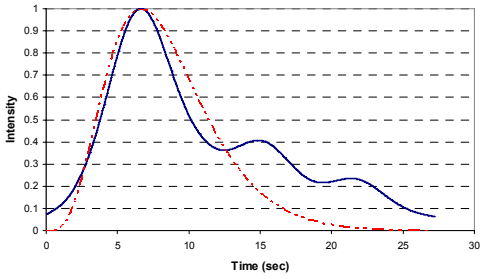

(c) Vertical component from NGA1158 (UP)

Figure 4.37: Approximated Exponential Intensity Functions for the Second Set of Synthetic Accelerograms

Table 4.14: The properties of the Selected Ground Motions and Recording Stations

Ground Motion Record	V_s (m/s)	*Geomatrix*			*D* (km)	# of data	*dt* (sec)	Component	*PGA* (g)	*PGV* (cm/s)	*PGD* (cm)
		1	*2*	*3*							
NGA1158	276	A	-	D	13.6	5437	0.005	180	0.312	58.80	44.11
								270	0.358	46.40	17.61
								UP	0.229	20.40	17.01
NGA0764	338.5	B	Q	D	10.27	7991	0.005	160	0.284	41.97	11.12
								250	0.241	24.01	3.67
								UP	0.149	11.10	5.96
NGA0732	133.1	I	H	E	43.06	7165	0.005	43	0.274	53.63	12.63
								133	0.220	34.31	6.84
								UP	0.083	9.49	3.16

The fault mechanisms of Kocaeli and Loma Prieta earthquakes are strike-slip and reverse-oblique respectively. The properties of the existing accelerograms and the stations at which these motions are recorded are shown in Table 4.14. The parameters in Table 4.14 are given as:

V_s : Shear wave velocity

D : Joyner-Boore distance defined as shortest horizontal distance from the recording site to the vertical projection of the rupture

dt : Time increment

PGA : Peak ground acceleration

PGV : Peak ground velocity

PGD : Peak ground displacement

Geomatrix 1 is the classification regarding instrument housing where:

I = Free-field instrument or instrument shelter

A= One-story structure of lightweight construction

B = Two-to-four-story structure of lightweight construction

Geomatrix 2 is the classification regarding mapped local geology where:

H = Holocene (Recent) Quaternary

Q = Pleistotocene Quaternary

Geomatrix 3 is the classification regarding geotechnical subsurface characteristics where:

D = Deep broad soil

E = Soft deep soil

For selection of existing accelerograms to be modified, several factors such as magnitude of earthquake event, distance from station to fault, peak ground acceleration and local soil conditions of recording station are taken into consideration. Besides, the difference between target spectrum and original spectrum shall be as small as possible. The three records selected are obtained as a result of search in NGA database following the criteria below:

- Moment magnitude in the range of M_w = 6.5-8
- $D \geq 10$ km
- For competent soil conditions, V_s = 180-360 m/s
- For poor soil conditions $V_s \leq 180$ m/s

43 records related to competent and 4 records related to poor soil conditions are found suitable for use in this study. *PGV*/*PGA* ratios of the records related to competent soils have an average of 0.110 seconds for horizontal components and 0.073 seconds for vertical components. The records related to the poor soil conditions shows that the average of PGV/PGA ratios is 0.166 seconds and 0.092 seconds for horizontal and vertical components respectively.

The frequency contents of the generated accelerograms are expected to be similar to the existing records which are recorded under similar conditions. It is found that the ratio of v_{max}/a_{max} (*PGV*/*PGA*) should be related to the frequency content of the motion as peak velocities and peak accelerations are usually associated with motions of different frequency [30]. Table 4.15 shows the suggested representative values of v_{max}/a_{max} by Seed and Idriss [47] at different soil conditions less than 50 km from the source.

Table 4.15: Representative Values of v_{max}/a_{max} for Different Soil Conditions [47]

Site Condition	v_{max}/a_{max} (sec)
Rock	0.056
Stiff soils (< 200 ft)	0.112
Deep stiff soils (> 200 ft)	0.138

Table 4.15 indicates a shift toward longer-period motion on softer soil deposits. v_{max}/a_{max} ratios for the generated accelerograms at competent soil condition are shown in Table 4.16. The average of v_{max}/a_{max} ratios is 0.11 and 0.10 seconds for horizontal and vertical components, respectively. v_{max}/a_{max} ratios for the generated accelerograms at poor soil condition are shown in Table 4.17. The average of v_{max}/a_{max} ratios is 0.16 and 0.17 seconds for horizontal and vertical components, respectively. It may be concluded that the generated accelerograms at both type of soil conditions are acceptable in terms of frequency contents.

Table 4.16: v_{max}/a_{max} Ratios for the Generated Accelerograms at Competent Soil Condition

	Input Record			Generated Record			
Record Name	Component		v_{max}/a_{max} (sec)	Component	a_{max} (m/s^2)	v_{max} (m/s)	v_{max}/a_{max} (sec)
D_synth_1	*(synthetic)*		-	*N-S*	5.774	0.524	0.09
			-	*E-W*	5.202	0.625	0.12
			-	*Vertical*	4.686	0.371	0.08
D_synth_2	*(synthetic)*		-	*N-S*	5.752	0.532	0.09
			-	*E-W*	5.645	0.532	0.09
			-	*Vertical*	3.852	0.335	0.09
D_real_1	NGA 1158	270	0.13	*270*	5.708	0.678	0.12
		180	0.19	*180*	6.947	0.839	0.12
		UP	0.09	*Vertical*	3.563	0.408	0.11
D_real_2	NGA 0764	160	0.15	*160*	5.568	0.668	0.12
		250	0.10	*250*	5.329	0.780	0.15
		UP	0.08	*Vertical*	3.626	0.501	0.14

Table 4.17: v_{max}/a_{max} Ratios for the Generated Accelerograms at Poor Soil Condition

Record Name	Input Record			Generated Record			
	Component		v_{max}/a_{max} (sec)	Component	a_{max} (m/s^2)	v_{max} (m/s)	v_{max}/a_{max} (sec)
E_synth_1	*(synthetic)*		-	*N-S*	5.495	0.751	0.14
			-	*E-W*	4.781	0.791	0.17
			-	*Vertical*	2.994	0.606	0.20
E_synth_2	*(synthetic)*		-	*N-S*	5.108	0.727	0.14
			-	*E-W*	5.086	0.757	0.15
			-	*Vertical*	3.539	0.475	0.13
E_real_1	NGA 1158	270	0.13	*270*	5.319	0.899	0.17
		180	0.19	*180*	6.010	0.947	0.16
		UP	0.09	*Vertical*	3.362	0.536	0.16
E_real_2	NGA 0732	133	0.16	*133*	5.508	1.069	0.19
		43	0.20	*43*	5.328	0.915	0.17
		UP	0.12	*Vertical*	2.815	0.552	0.20

The horizontal components of each ground motion are applied in longitudinal and transverse directions interchangeably with the same vertical component as shown in Table 4.18

Table 4.18: Application Order of Generated Accelerogram Components

ITHA Analysis	**Competent Soil Models**				**Poor Soil Models**			
	Record	**Long.**	**Trans.**	**Vert.**	**Record**	**Long.**	**Trans.**	**Vert.**
ITHA-1	*D_synt_1*	*N-S*	*E-W*	*Vert.*	*E_synt_1*	*N-S*	*E-W*	*Vert.*
ITHA-2	*D_synt_1*	*E-W*	*N-S*	*Vert.*	*E_synt_1*	*E-W*	*N-S*	*Vert.*
ITHA-3	*D_synt_2*	*N-S*	*E-W*	*Vert.*	*E_synt_2*	*N-S*	*E-W*	*Vert.*
ITHA-4	*D_synt_2*	*E-W*	*N-S*	*Vert.*	*E_synt_2*	*E-W*	*N-S*	*Vert.*
ITHA-5	*D_real_1*	*270*	*180*	*Vert.*	*E_real_1*	*270*	*180*	*Vert.*
ITHA-6	*D_real_1*	*180*	*270*	*Vert.*	*E_real_1*	*180*	*270*	*Vert.*
ITHA-7	*D_real_2*	*160*	*250*	*Vert.*	*E_real_2*	*133*	*43*	*Vert.*
ITHA-8	*D_real_2*	*250*	*160*	*Vert.*	*E_real_2*	*43*	*133*	*Vert.*

The generated synthetic time-history records (the first two sets) are shown in Figures 4.38 and 4.39. The original and modified components of generated time-history records (the third and fourth sets) are shown in Figures 4.40 to 4.43. The response spectra of generated time-history records are presented in Appendix G.

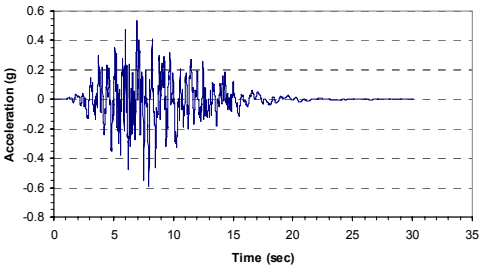

(a) *D_synth_1 N-S* Component

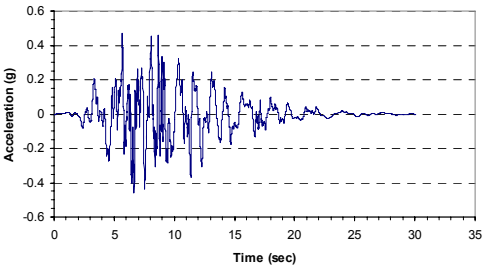

(d) *E_synth_1 N-S* Component

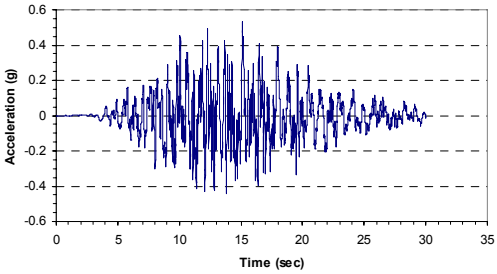

(b) *D_synth_1 E-W* Component

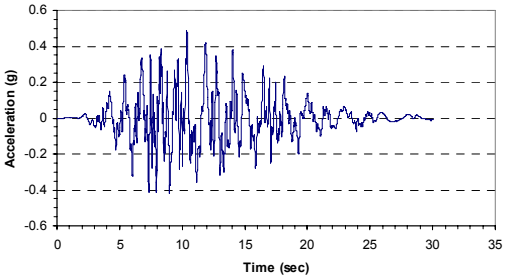

(e) *E_synth_1 E-W* Component

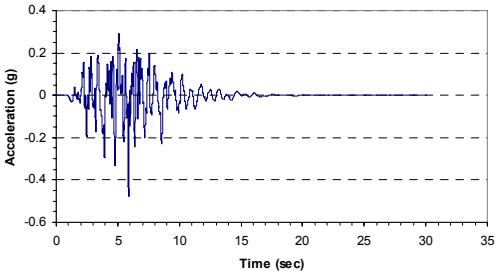

(c) *D_synth_1 Vertical* Component

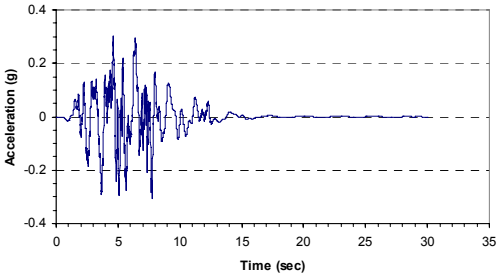

(f) *E_synth_1 Vertical* Component

Figure 4.38: Components of Synthetic Time-History Records *D_synth_1* and *E_synth_1*

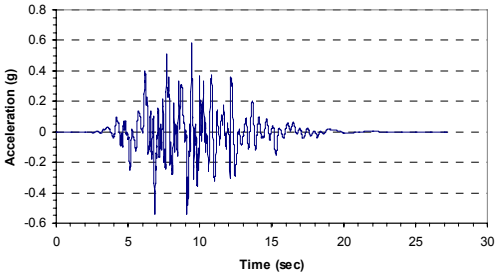

(a) *D_synth_2 N-S* Component

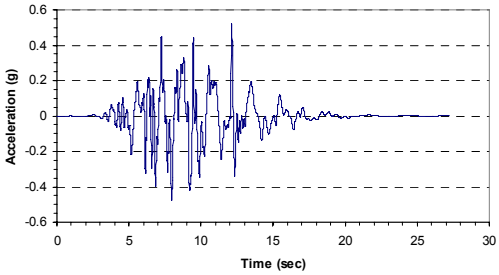

(d) *E_synth_2 N-S* Component

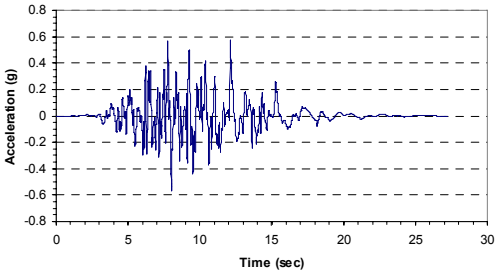

(b) *D_synth_2 E-W* Component

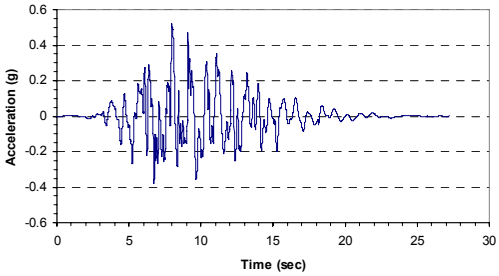

(e) *E_synth_2 E-W* Component

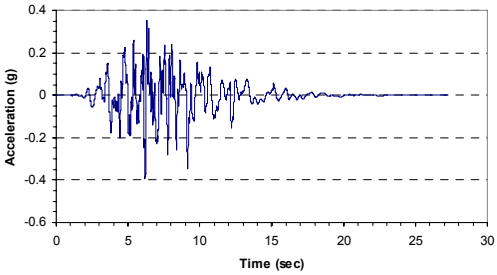

(c) *D_synth_2 Vertical* Component

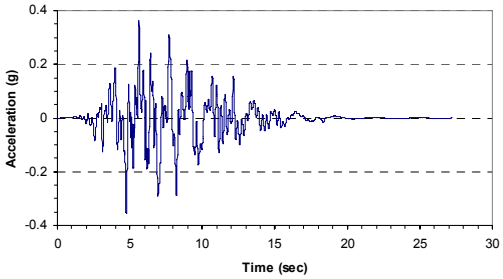

(f) *E_synth_2 Vertical* Component

Figure 4.39: Components of Synthetic Time-History Records *D_synth_2* and *E_synth_2*

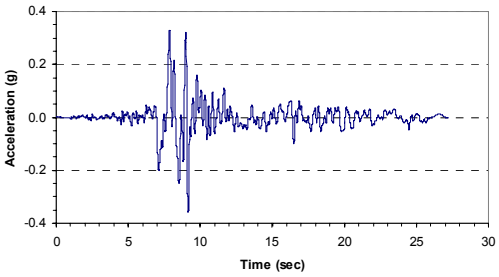

(a) Original “270” Component

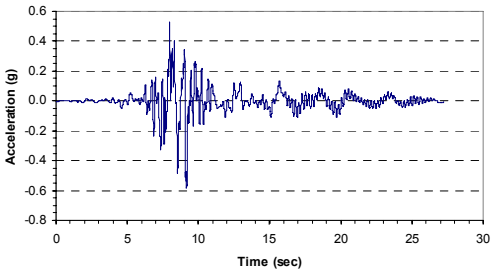

(b) Modified “270” Component

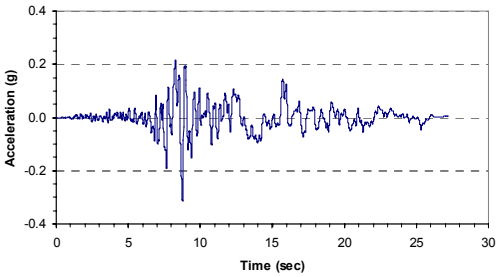

(c) Original “180” Component

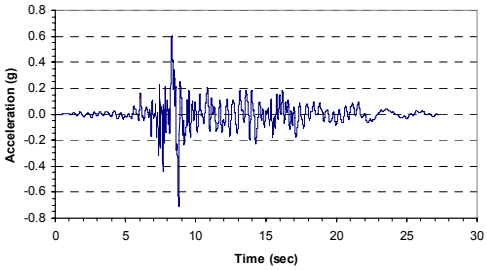

(d) Modified “180” Component

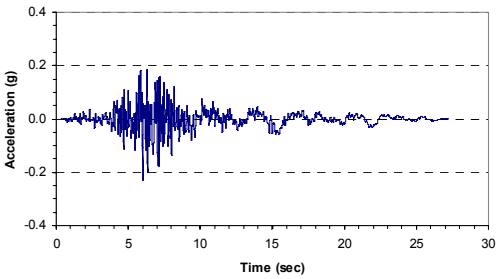

(e) Original “UP” Component

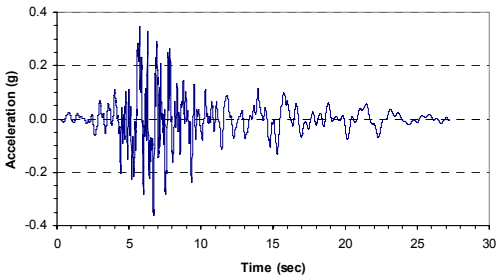

(f) Modified “UP” Component

Figure 4.40: Original and Modified Components of Time-History Record *D_real_1*

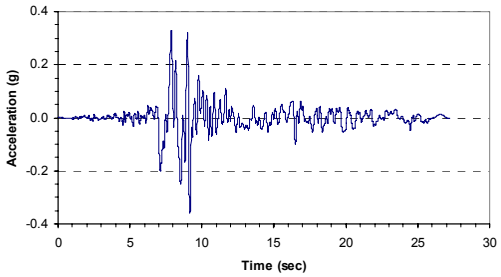

(a) Original “270” Component

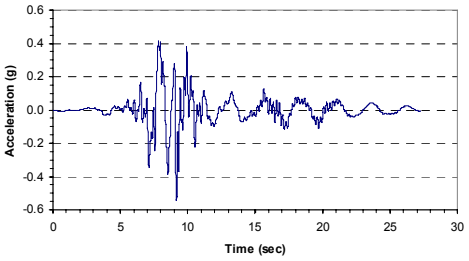

(b) Modified “270” Component

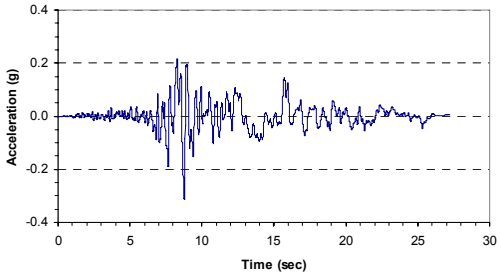

(c) Original “180” Component

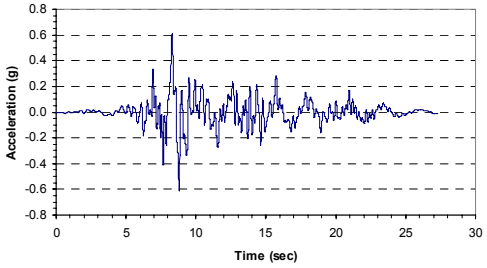

(d) Modified “180” Component

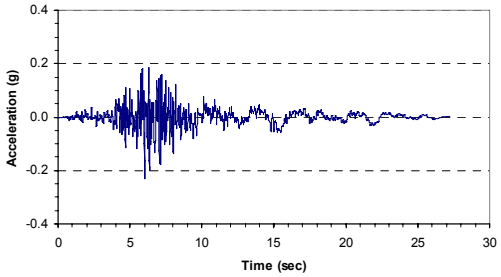

(e) Original “UP” Component

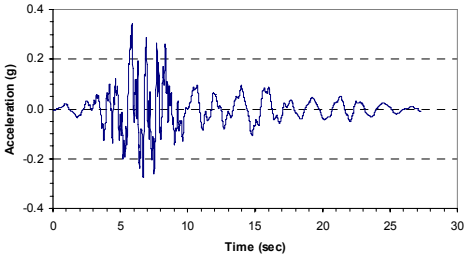

(f) Modified “UP” Component

Figure 4.41: Original and Modified Components of Time-History Record *E_real_1*

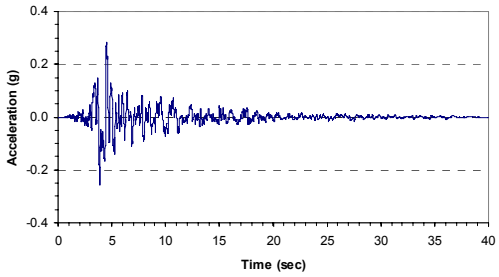

(a) Original “160” Component

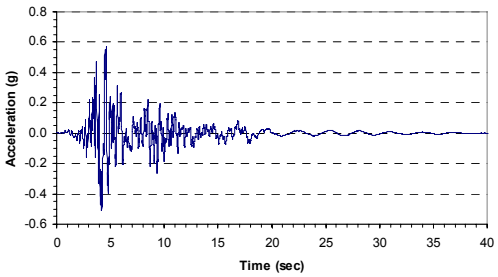

(b) Modified “160” Component

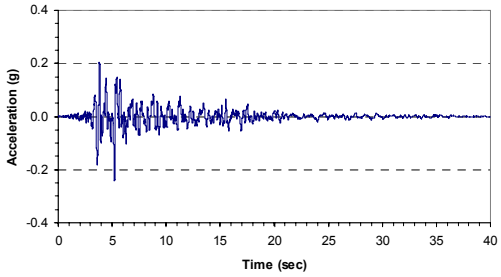

(c) Original “250” Component

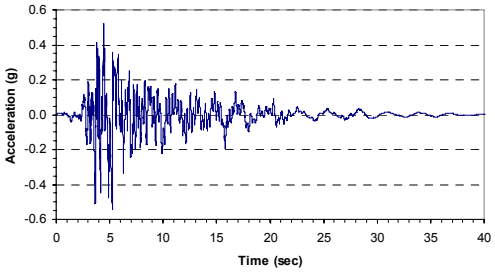

(d) Modified “250” Component

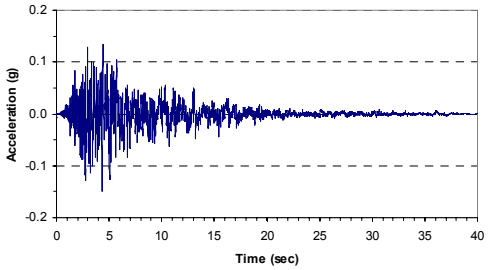

(e) Original “UP” Component

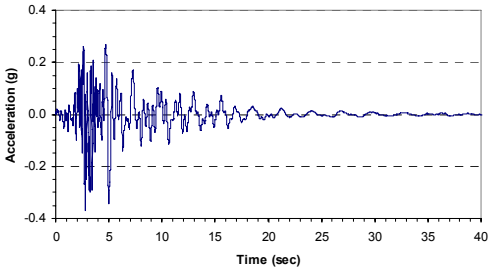

(f) Modified “UP” Component

Figure 4.42: Original and Modified Components of Time-History Record *D_real_2*

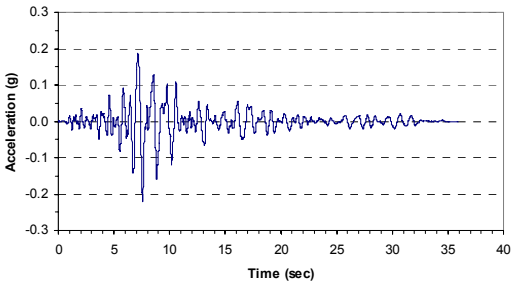

(a) Original "133" Component

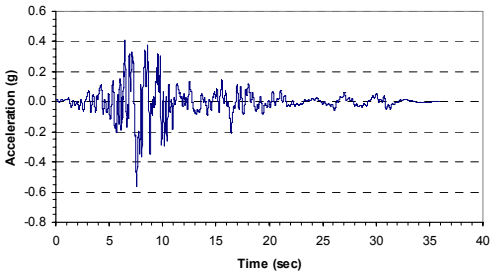

(b) Modified "133" Component

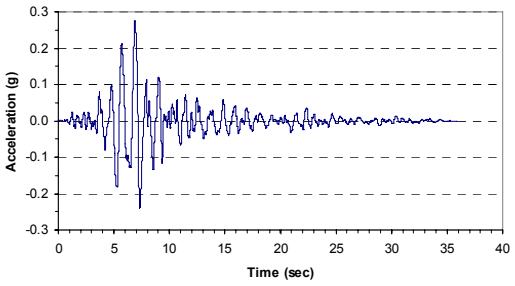

(c) Original "043" Component

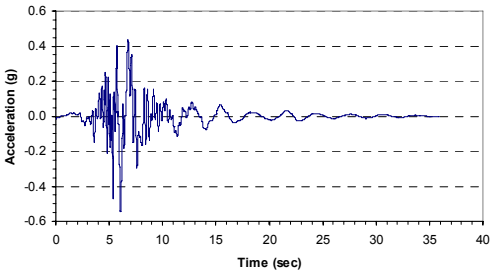

(d) Modified "043" Component

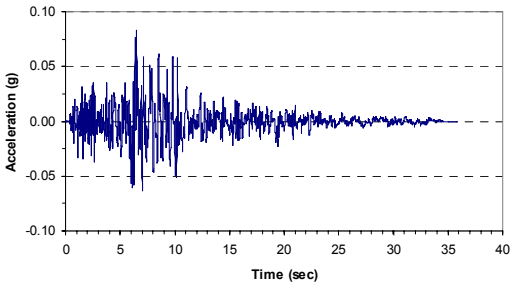

(e) Original "UP" Component

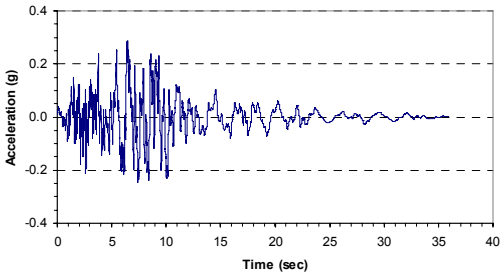

(f) Modified "UP" Component

Figure 4.43: Original and Modified Components of Time-History Record E_*real_2*

4.9.2 Rayleigh Damping

Rayleigh damping which is used in time-history analyses is defined as: [19]

$$c = a_0 m + a_1 k \tag{4.33}$$

where;

m : Mass matrix

k : Stiffness matrix

a_0 : Mass-proportional damping coefficient

a_1 : Stiffness proportional damping coefficient

The damping ratio for the nth mode:

$$\zeta_n = \frac{a_0}{2}\frac{1}{\omega_n} + \frac{a_1}{2}\omega_n \tag{4.34}$$

The coefficients a_0 and a_1 can be determined from specified damping ratios ζ_i and ζj for the ith and jth modes, respectively as:

$$\frac{1}{2}\begin{bmatrix} 1/\omega_i & \omega_i \\ 1/\omega_j & \omega_j \end{bmatrix}\begin{Bmatrix} a_0 \\ a_1 \end{Bmatrix} = \begin{Bmatrix} \zeta_i \\ \zeta_j \end{Bmatrix} \tag{4.35}$$

The relation defined in Equation 4.35 is applied for the first (in longitudinal direction) and the third mode (in vertical direction). Damping ratios of ζ_i = 0.05 and ζ_j =0.065 are specified for the 1st (in longitudinal direction) and 3rd (in vertical direction) modes respectively. The aim is to have damping ratios of the first and second (in transverse direction) modes close to the value of ζ = 0.05. As the responses in longitudinal and transverse directions are highly concerned in this study, a higher damping ratio of vertical mode is acceptable. Damping ratio versus period relationship of the case *C61* is shown in Figure 4.44 as an example. The coefficients a_0 and a_1 and damping ratios for the second mode are shown in Table 4.19.

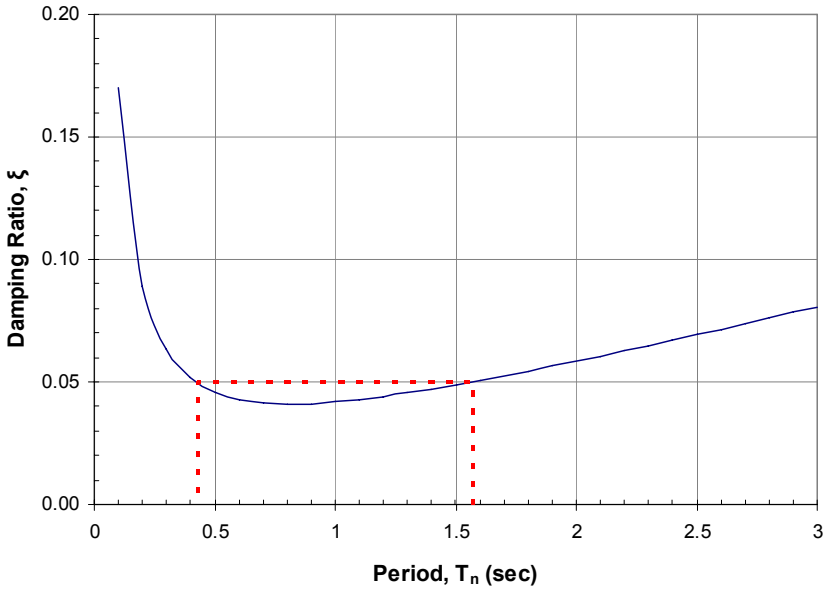

Figure 4.44: Damping Ratio versus Period for the Case *C61*

Table 4.19: Rayleigh Damping Coefficients and Damping Ratios for Second Mode

		Competent Soil			Poor Soil		
ρ_l	H_n / D	a_0 (sec^{-1})	a_1 (sec)	ζ_2	a_0 (sec^{-1})	a_1 (sec)	ζ_2
1%	5	0.3226	0.00531	0.042	0.3004	0.00537	0.040
	6	0.3148	0.00533	0.041	0.2916	0.00542	0.040
	7	0.3060	0.00535	0.041	0.2819	0.00548	0.040
	8	0.2947	0.00549	0.043	0.2705	0.00554	0.041
2%	5	0.3258	0.00531	0.042	0.3042	0.00535	0.041
	6	0.3179	0.00532	0.041	0.2957	0.00541	0.040
	7	0.3118	0.00534	0.041	0.2869	0.00546	0.040
	8	0.2994	0.00552	0.042	0.2757	0.00553	0.040
3%	5	0.3303	0.00514	0.042	0.3066	0.00533	0.041
	6	0.3210	0.00532	0.041	0.2985	0.00540	0.040
	7	0.3148	0.00533	0.041	0.2904	0.00545	0.040
	8	0.3035	0.00552	0.042	0.2801	0.00552	0.040
4%	5	0.3337	0.00513	0.042	0.3085	0.00530	0.041
	6	0.3226	0.00531	0.042	0.3006	0.00538	0.040
	7	0.3164	0.00533	0.041	0.2929	0.00544	0.040
	8	0.3064	0.00551	0.042	0.2839	0.00551	0.040

CHAPTER 5

ANALYSES RESULTS

5.1 Introduction

Outputs of push-over analyses, RSA-II, and inelastic time-history analyses are introduced in Appendix H. Resulting response measures are presented in the forthcoming sections of Chapter 5 in the form of figures and in Appendix I in the form of tables. Capacity curves, elastic displacement demands obtained from RSA-II analysis and inelastic displacement demands obtained from inelastic time-history analysis are all drawn on same graphs for comparison as shown in Appendix J.

5.2 Structural Displacement Ductility Capacities

Structural displacement ductility capacities (μ_C) are shown in Figure 5.1. The resulting values of structural displacement ductility capacities for the bridges over competent and poor soil are approximately equal since foundation displacements are eliminated. Trendlines are drawn for each series of longitudinal reinforcement ratio to see the variation of structural displacement capacities with respect to column aspect ratio.

- It is observed that the variation of structural displacement ductility capacities with respect to column aspect ratio is complicated. The reason may be supplying nonuniform amount of confining reinforcement to column sections as a result of the shear design explained in Section 4.7.2.
- Bridges having column longitudinal reinforcement ratios of ρ_l = 4 % and ρ_l = 3 % have the first and second highest structural displacement ductility

capacities, respectively. It is noticed that structural displacement ductility capacities of bridges having column longitudinal reinforcement ratios of ρ_l = 1 % are slightly higher than the ones having column longitudinal reinforcement ratios of ρ_l = 2 %.

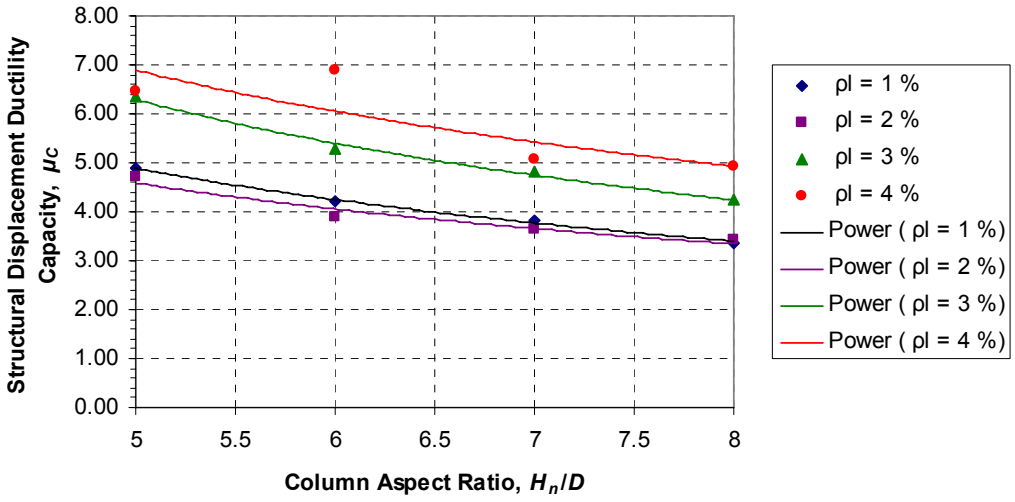

(a) Along Transverse Direction

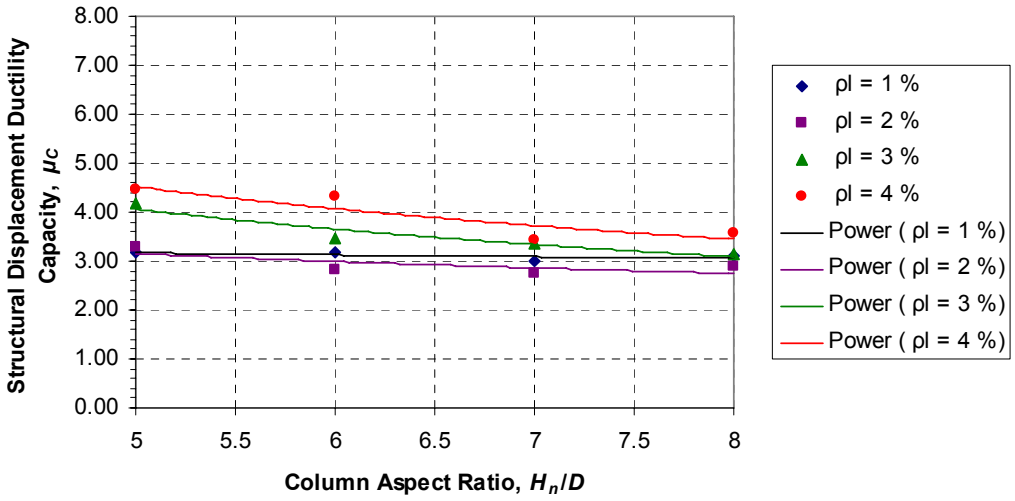

(b) Along Longitudinal Direction

Figure 5.1: Structural Displacement Ductility Capacities

- Structural displacement ductility capacities of bridges along transverse direction are higher than the ones along longitudinal direction. It is observed that resulting values of structural displacement ductility capacities along transverse and longitudinal directions do not fall below $\mu_C = 3.0$ and $\mu_C = 2.5$, respectively.

5.3 Maximum Displacement Ratios

The variation of maximum displacement ratios (C_1) with respect to column aspect ratio (H_n/D) is shown in Figure 5.2.

- Maximum displacement ratios computed along transverse direction range from 1.02 to 1.28 and from 1.0 to 1.27 at competent and poor soil conditions, respectively; while the resulting values along longitudinal direction range from 1.26 to 1.62 and from 1.15 to 1.63 at competent and poor soil conditions, respectively.
- Maximum displacement ratios computed along transverse direction are less scattered than the ones computed along longitudinal direction. The resulting values along transverse direction are closer to the border value of $C_1 = 1.0$ at which equal displacement rule is valid.
- Trendlines are drawn on the plotted data to estimate the variation of maximum displacement ratios with respect to column aspect ratio. A slight decreasing trend of maximum displacement ratios with increasing column aspect ratio is obtained along transverse direction while the opposite trend is observed with increasing column aspect ratio along longitudinal direction.
- Maximum displacement ratios computed along transverse direction for the investigated cases *P71*, *P81* and *P82* are disregarded as these models fail along transverse direction.

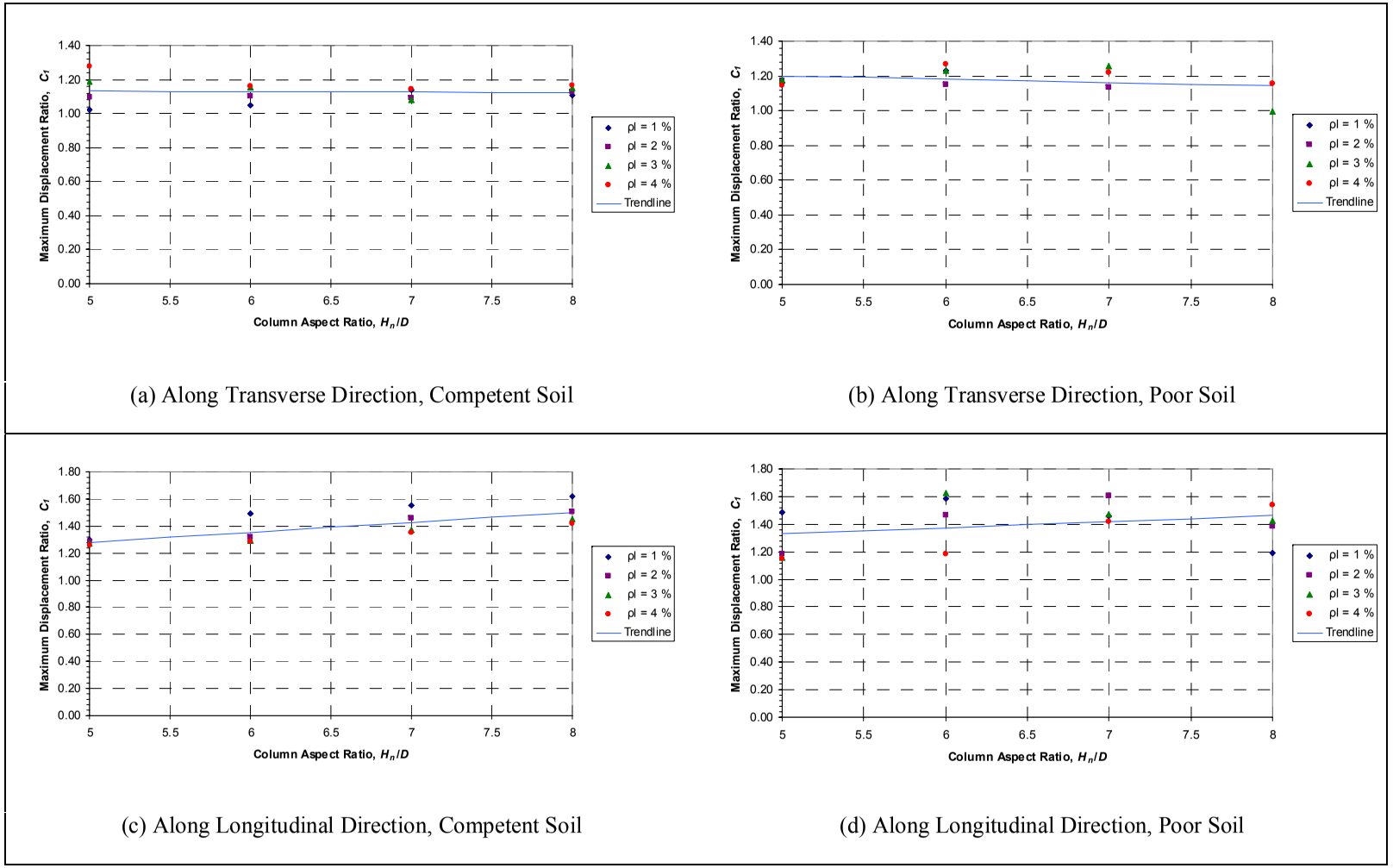

(a) Along Transverse Direction, Competent Soil

(b) Along Transverse Direction, Poor Soil

(c) Along Longitudinal Direction, Competent Soil

(d) Along Longitudinal Direction, Poor Soil

Figure 5.2: Maximum Displacement Ratios versus Column Aspect Ratio

Maximum displacement ratios versus fundamental periods of the investigated cases are plotted in Figure 5.3.

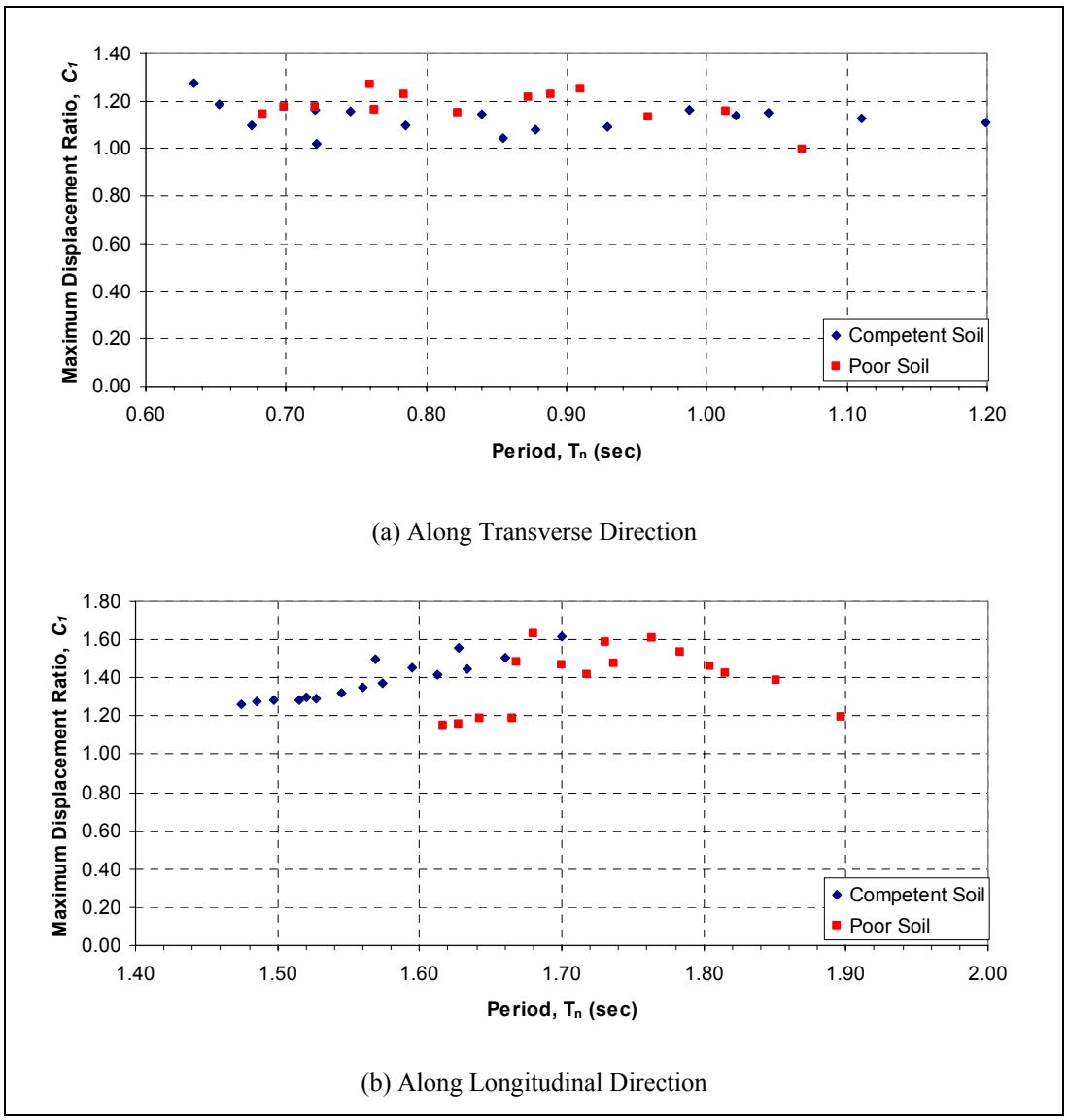

(a) Along Transverse Direction

(b) Along Longitudinal Direction

Figure 5.3: Maximum Displacement Ratios versus Period

5.4 Displacement Capacity over Demand Ratios

The variations of displacement capacity over demand ratios (*C*/*D* ratios), with either using elastic displacement demands or inelastic displacement demands, along transverse and longitudinal directions with respect to column aspect ratio (H_n/D) are shown in Figures 5.4 to 5.7. Based on these figures, the following interpretations are made:

- Displacement capacity over demand ratios decrease as bent columns get slender (from low column aspect ratio to high).
- *C*/*D* ratios get higher as column longitudinal reinforcement ratio is increased. The difference between *C*/*D* ratios resulting from different column longitudinal reinforcement ratios almost diminish at high column aspect ratios. This implies that supplying additional reinforcement to a column with low aspect ratio is more effective than supplying to a column with high aspect ratio in terms of enhancing reserved displacement capacity.
- *C*/*D* ratios of bridges at competent soil are generally larger than the *C*/*D* ratios of bridges at poor soil. The only exception observed is along transverse direction where column aspect ratio is $H_n/D = 5$ with high longitudinal reinforcement ratios. This is mostly due to additional flexibility supplied from foundation.
- *C*/*D* ratios of bridges reach to the failure limit of 1.0 at high column aspect ratios. No failure is assessed for the bridges at competent soil; while some of the bridges having high column aspect ratios and low column longitudinal reinforcement ratios are assessed to fail along transverse and longitudinal directions at poor soil. The failing cases are evaluated from the global displacement capacity over demand ratios using inelastic displacement demands and stated as follows:

  Along transverse direction : *P61*, *P71*, *P72*, *P81*, *P82*

  Along longitudinal direction : *P71*, *P81*, *P82*

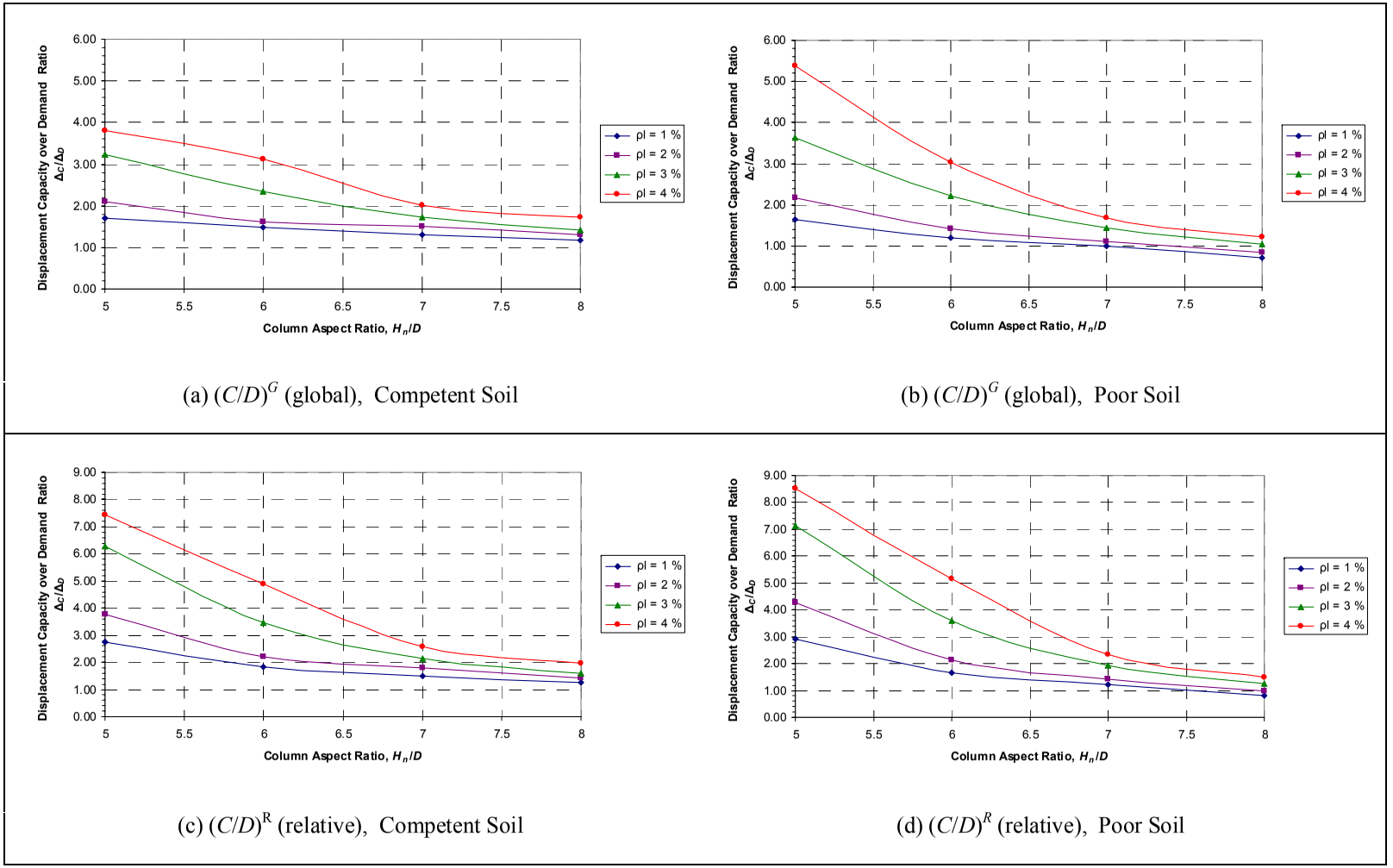

Figure 5.4: Displacement Capacity over Demand Ratios along Transverse Direction Using Elastic Displacement Demands

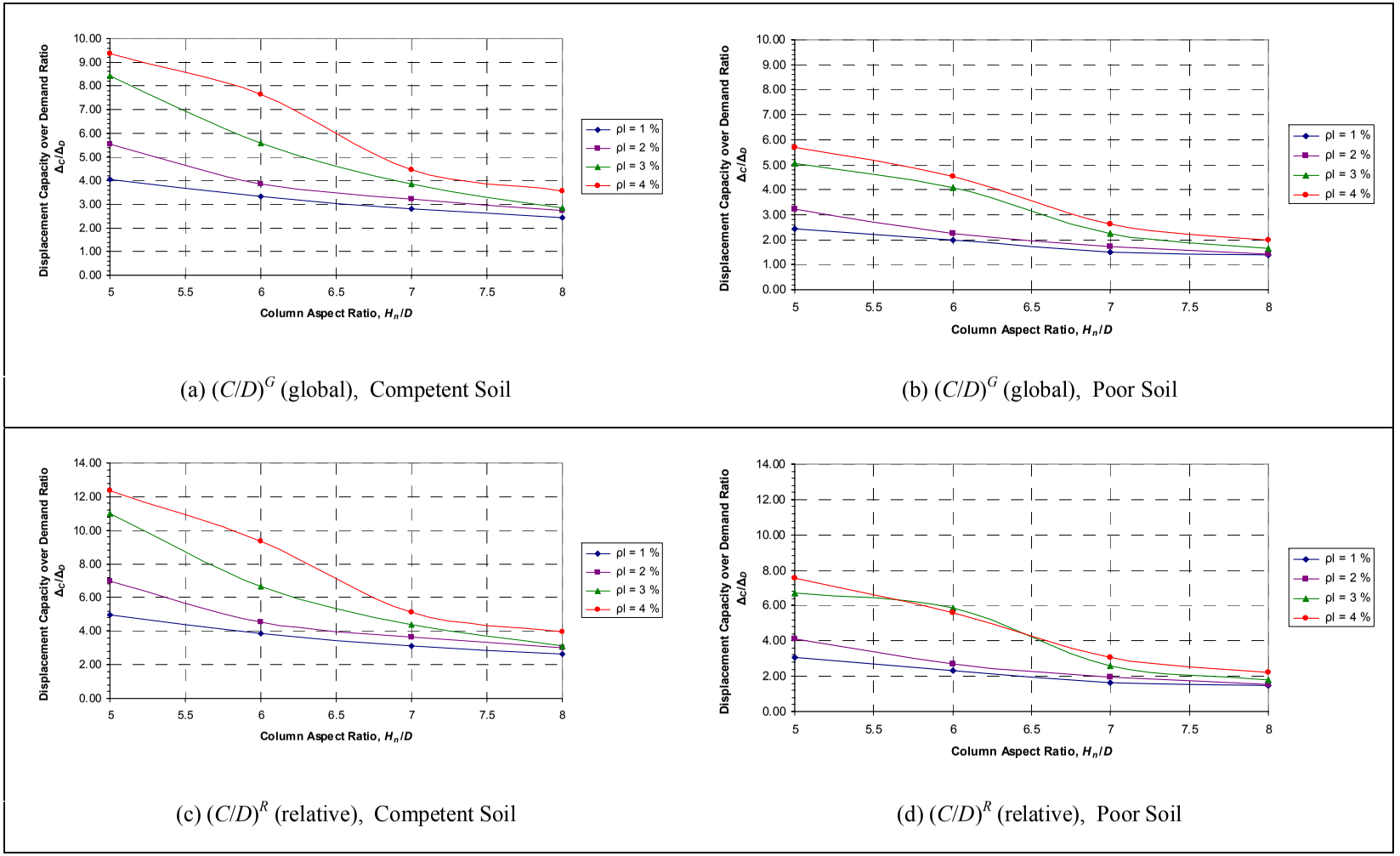

Figure 5.5: Displacement Capacity over Demand Ratios along Longitudinal Direction Using Elastic Displacement Demands

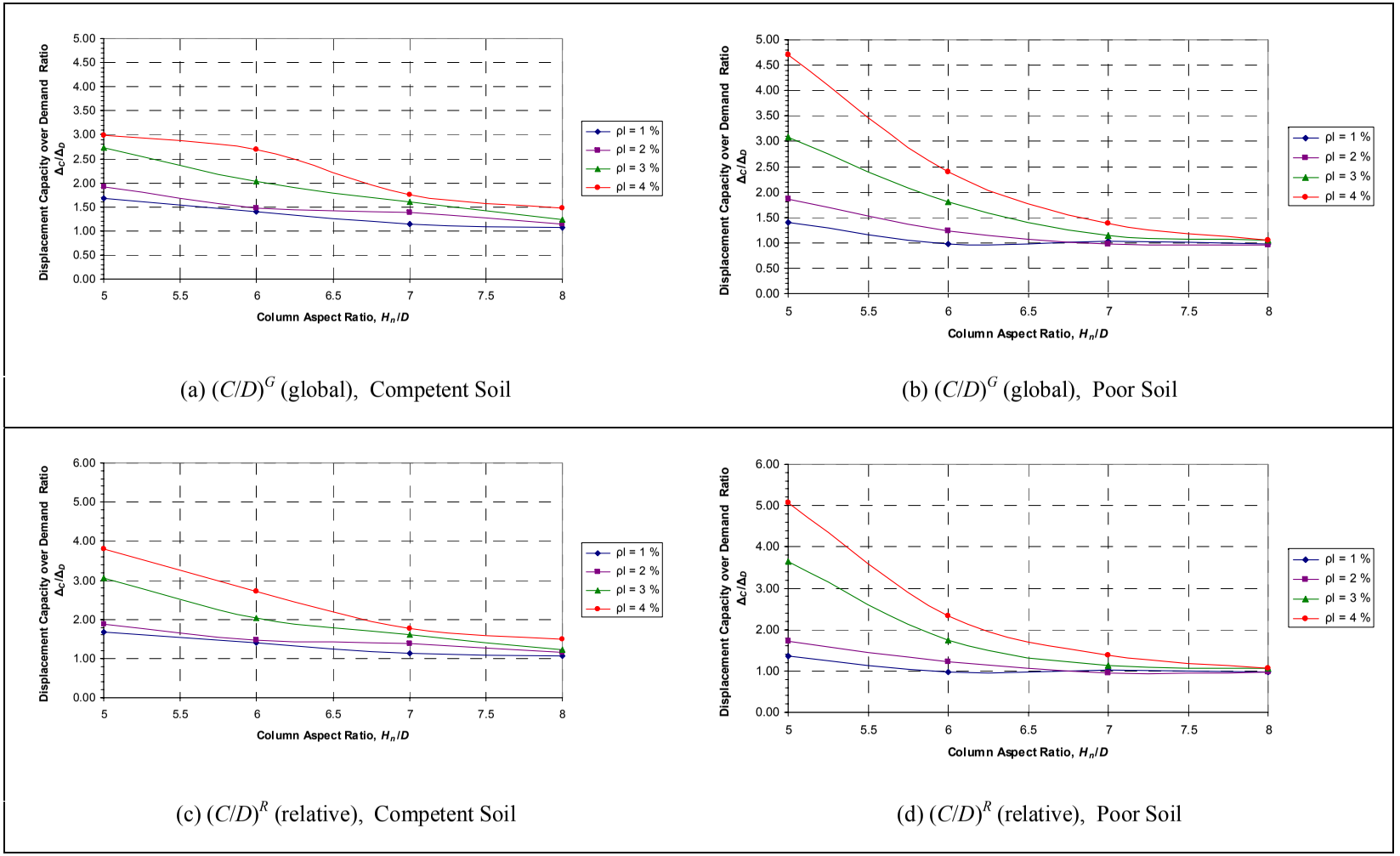

(a) $(C/D)^G$ (global), Competent Soil

(b) $(C/D)^G$ (global), Poor Soil

(c) $(C/D)^R$ (relative), Competent Soil

(d) $(C/D)^R$ (relative), Poor Soil

Figure 5.6: Displacement Capacity over Demand Ratios along Transverse Direction Using Inelastic Displacement Demands

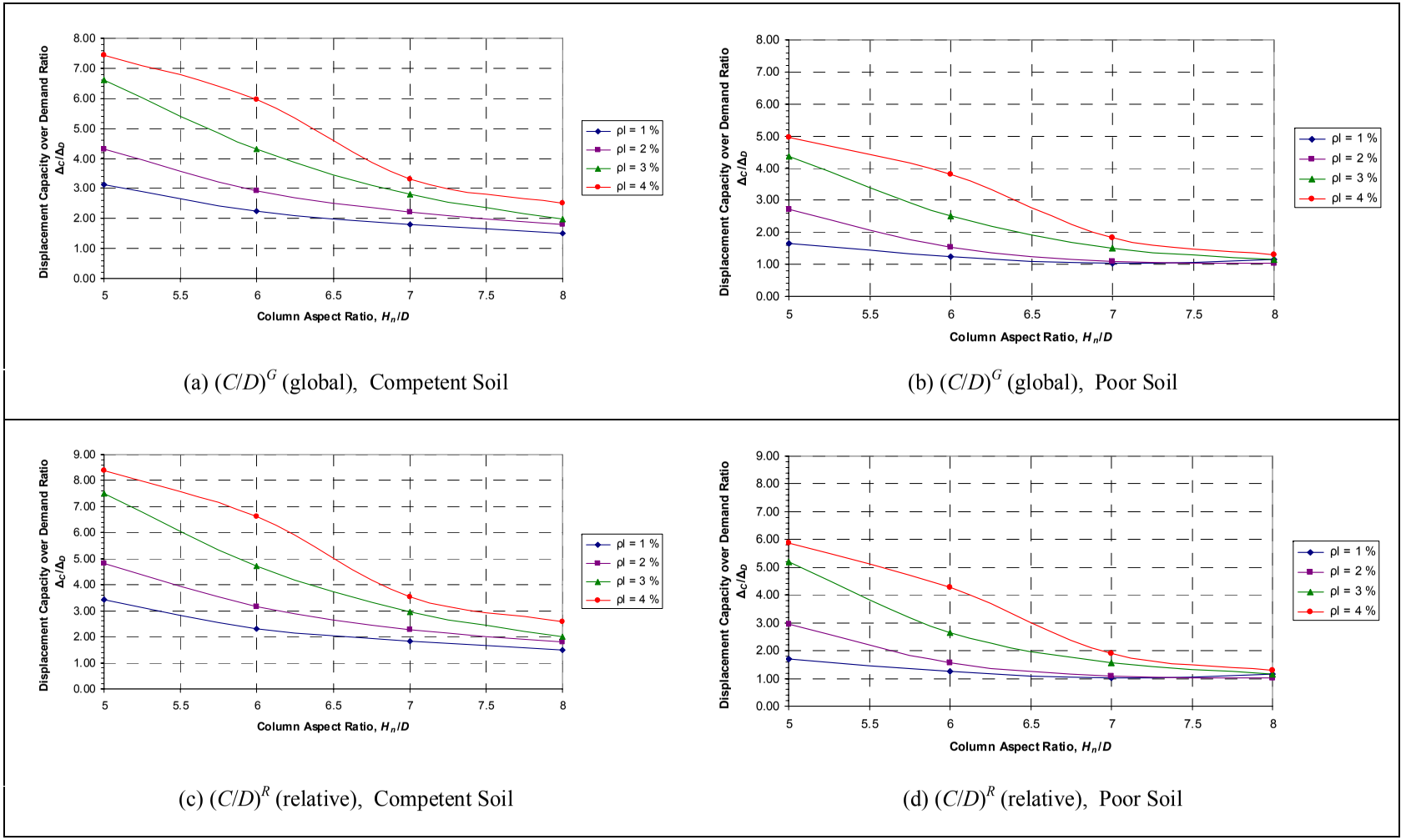

Figure 5.7: Displacement Capacity over Demand Ratios along Longitudinal Direction Using Inelastic Displacement Demands

- *C*/*D* ratios computed using relative displacements are generally higher than the ones computed in global. The difference between global and relative *C*/*D* ratios gets smaller as column aspect ratio increases, and even in some cases with slender columns they are identical. The reason is that contribution of foundation flexibility decreases as columns get slender. This effect is smaller when *C*/*D* ratios are computed using inelastic displacement demands.

5.5 Global Displacement Ductility Demands

The variations of global displacement ductility demands (μ_D), using elastic displacement demands and inelastic displacement demands, with respect to column aspect ratio (H_n/D) are shown in Figures 5.8 and 5.9. Based on these figures, the following interpretations are made:

- Global displacement ductility demands increase as columns get slender. This increase is greater for the bridges over poor soil than the ones over competent soil. Besides, bridges with high longitudinal reinforcement ratios have low global displacement ductility demands compared to others.
- Global displacement ductility demands computed at poor soil are generally higher than the ones computed at competent soil.
- Global displacement ductility demands (using inelastic displacement demands) are not considered for the failed models in which displacement capacity over demand ratios, $(\Delta_C)^G_{inelastic}/(\Delta_D)^G$ are smaller than one. The reason is that global inelastic displacement demand can reach to global displacement capacity at most. If these models had larger displacement capacities, it could be possible to capture higher inelastic displacement demands. This phenomenon can be observed in Figure 5.9(b) as increasing trend of μ_D along transverse direction stops after $H_n/D = 6$ for $\rho_l = 1\%$ and $H_n/D = 7$ for $\rho_l = 2\ \%$ and $\rho_l = 3\ \%$.

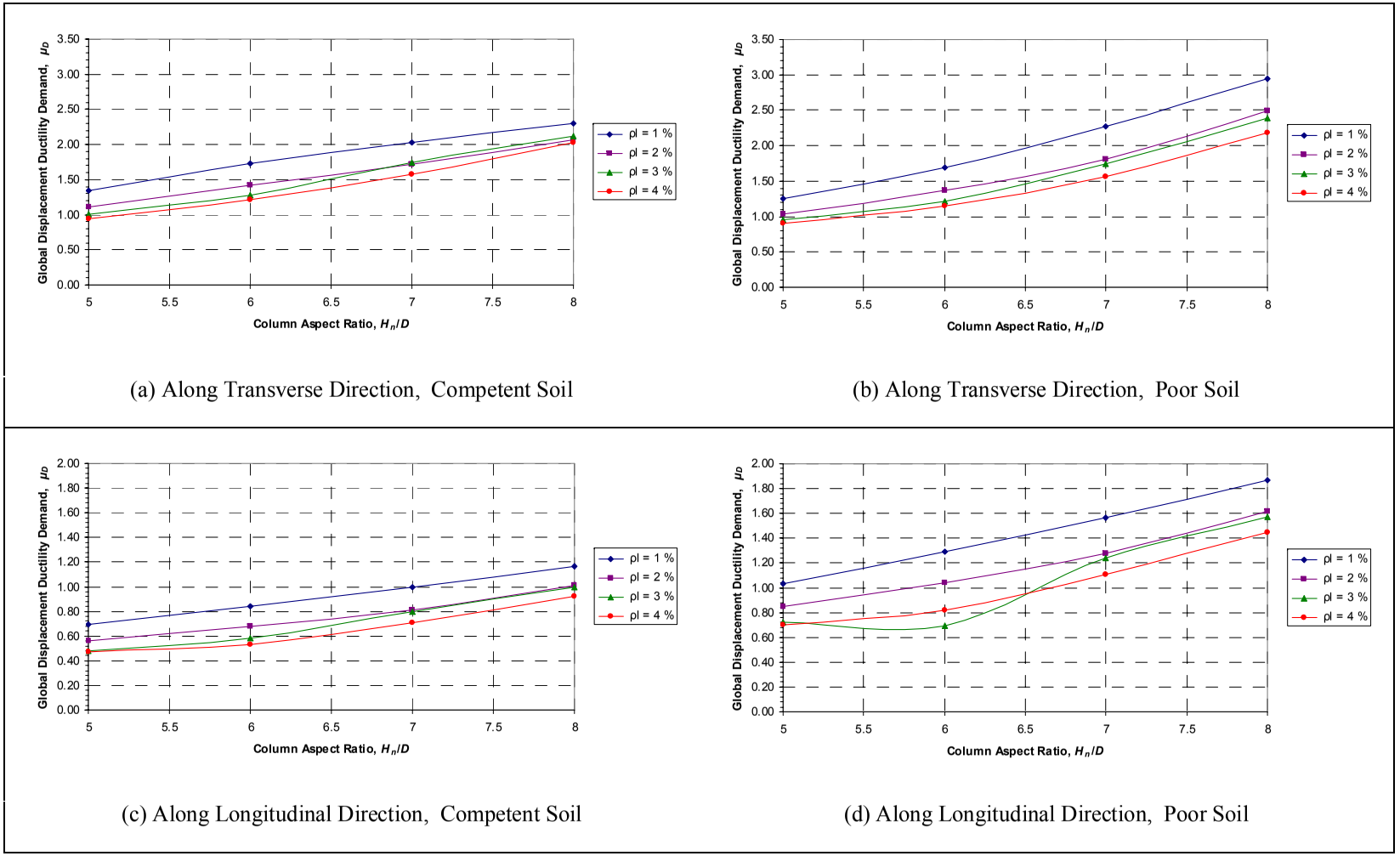

(a) Along Transverse Direction, Competent Soil

(b) Along Transverse Direction, Poor Soil

(c) Along Longitudinal Direction, Competent Soil

(d) Along Longitudinal Direction, Poor Soil

Figure 5.8: Global Displacement Ductility Demands Using Elastic Displacement Demands

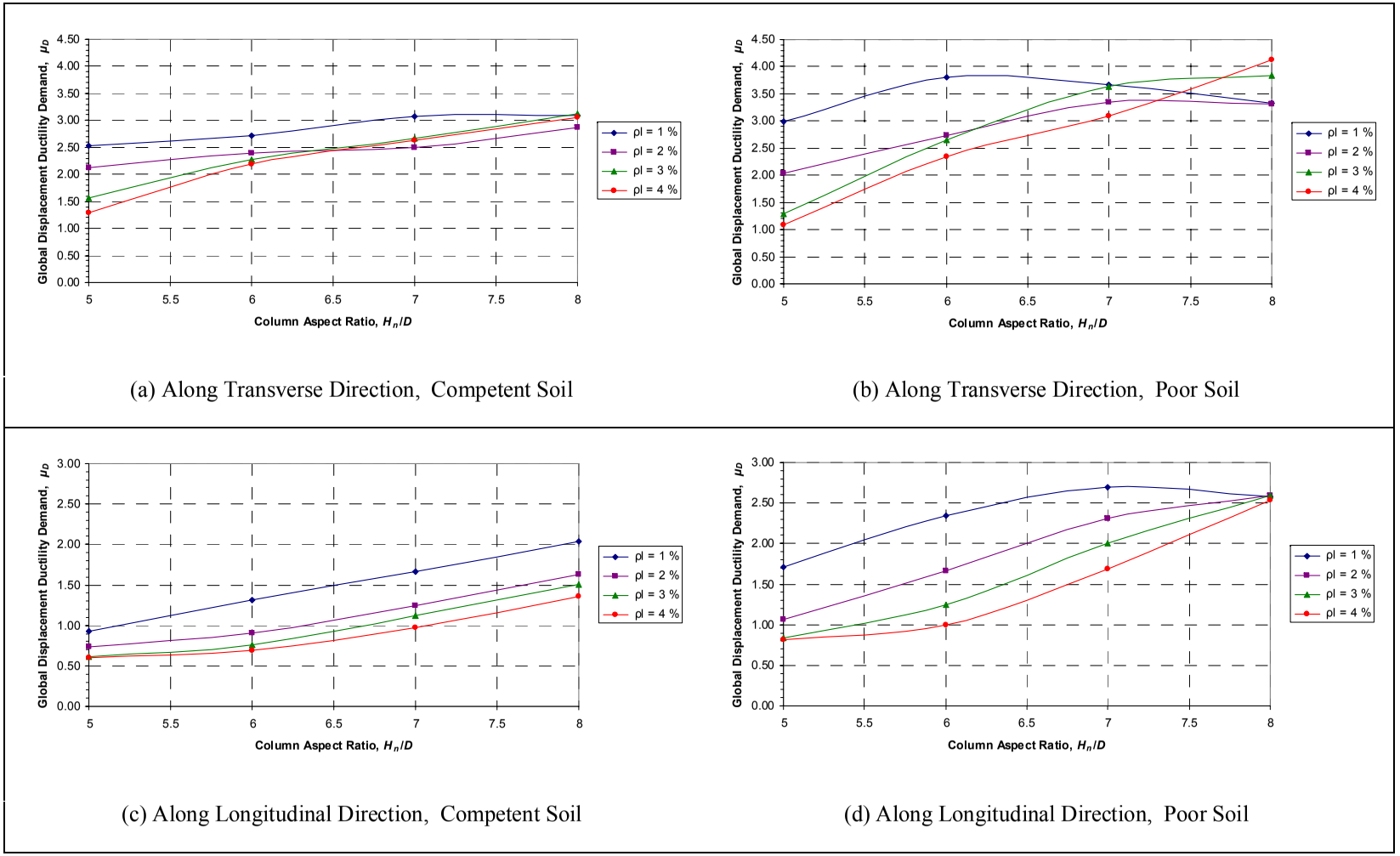

(a) Along Transverse Direction, Competent Soil

(b) Along Transverse Direction, Poor Soil

(c) Along Longitudinal Direction, Competent Soil

(d) Along Longitudinal Direction, Poor Soil

Figure 5.9: Global Displacement Ductility Demands Using Inelastic Displacement Demands

- Global displacement ductility demands determined along transverse direction are higher compared to the ones determined along longitudinal direction.
- Global displacement ductility demands determined using elastic displacements are lower than those determined from using inelastic displacements. This is mostly due to the contribution of foundation flexibility displacements to global yield displacement. It is observed that elastic displacements attributed to foundation flexibility determined as a result of the iteration performed in response spectrum analyses are higher as compared to those attained in inelastic time-history analyses.

5.6 Response Modification Factors for Columns

The variation of response modification factors for columns (R) with respect to column aspect ratio (H_n/D) is shown in Figure 5.10. Response modification factors computed are called "R-factor demand" throughout this section. Based on Figure 5.10, the following interpretations are made:

- As bent columns get slender, R-factor demands increase. Most of the fundamental periods of the investigated bridges fall on the descending portion of the design response spectra that results in a decrease in spectral accelerations and implicitly force demands as columns get slender (periods elongate). Maximum range of spectral accelerations is 0.79 – 0.51 g along transverse direction at competent soil conditions. This range is much narrower along longitudinal direction. However, decrease in moment capacities of sections with the decrease in section dimension governs the increase in R-factor demands.

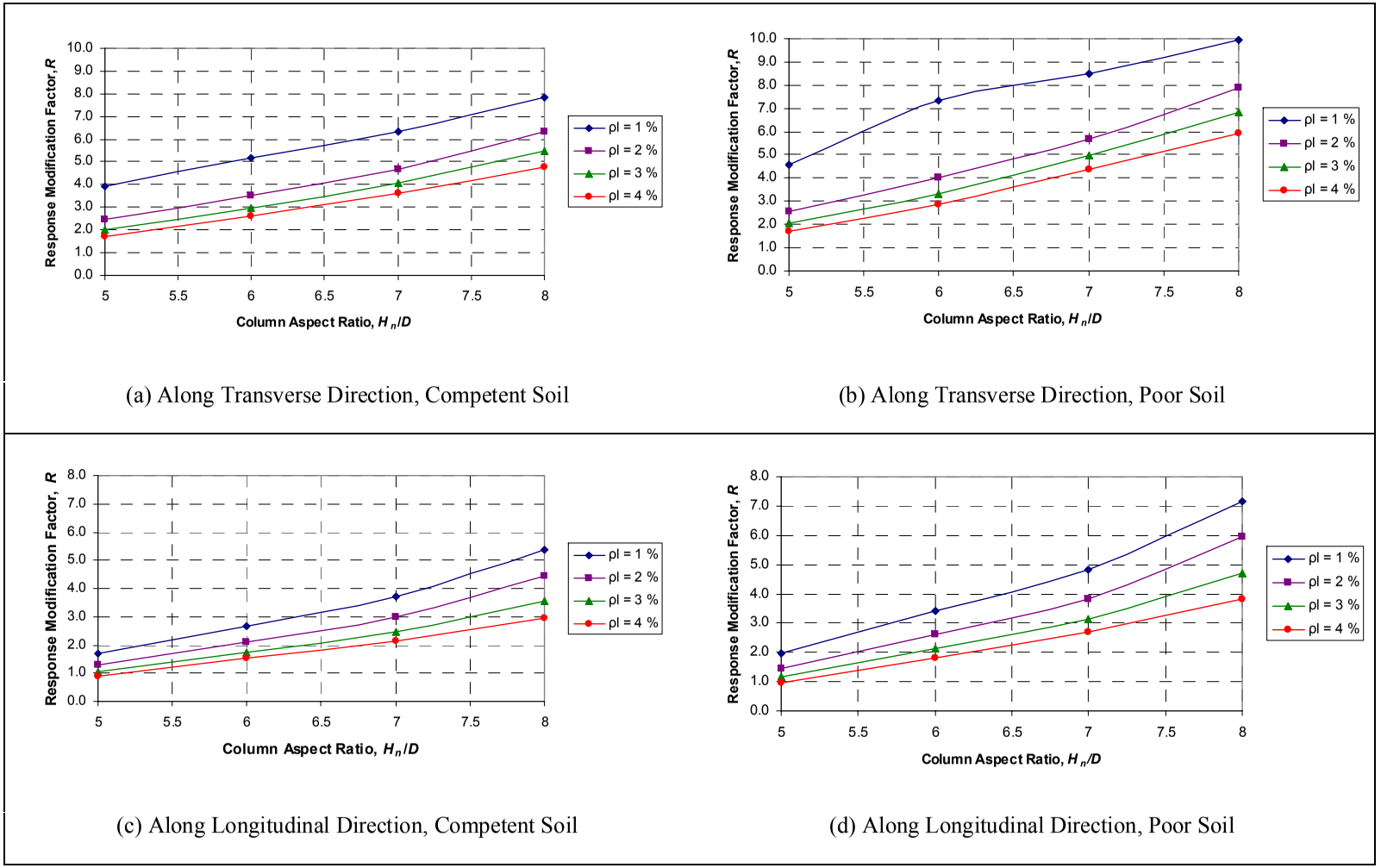

(a) Along Transverse Direction, Competent Soil

(b) Along Transverse Direction, Poor Soil

(c) Along Longitudinal Direction, Competent Soil

(d) Along Longitudinal Direction, Poor Soil

Figure 5.10: Response Modification Factors for Columns

- Columns having higher longitudinal reinforcement ratios have smaller *R*-factor demands due to the increase of moment strength provided by reinforcement. Increasing longitudinal reinforcement of stiff bridge columns is not as effective as increasing longitudinal reinforcement of less stiff bridge columns in terms of decreasing *R*-factor demands.
- *R*-factor demands of bridges computed at poor soil conditions are mainly higher than the ones computed at competent soil conditions due to the higher force demands of bridges over poor soil. However, the contribution of foundation flexibility reduces the moment demands of very stiff columns making the difference of *R*-factor demands at different soil conditions diminish.
- *R*-factor demands computed along longitudinal direction are lower than the ones computed along transverse direction. The main reason is that total longitudinal moment demands are almost distributed equally to each pier. On the other hand, the middle pier gets the greatest moment demand among all piers in transverse direction. Besides, the increase in axial tension occurring along transverse direction decrease moment capacities significantly. The other reason is that fundamental periods along longitudinal direction are all longer than the periods along transverse direction causing seismic demands along longitudinal direction reduced compared to transverse direction.

5.7 Concrete and Steel Strains

The variations of maximum concrete strains (ε_c) and steel strains (ε_s) computed along transverse and longitudinal directions with respect to column aspect ratio (H_n/D) are shown in Figures 5.11 and 5.12. Based on these figures, the following interpretations are made:

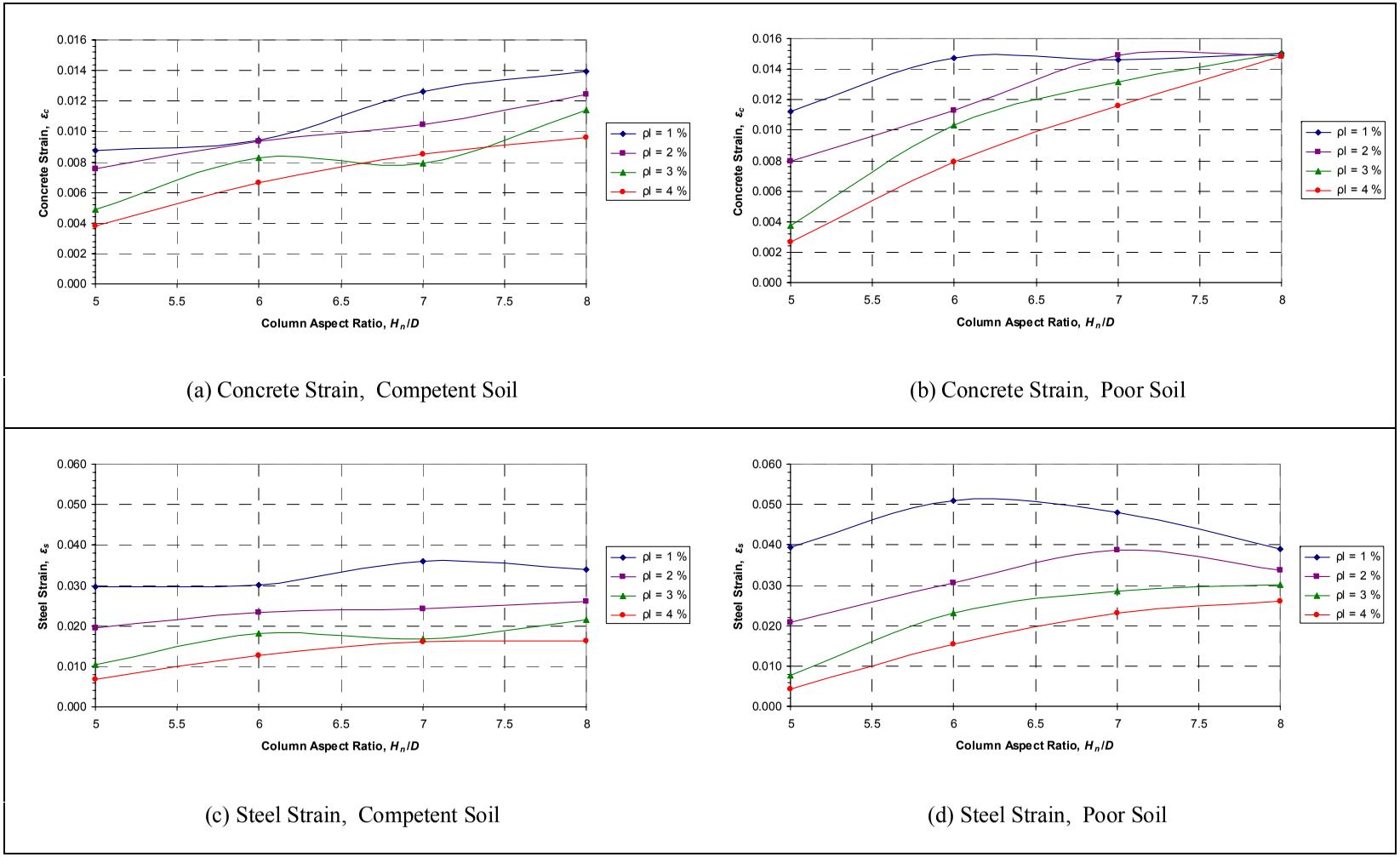

(a) Concrete Strain, Competent Soil

(b) Concrete Strain, Poor Soil

(c) Steel Strain, Competent Soil

(d) Steel Strain, Poor Soil

Figure 5.11: Maximum Concrete and Steel Strains for Loading in Transverse Direction

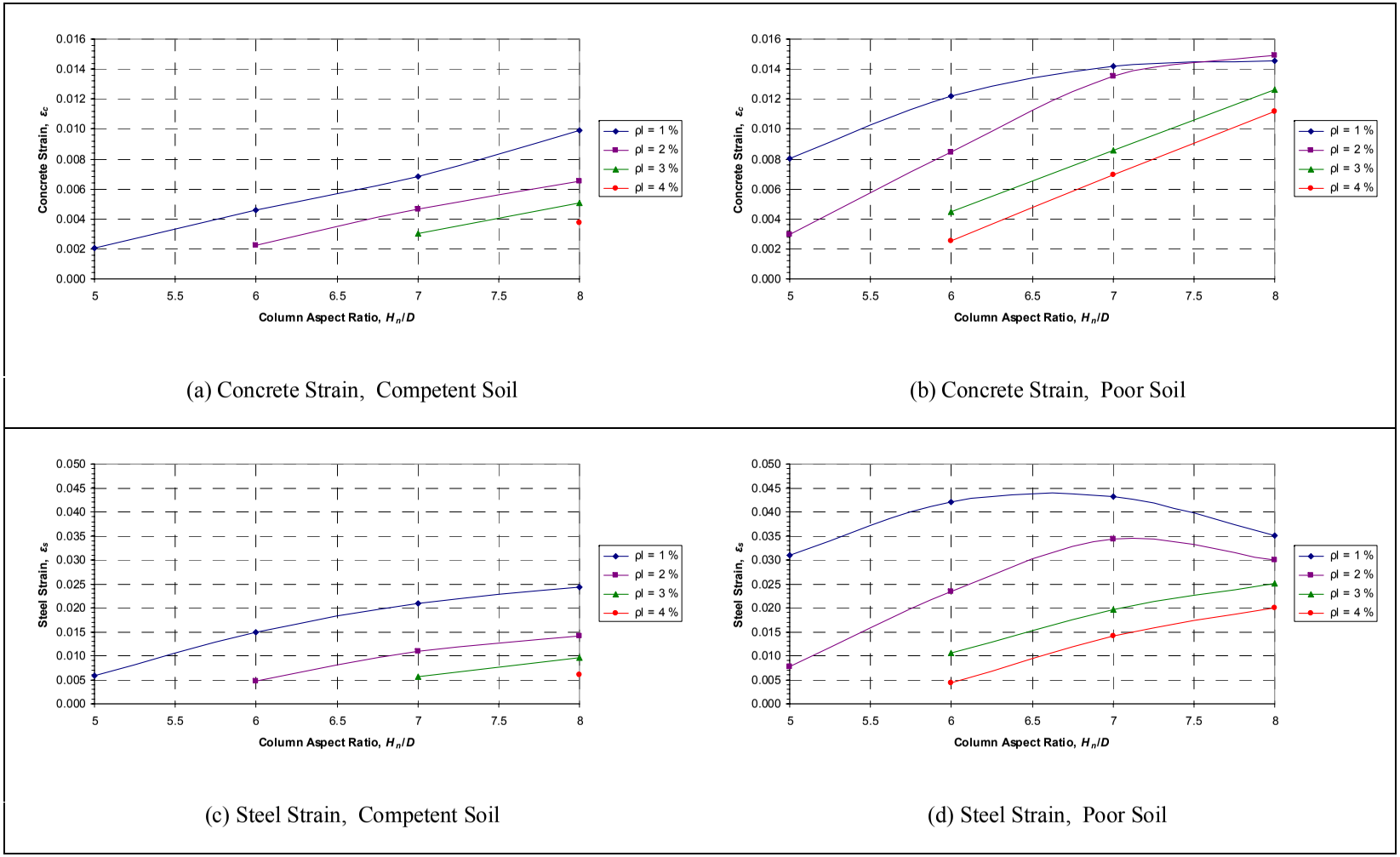

(a) Concrete Strain, Competent Soil

(b) Concrete Strain, Poor Soil

(c) Steel Strain, Competent Soil

(d) Steel Strain, Poor Soil

Figure 5.12: Maximum Concrete and Steel Strains for Loading in Longitudinal Direction

- Slender columns are more strained than stiff columns.
- Strain values of bridge columns computed at poor soil are generally higher than the ones computed at competent soil except for the bridges having stiff columns with H_n/D = 5 and ρ_l = 3 % and ρ_l = 4 % in transverse direction.

  As column aspect ratios reach H_n/D = 8, the concrete strains of failing models converge to a strain value of approximately ε_c = 0.015 which is the corresponding ultimate crushing strain of confined concrete. The same behavior is not observed for the cases having high longitudinal and high confining reinforcement which postpone failure beyond the aspect ratio of H_n/D = 8. For the bridges having column longitudinal reinforcement ratios of 1 % and 2 %, the decreasing trend of steel strains with increasing column aspect ratio beyond the first failing case is disregarded.
- It is observed that the graphs drawn for longitudinal direction have some missing points. The reason is that critical bent columns of some investigated bridges do not encounter any plastic rotation in longitudinal direction at any inelastic time history analysis. Hence, strain values corresponding to maximum displacement demands of these bridges are not captured and plotted on the graphs of concrete and steel strains. These bridges are designated as elastic along longitudinal direction and are listed as follows:

  At competent soil : *C52*, *C53*, *C63*, *C54*, *C64*, *C74*

  At poor soil : *P53*, *P54*

5.8 Correlation of Damage Levels with Response Measures

In order to correlate damage levels with computed seismic response measures, the input parameters of column aspect ratio and column longitudinal reinforcement ratio are eliminated by plotting computed seismic response measure values for

each investigated case with the corresponding maximum concrete and steel strains. Correlations constructed for three types of seismic response measures are listed as:

Figures 5.13-5.16: Global and relative displacement capacity over demand ratios (C/D) with using either elastic displacement demands or inelastic displacement demands
Figures 5.17-5.18: Global displacement ductility demands (μ_D) using either elastic displacement demands or inelastic displacement demands
Figures 5.19-5.20: Response modification factors for columns (R) along transverse and longitudinal directions

For constructing the correlations of displacement capacity over demand ratios and global displacement ductility demands with concrete and steel strains, the data coming from both directions are utilized. Thus, direction parameter is taken out of consideration giving more importance to the governing direction indirectly. Besides, reliability of trendlines increases as number of data increases.

Response modification factor is a forced based design parameter which is considered separately along different directions in practice. Therefore, throughout the process related to response modification factor, data obtained from both directions are not combined. As a result; at competent soil condition extrapolation of limited data is necessitated for determination of estimated R-factor value in longitudinal direction corresponding to significant damage level using concrete strains. (Figure 5.20 (a))

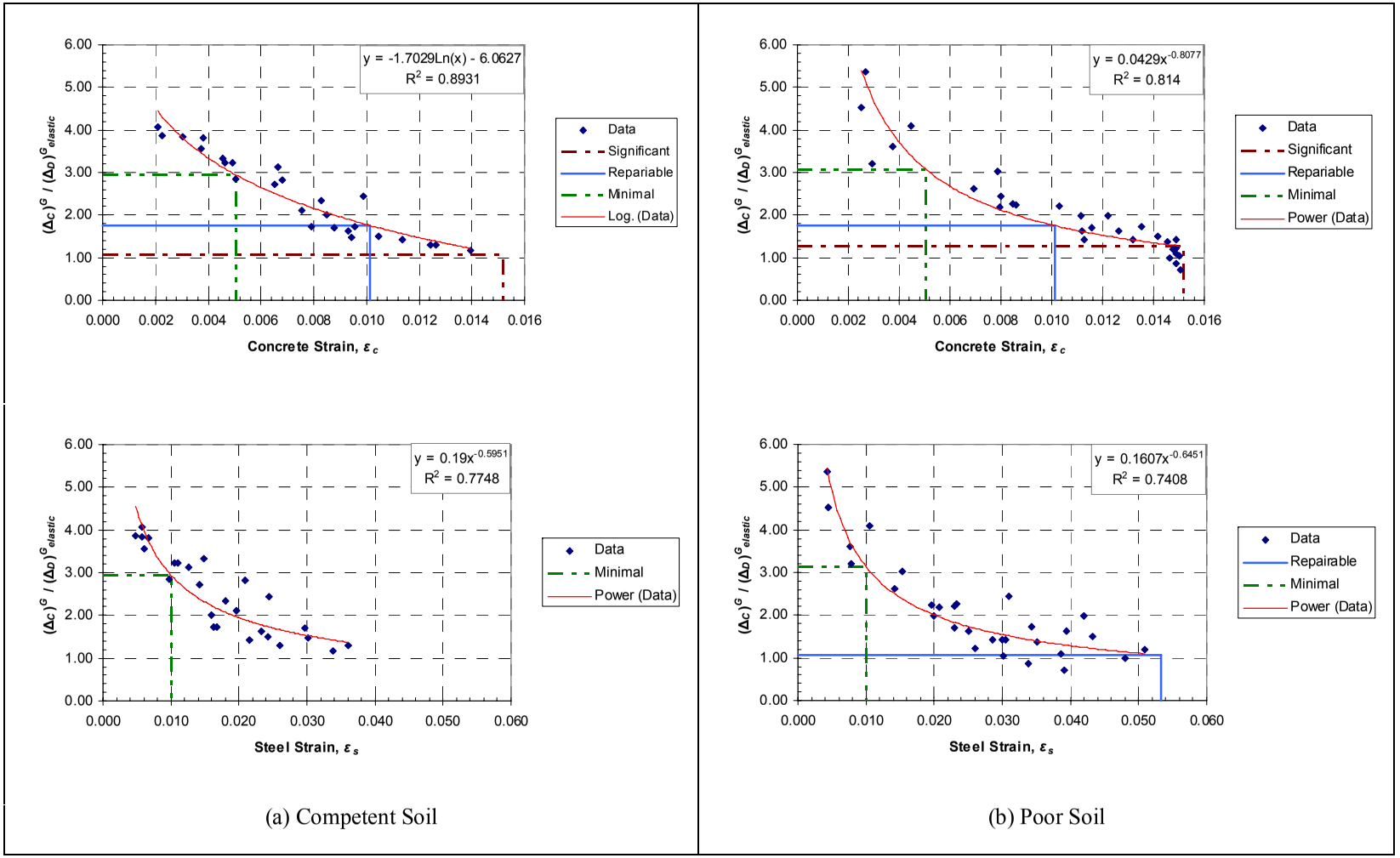

(a) Competent Soil

(b) Poor Soil

Figure 5.13: Global Displacement capacity over Demand Ratios (Δ_D = elastic) versus Concrete and Steel Strains

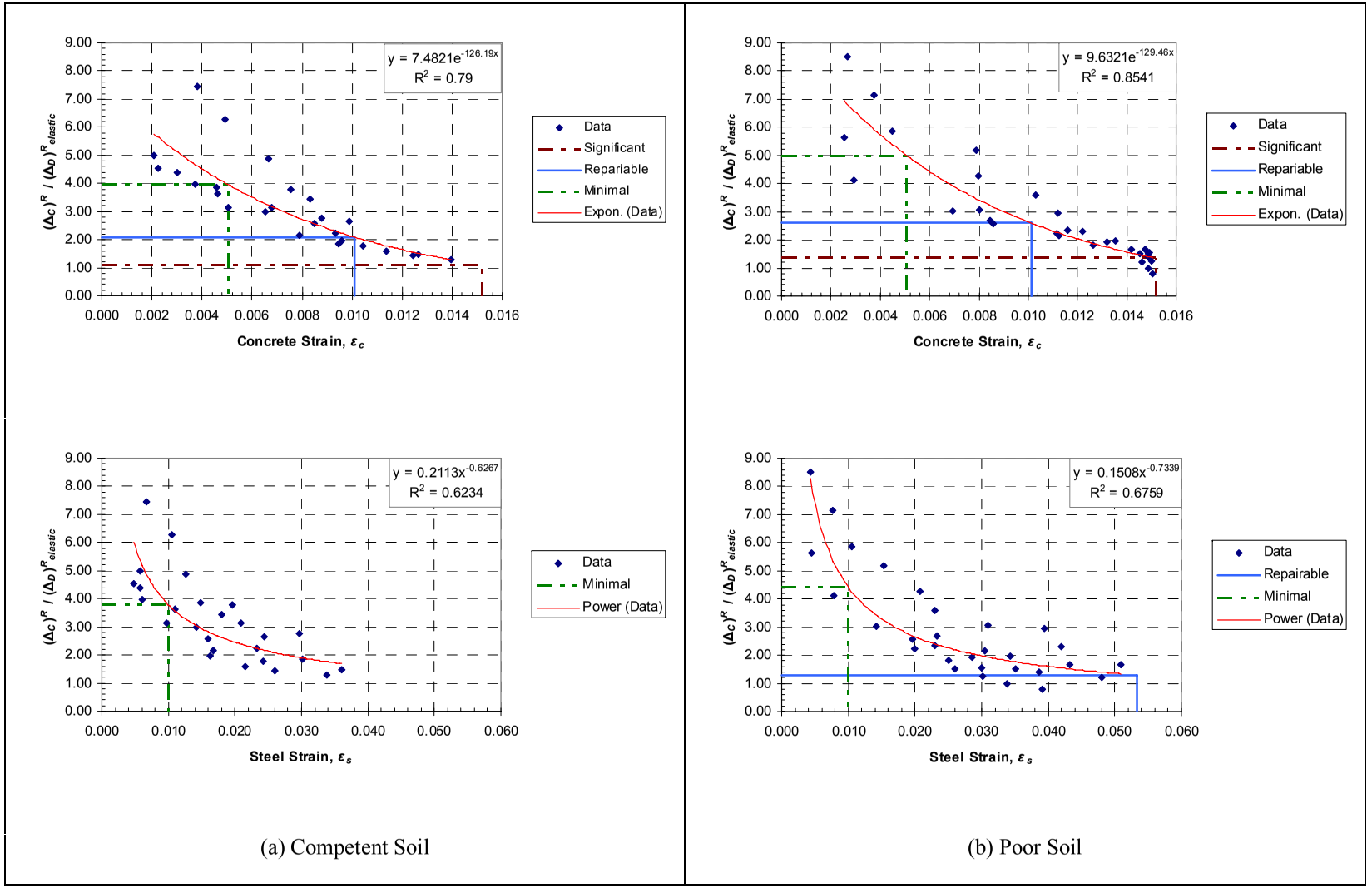

(a) Competent Soil

(b) Poor Soil

Figure 5.14: Relative Displacement Capacity over Demand Ratios (Δ_D = elastic) versus Concrete and Steel Strains

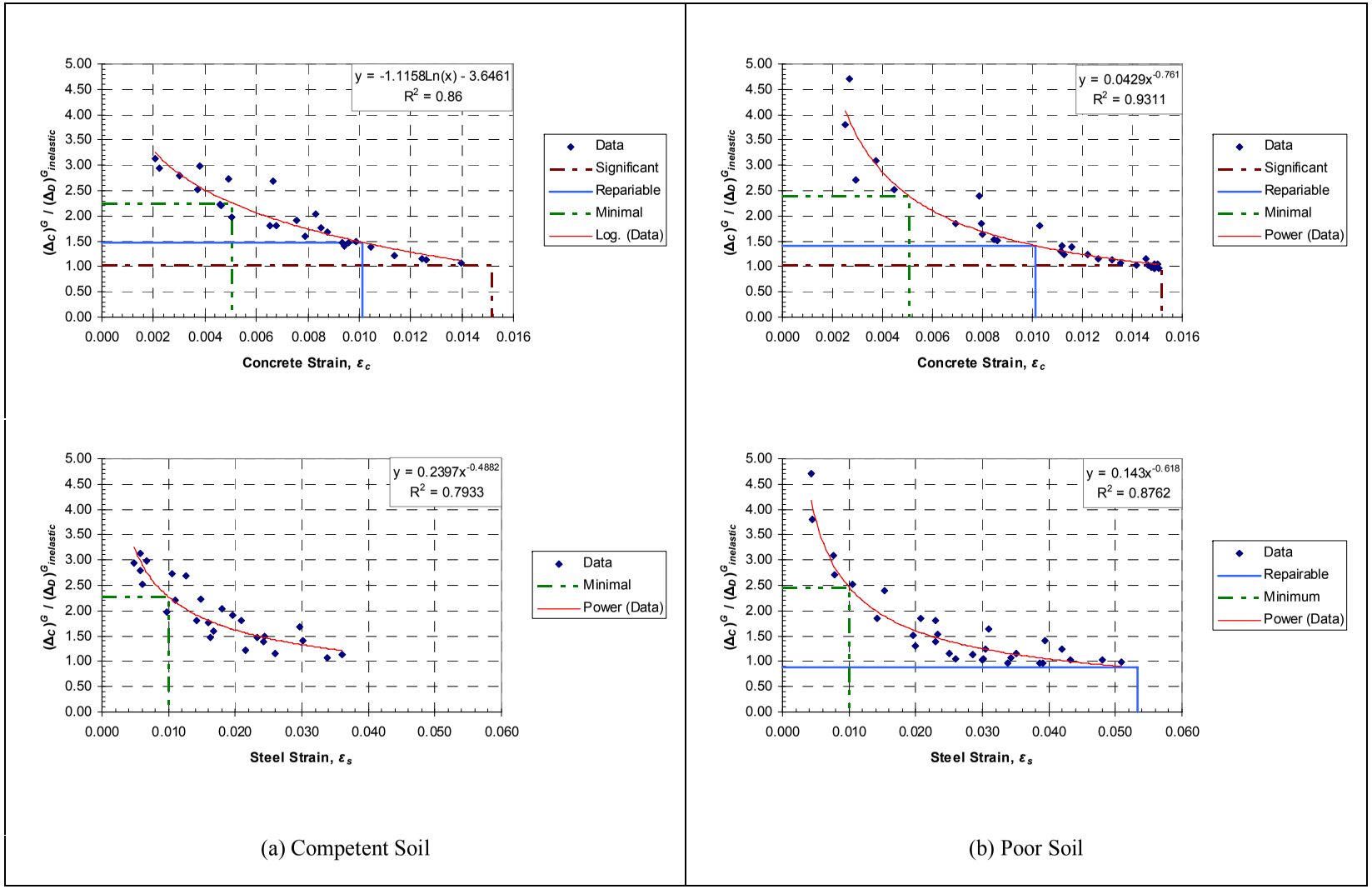

(a) Competent Soil

(b) Poor Soil

Figure 5.15: Global Displacement Capacity over Demand Ratios (Δ_D = inelastic) versus Concrete and Steel Strains

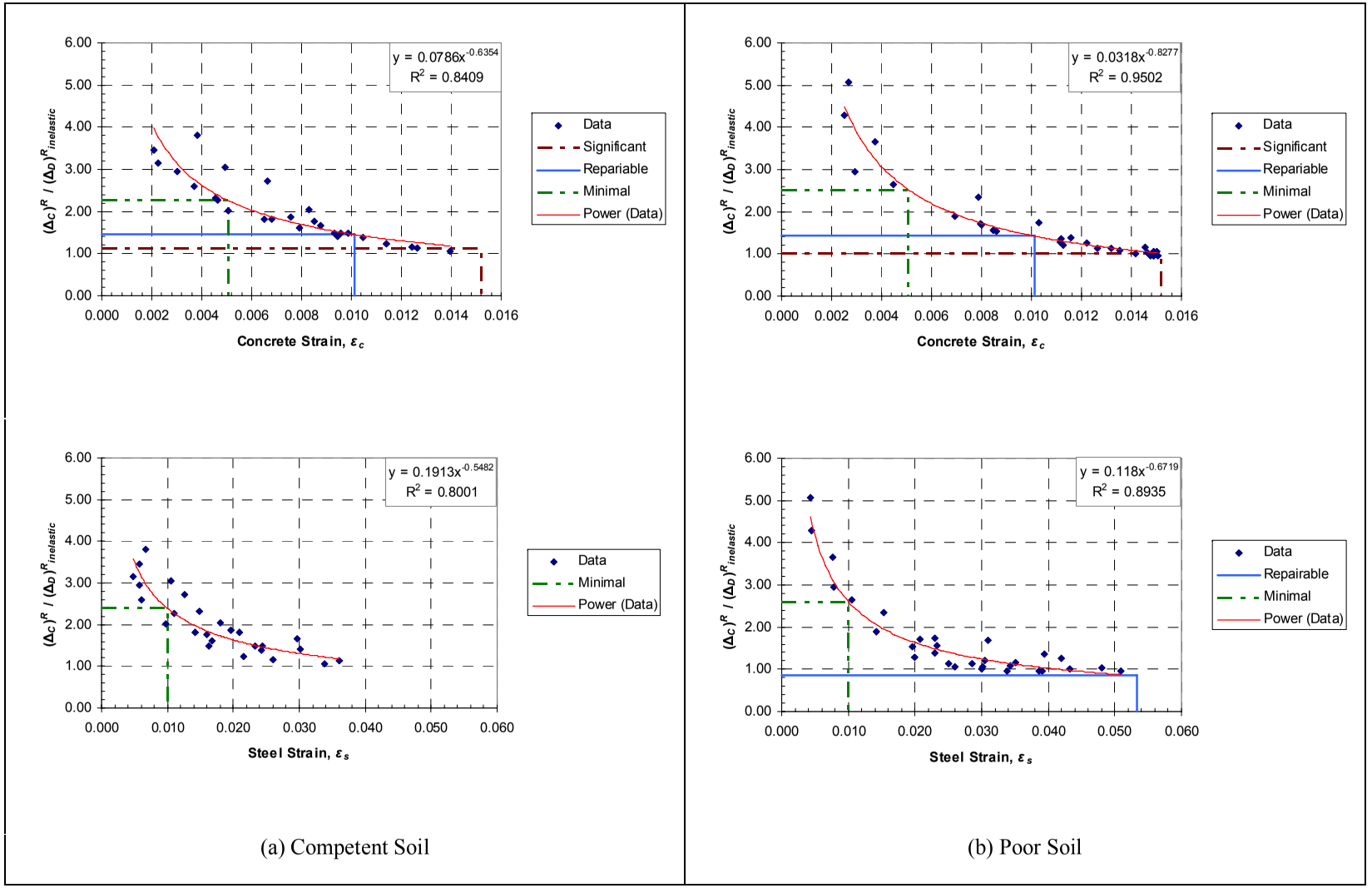

(a) Competent Soil

(b) Poor Soil

Figure 5.16: Relative Displacement Capacity over Demand Ratios (Δ_D = inelastic) versus Concrete and Steel Strains

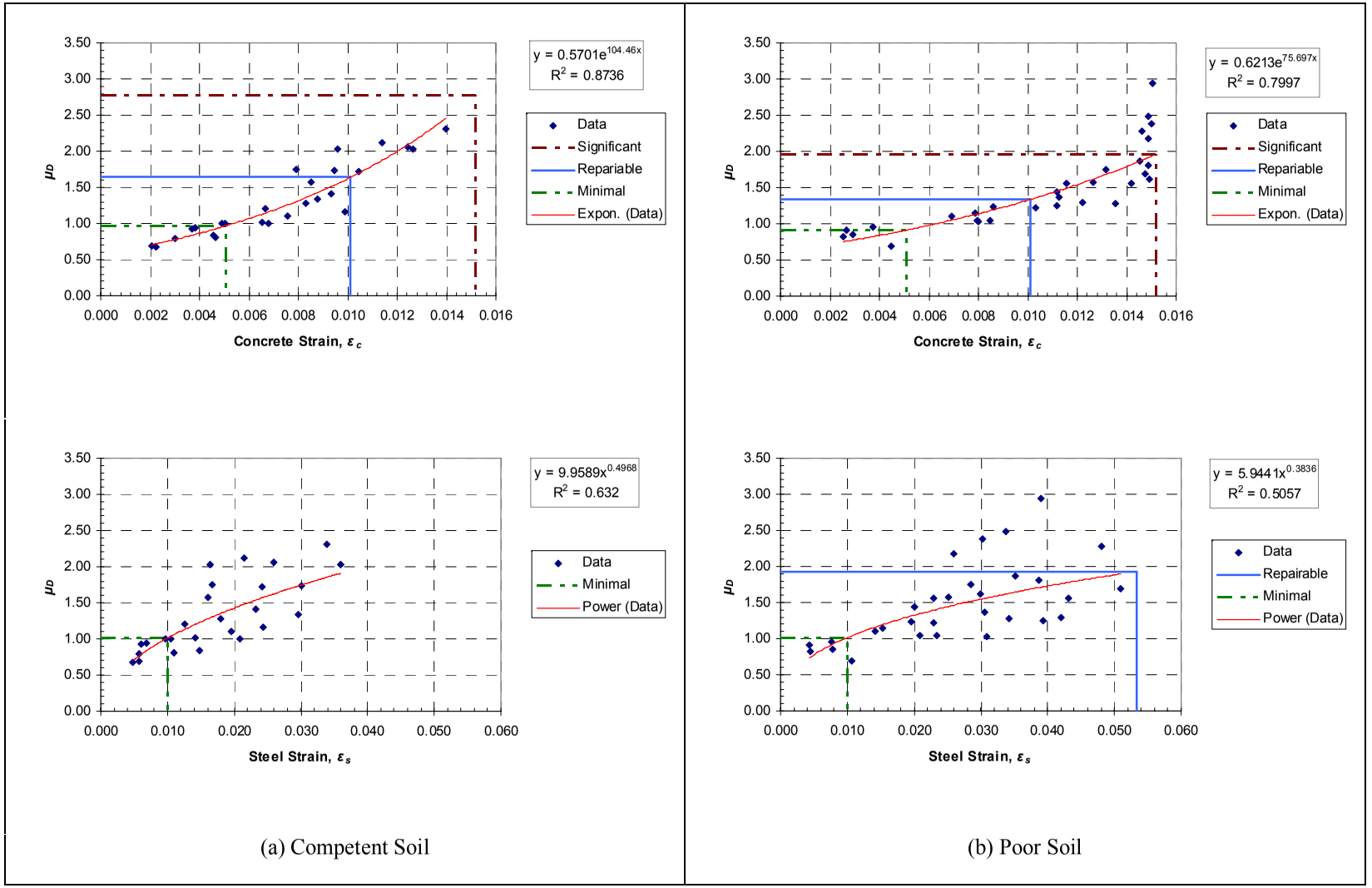

(a) Competent Soil

(b) Poor Soil

Figure 5.17: Global Displacement Ductility Demand (Δ_D = elastic) versus Concrete and Steel Strains

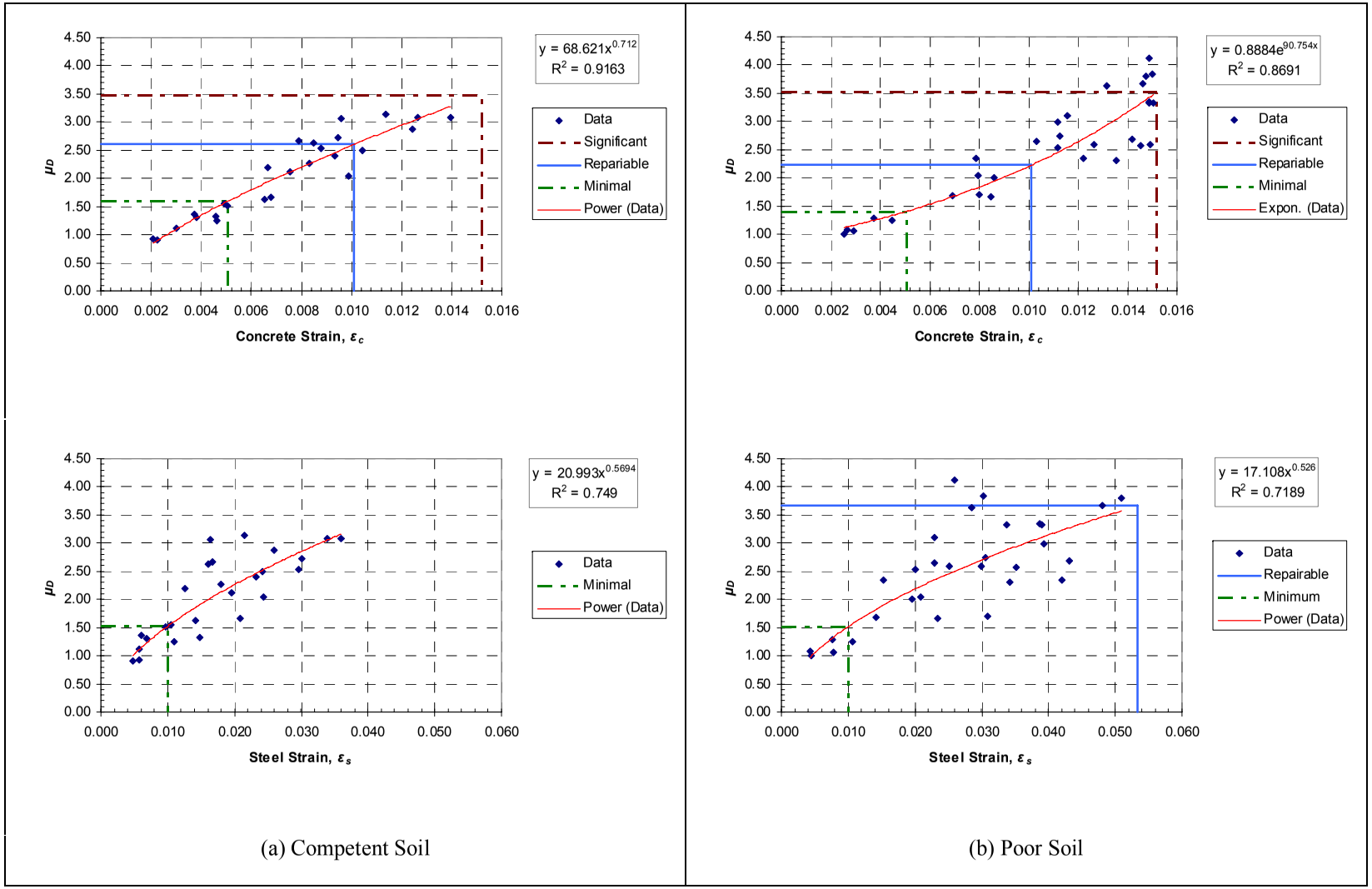

(a) Competent Soil

(b) Poor Soil

Figure 5.18: Global Displacement Ductility Demand (Δ_D = inelastic) versus Concrete and Steel Strains

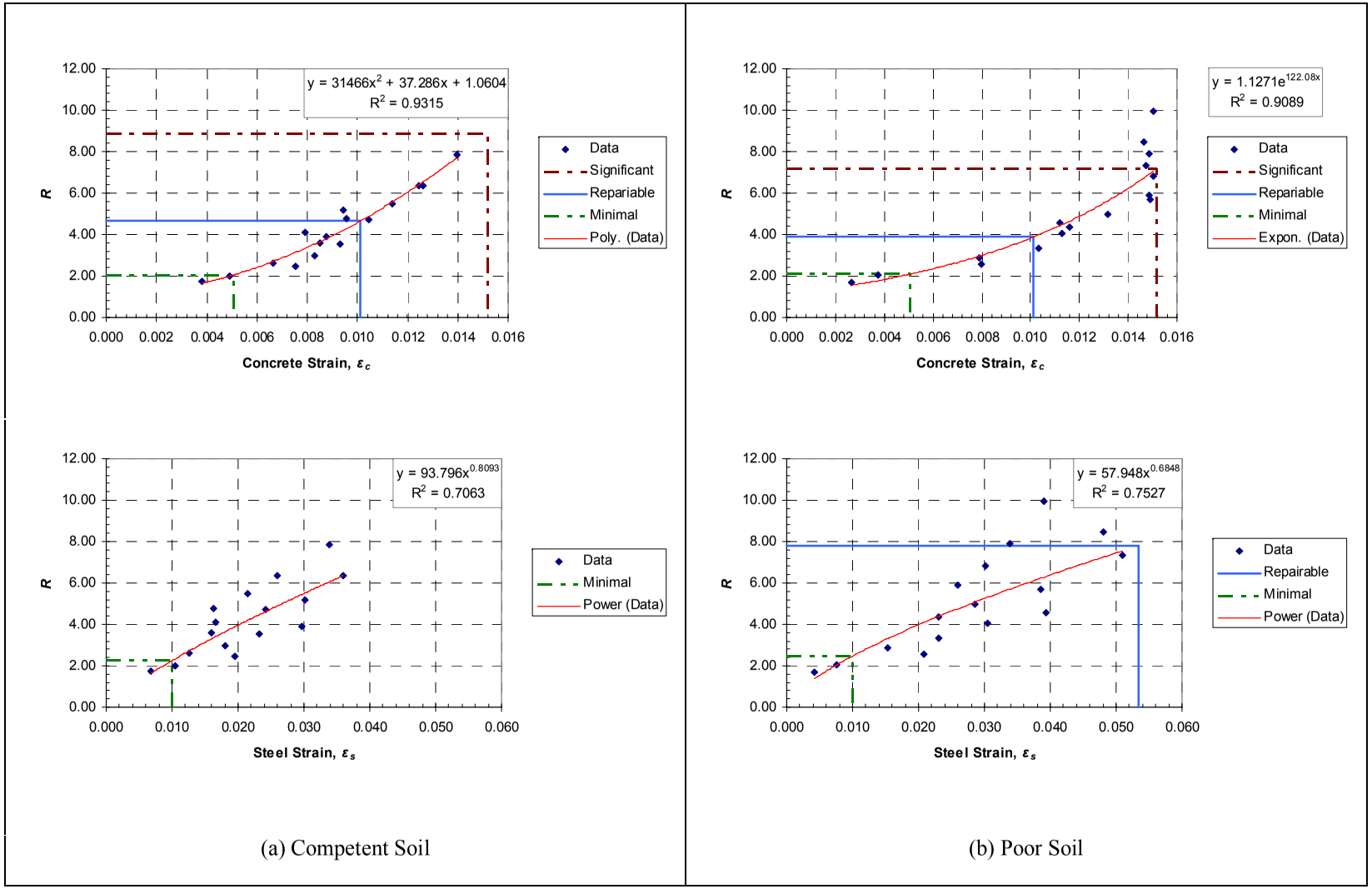

(a) Competent Soil

(b) Poor Soil

Figure 5.19: Response Modification Factor along Transverse Direction versus Concrete and Steel Strains

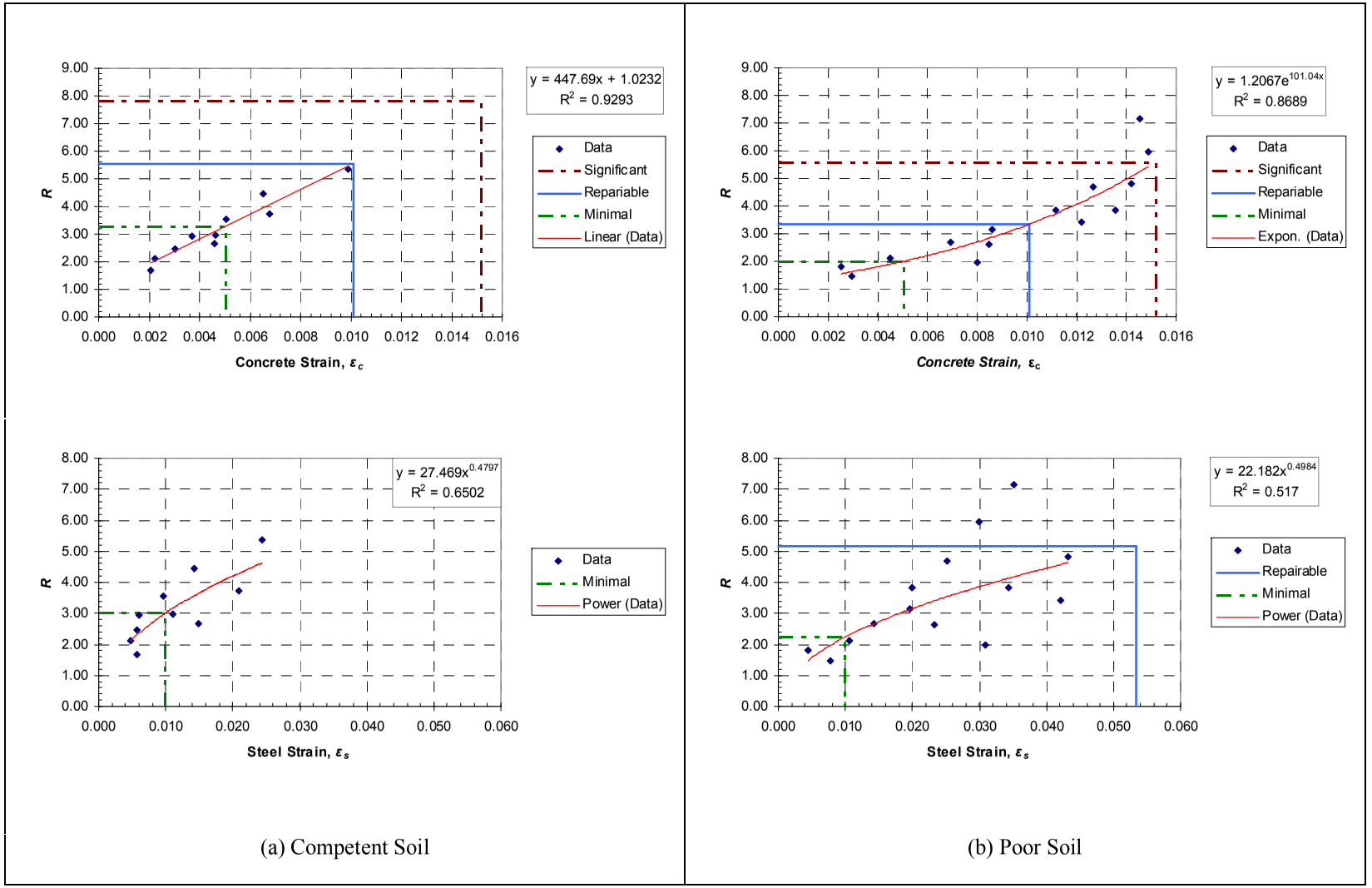

(a) Competent Soil

(b) Poor Soil

Figure 5.20: Response Modification Factor along Longitudinal Direction versus Concrete and Steel Strains

It can be observed from Figures 5.13 to 5.20 that seismic response measure values corresponding to significant damage are not captured by the available resulting steel strains obtained from analyses. The same observation is also true for determination of seismic response measure values corresponding to repairable damage at competent soil conditions. Therefore; on the graphs of seismic response measures versus steel strains for competent soil condition, only steel strain corresponding to minimal damage is marked, while on the graphs for poor soil condition, steel strains corresponding to minimal and repairable damage levels are marked.

Among the values obtained from concrete strain and steel strain plots, the most critical one which causes a conservative design is taken as the final estimated seismic response measure value corresponding to a certain damage level. It is found out that repairable and significant damages are always governed by concrete strain and minimal damage is either governed by concrete strain or steel strain. Estimated seismic response measure values for different damage levels are shown in Table 5.1.

Table 5.1: Estimated Seismic Response Measure Values for Different Damage Levels

			Competent Soil			**Poor Soil**		
Figure #	**Response Measure**		Significant	Repairable	Minimal	Significant	Repairable	Minimal
5.13	$(\Delta_C)^G / (\Delta_D)^G_{elastic}$		1.07	1.76	2.94	1.26	1.75	3.13
5.14	$(\Delta_C)^R / (\Delta_D)^R_{elastic}$		1.10	2.09	3.95	1.35	2.60	5.00
5.15	$(\Delta_C)^G / (\Delta_D)^G_{inelastic}$		1.03	1.48	2.27	1.04	1.41	2.46
5.16	$(\Delta_C)^R / (\Delta_D)^R_{inelastic}$		1.12	1.46	2.39	1.02	1.42	2.60
5.17	μ_D (Δ_D = elastic)		2.78	1.64	0.97	1.96	1.34	0.91
5.18	μ_D (Δ_D = inelastic)		3.48	2.61	1.53	3.52	2.23	1.41
5.19	*R*	Trans.	8.87	4.66	2.05	7.19	3.88	2.09
5.20		Long.	7.82*	5.55	3.02	5.59	3.35	2.01

*: Based on extrapolation of limited data

CHAPTER 6

DISCUSSION OF RESULTS AND CONCLUSIONS

6.1 Discussion of Results

The figures showing the variation of displacement capacity over demand (*C*/*D*) ratios with respect to column aspect ratio can be interpreted such that stiff columns are better for a bridge design. However this argument should be investigated in terms of the required performance objective for the design considered. The components, global displacement capacities and inelastic displacement demands, forming displacement capacity over demand ratios are shown in Figure 6.1. For low longitudinal reinforcement ratios such as ρ_l = 1 %, the decrease of demands are greater with decreasing column aspect ratio as compared to capacities making the *C*/*D* ratio increase as well. For high longitudinal reinforcement ratios such as ρ_l = 4 %, capacities increase with decreasing column aspect ratio while demands also decrease making the *C*/*D* ratio increase. This may be due to the great contribution of foundation flexibility effects to displacement capacities as a result of stiff columns. Therefore, using stiff column yields high displacement capacity over demand ratios, but foundation level displacement may be extensive which may make the design of foundation elements difficult.

The trend of displacement capacity over demand ratios using relative displacements is similar to the one using global displacements. This implies that structural deformation capacity of well-confined columns is also an important factor for this behavior that can be observed from the structural displacement ductility capacities shown in Section 5.2 and the structural drift ratio capacities

shown in Table 6.1. Structural drift ratio capacity which mainly originate from deformations of columns is defined as:

$$Structural\ Drift\ Ratio\ Capacity = \frac{(\Delta_C)^R}{H_n} \tag{6.1}$$

Structural drift ratios along transverse direction range between 6.36 % and 3.56 % while those along longitudinal direction range between 4.08 % and 7.41 %. These values are consistent with the drift ratios of columns found in other researches. A maximum drift limit of approximately 7.5 % can be observed from the histogram for ultimate level in the research of Lu et al. [33]. A maximum drift ratio of nearly 10 % was obtained according to one of the test results of several well-confined, circular-cross-section, reinforced concrete bridge columns in the research of Lehman et al. [32]. It should be remembered that columns utilized in this research are well-confined complying with the minimum requirements of AASHTO-LRFD [2].

Table 6.1: Structural Drift Ratio Capacities (in %)

ρ_l	H_n/D	*Transverse*	*Longitudinal*
1%	5	3.56	4.08
	6	3.69	4.32
	7	4.11	4.35
	8	4.20	4.85
2%	5	3.80	4.63
	6	3.67	4.32
	7	4.03	4.38
	8	4.28	4.64
3%	5	5.22	6.54
	6	5.04	5.72
	7	4.52	5.02
	8	4.52	4.66
4%	5	5.26	6.55
	6	6.36	7.41
	7	4.93	5.44
	8	4.94	5.31

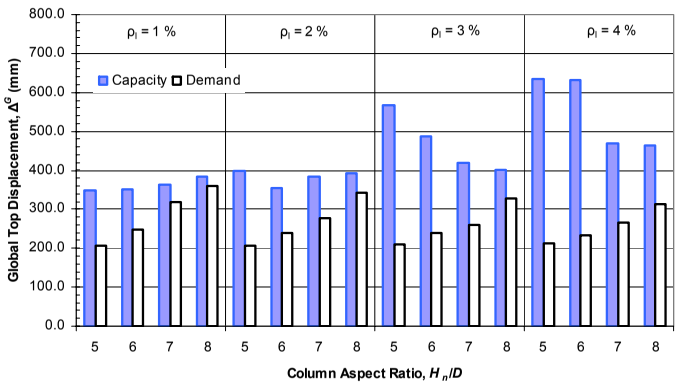

(a) Along Transverse Direction, Competent Soil

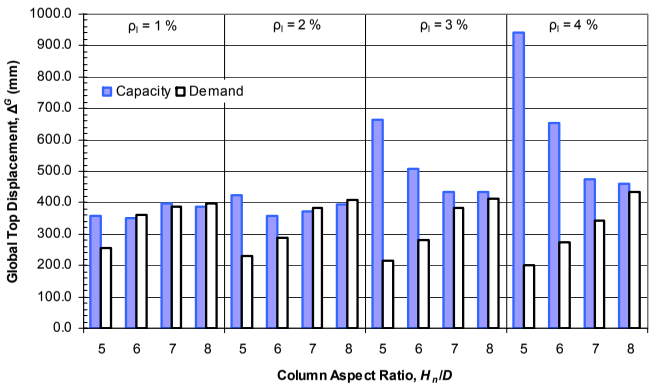

(b) Along Transverse Direction, Poor Soil

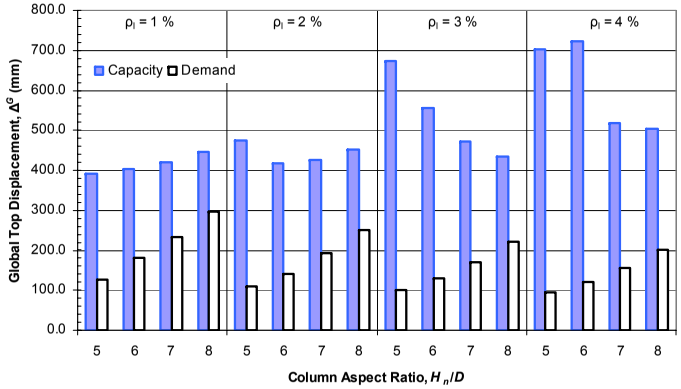

(c) Along Longitudinal Direction, Competent Soil

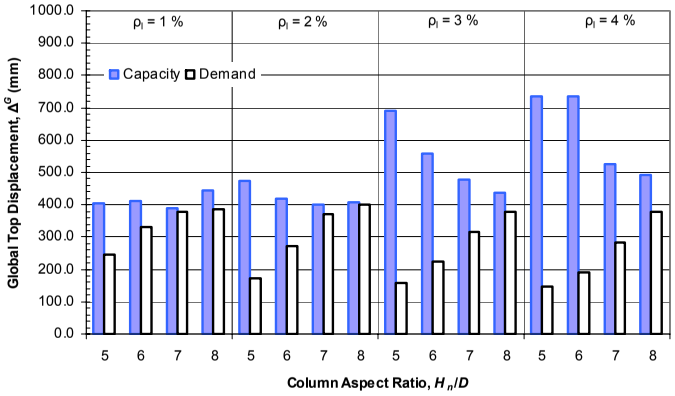

(d) Along Longitudinal Direction, Poor Soil

Figure 6.1: Comparison between Global Displacement Capacities and Inelastic Displacement Demands

Displacement capacity over demand ratio (C/D) and displacement ductility demand (μ_D) are two major response measures for displacement based design. [13, 21] In Section 5.8, damage state limits are estimated with computed seismic response measures. For comparison only, two extreme cases - one having the stiffest column and the other one having the most flexible column - along transverse direction are investigated at competent and poor soil conditions:

Case 1: Column aspect ratio of H_n/D = 5 and column longitudinal reinforcement ratio of ρ_l = 4 % (models: *C54* and *P54*)

Case 2: Column aspect ratio of H_n/D = 8 and column longitudinal reinforcement ratio of ρ_l = 1 % (models: *C81* and *P81*)

Six different types of seismic response measure values for different damage levels, which are estimated from Figures 5.13 to 5.20, are utilized to mark displacement demands on capacity curves. The comparisons made are shown in Figures 6.2 to 6.4:

The following outcomes can be stated as observed in Figures 6.2 to 6.4:

- Global displacement ductility demand is not a good measure for estimation of damage levels especially when the foundation flexibility effect is extensive. For Case 1, foundation flexibility effect exists at both soil conditions as bent columns are relatively stiff. This effect is extensive at poor soil conditions where the foundation level displacement including soil yielding corresponds to nearly 50 % of the total displacement capacity. It is observed in Figure 6.4 that damage levels shift towards the global yield displacement point of capacity curve. The reason is that the computation of global displacement ductility demands is performed according to this point. This results in unrealistic damage levels as foundation yielding occurs prior to or with column deformation and idealization of the system with a single yield point does not account for

these phenomenon. The same behavior is not observed in case 2 where contribution of foundation flexibility is very low since foundation level displacement corresponds to nearly 2 % of the total displacement capacity at poor soil condition.

- Displacement capacity over demand ratios are better for estimation of damage levels since formulation is not a function of system yielding which includes not only structural yielding but also soil yielding. The favor of this measure is shown in Figure 6.3 for case 1 that damage levels estimated using global or relative displacements are well-distributed over the capacity curves. It has been observed that excluding foundation effects both from bridges over competent soil and poor soil resulted similar responses. Therefore, using relative displacements is an innovative way to assess only structural response in absence of foundation flexibility effects.
- For estimation of damage levels, displacement capacity over demand ratios obtained from inelastic displacement demands can be favored over the ones obtained from elastic displacements. As shown in Section 5.3, for some cases investigated in this study, true displacements are found to be underestimated by elastic analyses. It is observed that estimated damage levels are shifted away from the failure point along the capacity curves when elastic displacements are used.

Table 6.2 shows the comparison made between the estimated global displacement ductility demands (μ_D) corresponding to different damage levels obtained in this study and the proposed ranges for the same damage levels presented in reference [22] and shown in Table 2.5. For the comparison of displacement ductility demand limits, the ones obtained from inelastic displacements at competent soil conditions is considered only.

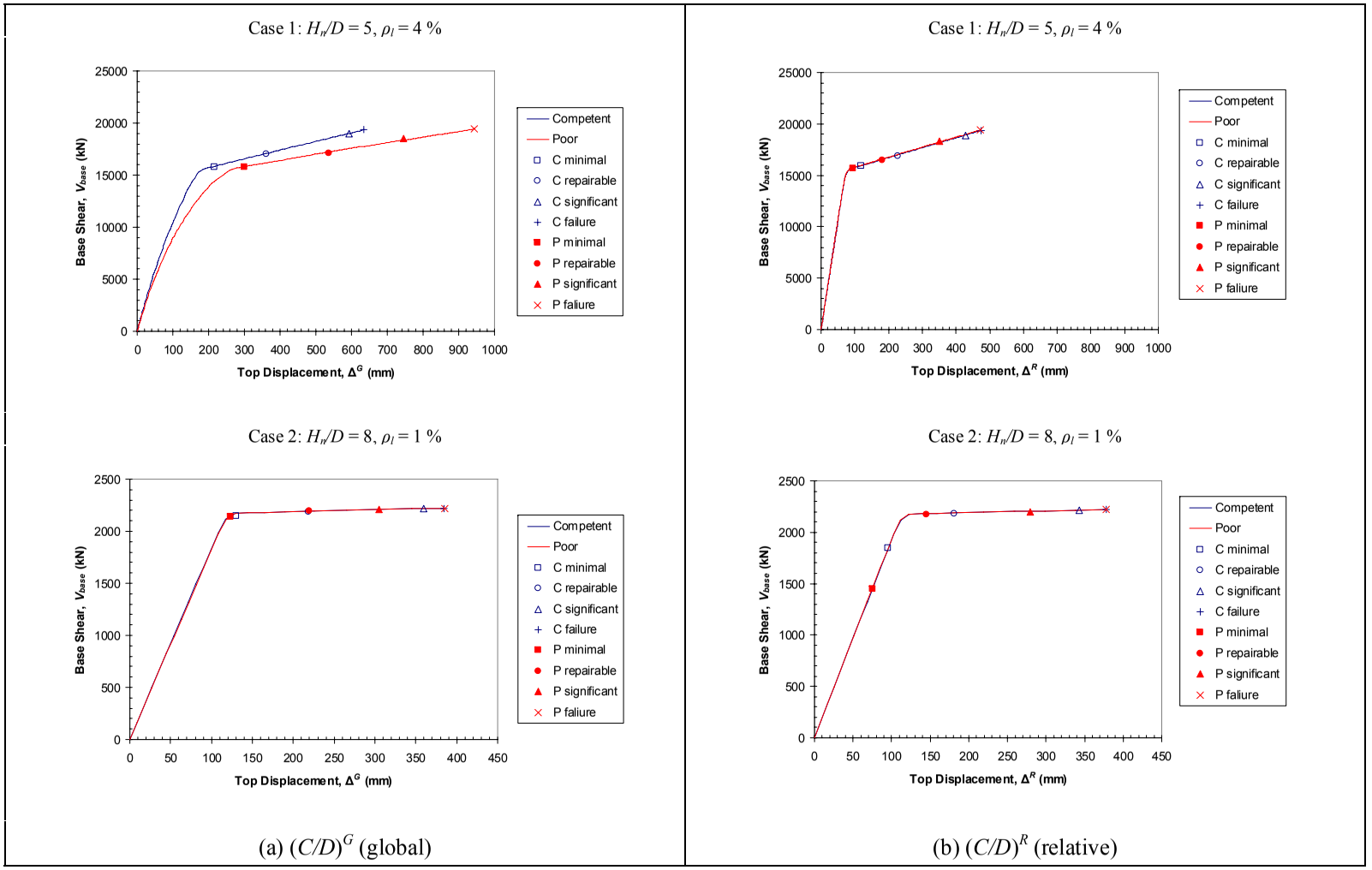

Figure 6.2: Comparison of Displacement Capacity over Demand Ratios (Δ_D = elastic) for Different Damage Levels

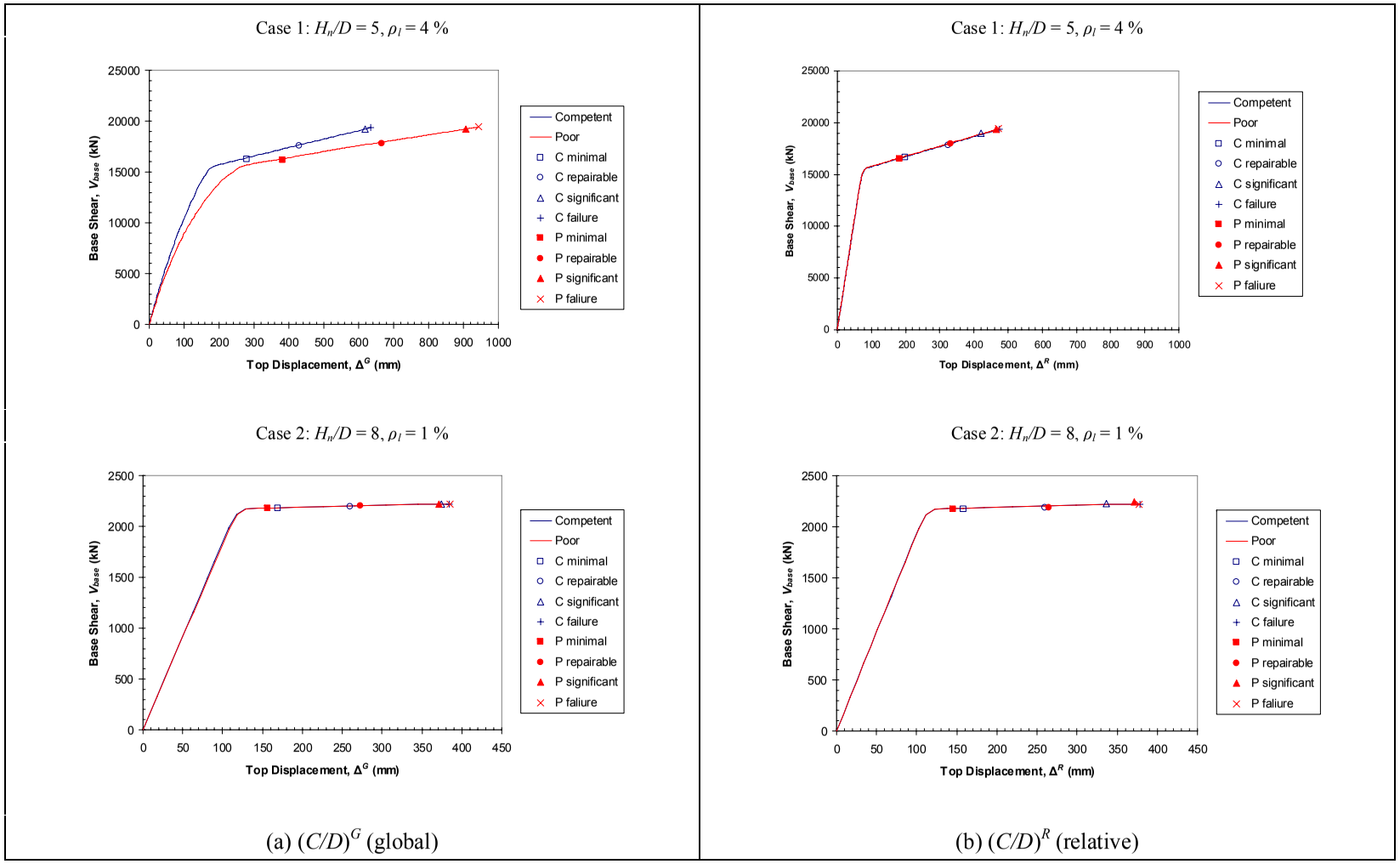

(a) $(C/D)^G$ (global) (b) $(C/D)^R$ (relative)

Figure 6.3: Comparison of Displacement Capacity over Demand Ratios (Δ_D = inelastic) for Different Damage Levels

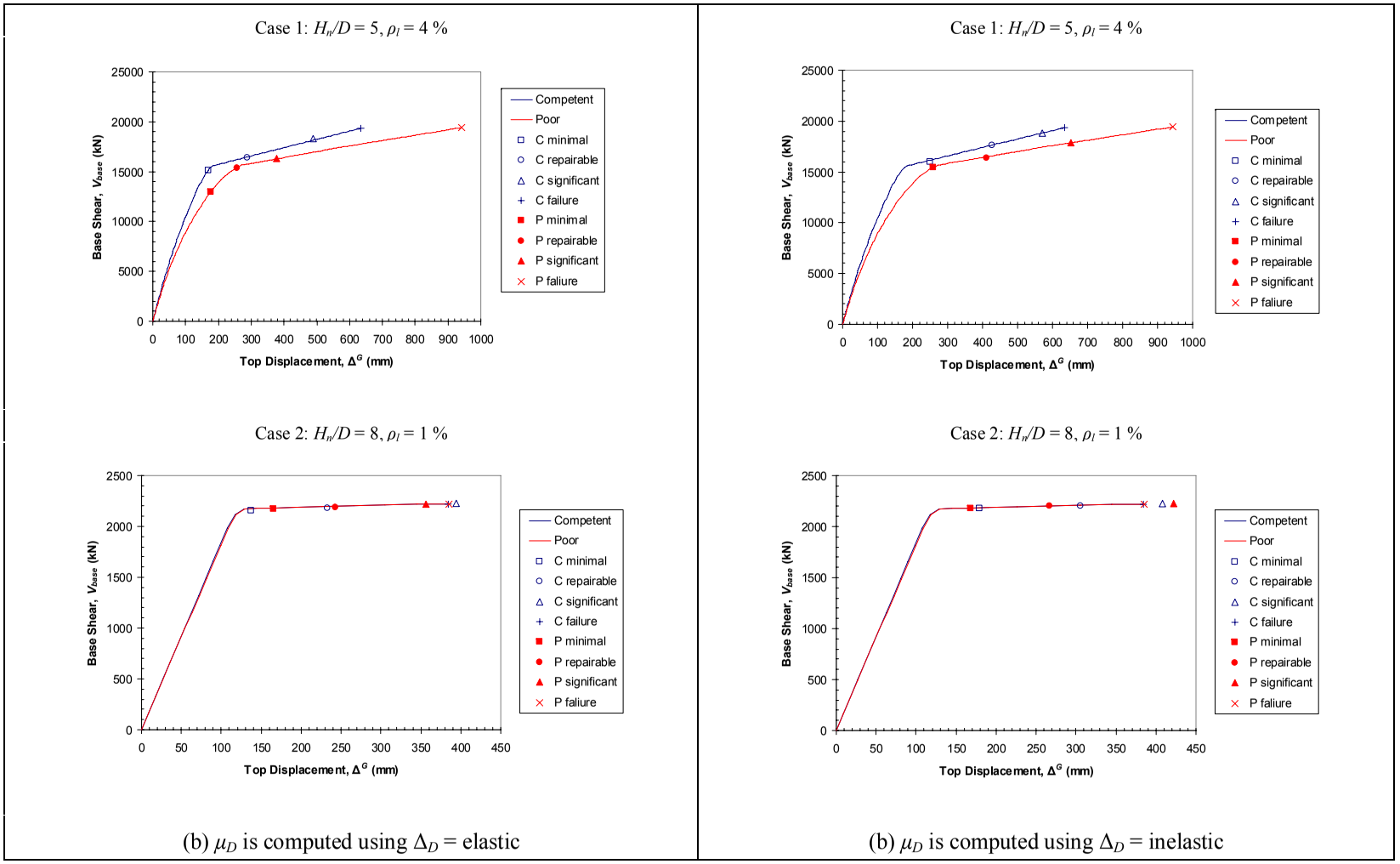

(b) μ_D is computed using Δ_D = elastic

(b) μ_D is computed using Δ_D = inelastic

Figure 6.4: Comparison of Global Displacement Ductility Demands for Different Damage Levels

Table 6.2: Comparison of Displacement Ductility Demands for Estimation of Damage Levels

	Reference [22]	**This Study**
Damage Level	μ_D	μ_D
Minimal	1~2	< 1.53
Repairable	2~4	1.53 ~ 2.61
Significant	4~6	2.61 ~ 3.48

Estimated displacement ductility demand values corresponding to different damage levels in this study are conservative as compared to the ranges given in reference [22] as shown in Table 6.2. However, any explanation on the derivation of proposed ranges of displacement ductility demands for different damage levels presented in Table 2.5 is not included in the reference document. Assumptions made, methodology followed or the type of bridges utilized may be effective in assigning these ranges.

Global displacement capacity over demand ratios $(C/D)^G$ of each investigated case are shown in Figure 6.5. The estimated global displacement capacity over demand ratios corresponding to different damage levels are also drawn on the same figure to demonstrate the limits for minimal, repairable and significant damage states.

Damage states of each investigated bridge along transverse or longitudinal direction at safety evaluation earthquake hazard can be determined from Figure 6.5. For a complete bridge system, a single performance objective is specified without consideration of direction. Hence, estimated damage states of all bridge systems - obtained from taking the smaller value of $(C/D)^G$ ratios resulted from both directions and comparing with the limits - are shown in Table 6.3.

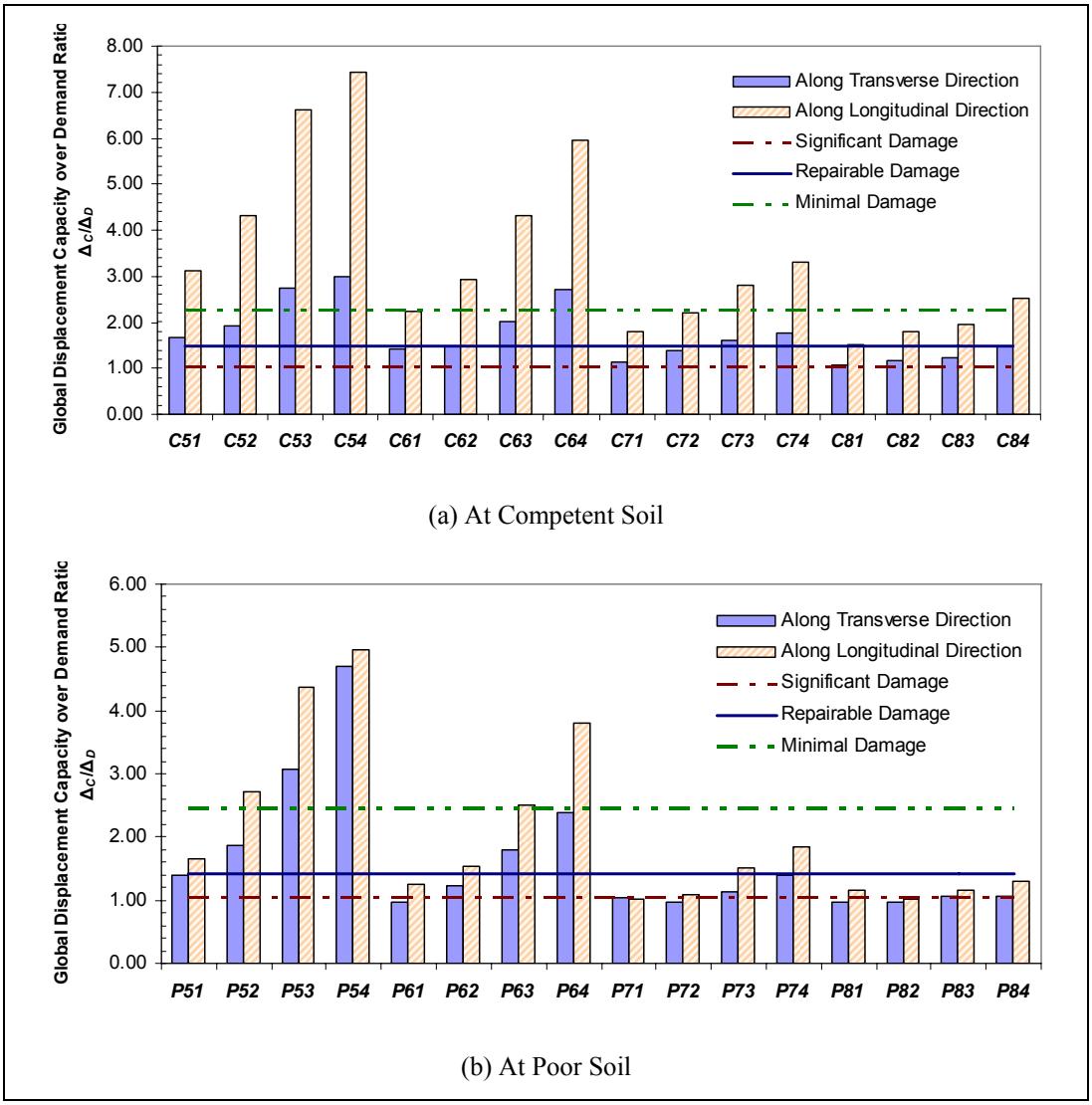

Figure 6.5: Demonstration of Estimated Damage States of Investigated Cases

The following interpretations can be made according to Table 6.3:

- Some bridges satisfy the same damage state at both soil conditions, while some bridges perform worse at poor soil compared to competent soil.
- It is possible for bridges to satisfy different damage states at a certain soil condition by changing only column longitudinal reinforcement ratio and keeping column size as constant. For instance, the estimated damage states of the cases *C64*, *C63* and *C62* are minimal, repairable and significant, respectively.

- It is also possible for bridges to satisfy different damage states at a certain soil condition by changing only column aspect ratio and keeping column longitudinal reinforcement ratio as constant. For instance, the estimated damage states of the cases *C64*, *C74* and *C84* are minimal, repairable and significant, respectively.
- The proper combination of column size and longitudinal reinforcement ratio can be obtained for design purposes from Table 6.3 according to the required performance objective under the safety evaluation earthquake with a return period of 1000 years.

Table 6.3: Estimated Damage States of the Investigated Bridges

Minimal Damage		**Repairable Damage**		**Significant Damage**	
Competent	Poor	Competent	Poor	Competent	Poor
C64	*(repairable)*	*(minimal)*	*P64*	*C62*	*P62*
C53	*P53*	*C51*	*(significant)*	*(repairable)*	*P51*
C54	*P54*	*C73*	*(significant)*	*(repairable)*	*P73*
		C74	*(significant)*	*(repairable)*	*P74*
		C52	*P52*	*C83*	*P83*
		C63	*P63*	*C84*	*P84*
				C61	*(fails)*
				C71	*(fails)*
				C72	*(fails)*
				C81	*(fails)*
				C82	*(fails)*

Both Caltrans-SDC [15] and AASHTO-Seismic [28] require displacement capacity over demand ratios be larger than 1.0 for ordinary bridges. The expected damage state for ordinary bridges is significant damage according to the performance objectives defined in ATC-32 [8] which is also adopted in Caltrans-SDC [15] and AASHTO-Seismic [28]. The global displacement criteria of Caltrans and AASHTO-Seismic is verified in this study as limiting values of global displacement capacity over demand ratios corresponding to significant damage level are $(C/D)^G$ = 1.03 and $(C/D)^G$ = 1.04 at competent and poor soil conditions as shown in Table 6.4. However, these documents do not state any minimum criteria of displacement capacity over demand ratios for important

bridges for which at least repairable damage state shall be satisfied under the safety evaluation earthquake. Therefore, limiting displacement capacity over demand ratios are suggested for different damage levels based on the estimated values shown in Table 5.1 under the safety evaluation earthquake with a return period of 1000 years.

Table 6.4: Comparison of Limiting Displacement Capacity over Demand Ratios

		Significant	**Repairable**	**Minimal**
Competent Soil	$(\Delta_C)^G / (\Delta_D)^G_{inelastic}$	1.03	1.48	2.27
	$(\Delta_C)^R / (\Delta_D)^R_{inelastic}$	1.12	1.46	2.39
Poor Soil	$(\Delta_C)^G / (\Delta_D)^G_{inelastic}$	1.04	1.41	2.46
	$(\Delta_C)^R / (\Delta_D)^R_{inelastic}$	1.02	1.42	2.60
Suggested	$(\Delta_C) / (\Delta_D)_{inelastic}$	**1.10**	**1.50**	**2.50**

In Table 6.5 the estimated response modification factors (*R*-factors) corresponding to different damage levels are compared with the *R*-factors specified by AASHTO-LRFD [2] which makes different recommendations for multiple-column bents and single columns. Although the seismic behavior of a pier along longitudinal direction is sometimes similar to single column behavior, contra-flexure length may fluctuate along the column length depending on the load level. Therefore, only the *R*-factors for multiple columns specified in AASHTO-LRFD are compared with the *R*-factors along transverse direction estimated in this study.

Table 6.5: Comparison of Response Modification Factors

AASHTO-LRFD	Return period of design earthquake		475 years		
	Importance of bridge		**Critical**	**Essential**	**Other**
	Recommended *R*-factors		1.5	3.5	5
This study	Return period of SEE		1000 years		
	Expected damage level		**Minimal**	**Repairable**	**Significant**
	Estimated *R*-factors	at competent soil	2.05	4.66	8.87
		at poor soil	2.09	3.88	7.19
Suggested limits under SEE			**2.0**	**3.5**	**5.0**

It should be remembered that the derivation of estimated response modification factors corresponding to different damage levels are made using the strains resulting from the safety evaluation earthquake (SEE) with a return period of 1000 years and response modification factors computed for a design earthquake with a return period of 475 years. Thus, *R*-factors consistent with the design procedure of AASHTO-LRFD [2] and the performance objectives under safety evaluation earthquake hazard level are attained.

AASHTO-LRFD uses a single earthquake hazard definition -the design earthquake with a return period of 475 years- adjusting designs according to its required performance objectives in background by the use of *R*-factors. A designer confronts with only the design earthquake and the importance classification and is not interested in damage states. It is possible to match the damage state definitions of ATC-32 [8] used in this study with the importance classification of AASHTO-LRFD as shown in Table 6.5. It is observed in Table 6.5 that the response modification factors for different importance categories specified in AASHTO-LRFD are smaller than the values estimated in this study for the equivalent damage levels. This may be due to the additional conservatism required or the consideration of a higher earthquake hazard as compared to the one utilized in this study for displacement-based assessment performed in background without changing the design earthquake definition in AASHTO-LRFD. It is known that serviceability conditions of important bridges are required to be checked for a large earthquake event with a return period of 2500 years in AASHTO-LRFD.

It is also noticed in Table 6.5 that lower values are estimated for *R*-factors corresponding to repairable and significant damage levels at poor soil conditions compared to competent soil conditions. Based on the comparison mentioned above, response modification factors corresponding to minimal, repairable and significant damage levels under the safety evaluation earthquake with a return period of 1000 years are suggested as shown in Table 6.5.

6.2 Summary and Conclusions

Thirty two bridge models were investigated in this study to find the effect of foundation and column flexibility on seismic behavior of multi-column highway bridges with two-column reinforced concrete bents. From the results of a series of analyses, seismic responses of the investigated bridges are compared according to several response measures. Then an approach is developed to correlate seismic response measures with damage levels.

The following conclusions can be drawn for this study:

- Damage states of bridges under a large earthquake hazard, such as the safety evaluation earthquake with a return period of 1000 years, can significantly vary with different combination of column sizes and column longitudinal reinforcement ratios.
- Global displacement ductility demand is not a favorable response measure for assessing damage levels. For the cases where foundation flexibility effect is dominant, especially for bridges over poor soil, yielding at foundation level may result in complexity in assessing structural ductility demands which are not a function of soil yielding.
- Displacement capacity over demand ratios are suggested for estimation of damage levels as system yielding is not taken into consideration. However, in this case push-over analysis is needed to obtain ultimate displacement capacity.
- Displacement capacity over demand ratios obtained from using global and relative displacements results in similar responses at investigated damage levels. Nevertheless, it is possible to assess only structural response isolated from foundation flexibility effects by using relative displacements.
- Based on the correlation of seismic response measures with damage levels, global displacement capacity over demand ratio of (C/D) = 1.1, (C/D) =1.5

and (C/D) = 2.5 are suggested for minimal, repairable and significant damage levels, respectively for the safety evaluation earthquake which has a return period of 1000 years. The same values can be taken when relative displacements are used.

- For forced based design procedures, response modification factors for columns of R = 2.0, R = 3.5 and R = 5.0 are suggested for minimal, repairable and significant damage levels, respectively for the safety evaluation earthquake.
- Although inelastic displacements are the most accurate way of determining displacement demands, they are obtained from inelastic time history analysis which includes several issues such as selection of ground motions, determination of expected material properties, determination of damping, modeling of elements having inelastic behavior and the exhaustive effort involved in terms of processing of outputs and run times. Therefore, elastic analysis can be used to estimate displacement demands with proposed relationships in literature for scaling of elastic displacements in order to eliminate such complex issues.

6.3 Recommendations for Further Studies

Case studies can be expanded to investigate other types of substructures.

REFERENCES

[1] AASHTO, 1999, *Guide Specifications for Seismic Isolation Design*, American Association of State Highway and Transportation Officials, Washington D.C.

[2] AASHTO, 2007, *LRFD Bridge Design Specifications*, American Association of State Highway and Transportation Officials, Washington D.C.

[3] Abrahamson N., Silva W., 1996, *Empirical Ground Motion Models,* Draft Report, Brookhaven National Laboratory.

[4] ACI, 1999, *ACI 318, Building Code Requirement for Structural Concrete and Commentary*, American Concrete Institute.

[5] Akkari M., Duan L., 2003, *Nonlinear Analysis of Bridge Structures,* Chapter of Bridge Engineering Seismic Design, edited by Chen W.F., W.K., Duan L., CRC Press, Florida.

[6] API, 1993, *Recommended Practice for Planning, Designing and Constructing Fixed Offshore Platforms - Working Stress Design*, American Petroleum Institute.

[7] ATC, 1981, *ATC 6*, *Seismic Design Guidelines for Highway Bridges,* Applied Technology Council, Redwood City, CA.

[8] ATC, 1996, *ATC 32, Improved Seismic Design Criteria for California Bridges*, Applied Technology Council, Redwood City, CA.

[9] ATC, 1997, *ATC 18, Seismic Design Criteria for Bridges and Other Highway Structures*, Applied Technology Council, Redwood City, CA.

[10] ATC/MCEER, 2001, *Recommended LRFD Guidelines for the Seismic Design of Highway Bridges*, Applied Technology Council/ Multidisciplinary Center for Earthquake Engineering Joint Venture, Redwood City, CA, and Buffalo, NY.

[11] ATC/MCEER, 2001, *NCHRP 12-49, Comprehensive Specification for the Seismic Design of Bridges, Third Draft of Specifications and Commentary*, Applied Technology Council/Multidisciplinary Center for Earthquake Engineering Joint Venture for NCHRP, Washington D.C.

[12] ATC/MCEER, 2001, *Report 472, Comprehensive Specification for the Seismic Design of Bridges*, Applied Technology Council/Multidisciplinary Center for Earthquake Engineering Joint Venture for NCHRP, Washington D.C.

[13] Budek A.M., Priestley M.J.N., Benzoni G., 2000, *Inelastic Seismic Response of Bridge Drilled-Shaft RC Pile/Columns,* Journal of Structural Division, American Society of Civil Engineers, Vol. 126, No. 4, 510-517.

[14] CALTRANS, 1999, *Bridge Memo to Designers 20-1: Seismic Design Methodology*, California Department of Transportation.

[15] CALTRANS, 2006, *Seismic Design Criteria Version 1.4*, California Department of Transportation.

[16] Caner, A., and Zia, P., 1998, *Behavior and Design of Link Slabs for Jointless Bridge Decks*, PCI Journal, 43(3), 68 – 80.

[17] Caner A., Yanmaz A. M., Yakut A., Avsar Ö., Yılmaz T, 2008, *Service Life Assessment of Existing Highway Bridges with no Planned Regular Inspections,* Journal of Performance of Constructed Facilities, ASCE, March/April, 108 – 114.

[18] Chai Y.H, 2002, *Flexural Strength and Ductility of Extended Pile-Shafts. I: Analytical Model*, Journal of Structural Division, American Society of Civil Engineers, Vol. 128, No. 5, 586-594.

[19] Chopra A. K., 2000, *Dynamics of Structures*, Second Edition, Prentice Hall, New Jersey.

[20] Ciampoli M., Pinto E. P., 1995, *Effects of Soil-Structure Interaction on Inelastic Seismic Response of Bridge Piers,* Journal of Structural Division, American Society of Civil Engineers, Vol. 121, No. 5, 806-814.

[21] Domaniç K.A., 2008, *Effects of Vertical Excitation on Seismic Performance of Highway Bridges and Hold-Down Device Requirements*, Master Thesis, Department of Civil Engineering, METU, Ankara.

[22] Duan L., Li F., 2003, *Seismic Design Philosophies and Performance-Based Design Criteria*, Chapter of Bridge Engineering Seismic Design, edited by Chen W.F., W.K., Duan L., CRC Press, Florida.

[23] Dunhum J. W., 1954, *Pile Foundations for Buildings*, Proc. of the ASCE, Journ. SMF Div., Vol. 80, SM 1, Proc. Paper 385, 1-21.

[24] FEMA, 1997*, FEMA 273, NEHRP Guidelines for the Seismic Rehabilitation of Buildings*, Federal Emergency Management Agency, Washington D.C.

[25] FEMA, 2000*, FEMA 356, Prestandard and Commentary for the Seismic Rehabilitation of Buildings*, Federal Emergency Management Agency, Washington D.C.

[26] General Directorate of Disaster Affairs Earthquake Research Department, Republic of Turkey, *Türkiye Deprem Bölgeleri Haritası*, www.deprem.gov.tr, last visited: 20.08.2008.

[27] Idriss I.M., 2005, *Attenuation Relationships*, Seismic Analysis and Retrofitting of Lifeline Buildings in Delhi, India*,* www.quakesafedelhi.net, last visited: 27.11.2008.

[28] Imbsen Consulting, 2007, *Proposed AASHTO Guide Specifications for LRFD Seismic Bridge Design*, project no. 20-07/Task 193, Imbsen Consulting for NCHRP.

[29] Kowalsky M., 2000, *Deformation Limit States for Circular Reinforced Concrete Bridge Columns*, Journal of Structural Division, American Society of Civil Engineers, Vol. 126, No. 8, 869-878.

[30] Kramer S.L., 1996, *Geotechnical Earthquake Engineering*, Prentice Hall, New Jersey.

[31] LARSA 4D, 2008, *Structural and Earthquake Engineering Integrated Analysis and Design Software*, LARSA Inc., New York, USA.

[32] Lehman D., Moehle J., Mahin S., Calderone A., Henry L., 2004, *Experimental Evaluation of the Seismic Performance of Reinforced Concrete Bridge Columns*, Journal of Structural Division, American Society of Civil Engineers, Vol. 130, No. 6, 869-879.

[33] Lu Y., Gu X., Guan J., 2005, *Probabilistic Drift Limits and Performance Evaluation of Reinforced Concrete Columns,* Journal of Structural Division, American Society of Civil Engineers, Vol. 131, No. 6, 966-978.

[34] Mander J.B., Priestley M.J.N., Park R., 1988, *Theoretical Stress-Strain Model for Confined Concrete*, Journal of Structural Division, American Society of Civil Engineers, Vol. 114, No. 8, 1804-1826.

[35] MCEER, 1999, *Impact Assessment of Selected MCEER Highway Project Research on the Seismic Design of Highway Structures*, Multidisciplinary Center for Earthquake Engineering.

[36] Megally S.H., Silva P. F., Seible F., 2002, *Seismic Response of Sacrificial Shear Keys in Bridge Abutments*, Report No. SSRP-2001/23, Department of Structural Engineering, University of California San Diego.

[37] Ministry of Public Works and Settlement, Republic of Turkey, 2007, *Deprem Bölgelerinde Yapılacak Binalar Hakkında Yönetmelik*, Ankara.

[38] Moyer, M.J., Kowalsky, M.J., 2002, *Influence of Tension Strain on Buckling of Reinforcement in RC Bridge Columns*, ACI Structural Journal.

[39] NYCDOT, 2002, *Standard Specifications for Highway Bridges*, New York State Department of Transportation.

[40] Özkaya C., Caner A., 2007, *Sismik İzolasyonlu ve Ters T Başlık Kirişli Standart Karayolu Köprülerinin Deprem Davranışının Belirlenmesi*, 1. Symposium on Bridges and Viaducts, Antalya.

[41] Pacific Earthquake Engineering Research Center, *PEER NGA Database*, Pacific Earthquake Engineering Research Center, University of California, Berkeley, last visited: 27.11.2008.

[42] Pacific Earthquake Engineering Research Center, *Structural Performance Database*, Pacific Earthquake Engineering Research Center, University of California, Berkeley, last visited: 27.11.2008.

[43] Priestley N., Seible F., Calvi M., 1996, *Seismic Design and Retrofit of Bridges*, John Wiley & Sons, New York.

[44] Priestley M.J.N., Calvi G.M., Kowalsky M.J., 2007, *Displacement Based Design of Structures*, IUSS Press, Pavia, Italy.

[45] Saatcioglu M., Baingo D., March 1999, *Circular High-Strength Concrete Columns under Simulated Seismic Loading*, Journal of Structural Engineering, 272-280.

[46] SCDOT, 2002, *Seismic Design Specifications*, South Carolina Department of Transportation.

[47] Seed H. B., Idriss I. M., 1982, Ground Motions and Soil Liquefaction During Earthquake, Earthquake Engineering Research Institute, Berkeley, California, 134 pp.

[48] Sevgili G., 2007, *Seismic Performance of Multisimple-Span Skew Bridges Retrofitted with Link Slabs*, Master Thesis, Department of Civil Engineering, METU, Ankara.

[49] Sivaselvan M.V., Reinhorn A.M., 1999, *Hysteretic Models for Cyclic Behavior of Deteriorating Inelastic Structures*, Technical Report MCEER-99-0018, University at Buffalo, State University of New York.

[50] Thiele M. (2002), *Spectrum Compatible Accelerograms in Earthquake Engineering*, Universidad de La Serena, Chile.

[51] Ucak A., Tsopelas A. M., 2008, *Effect of Soil-Structure Interaction on Seismic Isolated Bridges,* Journal of Structural Division, American Society of Civil Engineers, Vol. 134, No. 7, 1154-1164.

[52] Vebe A. et al., 1977, *Moment-Curvature Relations of Reinforced Concrete Slab, Journal of Structural Division*, ASCE, 103(ST3), 515.

[53] Yüksekol Ü.T., 2007, *A Simple Assessment of Lateral Pier Response of Standard Highway Bridges on Pile Foundations*, Master Thesis, Department of Civil Engineering, METU, Ankara.

APPENDIX A

MATERIAL MODELS

Concrete under Compression, Mander's Model

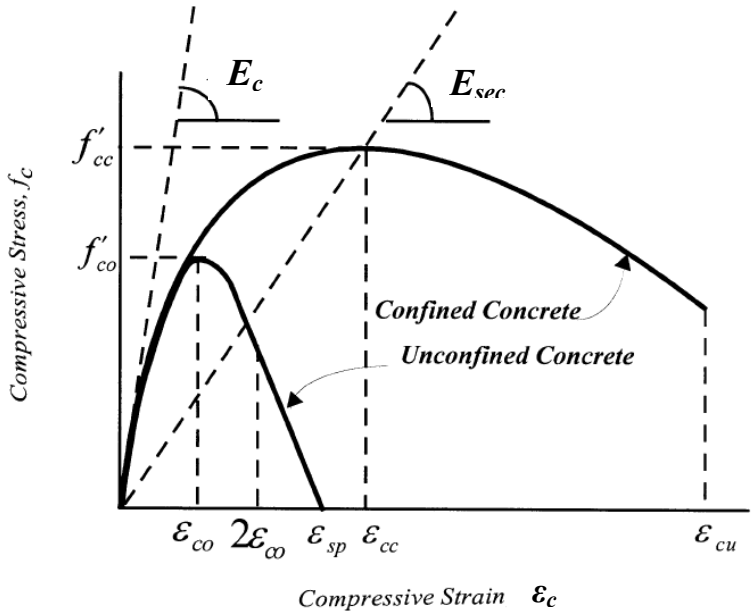

Figure A.1: Mander's Model (Printed in [5])

Mander's [34] model for concrete is shown in Figure A.1. Stress-strain relationship is given as:

$$f_c = \frac{f'_{cc}(\varepsilon_c / \varepsilon_{cc})r}{r - 1 + x} \tag{A.1}$$

$$f'_{cc} = f'_{co}\left(2.254\sqrt{1 + \frac{7.94 f'_l}{f'_{co}}} - \frac{2 f'_l}{f'_{co}} - 1.254\right) \tag{A.2}$$

$$\varepsilon_{cc} = 0.002\left[1 + 5\left(\frac{f'_{cc}}{f'_{co}} - 1\right)\right] \quad \text{(A.3)}$$

$$\varepsilon_{cu} = 0.004 + \frac{1.4\,\rho_s\, f_{yh}\, \varepsilon_{su}}{f'_{cc}} \quad \text{(A.4)}$$

$$r = \frac{E_c}{E_c - E_{\text{sec}}} \quad \text{(A.5)}$$

$$E_{\text{sec}} = \frac{f'_{cc}}{\varepsilon_{cc}} \quad \text{(A.6)}$$

$$f'_l = \frac{1}{2} K_e\, \rho_s\, f_{yh} \qquad \text{(For circular sections)} \quad \text{(A.7)}$$

$$\rho_s = \frac{4\,A_{sp}}{d_s\, s} \quad \text{(A.8)}$$

where;

f_{cc} : Peak compressive stress

f_{co} : Peak stress for unconfined concrete (cylindrical compression strength)

ε_{cc} : Strain corresponding to peak stress

ε_{cu} : Ultimate strain of confined concrete

ε_{su} : Steel strain at maximum tensile stress

E_c : Modulus of elasticity of concrete

f'_l : Effective lateral confining pressure

K_e : Confinement effectiveness coefficient (generally taken as 0.95 for circular sections)

f_{yh} : Yield stress of transverse reinforcement

ρ_s : Ratio of transverse confining steel volume to confined concrete core volume

A_{sp} : Bar area of transverse reinforcement

Although Mander's model originates from confined concrete; when effective lateral confining pressure $f_l' = 0$, stress-strain relationship for unconfined concrete can be obtained.

In this study, following strain values are used in Mander's model:

Strain at peak stress of unconfined concrete: $\varepsilon_{co} = 0.002$

Strain at onset of crushing of unconfined concrete: $2\varepsilon_{co} = 0.004$

Extreme compression strain of unconfined concrete: $\varepsilon_{sp} = 0.005$

Concrete Under Tension, Vebe's Model

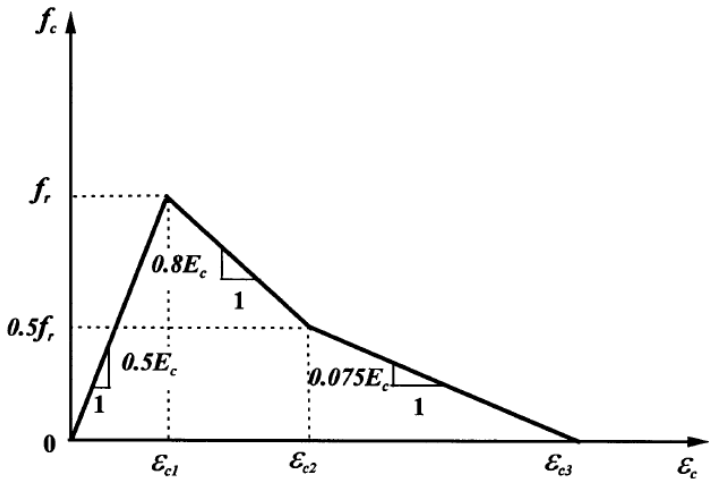

Figure A.2: Vebe's Model (printed in [5])

Vebe's [52] model for concrete in tension is shown in Figure A.2. Stress-strain relation is given as follows:

$$f_c = \begin{cases} 0.5\,E_c\,\varepsilon_c & \varepsilon_c \le \varepsilon_{c1} = 2\,f_r / E_c \\ f_r\left[1 - 0.8\,E_c\left(\varepsilon_c - \varepsilon_{c1}\right)\right] & \varepsilon_{c1} < \varepsilon_c \le \varepsilon_{c2} = 2.625\,f_r / E_c \\ f_r\left[0.5 - 0.075\,E_c\left(\varepsilon_c - \varepsilon_{c2}\right)\right] & \varepsilon_c < \varepsilon_{c3} = 9.292\,f_r / E_c \end{cases} \quad \text{(A.9)}$$

Where, f_r is the modulus of rupture of concrete.

Reinforcing Steel Model

Stress-strain relationship used for both longitudinal and confining reinforcing steel is shown in Figure A.3.

$$f_s = \begin{cases} E_s \varepsilon_s & \varepsilon_s \le \varepsilon_y \\ f_y & \varepsilon_y < \varepsilon_s \le \varepsilon_{sh} \\ f_{su} - (f_{su} - f_y)\left((\varepsilon_{su} - \varepsilon_s)/(\varepsilon_{su} - \varepsilon_{sh})\right)^2 & \varepsilon_{sh} < \varepsilon_s \le \varepsilon_{su} \end{cases} \quad \text{(A.10)}$$

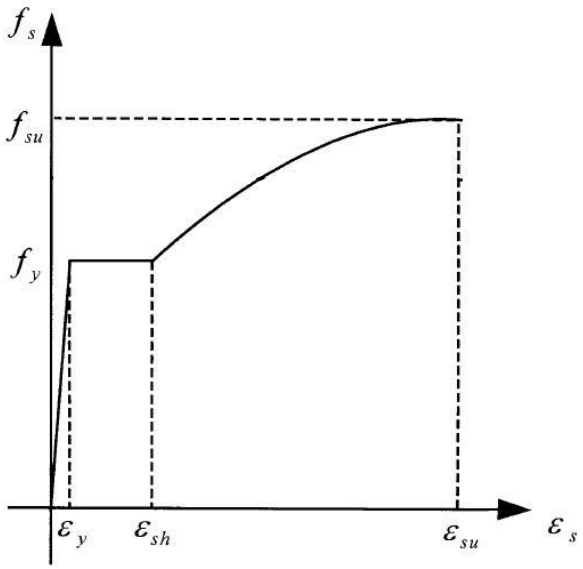

Figure A.3: Reinforcing Steel Model

APPENDIX B

ATTENUATION RELATIONSHIPS

Attenuation Model of Abrahamson and Silva [3]

Spectral accelerations, S_a (in g) can be estimated from the following formula:

$$\ln S_a(g) = f_1(m,r) + F\, f_3(m) + HW\, f_4(m,r) + S\, f_5(pga_{rock}) \qquad \text{(B.1)}$$

where;

$$f_1(m,r) = \begin{cases} a_1 + a_2(m-m_1) + a_{12}(8.5-m)^n + \left[a_3 + a_{13}(m-m_1)\right]\ln R & for\ m \le m_1 \\ a_1 + a_2(m-m_1) + a_{12}(8.5-m)^n + \left[a_3 + a_{13}(m-m_1)\right]\ln R & for\ m > m_1 \end{cases}$$

$$R = \sqrt{r^2 + c_4^2}$$

$$f_3(m) = \begin{cases} a_5 & for\ m < 5.8 \\ a_5 + \dfrac{(a_6 - a_5)}{(m_1 - 5.8)}(m - 5.8) & for\ 5.8 < m < m_1 \\ a_6 & for\ m \ge m_1 \end{cases}$$

$$f_4(m,r) = f_{HW}(m)\, f_{HW}(r)$$

$$f_{HW}(m) = \begin{cases} 0 & for\ m \le 5.5 \\ m - 5.5 & for\ 5.5 < m < 6.5 \\ 1 & for\ m \ge 6.5 \end{cases}$$

$$f_{HW}(r) = \begin{cases} 0 & r < 4 \\ a_9(r-4)/4 & 4 < r < 8 \\ a_9 & 8 < r < 18 \\ a_9(1-(r-18)/7) & 18 < r < 25 \\ 0 & 25 < r \end{cases}$$

$$f_5(pga_{rock}) = a_{10} + a_{11}\ln(pga_{rock} + c_5)$$

Total standard error is given as:

$$\sigma_{total}(m)=\begin{cases} b_5 & for\ m \le 5.0 \\ b_5 - b_6(m-5) & for\ 5.0 < m < 7.0 \\ b_5 - 2b_6 & for\ m \ge 7.0 \end{cases} \quad \text{(B.2)}$$

The parameters included in the equations above are as follows:

m : Moment magnitude

r : Closest distance to the rupture plane in km

F : Fault type (1 for reverse, 0.5 fo reverse/oblique and 0 otherwise)

HW : Dummy variable for hanging wall sites (1 for sites over the hanging wall, 0 othewise)

S : Dummy variable for the site class (0 for rock or shallow soil, 1 for deep soil)

c_4, a_1, a_2, a_3, a_4, a_5, a_6, a_9, a_{10}, a_{11}, a_{12}, a_{13}, m_1, c_5, n are the parameters specified for different periods and can be obtained from reference [3].

Attenuation Model of Idriss [27]

The median spectral acceleration, y (in g) can be estimated from the following formula:

$$\ln y = (\alpha_1 + \alpha_2 M) - (\beta_1 + \beta_2 M)\ln(R+10) + \varphi F \quad \text{(B.3)}$$

Standard error terms are obtained using the following expressions:

$$SE=\begin{cases} \varepsilon_{\max} & for\ M \le 5 \\ \varepsilon_1 - 0.12M & for\ 5 \le M \le 7.25 \\ \varepsilon_{\min} & for\ M \ge 7.25 \end{cases}$$

M : Moment magnitude

R : Closest distance to the rupture plane in km

F : Fault type (1 for reverse and reverse/oblique, and 0 otherwise)

α_1, α_2, β_1, β_2, φ, ε_{max}, ε_1, ε_{min} are the parameters specified for different periods and can be obtained from reference [27].

APPENDIX C

LOAD-DEFLECTION (P-Y) CURVES FOR SAND

The lateral soil resistance-deflection (p-y) relationships for sand are nonlinear and can be approximated at any specific depth *H*, by the following expression [6]:

$$P = A \cdot p_u \cdot \tanh\left[\frac{k \cdot H}{A \cdot p_u} \cdot y\right] \tag{C.1}$$

where;

A = Factor to account for cyclic or static loading condition. Evaluated by:

$A = 0.9$ for cyclic loading.

$A = \left(3.0 - 0.8\frac{H}{D}\right) \geq 0.9$ for static loading

k = Initial modulus of subgrade reaction, lb/in.^{3} (kN/m^3). Determine from Figure C.1 as function of angle of internal friction, ϕ'

y = Lateral deflection, in. (m)

H = Depth, in. (m)

D = Average pile diameter from surface to depth, in. (m)

p_u = Ultimate bearing capacity at depth *H*, lbs/in. (kN/m)

The smaller value of the following p_u should be used as the ultimate bearing capacity:

p_u for shallow depths; $p_{us} = (C_1 \cdot H + C_2 \cdot D) \cdot \gamma \cdot H$ (C.2)

p_u for deep depths; $p_{ud} = C_3 \cdot D \cdot \gamma \cdot H$ (C.3)

where;

C_1, C_2, C_3 = Coefficients determined from Figure C.2

γ = Effective soil weight, lb/in.^{3} (kN/m^3)

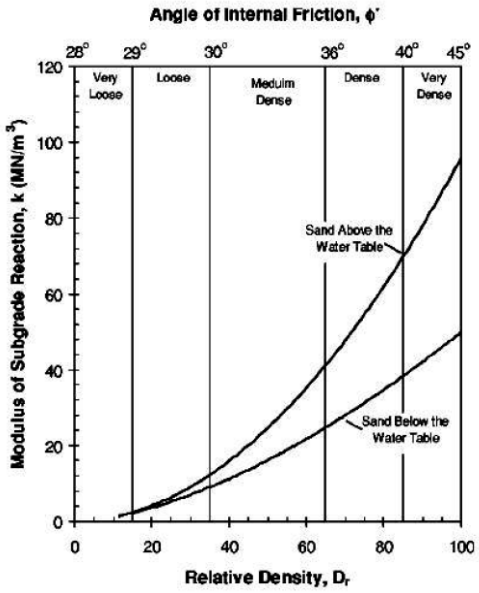

Figure C.1: Modulus of Subgrade Reaction for Sands [6]

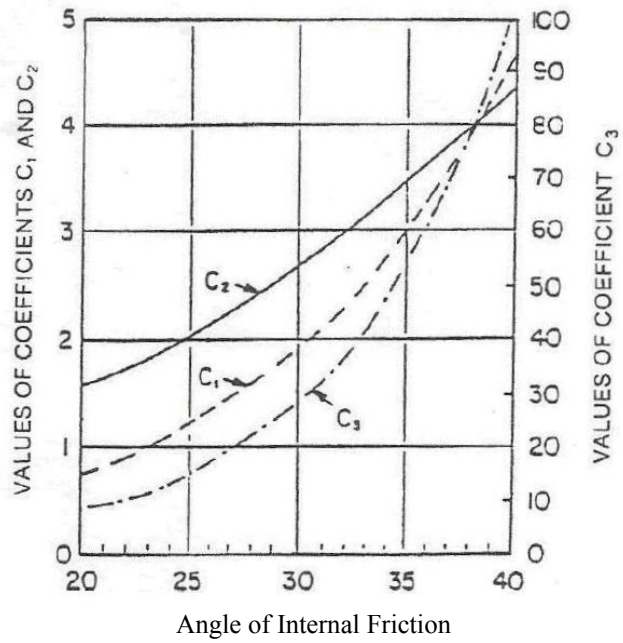

Figure C.2: Coefficients for Computation of Ultimate Bearing Capacity [6]

APPENDIX D

CONSTRUCTION OF RESPONSE SPECTRA CURVES

AASHTO-LRFD [2] Response Spectrum

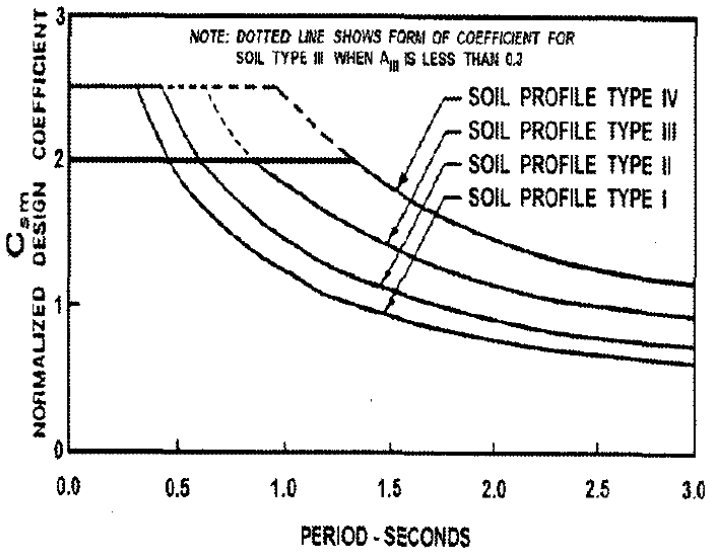

Figure D.1: AASHTO-LRFD [2] Response Spectra Curves for Different Soil Profiles

Elastic seismic response coefficient with respect to period is given as:

$$C_s = \frac{1.2\,AS}{T^{2/3}} \leq 2.5\,A \qquad \text{(D.1)}$$

where;

A : Acceleration coefficient

T : Period

S : Site coefficient (determined from Table D.1)

For soil profiles III and IV where $A \geq 0.30$, C_s need not exceed $2.0A$. (Figure D.1)

Table D.1: Site Coefficient

	Soil Profile Type			
	I	II	III	IV
S	1	1.2	1.5	2

AASHTO-Seismic [28] Response Spectrum

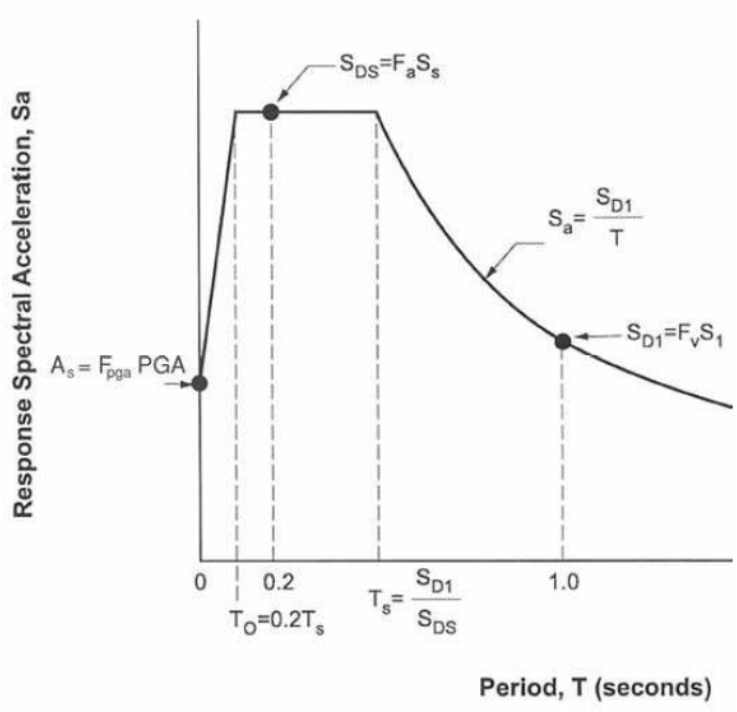

Figure D.2: AASHTO-Seismic Response Spectra [28]

Referring to the nomenclature of Figure D.2, response spectrum is constructed as:

$$S_a = (S_{DS} - A_S)\frac{T}{T_O} + A_S \qquad \text{for } T \leq T_O$$

$$S_a = S_{DS} \qquad \text{for } T_O < T \leq T_S$$

$$S_a = \frac{S_{D1}}{T} \qquad \text{for } T > T_S$$

where;

F_{PGA} : Site coefficient for peak ground acceleration

PGA : Peak horizontal ground acceleration on Class B rock

F_a : Site coefficient for 0.2 second period spectral acceleration

S_S : 0.2 second period spectral acceleration

F_v : Site coefficient for 1.0 second period spectral acceleration

S_1 : 1.0 second period spectral acceleration

F_{PGA}, F_a and F_v are determined from Table D.2 and D.3. For site class E, site-specific geotechnical investigation and dynamic site response analyses shall be performed.

Table D.2: F_{PGA} and F_a as a function of Site Class and Peak Ground Acceleration or Short Period Spectral Acceleration

Site Class	$PGA \leq 0.1$	$PGA = 0.20$	$PGA = 0.30$	$PGA = 0.40$	$PGA \geq 0.50$
	$S_s \leq 0.25$	$S_s = 0.50$	$S_s = 0.75$	$S_s = 1.00$	$S_s \geq 1.25$
A	0.8	0.8	0.8	0.8	0.8
B	1	1	1	1	1
C	1.2	1.2	1.1	1	1
D	1.6	1.4	1.2	1.1	1
E	2.5	1.7	1.2	0.9	0.9

Table D.3: F_v as a function of Site Class and 1 Second Period Spectral Acceleration

Site Class	$S_1 \leq 0.1$	$S_1 = 0.20$	$S_1 = 0.30$	$S_1 = 0.40$	$S_1 \geq 0.50$
A	0.8	0.8	0.8	0.8	0.8
B	1	1	1	1	1
C	1.7	1.6	1.5	1.4	1.3
D	2.4	2	1.8	1.6	1.5
E	3.5	3.2	2.8	2.4	2.4

APPENDIX E

SHEAR STRENGTH FORMULAS

Factored capacity should be greater than design shear force, V_d:

$$\phi_s V_n \geq V_d \tag{E.1}$$

$$V_n = V_c + V_s \tag{E.2}$$

where;

ϕ_s = 0.85 for shear in reinforced concrete

V_n = Nominal shear capacity of member (kip)

V_c = Concrete contribution to shear capacity (kip)

V_s = Reinforcing steel contribution to shear capacity (kip)

Concrete Contribution to Shear Capacity

$$V_c = \nu_c A_e \tag{E.3}$$

$$A_e = 0.8 A_g \tag{E.4}$$

If P_u is compressive;

$$\nu_c = 0.032\alpha' \left(1 + \frac{P_u}{2A_g}\right)\sqrt{f_c'} \leq \min\begin{cases} 0.11\sqrt{f_c'} \\ 0.047\alpha'\sqrt{f_c'} \end{cases} \tag{E.5}$$

Otherwise; $\nu_c = 0$ (E.6)

For circular columns with spiral or hoop reinforcing:

$$0.3 \leq \alpha' = \frac{f_s}{0.15} + 3.67 - \mu_D \leq 3 \tag{E.7}$$

$$f_s = \rho_s f_{yh} \leq 0.35 \tag{E.8}$$

$$\rho_s = \frac{4\,A_{sp}}{s\,D'} \tag{E.9}$$

Reinforcing Steel Contribution to Shear Capacity

$$V_s = \frac{\pi}{2}\left(\frac{n\,A_{sp}\,f_{yh}\,D'}{s}\right) \tag{E.10}$$

The symbols used in Equations E.3 to E.10 are:

A_g = gross area of member cross section (in^2)

A_e = effective area of cross section for shear resistance (in^2)

P_u = ultimate compressive force acting on section (kip)

s = pitch of spiral or spacing of hoops or ties (in)

D' = diameter of spiral or hoop for circular column (in)

f_{yh} = nominal yield stress of transverse reinforcing (ksi)

f_c' = nominal concrete compressive strength (ksi)

n = number of individual interlocking spiral or hoop core sections

A_{sp} = area of spiral or hoop reinforcing bar (in^2)

Maximum local displacement ductility ratio of a member, μ_D is defined as:

$$\mu_D = \frac{\Delta_{total}}{\Delta_{yi}} \tag{E.11}$$

Δ_{total} is the total displacement demand. As shear design is performed before inelastic analysis, elastic displacements are used for Δ_{total} assuming that elastic and inelastic displacements are equal. Δ_{yi} is the yield displacement corresponding to the idealized yield curvature of the member. These displacements are the relative displacements measured between the point of maximum moment to the point of contra-flexure.

Shear strength provided by the reinforcing steel, V_s, shall not be greater than:

$$V_s \le 0.25\sqrt{f_c'}\,A_e \tag{E.12}$$

APPENDIX F

MODAL ANALYSES RESULTS

Table F.1: First Two Periods Computed in RSA-I and RSA-II (in Seconds)

			Longitudinal		Transverse	
	ρ_l	H_n/D	*competent*	*poor*	*competent*	*poor*
RSA-I	1%	5	1.47	1.51	0.70	0.74
		6	1.49	1.56	0.84	0.87
		7	1.51	1.63	1.02	1.04
		8	1.58	1.70	1.21	1.22
	2%	5	1.47	1.49	0.66	0.71
		6	1.48	1.54	0.78	0.82
		7	1.50	1.60	0.94	0.97
		8	1.55	1.66	1.12	1.13
	3%	5	1.47	1.48	0.64	0.68
		6	1.48	1.52	0.74	0.78
		7	1.50	1.57	0.89	0.91
		8	1.52	1.63	1.05	1.07
	4%	5	1.46	1.46	0.62	0.67
		6	1.47	1.50	0.71	0.75
		7	1.49	1.56	0.84	0.87
		8	1.51	1.61	1.00	1.02
RSA-II	1%	5	1.52	1.67	0.72	0.76
		6	1.57	1.73	0.85	0.89
		7	1.63	1.80	1.02	1.04
		8	1.70	1.90	1.20	1.22
	2%	5	1.50	1.64	0.68	0.72
		6	1.55	1.70	0.78	0.82
		7	1.59	1.76	0.93	0.96
		8	1.66	1.85	1.11	1.13
	3%	5	1.49	1.63	0.65	0.70
		6	1.53	1.68	0.75	0.78
		7	1.57	1.74	0.88	0.91
		8	1.63	1.81	1.04	1.07
	4%	5	1.47	1.62	0.63	0.68
		6	1.52	1.67	0.72	0.76
		7	1.56	1.72	0.84	0.87
		8	1.61	1.78	0.99	1.01

APPENDIX G

RESPONSE SPECTRA OF TIME-HISTORY RECORDS

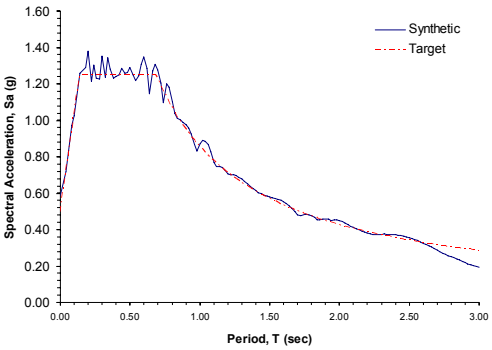

(a) *D_synth_1 N-S*

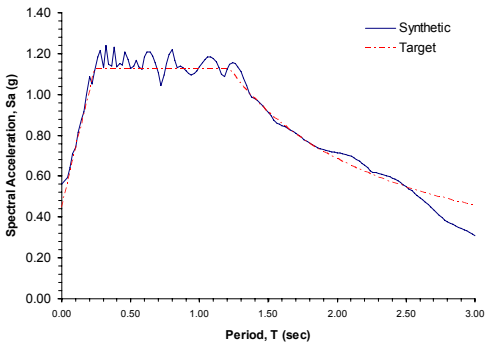

(d) *E_ synth_1 N-S*

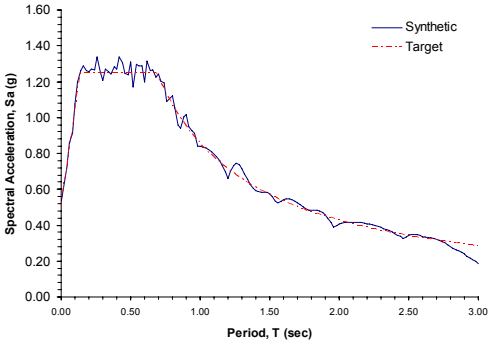

(b) *D_synth_1 E-W*

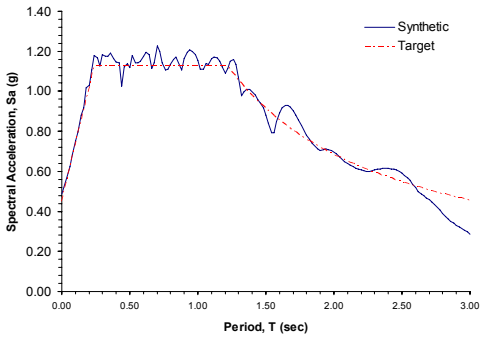

(e) *E_ synth_1 E-W*

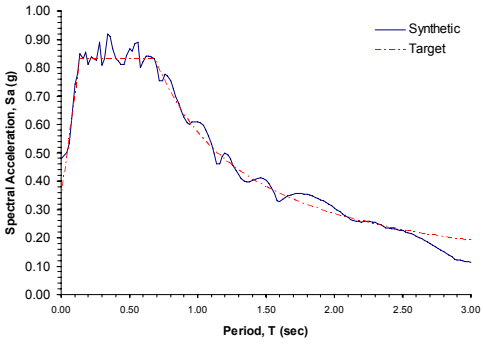

(c) *D_synth_1 vertical*

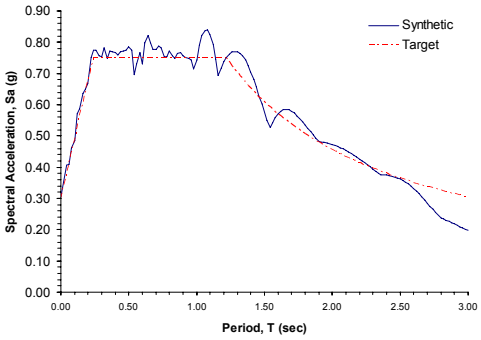

(f) *E_ synth_1 vertical*

Figure G.1: Response Spectra of Synthetic Accelerograms *D_synth_1* and *E_synth_1*

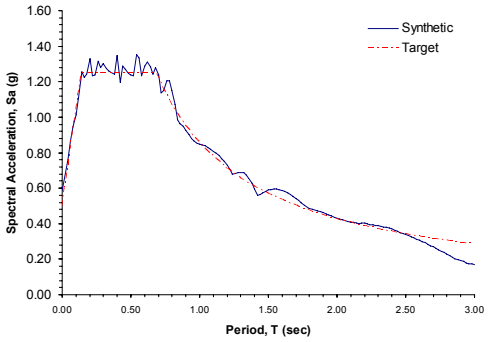

(a) *D_synth_2 N-S*

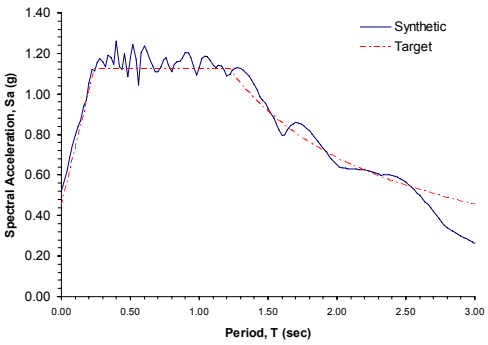

(d) *E_ synth_2 N-S*

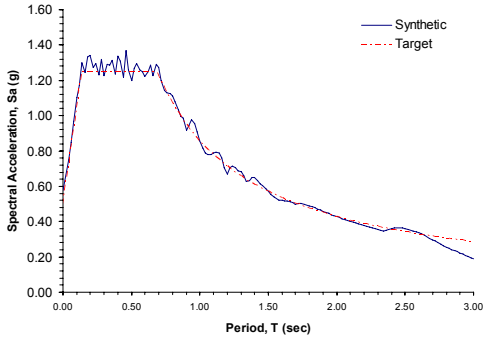

(b) *D_synth_2 E-W*

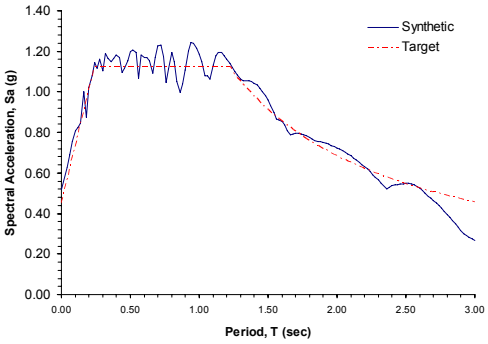

(e) *E_ synth_2 E-W*

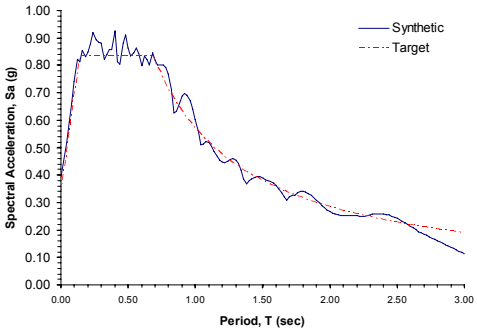

(c) *D_ synth_2 vertical*

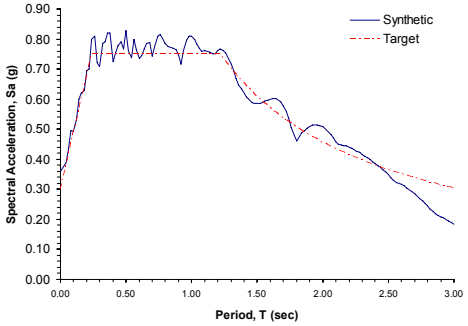

(f) *E_ synth_2 vertical*

Figure G.2: Response Spectra of Synthetic Accelerograms *D_synth_2* and *E_synth_2*

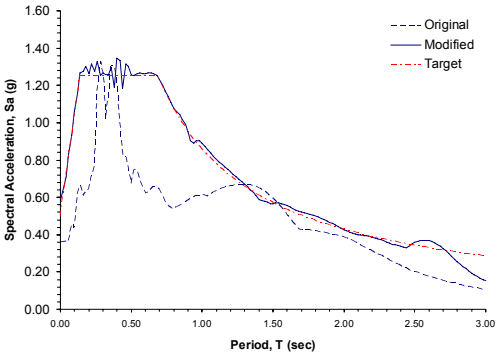

(a) *D_real_1 270*

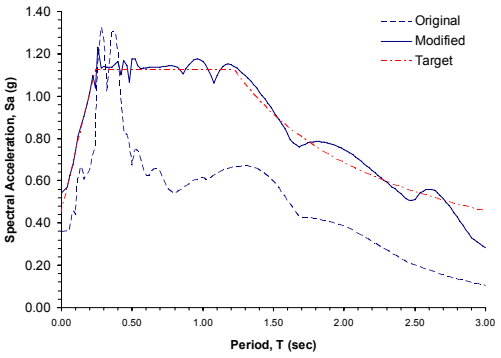

(d) *E_real_1 270*

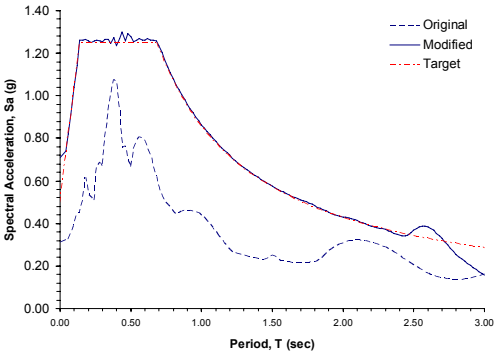

(b) *D_real_1 180*

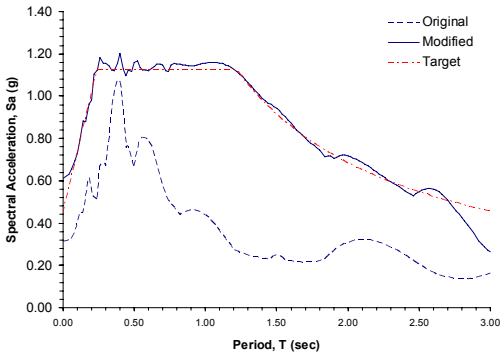

(e) *E_real_1 180*

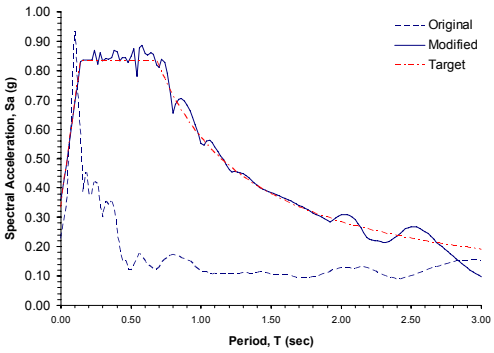

(c) *D_real_1 vertical*

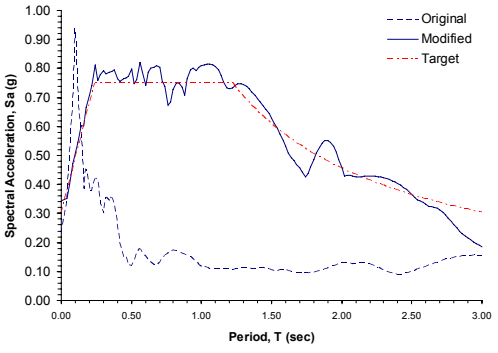

(f) *E_real_1 vertical*

Figure G.3: Response Spectra of Original and Modified Components of Accelerograms *D_real_1* and *E_real_1*

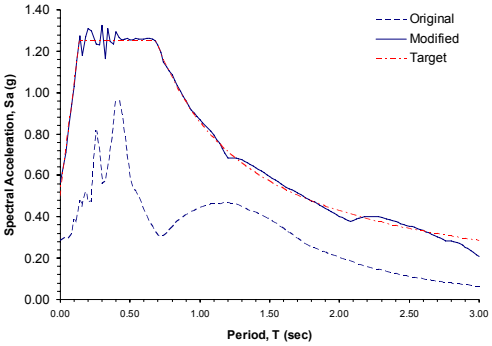

(a) *D_real_2 160*

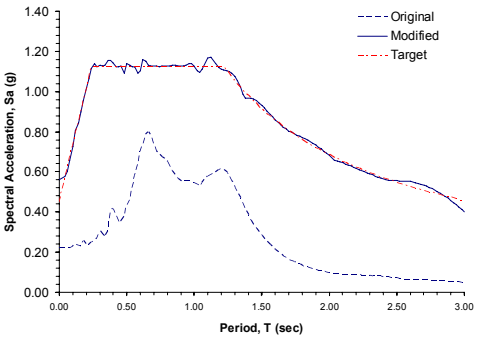

(d) *E_real_2 133*

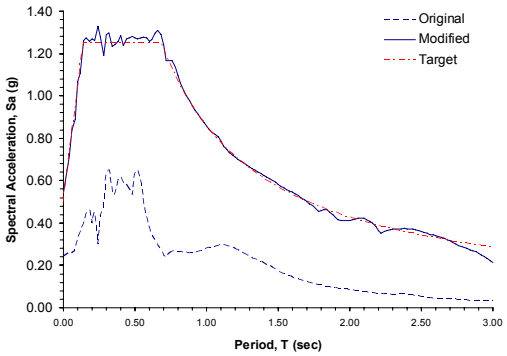

(b) *D_real_2 250*

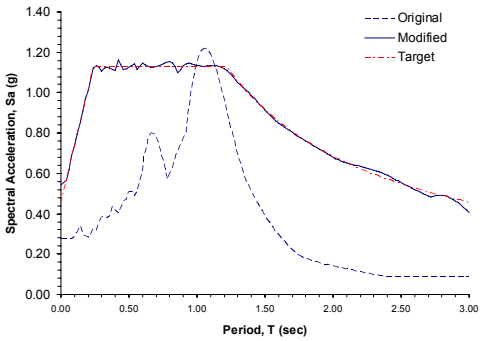

(e) *E_real_2 043*

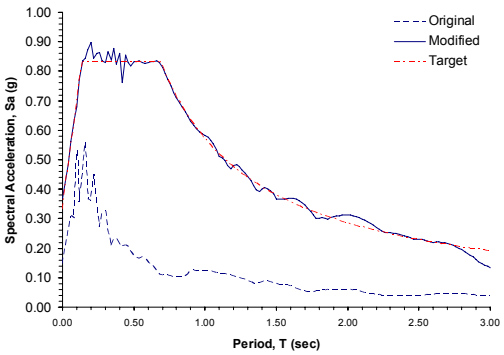

(c) *D_real_2 vertical*

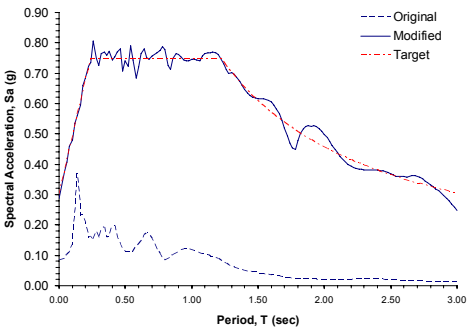

(f) *E_real_2 vertical*

Figure G.4: Response Spectra of Original and Modified Components of Accelerograms *D_real_2* and *E_real_2*

APPENDIX H

ANALYSES OUTPUTS

Table H.1: Structural Yield Displacements, Global and Relative Displacement Capacities Resulting from Push-over Analysis

	Transverse			Longitudinal		
Model	Δ_y (mm)	$(\Delta_C)^R$ (mm)	$(\Delta_C)^G$ (mm)	Δ_y (mm)	$(\Delta_C)^R$ (mm)	$(\Delta_C)^G$ (mm)
C51	65.5	321.2	347.8	115.5	363.4	392.2
C52	72.5	343.8	398.8	127.0	423.4	474.8
C53	74.0	470.6	568.2	141.0	590.3	673.6
C54	73.0	473.4	635.0	132.0	591.4	702.6
C61	78.5	330.9	350.1	123.0	385.1	402.6
C62	85.0	332.5	355.4	137.0	389.1	416.4
C63	86.0	451.7	488.0	148.0	515.2	554.7
C64	83.0	575.1	630.3	155.0	666.4	721.0
C71	96.5	354.0	362.7	131.0	409.1	421.2
C72	100.0	371.2	384.5	143.0	409.5	427.1
C73	84.5	402.2	419.7	134.0	450.8	473.3
C74	87.5	444.4	468.1	142.0	488.0	516.8
C81	112.0	378.0	384.2	140.0	437.4	446.4
C82	112.5	385.0	393.5	145.0	438.6	450.6
C83	96.0	391.4	402.2	134.0	419.2	433.9
C84	90.5	448.4	462.2	134.0	485.5	504.1
P51	65.5	320.1	357.6	115.5	371.0	404.9
P52	72.5	341.0	424.8	126.5	410.8	472.8
P53	74.0	468.9	664.1	141.0	587.6	691.9
P54	73.0	472.7	942.1	132.0	588.3	733.6
P61	79.5	333.5	351.4	123.0	392.5	412.5
P62	85.0	327.4	358.7	137.0	388.3	420.2
P63	86.0	455.7	508.8	148.0	513.5	560.6
P64	83.0	570.3	654.8	155.0	667.7	734.8
P71	96.5	386.2	397.3	131.0	374.1	387.9
P72	100.0	353.9	370.5	143.0	379.4	399.3
P73	84.5	412.0	435.3	134.0	451.9	478.1
P74	87.5	443.6	475.7	142.0	490.5	524.3
P81	112.0	377.7	385.3	140.0	435.8	446.0
P82	112.5	384.7	395.2	145.0	396.1	409.8
P83	96.0	422.1	435.5	134.0	419.0	435.9
P84	90.5	441.7	459.0	134.0	470.4	491.4

Table H.2: Elastic Displacement Demands Resulting from RSA-II

Model	Transverse			Longitudinal		
	$(\Delta_D)^G$ (mm)	Δ_f (mm)	$(\Delta_D)^R$ (mm)	$(\Delta_D)^G$ (mm)	Δ_f (mm)	$(\Delta_D)^R$ (mm)
C51	203.3	86.3	117.0	96.5	23.6	72.9
C52	189.2	98.4	90.8	85.8	25.2	60.6
C53	176.0	101.0	75.1	79.9	26.3	53.6
C54	166.5	103.0	63.6	75.1	27.2	47.8
C61	237.4	58.3	179.1	120.7	20.8	99.9
C62	218.6	69.1	149.6	107.6	21.7	85.9
C63	208.0	77.2	130.8	99.6	22.4	77.2
C64	201.3	83.4	117.9	94.2	23.0	71.1
C71	279.3	40.9	238.4	149.7	19.2	130.6
C72	255.1	48.4	206.8	132.6	19.8	112.8
C73	242.0	54.2	187.8	122.9	20.3	102.6
C74	232.2	59.5	172.7	115.7	20.7	95.0
C81	326.7	29.9	296.9	183.7	17.9	165.8
C82	302.8	34.2	268.6	165.4	18.4	146.9
C83	284.6	38.3	246.2	152.3	18.9	133.4
C84	269.1	42.5	226.6	141.6	19.3	122.3
P51	218.9	109.7	109.2	165.9	44.7	121.2
P52	195.0	115.4	79.6	147.3	47.4	99.8
P53	183.4	117.8	65.6	136.8	49.1	87.8
P54	175.2	119.8	55.4	128.6	50.6	78.0
P61	292.7	94.1	198.6	209.2	39.4	169.8
P62	251.9	99.8	152.1	186.3	41.4	144.9
P63	229.4	103.0	126.4	136.8	49.1	87.8
P64	215.7	105.5	110.2	162.8	44.0	118.8
P71	397.7	78.5	319.2	260.7	35.7	225.0
P72	336.5	85.6	250.9	230.7	37.5	193.3
P73	304.6	90.0	214.6	213.6	38.5	175.1
P74	281.0	92.6	188.3	200.9	39.5	161.4
P81	535.9	69.8	466.1	322.1	32.5	289.5
P82	463.7	73.7	390.0	289.8	34.1	255.7
P83	414.3	77.8	336.5	266.1	35.2	230.9
P84	374.6	81.4	293.1	246.5	36.2	210.3

Inelastic displacement demands, which are determined from taking the average value of resulting maximum displacements of each inelastic time-history analysis, are shown in Table H.3. Maximum global displacement demand and relative displacement demand may not necessarily occur at the same moment. Outputs of each inelastic time-history analysis are given in Tables H.4 to H.19.

Table H.3: Inelastic Displacement Demands Resulting from ITHA

	Transverse			Longitudinal		
Model	$(\Delta_D)^G$ (mm)	Δ_f (mm)	$(\Delta_D)^R$ (mm)	$(\Delta_D)^G$ (mm)	Δ_f (mm)	$(\Delta_D)^R$ (mm)
C51	207.9	16.6	192.5	125.5	20.4	105.5
C52	207.5	25.5	183.8	110.0	23.0	87.7
C53	208.5	59.9	154.2	101.8	24.1	78.7
C54	212.9	91.1	124.5	94.5	25.1	70.5
C61	248.5	12.9	236.5	180.4	14.3	166.6
C62	240.6	15.5	225.3	142.0	19.1	123.4
C63	240.3	19.8	221.1	128.4	20.1	109.2
C64	233.7	23.5	211.8	120.9	21.2	100.8
C71	317.6	6.8	311.1	232.9	8.9	224.8
C72	278.9	11.5	268.1	193.1	12.6	180.9
C73	261.2	13.3	249.0	168.9	16.1	153.2
C74	266.2	13.6	253.1	156.1	19.2	137.6
C81	361.6	5.2	356.5	297.5	5.9	292.2
C82	342.0	6.7	335.6	249.0	7.7	241.7
C83	327.6	8.6	319.4	220.7	12.7	208.6
C84	313.4	11.8	302.2	200.5	14.0	187.3
P51	254.5	19.5	237.0	246.2	28.4	218.6
P52	228.7	39.5	199.0	174.6	38.2	139.0
P53	215.8	93.4	128.7	158.2	46.6	113.0
P54	200.2	112.0	93.2	147.6	48.9	99.9
P61	359.6	15.2	344.6	331.3	18.2	313.2
P62	289.6	20.8	269.7	272.8	27.4	246.6
P63	282.1	20.3	262.5	222.9	30.6	193.6
P64	273.7	33.7	243.6	193.0	38.1	155.6
P71	385.3	8.4	376.9	380.0	10.0	370.0
P72	381.8	14.0	367.8	370.4	17.7	352.7
P73	381.9	20.4	361.8	314.8	22.7	292.2
P74	342.0	23.0	319.7	284.3	27.1	257.9
P81	397.7	7.7	390.0	384.6	9.2	375.4
P82	408.7	10.7	398.1	400.9	9.4	391.5
P83	411.7	11.3	400.4	379.1	12.5	366.8
P84	433.6	14.7	419.0	378.7	15.5	363.3

The additional output parameters shown in Tables H.4 to H.19 are defined as:

θ_{Left} : Maximum plastic rotation of left column at the moment when maximum global displacement occurs (left column can be determined from transverse plane along the direction of +Y)

θ_{Right} : Maximum plastic rotation of right column at the moment when maximum global displacement occurs

N_{Left} : Axial force on left column (compression is taken as positive)

N_{Right} : Axial force on right column

Table H.4: Global and Relative Inelastic Displacement Demands along Transverse Direction Resulting from ITHA-1

	At the Moment When Max. Global Displacement Occurs						
Model	$(\Delta_D)^G$	Δ_f	θ_{Left}	θ_{Right}	N_{left}	N_{right}	$(\Delta_D)^R$
C51	189.4	14.5	0.0113	0.0112	685.2	11855.1	174.9
C52	188.5	32.2	0.0079	0.0079	-2517.8	15147.6	159.4
C53	186.9	63.7	0.0039	0.0039	-5322.6	17844.6	129.5
C54	207.2	91.5	0.0027	0.0026	-7720.1	20185.9	119.1
C61	254.4	11.8	0.0162	0.0162	2099.6	10021.5	242.8
C62	266.8	16.9	0.0165	0.0165	656.9	11529.6	249.9
C63	251.0	18.6	0.0140	0.0139	-729.7	12950.3	232.4
C64	207.1	23.0	0.0080	0.0080	-2067.6	15114.8	185.0
C71	284.0	8.6	0.0177	0.0177	3376.7	8598.3	275.4
C72	273.7	12.5	0.0153	0.0152	2383.6	9589.1	261.3
C73	303.6	13.4	0.0177	0.0176	1402.9	10536.6	290.2
C74	301.6	16.7	0.0166	0.0166	481.0	11489.9	284.9
C81	310.6	4.1	0.0196	0.0196	4068.4	7645.2	306.9
C82	303.1	7.4	0.0169	0.0170	3607.8	8242.6	295.8
C83	327.6	11.3	0.0187	0.0187	3004.5	8846.6	316.3
C84	329.3	11.6	0.0183	0.0170	2288.5	9560.7	317.7
P51	251.6	12.1	0.0178	0.0177	146.7	12094.3	239.7
P52	191.9	44.5	0.0071	0.0071	15204.5	-2566.7	150.0
P53	232.3	98.1	0.0054	0.0053	-5473.0	17533.8	142.0
P54	229.4	127.2	0.0017	0.0017	-7237.6	19696.7	108.3
P61	338.9	12.9	0.0257	0.0257	2867.1	10128.6	325.9
P62	248.7	14.7	0.0143	0.0143	260.0	11239.1	234.0
P63	287.5	22.9	0.0169	0.0168	-1402.6	13256.6	265.9
P64	251.3	31.3	0.0119	0.0120	13986.8	-2949.5	220.9
P71	393.6	6.7	0.0313	0.0310	3769.1	9031.2	386.9
P72	395.1	15.7	0.0295	0.0293	2254.8	8852.5	379.4
P73	345.5	18.4	0.0222	0.0221	1745.7	10518.9	327.2
P74	275.3	12.7	0.0144	0.0143	-297.0	10261.3	262.7
P81	(failed along longitudinal direction)						
P82	(failed along longitudinal direction)						
P83	415.2	10.5	0.0285	0.0284	3187.6	9383.9	404.7
P84	433.5	12.7	0.0301	0.0301	2402.7	9706.8	420.9

Table H.5: Global and Relative Inelastic Displacement Demands along Transverse Direction Resulting from ITHA-2

	At the Moment When Max. Global Displacement Occurs						
Model	$(\Delta_D)^G$	Δ_f	θ_{Left}	θ_{Right}	N_{left}	N_{right}	$(\Delta_D)^R$
C51	198.3	17.3	0.0116	0.0116	12030.7	-162.6	181.8
C52	209.8	24.6	0.0113	0.0112	15121.3	-2786.2	185.9
C53	189.6	63.7	0.0040	0.0040	16075.8	-7168.1	130.0
C54	236.0	87.8	0.0063	0.0063	19361.2	-9186.6	148.7
C61	254.8	16.1	0.0163	0.0162	1578.1	8493.6	240.8
C62	197.3	23.3	0.0083	0.0082	809.6	10987.7	174.7
C63	231.3	22.8	0.0111	0.0111	12868.5	-1439.7	208.9
C64	247.8	25.2	0.0119	0.0119	14582.1	-2844.6	222.9
C71	324.8	5.3	0.0232	0.0231	5149.0	9988.0	319.9
C72	298.9	15.0	0.0183	0.0183	2090.8	8945.4	286.5
C73	266.5	15.5	0.0142	0.0142	425.3	9089.8	255.5
C74	245.4	11.4	0.0113	0.0113	-398.9	10785.5	234.9
C81	334.4	5.7	0.0225	0.0224	5785.7	9098.5	328.8
C82	314.2	4.2	0.0191	0.0191	7907.4	3611.5	310.8
C83	312.8	11.5	0.0177	0.0177	8593.7	3421.4	301.7
C84	306.1	13.6	0.0159	0.0159	2607.5	9479.2	294.2
P51	225.3	16.0	0.0148	0.0148	574.0	11881.1	209.6
P52	202.8	35.8	0.0094	0.0094	-2522.2	15005.2	170.5
P53	205.4	81.7	0.0042	0.0043	15920.8	-7220.0	129.0
P54	206.5	120.7	0.0006	0.0005	-6308.3	17128.4	97.4
P61	(failed along longitudinal direction)						
P62	256.0	13.2	0.0153	0.0154	10554.7	-417.0	243.1
P63	272.6	19.8	0.0158	0.0158	-882.7	12983.9	252.8
P64	253.7	40.6	0.0113	0.0112	-2336.1	14531.0	217.7
P71	394.3	7.6	0.0315	0.0311	3566.8	8673.8	386.8
P72	(failed along longitudinal direction)						
P73	351.7	23.3	0.0223	0.0223	1241.9	10240.3	328.8
P74	319.9	26.7	0.0178	0.0178	228.3	10840.4	293.9
P81	394.8	4.6	0.0295	0.0294	4171.5	7612.6	390.3
P82	412.5	10.6	0.0298	0.0295	3442.5	8056.7	402.0
P83	392.3	10.0	0.0258	0.0258	2996.9	9214.4	382.5
P84	394.3	15.4	0.0250	0.0250	2314.4	9883.2	379.8

Table H.6: Global and Relative Inelastic Displacement Demands along Transverse Direction Resulting from ITHA-3

	At the Moment When Max. Global Displacement Occurs						
Model	$(\Delta_D)^G$	Δ_f	θ_{Left}	θ_{Right}	N_{left}	N_{right}	$(\Delta_D)^R$
C51	174.5	14.1	0.0095	0.0094	211.3	11227.9	160.4
C52	201.3	27.7	0.0099	0.0099	16154.6	-2443.5	175.4
C53	223.0	53.2	0.0090	0.0090	19215.2	-5158.4	174.9
C54	236.9	88.4	0.0063	0.0063	21533.9	-7751.6	155.8
C61	210.5	18.8	0.0102	0.0104	5233.3	4778.7	192.3
C62	210.2	13.1	0.0104	0.0104	10620.4	-249.7	197.1
C63	199.1	20.0	0.0080	0.0080	12826.2	-407.5	179.9
C64	213.1	27.3	0.0083	0.0083	14692.7	-1844.4	192.7
C71	267.5	7.9	0.0169	0.0169	4953.4	9067.7	260.9
C72	214.1	10.3	0.0097	0.0096	4675.4	11006.9	204.2
C73	219.6	13.6	0.0088	0.0088	9455.6	711.2	206.0
C74	226.9	12.0	0.0095	0.0095	1710.3	11553.4	214.9
C81	348.0	6.5	0.0236	0.0235	4935.1	8306.1	341.8
C82	294.5	4.9	0.0164	0.0163	4462.3	8854.1	289.6
C83	298.4	10.5	0.0161	0.0160	4458.2	9584.0	288.6
C84	286.5	9.7	0.0145	0.0145	3388.3	9942.0	277.5
P51	233.0	18.6	0.0154	0.0154	-660.9	11127.0	215.1
P52	219.6	31.4	0.0116	0.0116	-3996.8	14109.8	190.7
P53	230.9	97.4	0.0049	0.0049	18296.5	-5288.1	135.0
P54	223.6	127.1	0.0009	0.0010	18592.8	-7245.9	99.9
P61	319.3	10.7	0.0238	0.0237	3340.7	10913.6	309.5
P62	244.8	15.4	0.0144	0.0143	-1264.1	8959.1	229.4
P63	262.5	18.9	0.0149	0.0149	-1740.0	12364.7	243.5
P64	234.1	40.6	0.0091	0.0092	14274.1	-2890.6	200.2
P71	342.3	5.6	0.0251	0.0251	1934.0	6408.7	336.8
P72	343.1	9.5	0.0234	0.0233	3743.2	10825.4	333.9
P73	353.1	16.1	0.0234	0.0235	11773.5	2927.7	337.0
P74	318.4	29.7	0.0173	0.0173	9991.5	-988.1	288.7
P81	396.0	7.2	0.0297	0.0296	2911.1	5878.8	388.9
P82	(failed along longitudinal direction)						
P83	378.7	6.4	0.0251	0.0251	3702.8	9218.1	372.4
P84	382.3	10.0	0.0244	0.0244	3745.3	10838.3	372.5

Table H.7: Global and Relative Inelastic Displacement Demands along Transverse Direction Resulting from ITHA-4

	At the Moment When Max. Global Displacement Occurs						
Model	$(\Delta_D)^G$	Δ_f	θ_{Left}	θ_{Right}	N_{left}	N_{right}	$(\Delta_D)^R$
C51	220.2	21.7	0.0137	0.0137	13040.7	1899.4	199.3
C52	166.3	24.8	0.0067	0.0068	14834.9	-1978.6	143.4
C53	200.9	57.8	0.0061	0.0061	-5973.3	16794.9	145.8
C54	216.5	103.6	0.0023	0.0024	20536.9	-7416.2	113.6
C61	226.3	10.5	0.0136	0.0136	2981.9	10207.1	216.0
C62	261.8	15.0	0.0159	0.0160	12386.0	1764.2	246.9
C63	265.6	20.2	0.0149	0.0150	14446.8	363.9	245.4
C64	246.5	26.3	0.0118	0.0119	15588.6	-1551.3	220.6
C71	257.5	4.3	0.0159	0.0160	6398.8	2036.9	253.2
C72	284.0	10.6	0.0170	0.0169	2979.7	9894.4	273.4
C73	263.7	8.8	0.0142	0.0143	9842.8	1388.5	255.0
C74	292.2	12.7	0.0161	0.0162	11855.4	1285.3	279.5
C81	352.2	7.6	0.0244	0.0244	6324.3	3263.9	344.8
C82	309.2	8.1	0.0181	0.0181	8068.3	3744.4	302.2
C83	288.0	7.5	0.0151	0.0152	6341.6	989.1	281.1
C84	327.3	13.5	0.0182	0.0182	2680.9	9681.7	313.8
P51	227.8	20.5	0.0145	0.0145	11690.0	-128.7	207.6
P52	200.1	45.6	0.0081	0.0080	-2322.2	15319.6	158.5
P53	232.0	102.2	0.0047	0.0047	17122.4	-5622.7	131.8
P54	193.6	109.6	0.0000	0.0000	16630.3	-6081.1	85.6
P61	327.9	12.9	0.0246	0.0246	7051.8	489.1	315.1
P62	288.5	23.3	0.0181	0.0181	9482.6	-620.8	265.7
P63	252.0	25.0	0.0129	0.0130	13220.1	-934.4	229.1
P64	276.5	41.6	0.0136	0.0135	-1660.0	15479.0	239.8
P71	389.4	6.2	0.0310	0.0311	5671.8	1357.3	383.3
P72	366.4	13.0	0.0258	0.0258	6975.0	639.9	353.5
P73	312.2	14.3	0.0189	0.0189	8341.6	76.7	298.2
P74	329.4	16.6	0.0198	0.0198	9504.2	-811.1	313.1
P81	(failed along longitudinal direction)						
P82	396.2	6.9	0.0277	0.0277	5688.1	1421.1	389.3
P83	416.6	10.1	0.0295	0.0295	5745.9	537.1	406.5
P84	417.0	14.4	0.0278	0.0278	4831.0	11574.5	402.8

Table H.8: Global and Relative Inelastic Displacement Demands along Transverse Direction Resulting from ITHA-5

	At the Moment When Max. Global Displacement Occurs						
Model	$(\Delta_D)^G$	Δ_f	θ_{Left}	θ_{Right}	N_{left}	N_{right}	$(\Delta_D)^R$
C51	240.7	16.6	0.0165	0.0165	12345.8	1310.3	227.1
C52	248.2	16.5	0.0160	0.0161	15752.4	-2893.7	232.6
C53	221.7	51.1	0.0092	0.0092	18021.9	-5613.6	178.6
C54	194.0	78.3	0.0028	0.0029	20161.8	-8040.0	119.0
C61	241.0	11.8	0.0151	0.0151	1883.5	9350.9	229.2
C62	254.1	19.0	0.0147	0.0148	12005.1	1673.9	235.5
C63	277.9	18.6	0.0164	0.0164	13599.6	-352.5	260.0
C64	262.8	21.9	0.0138	0.0139	14950.8	-2143.4	241.0
C71	359.0	5.0	0.0268	0.0267	4085.2	9072.6	354.1
C72	284.5	11.4	0.0169	0.0169	2013.6	9239.7	273.3
C73	239.7	14.0	0.0111	0.0111	11048.9	1821.3	226.3
C74	273.0	17.4	0.0137	0.0137	12088.0	1636.5	255.7
C81	396.8	2.9	0.0299	0.0297	4612.8	7955.4	393.9
C82	375.8	5.2	0.0254	0.0253	4246.5	8867.4	370.5
C83	345.9	7.5	0.0211	0.0211	3265.1	9261.7	338.4
C84	308.7	11.4	0.0163	0.0163	1991.3	9285.1	297.5
P51	253.9	9.2	0.0184	0.0185	12184.9	950.9	246.2
P52	251.0	35.1	0.0147	0.0147	15513.8	-2412.2	222.1
P53	203.7	93.2	0.0028	0.0028	16880.1	-5682.2	122.6
P54	190.8	107.5	0.0001	0.0002	18035.7	-4353.6	94.1
P61	380.0	14.9	0.0311	0.0309	2355.1	9319.3	365.1
P62	287.1	20.4	0.0187	0.0187	10891.0	1043.3	272.5
P63	298.2	11.1	0.0193	0.0194	13612.2	-412.5	287.5
P64	303.2	28.7	0.0179	0.0180	15041.8	-2029.8	281.3
P71	(failed along longitudinal direction)						
P72	386.4	8.2	0.0283	0.0282	3208.3	10199.5	378.2
P73	404.7	25.9	0.0278	0.0279	754.2	9622.0	379.1
P74	326.5	21.4	0.0192	0.0192	311.5	10771.2	307.5
P81	(failed along longitudinal direction)						
P82	408.2	12.5	0.0287	0.0286	3243.3	7260.5	395.7
P83	417.4	10.0	0.0292	0.0291	3208.8	8589.6	407.4
P84	470.5	13.3	0.0339	0.0339	2397.9	9211.5	457.2

Table H.9: Global and Relative Inelastic Displacement Demands along Transverse Direction Resulting from ITHA-6

	At the Moment When Max. Global Displacement Occurs						
Model	$(\Delta_D)^G$	Δ_f	θ_{Left}	θ_{Right}	N_{left}	N_{right}	$(\Delta_D)^R$
C51	192.6	18.7	0.0109	0.0110	12706.9	1454.0	174.8
C52	191.8	22.2	0.0093	0.0094	14391.1	-4091.6	171.7
C53	222.9	70.0	0.0072	0.0072	16613.3	-6767.3	159.9
C54	201.2	93.9	0.0019	0.0020	18521.1	-7993.2	108.6
C61	250.3	9.8	0.0164	0.0163	2866.4	10160.4	242.7
C62	245.1	16.8	0.0140	0.0140	11346.4	559.4	228.3
C63	220.2	22.8	0.0099	0.0099	13996.5	26.2	197.4
C64	200.2	18.9	0.0078	0.0077	-2765.6	14023.6	183.7
C71	359.2	4.9	0.0269	0.0269	3542.7	8251.1	354.7
C72	272.5	7.5	0.0160	0.0160	2876.1	9860.9	266.2
C73	270.7	16.4	0.0142	0.0143	10307.6	1640.4	254.8
C74	286.9	16.3	0.0153	0.0153	10914.0	193.4	271.2
C81	394.4	1.8	0.0298	0.0297	4730.2	7838.1	392.6
C82	407.7	4.1	0.0299	0.0297	3788.9	8332.4	403.6
C83	346.7	5.4	0.0215	0.0215	3203.1	8973.3	341.3
C84	293.7	7.8	0.0151	0.0151	2754.0	9764.4	286.2
P51	172.8	20.9	0.0085	0.0085	12685.5	1365.2	158.7
P52	255.0	45.9	0.0139	0.0139	14558.5	-4197.8	224.3
P53	211.3	104.3	0.0022	0.0022	16204.2	-6272.0	116.5
P54	189.9	112.1	0.0000	0.0000	15830.2	-5677.0	84.6
P61	381.6	16.1	0.0304	0.0303	3585.0	11084.5	365.5
P62	242.4	23.2	0.0130	0.0130	11751.4	1195.3	219.3
P63	212.7	15.2	0.0098	0.0098	-854.4	13011.4	197.6
P64	262.6	16.4	0.0145	0.0145	14545.2	-2995.0	246.8
P71	397.6	11.0	0.0314	0.0312	4574.3	9422.8	386.6
P72	396.3	14.7	0.0294	0.0292	3228.9	10417.4	381.5
P73	415.4	21.2	0.0295	0.0295	1933.7	11348.1	395.3
P74	327.1	25.2	0.0188	0.0188	1638.2	12706.4	302.7
P81	398.6	9.8	0.0297	0.0296	5625.1	8821.6	388.8
P82	410.0	9.3	0.0291	0.0290	4814.0	9479.0	400.7
P83	421.3	10.8	0.0299	0.0296	4009.5	9982.1	410.5
P84	478.6	19.8	0.0345	0.0343	3549.2	10921.0	458.7

Table H.10: Global and Relative Inelastic Displacement Demands along Transverse Direction Resulting from ITHA-7

	At the Moment When Max. Global Displacement Occurs						
Model	$(\Delta_D)^G$	Δ_f	θ_{Left}	θ_{Right}	N_{left}	N_{right}	$(\Delta_D)^R$
C51	226.0	21.1	0.0142	0.0142	13807.6	1326.4	209.0
C52	215.9	30.3	0.0111	0.0112	14034.6	-4545.3	185.7
C53	231.7	58.3	0.0095	0.0095	17324.9	-6369.9	179.5
C54	214.8	99.2	0.0028	0.0028	19231.9	-8744.1	119.4
C61	276.0	10.6	0.0192	0.0193	11714.5	5377.7	266.0
C62	251.3	10.4	0.0150	0.0151	13854.6	2878.9	240.9
C63	209.1	23.7	0.0086	0.0086	13891.2	-508.1	188.1
C64	229.6	23.9	0.0101	0.0101	-1238.2	16210.9	205.7
C71	295.7	8.8	0.0200	0.0201	9790.9	6038.1	287.1
C72	262.0	10.3	0.0148	0.0149	11495.7	5446.0	253.1
C73	254.2	10.1	0.0132	0.0132	12515.4	4504.2	245.9
C74	249.4	9.6	0.0119	0.0119	13540.9	3306.6	240.6
C81	362.8	5.9	0.0258	0.0259	8340.5	6010.6	357.4
C82	319.3	8.9	0.0193	0.0194	9708.6	6088.5	310.4
C83	292.0	8.8	0.0154	0.0154	3916.1	9745.7	283.2
C84	286.3	12.0	0.0141	0.0140	3522.5	10338.4	274.3
P51	328.7	21.9	0.0254	0.0254	14447.7	2442.1	310.2
P52	252.7	41.8	0.0139	0.0139	15675.7	-3168.8	217.2
P53	201.2	84.6	0.0033	0.0033	16727.9	-6284.3	121.7
P54	180.1	94.5	0.0000	0.0000	17018.9	-6744.6	85.6
P61	385.4	21.5	0.0302	0.0301	1798.0	9240.6	363.9
P62	360.1	24.5	0.0256	0.0256	713.1	11972.0	335.7
P63	313.7	18.9	0.0200	0.0201	15537.1	729.1	294.8
P64	300.0	35.4	0.0166	0.0167	16015.3	-1614.9	268.8
P71	394.3	13.1	0.0301	0.0301	3953.2	9058.4	381.2
P72	403.3	22.8	0.0294	0.0291	1937.5	9024.3	380.5
P73	455.9	26.4	0.0342	0.0340	1065.8	10338.4	429.5
P74	411.8	30.7	0.0273	0.0273	105.0	11455.8	382.4
P81	401.3	9.4	0.0302	0.0299	4783.2	8191.1	391.9
P82	416.7	14.1	0.0299	0.0297	3965.6	8735.9	402.6
P83	427.5	19.1	0.0297	0.0296	3039.5	8970.5	408.4
P84	480.9	21.9	0.0348	0.0346	2499.2	9889.9	459.1

Table H.11: Global and Relative Inelastic Displacement Demands along Transverse Direction Resulting from ITHA-8

	At the Moment When Max. Global Displacement Occurs						
Model	$(\Delta_D)^G$	Δ_f	θ_{Left}	θ_{Right}	N_{left}	N_{right}	$(\Delta_D)^R$
C51	221.4	9.2	0.0149	0.0148	3850.7	15153.2	212.7
C52	238.6	25.7	0.0142	0.0142	-14.5	18274.3	216.5
C53	191.2	61.6	0.0047	0.0047	-3761.8	19324.2	135.2
C54	196.3	86.4	0.0022	0.0022	16931.8	-10376.8	112.0
C61	274.9	13.4	0.0188	0.0188	9268.2	2078.3	261.9
C62	238.0	9.8	0.0139	0.0138	3940.1	13966.9	229.2
C63	268.3	11.5	0.0161	0.0160	2442.4	16292.8	256.8
C64	262.9	21.5	0.0142	0.0141	851.0	17798.4	243.2
C71	393.0	9.7	0.0307	0.0308	7270.4	2654.5	383.3
C72	341.1	14.7	0.0228	0.0229	10047.6	2947.6	326.9
C73	271.9	15.0	0.0146	0.0147	9058.0	495.6	258.1
C74	254.6	12.4	0.0122	0.0122	3479.0	13458.2	242.9
C81	393.4	7.2	0.0290	0.0290	6199.1	3220.0	386.1
C82	412.6	10.6	0.0296	0.0299	8004.2	3504.3	402.0
C83	409.7	6.4	0.0282	0.0283	10709.3	4643.4	404.9
C84	369.2	14.5	0.0226	0.0227	10432.7	3170.6	356.0
P51	343.3	36.8	0.0255	0.0255	12642.7	252.7	308.7
P52	256.5	36.1	0.0150	0.0150	16167.6	-2307.0	223.1
P53	209.3	85.3	0.0042	0.0042	18325.6	-4704.9	130.5
P54	187.4	97.1	0.0000	0.0000	19038.2	-5913.0	90.6
P61	384.0	17.1	0.0305	0.0306	10479.6	2871.2	366.9
P62	389.4	31.5	0.0282	0.0284	12301.5	661.1	357.9
P63	357.7	30.6	0.0239	0.0239	13715.5	-1209.9	329.2
P64	308.0	35.0	0.0174	0.0175	15268.6	-2294.1	273.6
P71	(failed along longitudinal direction)						
P72	(failed along longitudinal direction)						
P73	416.4	17.9	0.0299	0.0299	9073.4	364.8	399.1
P74	427.7	21.2	0.0298	0.0298	12014.9	521.0	406.6
P81	(failed along longitudinal direction)						
P82	(failed along longitudinal direction)						
P83	424.6	13.8	0.0297	0.0299	9851.0	3675.7	410.8
P84	411.5	10.4	0.0276	0.0276	2777.5	9723.6	401.2

Table H.12: Global and Relative Inelastic Displacement Demands along Longitudinal Direction Resulting from ITHA-1

	At the Moment When Max. Global Displacement Occurs						
Model	$(\Delta_D)^G$	Δ_f	θ_{Left}	θ_{Right}	N_{left}	N_{right}	$(\Delta_D)^R$
C51	93.7	16.6	0.0000	0.0000	5001.8	7182.8	77.2
C52	86.6	16.7	0.0000	0.0000	8339.7	4638.5	71.3
C53	84.1	16.1	0.0000	0.0000	9089.9	4075.6	68.5
C54	80.4	16.8	0.0000	0.0000	8419.9	4862.4	63.8
C61	132.0	14.3	0.0012	0.0004	4272.0	8211.1	118.5
C62	106.0	16.7	0.0000	0.0000	3554.1	9693.2	91.5
C63	91.9	14.3	0.0000	0.0000	5046.6	6736.2	79.0
C64	88.4	15.8	0.0000	0.0000	5298.0	6951.5	72.7
C71	176.7	9.5	0.0061	0.0053	7165.6	5096.2	167.2
C72	141.8	9.1	0.0000	0.0000	5474.9	5966.7	132.8
C73	130.1	10.2	0.0000	0.0000	5527.1	5841.0	120.3
C74	123.5	15.7	0.0000	0.0000	4050.0	8531.8	108.4
C81	209.8	7.1	0.0086	0.0071	6989.3	5346.8	203.2
C82	188.0	8.7	0.0039	0.0029	7076.6	4937.8	179.5
C83	169.7	13.6	0.0000	0.0000	7060.2	4841.8	156.8
C84	154.0	14.1	0.0000	0.0000	5913.5	5423.2	141.7
P51	233.1	25.0	0.0122	0.0129	5560.0	7206.8	208.0
P52	158.5	37.1	0.0006	0.0008	7450.8	5443.2	123.3
P53	144.2	41.1	0.0000	0.0000	8299.7	4707.8	108.8
P54	137.1	44.2	0.0000	0.0000	10820.9	2167.0	99.1
P61	335.6	19.5	0.0237	0.0242	6416.4	5515.9	316.2
P62	280.3	24.7	0.0147	0.0155	4769.4	7681.7	255.8
P63	213.8	27.3	0.0057	0.0055	4403.8	7403.8	188.9
P64	188.6	34.2	0.0006	0.0007	5388.8	6868.9	155.3
P71	(failed along transverse direction)						
P72	(failed along transverse direction)						
P73	294.1	25.2	0.0141	0.0145	5270.0	6657.4	268.9
P74	307.7	26.5	0.0142	0.0149	4759.1	7420.3	282.2
P81	383.9	9.2	0.0266	0.0285	3596.5	5847.1	374.7
P82	398.6	6.5	0.0263	0.0284	4759.7	7793.7	392.1
P83	337.6	8.5	0.0187	0.0204	4652.1	8027.3	329.2
P84	303.3	9.7	0.0151	0.0149	3666.9	6783.0	293.7

Table H.13: Global and Relative Inelastic Displacement Demands along Longitudinal Direction Resulting from ITHA-2

	At the Moment When Max. Global Displacement Occurs						
Model	$(\Delta_D)^G$	Δ_f	θ_{Left}	θ_{Right}	N_{left}	N_{right}	$(\Delta_D)^R$
C51	133.4	21.4	0.0017	0.0011	9438.9	3077.2	112.6
C52	115.3	20.8	0.0000	0.0000	7224.5	5467.1	96.0
C53	106.5	23.9	0.0000	0.0000	6305.0	6354.5	84.9
C54	97.8	24.1	0.0000	0.0000	6601.4	6002.1	75.2
C61	218.3	12.0	0.0116	0.0116	6832.3	5603.0	206.3
C62	159.8	22.1	0.0015	0.0011	7044.1	5168.3	138.1
C63	136.3	22.1	0.0000	0.0000	9284.2	2835.3	116.7
C64	127.0	22.9	0.0000	0.0000	9354.0	2797.9	109.3
C71	216.3	6.6	0.0111	0.0106	6427.9	6000.2	209.7
C72	236.4	10.8	0.0107	0.0106	6004.2	6235.9	225.7
C73	206.4	17.8	0.0046	0.0049	6154.3	5993.1	189.7
C74	179.4	22.8	0.0000	0.0000	6264.5	5704.3	156.7
C81	286.7	3.9	0.0172	0.0165	5692.6	6972.0	282.9
C82	246.5	5.1	0.0096	0.0109	6533.3	5525.0	241.4
C83	249.2	15.5	0.0097	0.0088	6240.9	5851.0	233.7
C84	243.1	10.7	0.0080	0.0074	6091.1	5977.2	232.3
P51	272.6	30.3	0.0170	0.0163	10674.7	2853.5	242.4
P52	165.4	31.8	0.0021	0.0016	11425.3	1993.0	133.6
P53	151.6	37.2	0.0000	0.0000	13088.9	361.4	114.5
P54	128.0	34.7	0.0000	0.0000	10913.6	2460.7	93.6
P61	380.0	21.9	0.0286	0.0282	8350.9	3998.1	358.1
P62	304.2	31.7	0.0175	0.0169	9377.0	3642.2	272.7
P63	235.4	31.5	0.0078	0.0069	10516.1	2552.4	204.6
P64	190.4	33.7	0.0011	0.0004	9703.0	3432.7	156.7
P71	(failed along transverse direction)						
P72	393.7	21.5	0.0271	0.0267	7779.4	4225.2	372.2
P73	352.9	27.1	0.0214	0.0205	8658.0	3563.4	325.9
P74	302.9	32.6	0.0142	0.0127	9523.5	3065.0	271.1
P81	(failed along transverse direction)						
P82	(failed along transverse direction)						
P83	410.7	14.4	0.0273	0.0270	6603.5	4809.4	396.8
P84	392.5	19.3	0.0241	0.0237	7517.3	4139.0	373.6

Table H.14: Global and Relative Inelastic Displacement Demands along Longitudinal Direction Resulting from ITHA-3

	At the Moment When Max. Global Displacement Occurs						
Model	$(\Delta_D)^G$	Δ_f	θ_{Left}	θ_{Right}	N_{left}	N_{right}	$(\Delta_D)^R$
C51	134.7	18.2	0.0017	0.0018	7139.2	7386.2	116.6
C52	116.6	20.5	0.0000	0.0000	7339.3	5800.1	96.2
C53	107.7	22.0	0.0000	0.0000	6222.6	6502.0	85.7
C54	100.4	25.4	0.0000	0.0000	3538.2	13106.1	76.3
C61	210.5	18.8	0.0102	0.0104	5233.3	4778.7	192.3
C62	152.6	17.2	0.0008	0.0011	8141.3	6246.6	135.7
C63	140.9	18.9	0.0000	0.0000	9517.1	3873.5	122.7
C64	133.0	19.0	0.0000	0.0000	8678.3	4326.2	114.2
C71	307.5	7.3	0.0205	0.0214	5940.9	3244.1	301.2
C72	221.5	17.9	0.0079	0.0087	6191.6	4052.8	204.3
C73	182.9	16.3	0.0018	0.0022	7022.9	6156.8	167.5
C74	168.9	22.8	0.0000	0.0000	9371.7	5291.3	150.6
C81	354.1	9.1	0.0241	0.0250	7571.7	5912.5	347.3
C82	311.3	6.0	0.0174	0.0185	5910.9	3422.6	305.7
C83	262.8	15.3	0.0101	0.0113	6138.2	2976.9	248.1
C84	225.0	17.6	0.0040	0.0055	7139.0	3832.6	208.1
P51	193.5	26.3	0.0074	0.0079	10550.4	3786.9	167.2
P52	142.8	35.7	0.0000	0.0000	11779.6	2062.2	107.5
P53	135.1	42.1	0.0000	0.0000	12224.6	-70.4	96.8
P54	130.8	45.2	0.0000	0.0000	11010.8	1395.4	86.7
P61	282.9	17.3	0.0177	0.0187	7922.2	4576.5	265.6
P62	247.1	26.8	0.0108	0.0114	10561.5	4933.1	220.4
P63	185.3	29.7	0.0014	0.0022	8311.8	995.2	156.5
P64	164.5	33.1	0.0000	0.0000	8980.7	-925.8	131.6
P71	383.8	13.6	0.0279	0.0283	2883.5	5071.5	370.4
P72	336.7	16.8	0.0207	0.0215	6805.6	4103.1	319.9
P73	300.0	24.1	0.0152	0.0158	8497.5	5191.8	276.0
P74	258.4	26.6	0.0082	0.0091	10477.3	5131.8	232.2
P81	(failed along transverse direction)						
P82	401.5	14.2	0.0265	0.0271	5043.7	7252.5	387.3
P83	389.0	14.6	0.0239	0.0255	6284.8	3178.5	374.4
P84	370.6	17.2	0.0211	0.0221	6461.4	4040.2	353.4

Table H.15: Global and Relative Inelastic Displacement Demands along Longitudinal Direction Resulting from ITHA-4

	At the Moment When Max. Global Displacement Occurs						
Model	$(\Delta_D)^G$	Δ_f	θ_{Left}	θ_{Right}	N_{left}	N_{right}	$(\Delta_D)^R$
C51	122.3	17.5	0.0005	0.0004	5247.6	8149.5	104.9
C52	106.9	20.1	0.0000	0.0000	3816.6	9510.1	87.0
C53	99.7	21.9	0.0000	0.0000	1546.9	11645.4	78.1
C54	92.5	23.3	0.0000	0.0000	-25.0	12987.8	69.5
C61	172.1	14.8	0.0057	0.0058	5737.6	7692.3	157.4
C62	138.0	15.8	0.0000	0.0000	7120.6	6107.4	122.2
C63	125.4	16.6	0.0000	0.0000	5293.7	7816.9	108.8
C64	117.6	17.5	0.0000	0.0000	4549.2	8516.2	100.2
C71	240.2	7.3	0.0132	0.0130	6554.6	4938.5	233.6
C72	178.9	13.9	0.0033	0.0031	5940.5	7224.7	165.1
C73	158.2	15.8	0.0000	0.0000	5856.4	7435.1	142.6
C74	149.2	15.3	0.0000	0.0000	6418.7	6768.1	134.0
C81	354.9	6.0	0.0245	0.0244	5782.5	5260.4	349.0
C82	263.5	8.3	0.0126	0.0119	6550.5	4671.2	255.6
C83	210.8	11.8	0.0054	0.0042	5500.6	7233.2	200.2
C84	187.4	14.9	0.0004	0.0001	6428.5	6746.4	172.6
P51	245.5	26.5	0.0142	0.0143	6785.3	4310.6	220.2
P52	169.9	42.4	0.0015	0.0013	5438.4	10239.9	136.0
P53	163.2	48.8	0.0000	0.0000	1160.4	8505.2	114.6
P54	154.7	51.7	0.0000	0.0000	4304.5	6157.7	103.1
P61	326.8	13.9	0.0241	0.0222	6819.1	2447.5	312.9
P62	275.0	21.8	0.0156	0.0152	5126.8	5004.6	253.9
P63	222.5	32.2	0.0059	0.0060	7861.6	5142.1	192.4
P64	190.7	41.5	0.0002	0.0001	8850.3	7049.9	149.2
P71	(failed along transverse direction)						
P72	360.0	14.6	0.0247	0.0225	7538.6	4009.4	345.3
P73	326.4	16.2	0.0202	0.0187	4373.6	5557.6	310.4
P74	286.5	19.6	0.0135	0.0129	4495.9	5408.0	267.5
P81	399.4	10.5	0.0297	0.0288	5419.3	6602.0	388.9
P82	(failed along transverse direction)						
P83	(failed along transverse direction)						
P84	372.3	16.3	0.0227	0.0202	8389.2	5043.5	356.1

Table H.16: Global and Relative Inelastic Displacement Demands along Longitudinal Direction Resulting from ITHA-5

	At the Moment When Max. Global Displacement Occurs						
Model	$(\Delta_D)^G$	Δ_f	θ_{Left}	θ_{Right}	N_{left}	N_{right}	$(\Delta_D)^R$
C51	137.1	23.9	0.0015	0.0019	5591.4	5547.9	114.1
C52	120.9	29.9	0.0000	0.0000	2731.6	7974.9	91.4
C53	111.2	31.7	0.0000	0.0000	233.7	10348.0	79.8
C54	102.9	32.6	0.0000	0.0000	-1175.6	11665.2	70.4
C61	211.3	14.2	0.0114	0.0106	7970.1	4628.4	197.3
C62	151.9	21.1	0.0009	0.0002	8110.2	5679.8	131.1
C63	137.9	23.2	0.0000	0.0000	5074.6	5557.2	116.7
C64	130.5	25.0	0.0000	0.0000	3610.0	6913.9	105.8
C71	237.9	6.5	0.0128	0.0128	6061.7	6183.6	231.3
C72	225.5	13.0	0.0100	0.0090	7484.5	4907.9	213.1
C73	190.6	19.9	0.0031	0.0021	8329.4	4657.2	171.2
C74	169.9	22.4	0.0000	0.0000	8673.7	5094.5	147.9
C81	(failed along transverse direction)						
C82	264.5	7.7	0.0122	0.0127	5570.6	6566.7	257.1
C83	252.4	9.3	0.0103	0.0101	6149.0	6112.8	243.1
C84	230.0	13.3	0.0062	0.0055	7008.4	5477.2	217.3
P51	242.7	35.7	0.0125	0.0133	7305.2	5196.5	211.1
P52	189.1	46.8	0.0032	0.0034	3275.4	9419.4	146.1
P53	170.8	56.5	0.0000	0.0000	451.3	11783.3	114.7
P54	160.1	58.8	0.0000	0.0000	911.3	11305.4	101.4
P61	(failed along transverse direction)						
P62	260.0	27.3	0.0123	0.0136	8158.5	4392.9	235.2
P63	225.3	33.8	0.0060	0.0066	6086.3	6520.2	194.2
P64	200.6	46.3	0.0007	0.0010	4463.3	7618.2	156.5
P71	372.7	8.1	0.0261	0.0288	5094.9	8694.1	364.6
P72	(failed along transverse direction)						
P73	288.1	18.1	0.0140	0.0159	9101.6	3468.2	270.2
P74	264.5	23.4	0.0093	0.0109	8712.4	3828.9	242.3
P81	369.9	8.0	0.0259	0.0259	6069.5	7330.5	361.9
P82	(failed along transverse direction)						
P83	(failed along transverse direction)						
P84	(failed along transverse direction)						

Table H.17: Global and Relative Inelastic Displacement Demands along Longitudinal Direction Resulting from ITHA-6

	At the Moment When Max. Global Displacement Occurs						
Model	$(\Delta_D)^G$	Δ_f	θ_{Left}	θ_{Right}	N_{left}	N_{right}	$(\Delta_D)^R$
C51	132.5	19.3	0.0012	0.0019	10128.5	3691.9	114.3
C52	116.4	25.6	0.0000	0.0000	11249.5	325.4	90.9
C53	108.0	26.2	0.0000	0.0000	12594.1	-1741.2	82.2
C54	101.4	26.6	0.0000	0.0000	12665.1	-1913.1	74.8
C61	187.4	11.9	0.0077	0.0084	7470.9	6654.6	176.4
C62	151.0	17.4	0.0003	0.0012	8886.4	5043.5	134.1
C63	140.4	21.6	0.0000	0.0000	9927.1	2739.0	119.3
C64	132.2	23.7	0.0000	0.0000	10473.5	1198.3	108.7
C71	245.4	14.5	0.0135	0.0134	6604.4	6209.4	232.8
C72	203.6	9.7	0.0068	0.0072	7048.3	7605.0	194.0
C73	172.7	13.2	0.0007	0.0014	7136.9	7268.7	159.7
C74	164.4	16.1	0.0000	0.0000	7530.7	6377.8	148.8
C81	(failed along transverse direction)						
C82	(failed along transverse direction)						
C83	240.3	16.0	0.0085	0.0085	6208.9	6632.9	227.0
C84	206.2	13.7	0.0030	0.0032	6391.2	7517.0	195.0
P51	258.8	23.6	0.0153	0.0163	9297.8	2675.9	235.9
P52	195.3	31.9	0.0048	0.0058	11468.4	-61.8	165.2
P53	173.9	49.5	0.0000	0.0000	12065.7	-1227.1	124.8
P54	166.1	54.3	0.0000	0.0000	11785.3	-1025.1	112.2
P61	(failed along transverse direction)						
P62	267.1	28.7	0.0131	0.0139	8801.8	2755.6	240.7
P63	223.4	23.6	0.0061	0.0074	9783.7	1797.1	199.8
P64	202.2	34.4	0.0014	0.0029	10755.2	120.6	169.0
P71	(failed along transverse direction)						
P72	(failed along transverse direction)						
P73	275.3	27.4	0.0114	0.0128	6388.7	4466.9	247.9
P74	251.3	28.6	0.0076	0.0080	6221.6	7768.7	222.7
P81	(failed along transverse direction)						
P82	(failed along transverse direction)						
P83	(failed along transverse direction)						
P84	(failed along transverse direction)						

Table H.18: Global and Relative Inelastic Displacement Demands along Longitudinal Direction Resulting from ITHA-7

	At the Moment When Max. Global Displacement Occurs						
Model	$(\Delta_D)^G$	Δ_f	θ_{Left}	θ_{Right}	N_{left}	N_{right}	$(\Delta_D)^R$
C51	119.5	22.3	0.0004	0.0000	11481.6	4133.7	97.7
C52	107.0	23.7	0.0000	0.0000	11670.7	3492.7	85.6
C53	101.5	25.3	0.0000	0.0000	9503.7	4927.5	80.0
C54	95.0	26.8	0.0000	0.0000	5814.1	7974.7	73.4
C61	154.7	14.0	0.0047	0.0030	8621.0	4548.3	141.7
C62	136.3	21.7	0.0000	0.0000	10918.7	4487.6	114.9
C63	123.3	21.2	0.0000	0.0000	11125.4	4114.7	102.6
C64	116.9	21.5	0.0000	0.0000	11264.1	3754.0	97.6
C71	206.7	10.3	0.0092	0.0089	5972.7	6268.6	197.6
C72	172.1	13.9	0.0036	0.0018	8335.2	4518.1	159.3
C73	160.3	20.1	0.0000	0.0000	9645.8	5044.1	140.4
C74	148.0	21.0	0.0000	0.0000	10264.3	4812.4	127.0
C81	281.8	3.4	0.0168	0.0160	5407.5	6334.6	278.6
C82	220.1	10.4	0.0073	0.0068	6211.4	6673.7	211.1
C83	196.9	8.4	0.0045	0.0024	6884.7	3656.7	188.6
C84	187.2	14.8	0.0013	0.0000	8209.2	4639.7	173.0
P51	251.5	26.4	0.0142	0.0147	7373.4	8724.9	225.8
P52	187.6	35.9	0.0041	0.0037	6151.5	5423.6	154.1
P53	162.6	46.4	0.0000	0.0000	4491.1	5839.4	117.2
P54	151.7	48.8	0.0000	0.0000	4432.9	5703.5	104.3
P61	(failed along transverse direction)						
P62	276.2	30.6	0.0139	0.0143	7916.2	5979.0	247.6
P63	241.8	34.1	0.0076	0.0080	5562.2	5694.8	208.9
P64	206.1	37.5	0.0023	0.0021	7803.6	3714.8	168.8
P71	(failed along transverse direction)						
P72	(failed along transverse direction)						
P73	(failed along transverse direction)						
P74	298.3	31.7	0.0128	0.0129	7107.4	4039.8	268.0
P81	(failed along transverse direction)						
P82	(failed along transverse direction)						
P83	(failed along transverse direction)						
P84	(failed along transverse direction)						

Table H.19: Global and Relative Inelastic Displacement Demands along Longitudinal Direction Resulting from ITHA-8

	At the Moment When Max. Global Displacement Occurs						
Model	$(\Delta_D)^G$	Δ_f	θ_{Left}	θ_{Right}	N_{left}	N_{right}	$(\Delta_D)^R$
C51	130.8	24.2	0.0006	0.0012	5252.2	7683.9	107.0
C52	110.4	26.8	0.0000	0.0000	2697.6	10872.2	83.6
C53	96.0	25.6	0.0000	0.0000	1289.2	12461.1	70.6
C54	85.3	24.7	0.0000	0.0000	2282.4	11057.2	60.8
C61	156.9	14.0	0.0039	0.0042	5012.2	6597.3	143.3
C62	140.3	20.9	0.0000	0.0000	6777.0	5731.9	119.5
C63	130.7	23.1	0.0000	0.0000	6522.8	6428.7	107.8
C64	121.5	24.1	0.0000	0.0000	5252.3	7915.4	97.5
C71	(failed along transverse direction)						
C72	164.9	12.4	0.0013	0.0021	5944.8	5521.3	152.6
C73	150.0	15.7	0.0000	0.0000	4883.8	6690.7	134.4
C74	145.4	17.9	0.0000	0.0000	6179.8	5805.9	127.6
C81	(failed along transverse direction)						
C82	(failed along transverse direction)						
C83	183.1	11.5	0.0010	0.0013	5356.5	6097.5	171.6
C84	170.9	12.7	0.0000	0.0000	4839.0	6545.4	158.3
P51	271.5	33.1	0.0155	0.0168	5409.2	5253.7	238.4
P52	188.0	43.7	0.0031	0.0034	2855.4	6127.2	146.5
P53	164.0	51.6	0.0000	0.0000	2409.6	8759.5	112.5
P54	152.3	53.3	0.0000	0.0000	1962.9	10006.1	99.0
P61	(failed along transverse direction)						
P62	(failed along transverse direction)						
P63	235.7	32.9	0.0067	0.0077	4737.3	3989.3	203.3
P64	200.9	43.8	0.0007	0.0014	5111.6	3891.2	157.3
P71	383.4	8.4	0.0284	0.0291	5210.5	6674.7	375.0
P72	391.1	17.8	0.0259	0.0285	8384.9	3556.1	373.3
P73	366.6	20.9	0.0218	0.0243	8739.4	4823.8	346.1
P74	305.0	27.8	0.0129	0.0153	8266.1	3411.4	277.2
P81	385.2	9.2	0.0269	0.0275	5966.3	7222.7	376.0
P82	402.7	7.7	0.0271	0.0278	5513.5	7226.4	395.0
P83	(failed along transverse direction)						
P84	454.6	15.0	0.0303	0.0319	6909.7	5495.5	439.6

APPENDIX I

RESPONSE MEASURE VALUES

Table I.1: Displacement Capacity over Demand Ratios along Transverse Direction

			Competent Soil		Poor Soil	
	ρ_l	H_n/D	*Global*	*Relative*	*Global*	*Relative*
Using Elastic Displacement Demands	1%	5	1.71	2.75	1.63	2.93
		6	1.47	1.85	1.20	1.68
		7	1.30	1.48	1.00	1.21
		8	1.18	1.27	0.72	0.81
	2%	5	2.11	3.79	2.18	4.28
		6	1.63	2.22	1.42	2.15
		7	1.51	1.79	1.10	1.41
		8	1.30	1.43	0.85	0.99
	3%	5	3.23	6.27	3.62	7.15
		6	2.35	3.45	2.22	3.61
		7	1.73	2.14	1.43	1.92
		8	1.41	1.59	1.05	1.25
	4%	5	3.81	7.45	5.38	8.52
		6	3.13	4.88	3.04	5.18
		7	2.02	2.57	1.69	2.36
		8	1.72	1.98	1.23	1.51
Using Inelastic Displacement Demands	1%	5	1.67	1.67	1.40	1.35
		6	1.41	1.40	0.98	0.97
		7	1.14	1.14	1.03	1.02
		8	1.06	1.06	0.97	0.97
	2%	5	1.92	1.87	1.86	1.71
		6	1.48	1.48	1.24	1.21
		7	1.38	1.38	0.97	0.96
		8	1.15	1.15	0.97	0.97
	3%	5	2.73	3.05	3.08	3.64
		6	2.03	2.04	1.80	1.74
		7	1.61	1.62	1.14	1.14
		8	1.23	1.23	1.06	1.05
	4%	5	2.98	3.80	4.71	5.07
		6	2.70	2.71	2.39	2.34
		7	1.76	1.76	1.39	1.39
		8	1.47	1.48	1.06	1.05

Table I.2: Displacement Capacity over Demand Ratios along Longitudinal Direction

			Competent Soil		Poor Soil	
	ρ_l	H_n/D	*Global*	*Relative*	*Global*	*Relative*
Using Elastic Displacement Demands	1%	5	4.06	4.98	2.44	3.06
		6	3.33	3.85	1.97	2.31
		7	2.81	3.13	1.49	1.66
		8	2.43	2.64	1.38	1.51
	2%	5	5.53	6.99	3.21	4.12
		6	3.87	4.53	2.26	2.68
		7	3.22	3.63	1.73	1.96
		8	2.72	2.99	1.41	1.55
	3%	5	8.43	11.00	5.06	6.69
		6	5.57	6.68	4.10	5.85
		7	3.85	4.39	2.24	2.58
		8	2.85	3.14	1.64	1.81
	4%	5	9.36	12.36	5.70	7.54
		6	7.66	9.37	4.51	5.62
		7	4.47	5.14	2.61	3.04
		8	3.56	3.97	1.99	2.24
Using Inelastic Displacement Demands	1%	5	3.12	3.44	1.64	1.70
		6	2.23	2.31	1.25	1.25
		7	1.81	1.82	1.02	1.01
		8	1.50	1.50	1.16	1.16
	2%	5	4.32	4.83	2.71	2.95
		6	2.93	3.15	1.54	1.57
		7	2.21	2.26	1.08	1.08
		8	1.81	1.81	1.02	1.01
	3%	5	6.61	7.50	4.37	5.20
		6	4.32	4.72	2.51	2.65
		7	2.80	2.94	1.52	1.55
		8	1.97	2.01	1.15	1.14
	4%	5	7.44	8.39	4.97	5.89
		6	5.96	6.61	3.81	4.29
		7	3.31	3.55	1.84	1.90
		8	2.51	2.59	1.30	1.29

Table I.3: Global Displacement Ductility Demands along Transverse Direction

		Competent Soil		Poor Soil	
ρ_l	H_n/D	Δ_D = *elastic*	Δ_D = *inelastic*	Δ_D = *elastic*	Δ_D = *inelastic*
1%	5	1.34	2.53	1.25	2.99
	6	1.74	2.72	1.69	3.80
	7	2.03	3.07	2.27	3.67
	8	2.30	3.08	2.95	3.32
2%	5	1.11	2.12	1.04	2.04
	6	1.42	2.39	1.36	2.74
	7	1.72	2.50	1.81	3.35
	8	2.06	2.87	2.49	3.32
3%	5	1.01	1.56	0.96	1.29
	6	1.27	2.27	1.21	2.65
	7	1.75	2.67	1.75	3.64
	8	2.12	3.13	2.38	3.84
4%	5	0.95	1.30	0.91	1.08
	6	1.21	2.19	1.14	2.35
	7	1.58	2.63	1.56	3.09
	8	2.02	3.06	2.18	4.12

* Filled cells represent failed models.

Table I.4: Global Displacement Ductility Demands along Longitudinal Direction

		Competent Soil		Poor Soil	
ρ_l	H_n/D	Δ_D = *elastic*	Δ_D = *inelastic*	Δ_D = *elastic*	Δ_D = *inelastic*
1%	5	0.69	0.92	1.04	1.71
	6	0.84	1.31	1.29	2.35
	7	1.00	1.67	1.56	2.69
	8	1.16	2.04	1.87	2.58
2%	5	0.56	0.73	0.85	1.06
	6	0.68	0.91	1.04	1.66
	7	0.81	1.24	1.28	2.30
	8	1.01	1.63	1.62	2.60
3%	5	0.48	0.62	0.72	0.84
	6	0.58	0.76	0.69	1.25
	7	0.80	1.12	1.24	2.01
	8	1.00	1.50	1.57	2.59
4%	5	0.47	0.60	0.70	0.82
	6	0.53	0.69	0.82	1.00
	7	0.71	0.97	1.11	1.68
	8	0.92	1.35	1.45	2.53

Table I.5: Response Modification Factors for Columns

		Transverse		Longitudinal	
ρ_l	H_n/D	*Competent*	*Poor*	*Competent*	*Poor*
1%	5	3.91	4.56	1.68	1.97
	6	5.19	7.34	2.66	3.41
	7	6.34	8.48	3.73	4.82
	8	7.84	9.94	5.36	7.14
2%	5	2.45	2.57	1.28	1.46
	6	3.53	4.03	2.11	2.62
	7	4.69	5.69	2.98	3.83
	8	6.35	7.91	4.46	5.95
3%	5	2.02	2.04	1.04	1.17
	6	2.97	3.33	1.74	2.12
	7	4.09	4.95	2.48	3.15
	8	5.48	6.81	3.55	4.69
4%	5	1.73	1.72	0.89	0.98
	6	2.62	2.86	1.52	1.82
	7	3.61	4.37	2.13	2.68
	8	4.78	5.92	2.94	3.83

Table I.6: Structural Displacement Ductility Capacities

ρ_l	H_n/D	Transverse	Longitudinal
1%	5	4.90	3.18
	6	4.21	3.16
	7	3.84	2.99
	8	3.37	3.12
2%	5	4.72	3.29
	6	3.88	2.84
	7	3.63	2.76
	8	3.42	2.88
3%	5	6.35	4.18
	6	5.28	3.48
	7	4.82	3.37
	8	4.24	3.13
4%	5	6.48	4.47
	6	6.90	4.30
	7	5.07	3.45
	8	4.92	3.57

Table I.7: Maximum Displacement Ratios

		Transverse		Longitudinal	
ρ_l	H_n/D	Competent	Poor	Competent	Poor
1%	5	1.02	1.16	1.30	1.48
	6	1.05	1.23	1.49	1.58
	7	1.14	0.97	1.56	1.46
	8	1.11	0.74	1.62	1.19
2%	5	1.10	1.17	1.28	1.19
	6	1.10	1.15	1.32	1.46
	7	1.09	1.13	1.46	1.61
	8	1.13	0.88	1.51	1.38
3%	5	1.18	1.18	1.27	1.16
	6	1.16	1.23	1.29	1.63
	7	1.08	1.25	1.37	1.47
	8	1.15	0.99	1.45	1.42
4%	5	1.28	1.14	1.26	1.15
	6	1.16	1.27	1.28	1.19
	7	1.15	1.22	1.35	1.42
	8	1.16	1.16	1.42	1.54

* Filled cells represent insignificant results as explained in Section 5.3.

Table I.8: Maximum Strain Values of Columns along Transverse Direction

		Concrete Strain, ε_c		Steel Strain, ε_s	
ρ_l	H_n/D	*Competent*	*Poor*	*Competent*	*Poor*
1%	5	0.0088	0.0112	0.0297	0.0394
	6	0.0094	0.0148	0.0301	0.0509
	7	0.0126	0.0146	0.0360	0.0481
	8	0.0140	0.0151	0.0339	0.0390
2%	5	0.0076	0.0080	0.0196	0.0208
	6	0.0093	0.0113	0.0232	0.0305
	7	0.0105	0.0149	0.0242	0.0386
	8	0.0124	0.0149	0.0259	0.0338
3%	5	0.0049	0.0037	0.0105	0.0076
	6	0.0083	0.0103	0.0180	0.0230
	7	0.0079	0.0132	0.0167	0.0286
	8	0.0114	0.0150	0.0215	0.0302
4%	5	0.0038	0.0027	0.0068	0.0043
	6	0.0067	0.0079	0.0126	0.0153
	7	0.0085	0.0116	0.0160	0.0230
	8	0.0096	0.0149	0.0164	0.0259

* Filled cells represent failed models.

Table I.9: Maximum Strain Values of Columns along Longitudinal Direction

		Concrete Strain, ε_c		Steel Strain, ε_s	
ρ_l	H_n/D	*Competent*	*Poor*	*Competent*	*Poor*
1%	5	0.0021	0.0080	0.0058	0.0309
	6	0.0046	0.0122	0.0148	0.0420
	7	0.0068	0.0142	0.0209	0.0432
	8	0.0099	0.0145	0.0244	0.0351
2%	5	*(elastic)*	0.0029	*(elastic)*	0.0078
	6	0.0022	0.0085	0.0048	0.0233
	7	0.0046	0.0136	0.0110	0.0343
	8	0.0065	0.0149	0.0142	0.0300
3%	5	*(elastic)*	*(elastic)*	*(elastic)*	*(elastic)*
	6	*(elastic)*	0.0045	*(elastic)*	0.0106
	7	0.0030	0.0086	0.0057	0.0196
	8	0.0050	0.0126	0.0097	0.0251
4%	5	*(elastic)*	*(elastic)*	*(elastic)*	*(elastic)*
	6	*(elastic)*	0.0025	*(elastic)*	0.0044
	7	*(elastic)*	0.0069	*(elastic)*	0.0142
	8	0.0037	0.0112	0.0060	0.0200

* Filled cells represent failed models.

APPENDIX J

DEMONSTRATION OF CAPACITIES AND DEMANDS

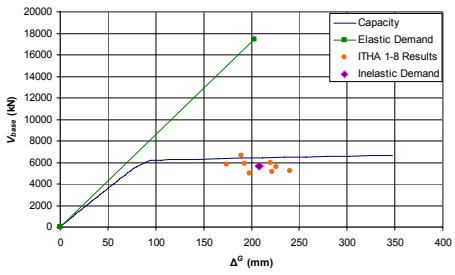

(a) *C51*

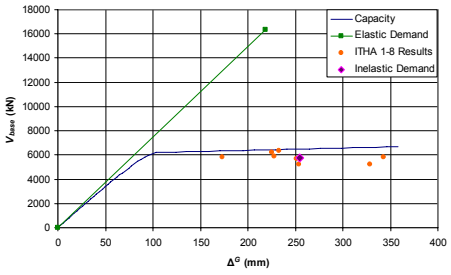

(e) *P51*

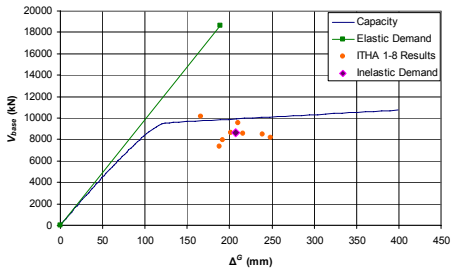

(b) *C52*

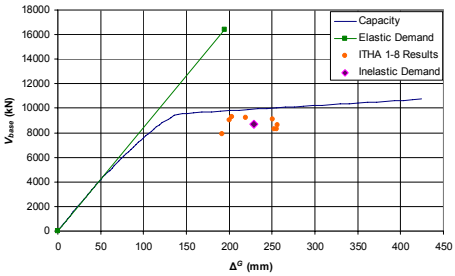

(f) *P52*

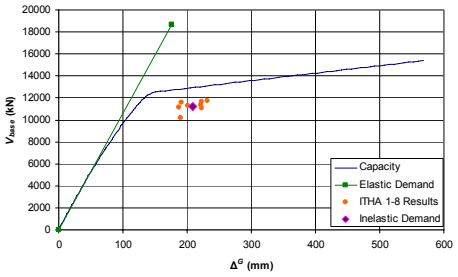

(c) *C53*

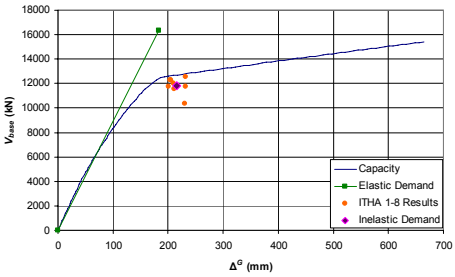

(g) *P53*

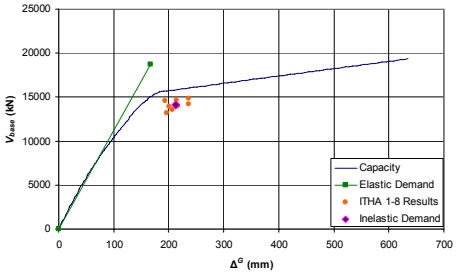

(d) *C54*

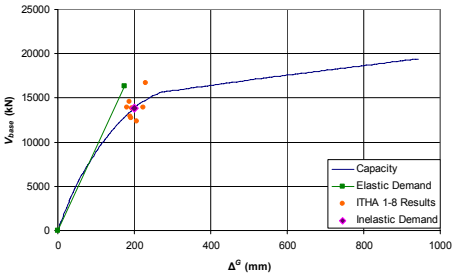

(h) *P54*

Figure J.1: Capacity Curves, Elastic and Inelastic Demands of the Bridges with H_n/D = 5 in Transverse Direction at Competent and Poor Soil

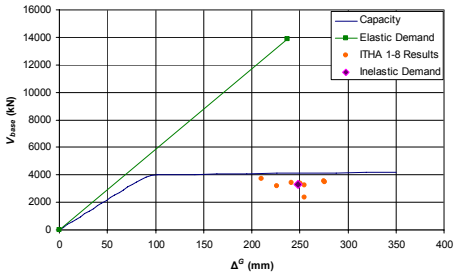

(a) *C61*

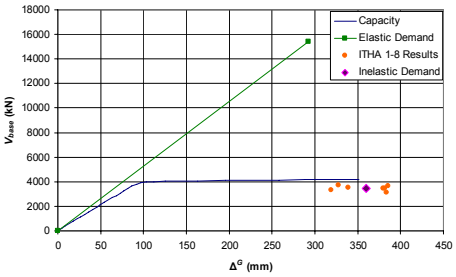

(e) *P61*

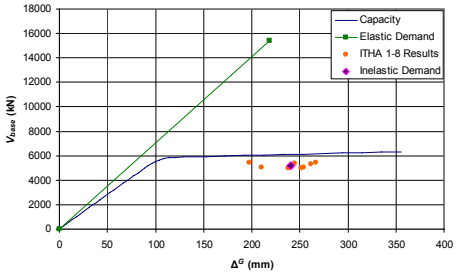

(b) *C62*

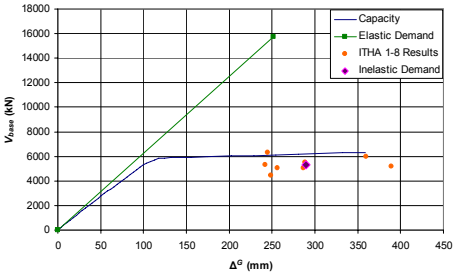

(f) *P62*

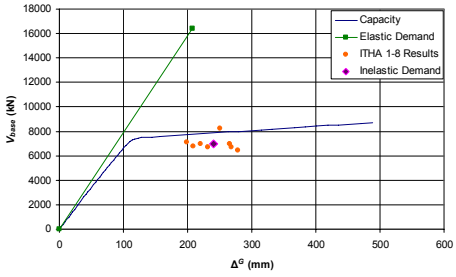

(c) *C63*

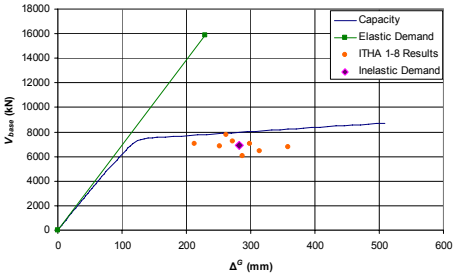

(g) *P63*

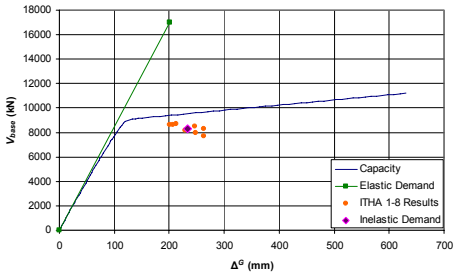

(d) *C64*

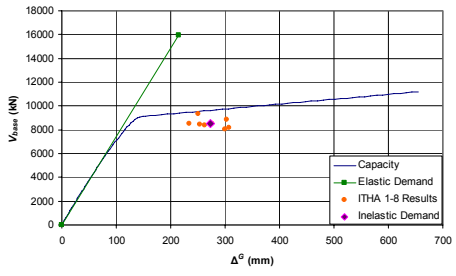

(h) *P64*

Figure J.2: Capacity Curves, Elastic and Inelastic Demands of the Bridges with H_n/D = 6 in Transverse Direction at Competent and Poor Soil

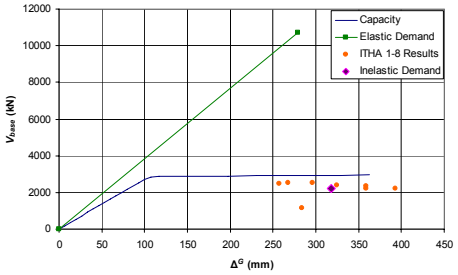

(a) *C71*

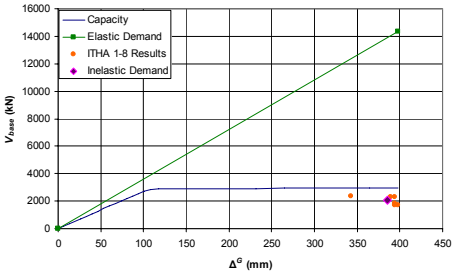

(e) *P71*

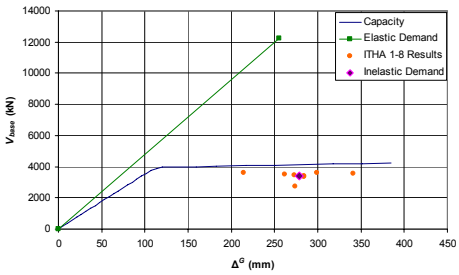

(b) *C72*

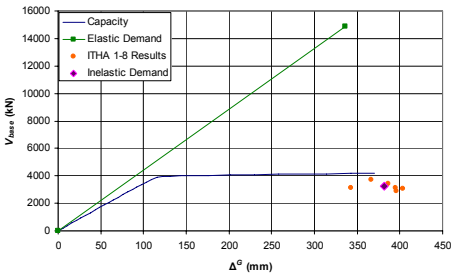

(f) *P72*

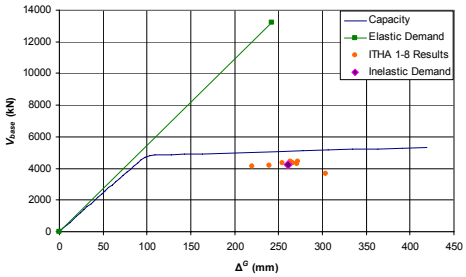

(c) *C73*

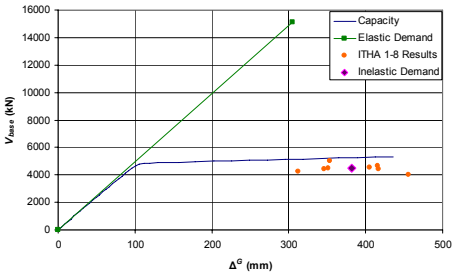

(g) *P73*

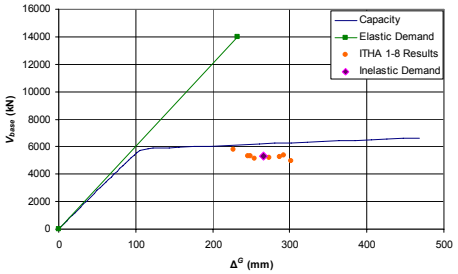

(d) *C74*

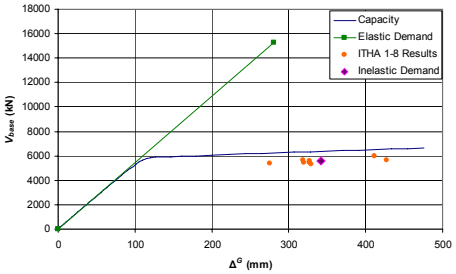

(h) *P74*

Figure J.3: Capacity Curves, Elastic and Inelastic Demands of the Bridges with $H_n/D = 7$ in Transverse Direction at Competent and Poor Soil

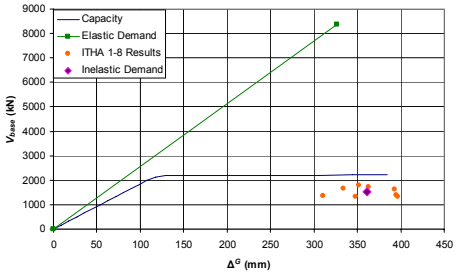

(a) *C81*

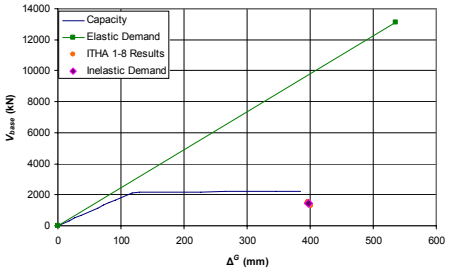

(e) *P81*

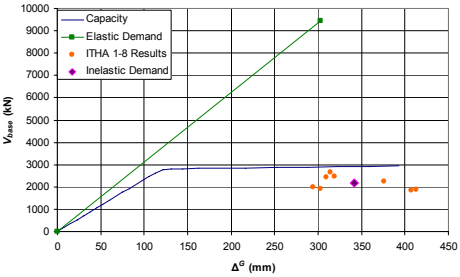

(b) *C82*

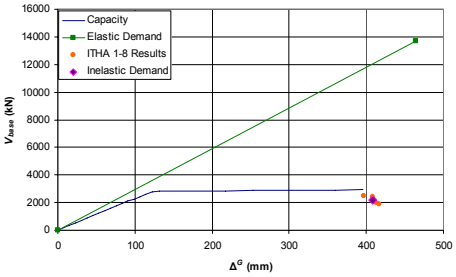

(f) *P82*

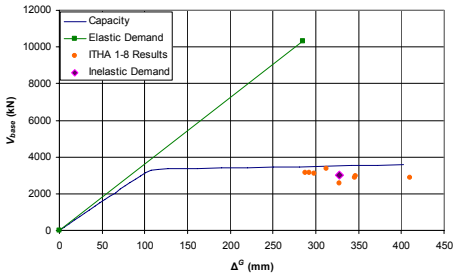

(c) *C83*

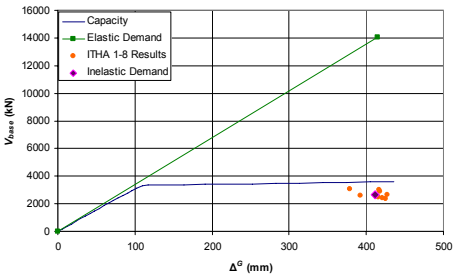

(g) *P83*

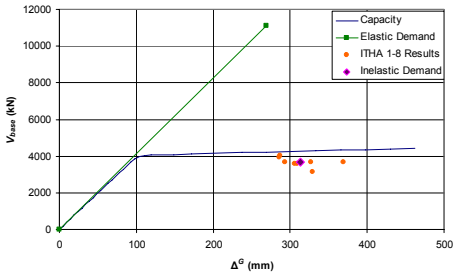

(d) *C84*

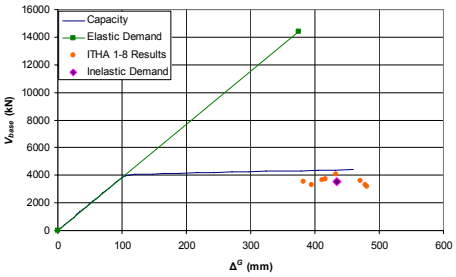

(h) *P84*

Figure J.4: Capacity Curves, Elastic and Inelastic Demands of the Bridges with H_n/D = 8 in Transverse Direction at Competent and Poor Soil

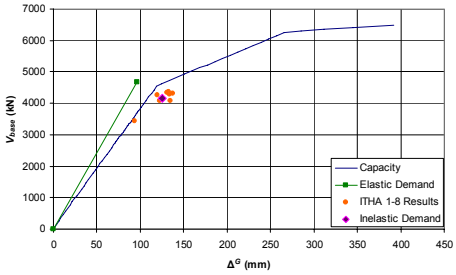

(a) *C51*

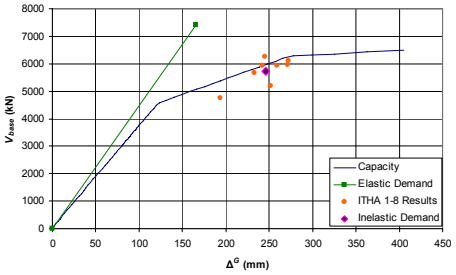

(e) *P51*

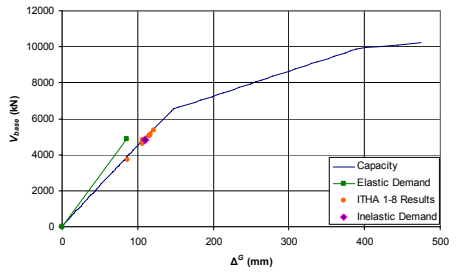

(b) *C52*

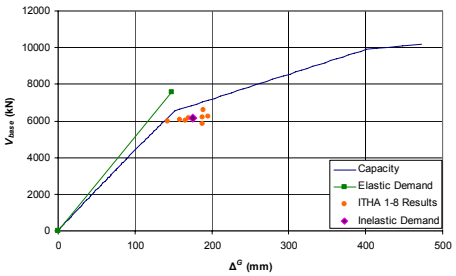

(f) *P52*

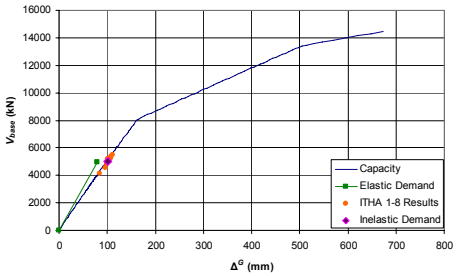

(c) *C53*

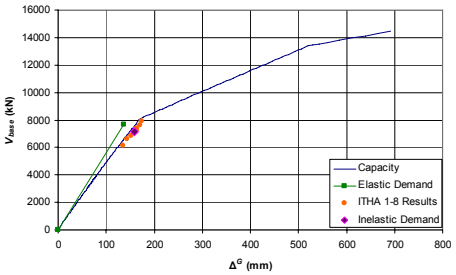

(g) *P53*

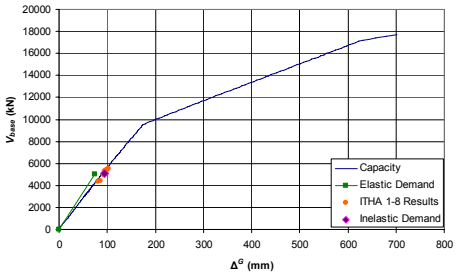

(d) *C54*

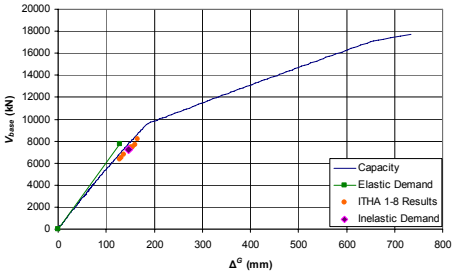

(h) *P54*

Figure J.5: Capacity Curves, Elastic and Inelastic Demands of the Bridges with H_n/D = 5 in Longitudinal Direction at Competent and Poor Soil

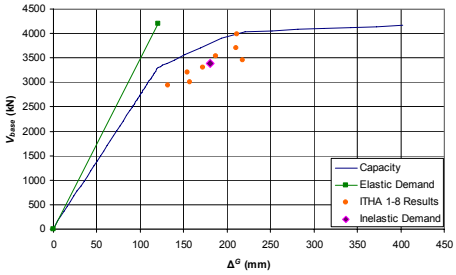

(a) *C61*

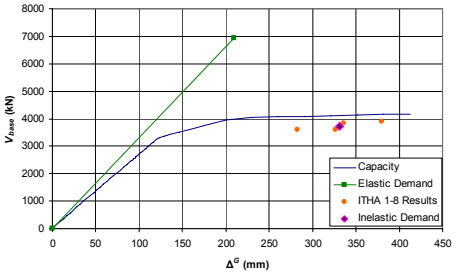

(e) *P61*

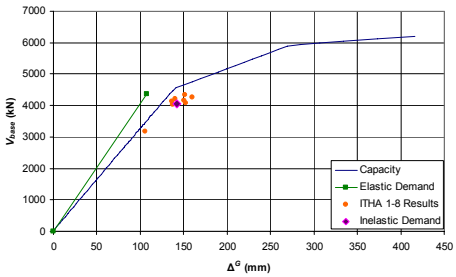

(b) *C62*

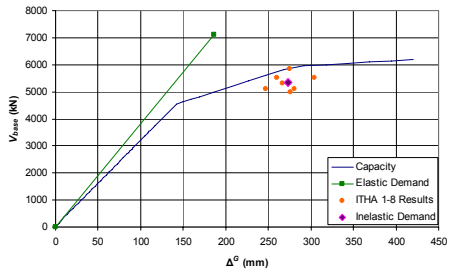

(f) *P62*

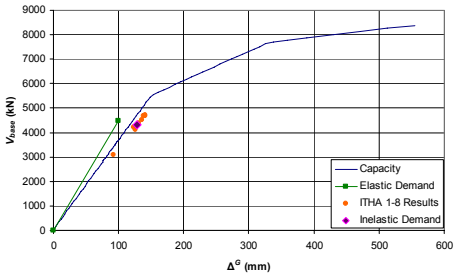

(c) *C63*

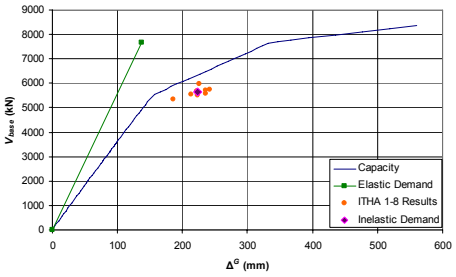

(g) *P63*

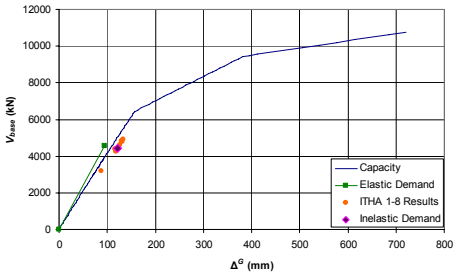

(d) *C64*

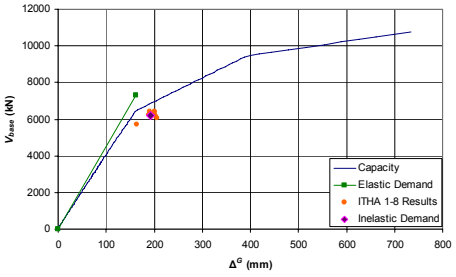

(h) *P64*

Figure J.6: Capacity Curves, Elastic and Inelastic Demands of the Bridges with H_n/D = 6 in Longitudinal Direction at Competent and Poor Soil

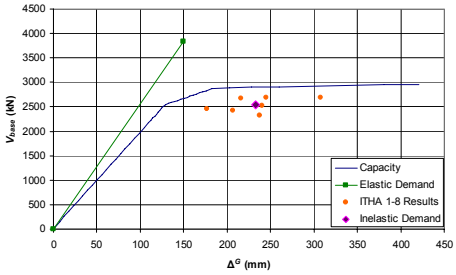

(a) *C71*

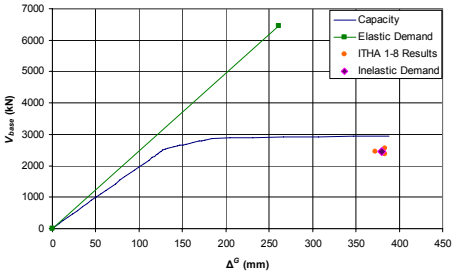

(e) *P71*

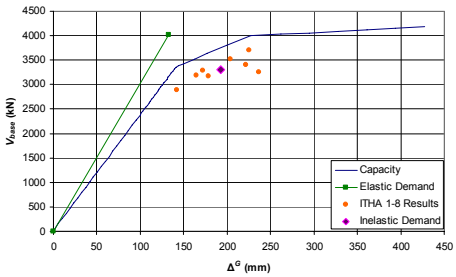

(b) *C72*

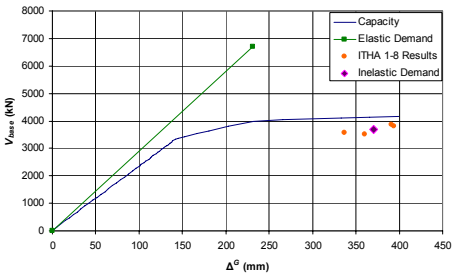

(f) *P72*

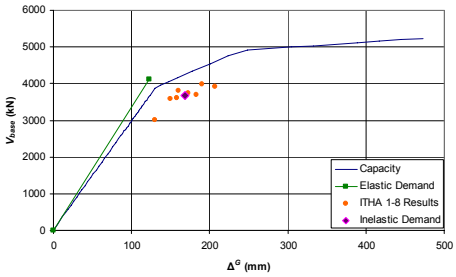

(c) *C73*

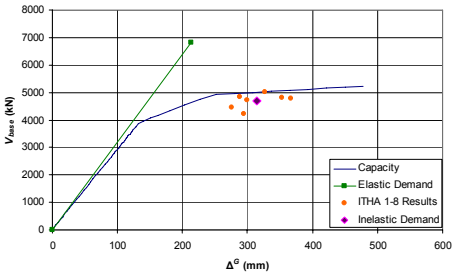

(g) *P73*

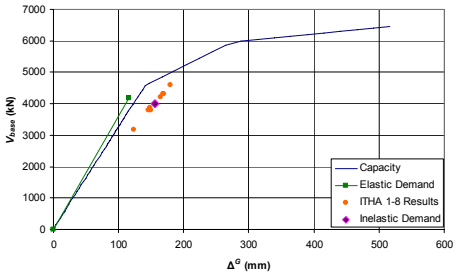

(d) *C74*

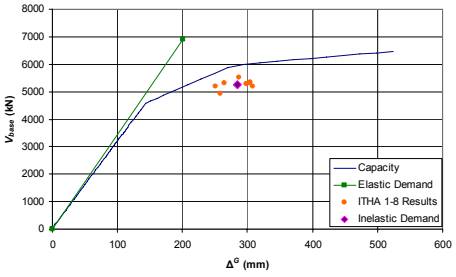

(h) *P74*

Figure J.7: Capacity Curves, Elastic and Inelastic Demands of the Bridges with H_n/D = 7 in Longitudinal Direction at Competent and Poor Soil

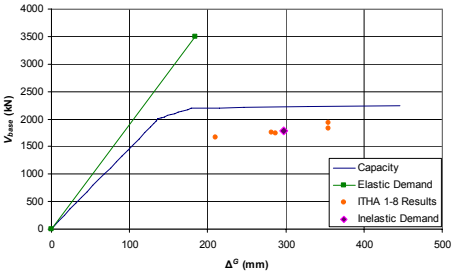

(a) *C81*

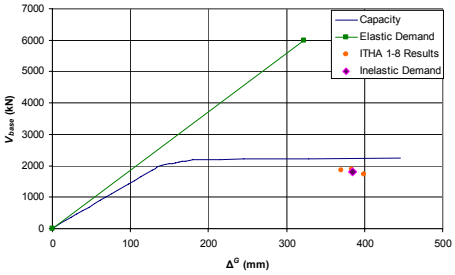

(e) *P81*

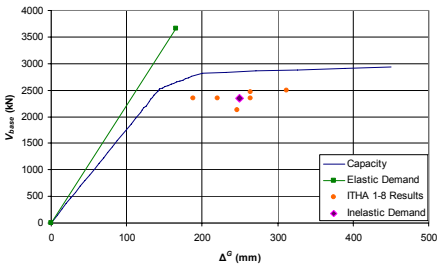

(b) *C82*

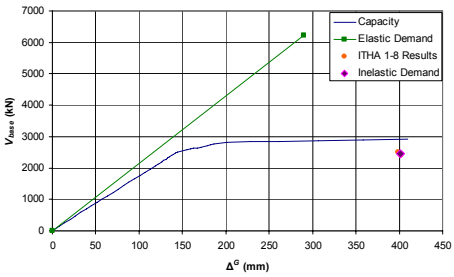

(f) *P82*

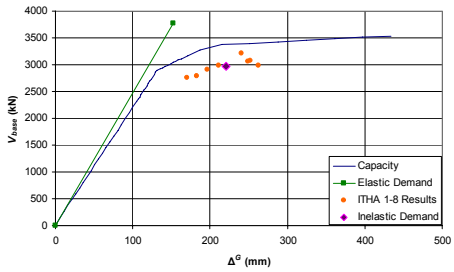

(c) *C83*

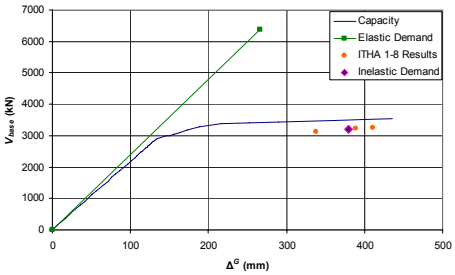

(g) *P83*

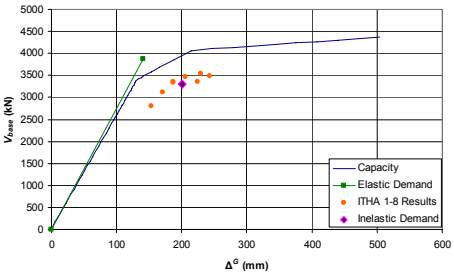

(d) *C84*

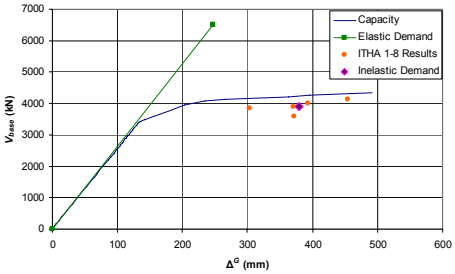

(h) *P84*

Figure J.8: Capacity Curves, Elastic and Inelastic Demands of the Bridges with H_n/D = 8 in Longitudinal Direction at Competent and Poor Soil